

**Development and Evaluation of Novel Lipid-Polymer Hybrid
Nanocarrier System for Targeted Delivery of HPPH and Olaparib
for Effective Triple Negative Breast Cancer Treatment**

THESIS

Submitted in partial fulfilment of
the requirements for the degree of
DOCTOR OF PHILOSOPHY

by

Rajesh Pradhan

Under the Supervision

of

Prof. Rajeev Taliyan

and Co-supervision of

Dr. Sunil Kumar Dubey



BITS Pilani
Pilani | Dubai | Goa | Hyderabad

**BIRLA INSTITUTE OF TECHNOLOGY & SCIENCE
PILANI-333031 (RAJASTHAN) INDIA**

2024

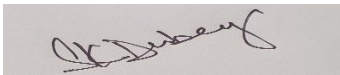
CERTIFICATE

This is to certify that the thesis entitled “**Development and Evaluation of Novel Lipid-Polymer Hybrid Nanocarrier System for Targeted Delivery of HPPH and Olaparib for Effective Triple Negative Breast Cancer Treatment**” submitted by **Mr. Rajesh Pradhan**, ID No. **2018PHXF0047P** for the award of Ph.D. Degree of the Institute, embodies the original work done by him under my supervision.

Signature of Supervisor

Name : Prof. Rajeev Taliyan
Designation: : Professor,
Department of Pharmacy,
BITS-Pilani, Pilani Campus

Signature of Co-supervisor

: 
Name : Dr. Sunil Kumar Dubey
Designation : General Manager,
Medical Research, R&D Healthcare Division,
Emami Ltd.,13, BT Road, Kolkata, India-700056

Date : 16-04-2024
Place : Pilani, Rajasthan

Table of Contents

Contents	Page no
Acknowledgments	i-ii
List of Abbreviations	iii-v
List of Tables	vi-vii
List of Figures	viii-xi
Abstract	xii-xxii
Chapter 1 Introduction	1-19
Chapter 2 Literature review	20-44
Chapter 3 Gap in existing research and Objectives	45-46
Chapter 4 Material and Methods	47-79
Chapter 5 Results	80-157
Chapter 6 Discussion	158-172
Chapter 7 Conclusion, Summary and Future Scope	173- 178
Chapter 8 Bibliography	179-210
Appendix I List of Publications, Patent, Book Chapter and Presentations	
Appendix II Biography	

Acknowledgments

Words fall short to express my gratitude to people who not only encouraged me during this rough patch of my life but also contributed both directly and indirectly in completing the thesis of my doctoral degree. To begin with, I shall thank my almighty for making me believe in myself and also always pushing me towards my extreme limits and right path. Next, I would like to thank my parents, **Mr. Ramesh Pradhan** and **Mrs. Saudamini Pradhan** for constantly persuading me in completing my thesis, giving me beneficial words of advice and bearing with me during my hard times. I thank them for trusting in me regarding all the decisions I have taken so far including joining PhD.

Next and most importantly, I am immensely thankful and grateful to my supervisor **Prof. Rajeev Taliyan** and my co-supervisor **Dr. Sunil Kumar Dubey** for his guidance, trust, patience, and support. This PhD journey would not have been memorable, insightful and knowledgeable if it wasn't for my supervisor. I will remain forever indebted to the trust he bestowed upon me during the times when I had completely lost faith in myself.

I am grateful to **Prof. Sudhir Kumar Barai**, Director, **Prof. V Ramgopal Rao**, Vice-Chancellor, BITS Pilani, and **Prof. A.K Sarkar**, Former-Director, BITS Pilani, Pilani Campus for permitting me to pursue my research work in the Institute. I also express my sincere thanks to **Prof. Shamik Chakraborty**, Associate Dean AGSRD, and **Prof. Jitendra Panwar**, former Associate Dean, AGSRD for their motivation, constant support and encouragement.

I am immensely thankful to my Doctoral approval committee (DAC) members **Prof. Gautam Singhvi**, Associate Professor, Department of Pharmacy and **Prof. Aniruddha Roy** Associate Professor, Department of Pharmacy, Pilani Campus for their words of advice and suggestions and also evaluating my thesis. I would like to acknowledge **Prof. Anil Jindal**, Convener and **Prof. Deepak Chitkara** former Convener, Departmental Research Committee, Department of Pharmacy, BITS Pilani, Pilani Campus for providing valuable comments.

A special vote of thanks to the head of the Department of Pharmacy, **Prof. Gaikwad Anil Bhanudas** who have constantly encouraged and motivated me during my PhD tenure. I am

honestly thankful for his support and encouragement. I would also like to thank **Prof. Hemant R. Jadhav** and **Prof. Atish T. Paul** former HODs of the Department of Pharmacy who provided immense encouragement during my PhD tenure.

I would like to thank all the extremely versatile faculty members **Prof. S. Murugesan, Prof. R. Mahesh, Prof. S. Sundriyal, Dr. Richa Shrivastava, Prof. Anupama Mittal, Prof. Murali M. Pandey, Dr. Pragyanshu Khare** for their insightful comments and suggestions.

I would like to convey a special thanks to my seniors, colleagues and juniors who had helped me to accomplish the completion stage of my thesis and would also like to extend my appreciation to the non-teaching staff of BITS Pilani for their invaluable support in conducting lab works. A big thanks to the non-teaching staffs-**Mr. Ram Suthar, Mr. Puran, Mr. Mahender, Mr. Tarachand, Mr. Laxman, Mr. Surender and Mr. Bikash Mr. Suman, Mr. Abhishek, Mr. Sandeep**, CAL facility and **Mr. Om Prakash** FESEM facility operator for their valuable help at each stage of my research work.

Last but not the least, I would like to pay homage to those experimental animals who have sacrificed their lives in making my endeavour successful. May GOD grant them eternal peace.

“Thank You”

Rajesh Pradhan

List of Abbreviations

Abbreviations	Description
% CDR	Percentage cumulative drug release
%	Percentage
% RSD	Percentage relative standard deviation
% EE	Percent entrapment efficiency
% w/w	Percentage weight by weight
% v/v	Percentage volume by volume
% w/v	Percentage weight by volume
<	Less than
≤	Less than equal to
>	More than
≥	More than equal to
~	Approximately equal to
±	Plus or minus
=	Equal to
λ _{max}	Wavelength of maximum absorbance
°C	Degree centigrade
μL	Microliter
μm	Micrometre
μg/mL	Micrometre per millilitre
cm	Centimetre
g	Gram
mg	Milligram
mg/mL	Milligram per millilitre
mL	Millilitre
ng/mL	Nanogram per millilitre
nm	Nanometre
ACN	Acetonitrile
API	Active pharmaceutical ingredient
ANOVA	Analysis of variance

AUC	Area under curve
BC	Breast Cancer
BSA	Bovine serum albumin
C _{max}	Maximum concentration
Conc.	Concentration
CPCSEA	Committee for the purpose of control and supervision of experiments on animals
DCIs	Ductal Carcinoma In Situ
DLS	Dynamic light scattering
DMSO	Dimethyl sulfoxide
DSC	Differential scanning calorimetry
EE	Entrapment Efficiency
EMA	European Medicine Agency
ERs	Estrogen Receptors
FDA	Food And Drug Administration
FESEM	Field emission scanning electron microscopy
FTIR	Fourier transform infrared spectrometer
G'	Storage modulus
G''	Loss modulus
HER2	Human Epidermal Growth Factor 2
HPPH	2-(1-Hexyloxyethyl)-2-devinyl pyropheophorbide-a
IDC	Invasive Ductal Carcinoma
ILC	Invasive Lobule Carcinoma
LCIS	Lobular Carcinoma In Situ
LPHNs	Lipid polymer hybrid nanoparticles
NPs	Nanoparticles
OLA	Olaparib
PARP	Poly (ADP-Ribose) Polymerase
PARPi	Poly (ADP-Ribose) Polymerase (PARP) Inhibitors
PDI	Polydispersity Index
PLGA	Polylactic -Co-Glycolic Acid
PRs	Progesterone Receptors
PVA	Polyvinyl alcohol

SPC 100	Soybean phosphatidylcholine grade 100)
TNBC	Triple Negative Breast Cancer

List of Tables

S. No	Title	Page no
1	Table-1.1: Different therapeutic approaches for TNBC	18
2	Table 2.1: Histologic Types of TNBCs and their essential genetic features/potential therapeutic targets	21
3	Table 4.1: List of instruments/ equipment with manufacturer's name used to conduct the experiments.	48
4	Table 4.2: List of software used to conduct the experiments	48
5	Table 4.3: Experimental design for the screening of HPPH and OLA and in combination of HPPH and OLA and their LPHNs in 4T1 bearing Balb/c mice	63
6	Table 4.4: Experimental design for the safety study of HPPH with nanocarrier systems in 4T1 bearing Balb/c mice	65
7	Table 4.5: Variable used in CCD response surface design	66
8	Table 5.1: Chromatographic condition for HPPH	80
9	Table 5.2: Accuracy and precision of HPPH	82
10	Table 5.3: Robustness of HPPH	82-83
11	Table 5.4: Different Stability studies of HPPH	83
12	Table 5.5: Chromatographic condition for OLA	85
13	Table 5.6: System Suitability Parameter of OLA	87
14	Table 5.7: Accuracy and precision of OLA	87
15	Table 5.8: Robustness of analytical method of OLA	88
16	Table 5.9: Different Stability studies of OLA	89
17	Table 5.10: Chromatographic condition of HPPH-OLA	89
18	Table 5.11: Standard calibration curves equation and correlation coefficients of HPPH-OLA	92
19	Table 5.12: Accuracy and Precision of HPPH-OLA	92
20	Table 5.13: Robustness (Different Analyst) HPPH-OLA	93
21	Table 5.14: Stability studies of HPPH-OLA	93-94
22	Table 5.15: Optimization of chromatographic condition of HPPH-OLA (Plasma)	94
23	Table 5.16: Standard calibration curves equation and correlation coefficients of HPPH-OLA(Plasma)	97
24	Table 5.17: Matrix effect of HPPH-OLA (Plasma)	98
25	Table 5.18: Accuracy and Precision of HPPH-OLA(Plasma)	98
26	Table 5.19: Robustness against different analyst of HPPH-OLA(Plasma)	99
27	Table 5.20: Stability studies of HPPH-OLA(Plasma)	99
28	Table 5.21: In vivo pharmacokinetic parameter of HPPH, OLA and their combination (n=5, Mean \pm SD)	107
29	Table 5.22: CCD based experimental runs and their corresponded responses.	110

30	Table 5.23: The analysis of variances for %EE as the response (Y1)	111
31	Table 5.24: The analysis of variances for particle size as the response (Y2)	111
32	Table 5.25: Predicted and experimental values of the responses obtained at optimum conditions	113
33	Table 5.26: Physiochemical characterisation of Optimised HPPH loaded LPHNs	114
34	Table 5.27: Lyophilization screening for HPPH loaded LPHNs with different cryoprotectant	114
35	Table 5.28: Physiochemical characterisation of Optimised HPPH loaded LPHNs (Lyophilized)	115
36	Table 5.29: In-vivo Pharmacokinetic profile of HPPH loaded LPHNs (Dose:5mg/kg.bw; Mean±SD; n=5)	123
37	Table 5.30: Biochemical analysis of HPPH and its LPHNs	127
38	Table 5.31: Physiochemical characterization of the OLA loaded LPHNs (Fresh LPHNs; n=3, Mean± SD)	128
39	Table 5.32: Lyophilization screening for OLA loaded LPHNs with different cryoprotectant	129
40	Table 5.33: Physiochemical characterization of optimised OLA loaded LPHNs	129
41	Table 5.34: In vivo pharmacokinetic study data of OLA (Dose: 30mg/kg.bw; n=5; Mean±SD)	137
42	Table 5.35: Physiochemical characterization HPPH and OLA co-loaded LPHNs (Fresh LPHNs n=3; Mean± SD)	140
43	Table 5.36: Lyophilization screening for HPPH and OLA co-loaded LPHNs with different cryoprotectant	141
44	Table 5.37: Physiochemical characterization HPPH and OLA co-loaded LPHNs (Lyophilised)	142
45	Table 5.38: In vivo pharmacokinetics studies of HPPH and OLA co-loaded LPHNs (HPPH-OLA, Biotin@HPPH/OLA-LPHNs and Biotin-ss-TPP@HPPH/OLA-LPHNs)	151

List of Figures

S. No	Title	Page no
1	Figure 1.1: Pathogenesis of triple negative breast cancer	3
2	Figure 1.2: Different types of nanoparticles used in treatment of TNBC	17
3	Figure 2.1: Pictorial representation of different novel therapies against TNBC	27
4	Figure 4.1: Synthesis scheme for Biotin-PEG-PLGA	58
5	Figure 4.2: Synthesis scheme for Linoleic acid-ss-TPP	60
6	Figure 4.3: Experimental schedule of animal model development and treatment	63
7	Figure 4.4: Schematic representation of LPHNs preparation procedure	66
8	Figure 4.5: Schematic representation of HPPH and OLA co-loaded LPHNs	76
9	Figure 5.1: Chromatogram of HPPH; A) Blank, B) LQC, C) HQC	81
10	Figure 5.2: Force degradation study of HPPH	84
11	Figure 5.3: Chromatogram of OLA; A) LQC (75ng/mL); B) HQC 1800ng/mL; C) Blank	86
12	Figure 5.4: Calibration curve and standard calibration equation of OLA	87
13	Figure 5.5: MRM based simultaneous chromatogram of HPPH and OLA; A) Blank; B) LQC (2ng/mL); C) MQC1 (90ng/mL); D) HQC (180ng/mL)	90-91
14	Figure 5.6: MRM based simultaneous chromatogram for HPPH and OLA; A) Blank; B) LQC (2ng/mL); C) HQC (300ng/mL)	95-96
15	Figure 5.7: Calibration curve of HPPH and OLA	97
16	Figure 5.8: MTT assay of HPPH and OLA	100
17	Figure 5.9: Dose-response effect and cytotoxicity study; (A) cytotoxicity of combination of HPPH and OLA (B) Combination index plot for HPPH-OLA	101
18	Figure 5.10: Body weight and tumour volume of each animal group i.e., Control, HPPH, OLA and HPPH-OLA	102
19	Figure 5.11: Luminescence imaging and intensity of each animal group i.e., control, HPPH, OLA and HPPH-OLA	102-103
20	Figure 5.12: In vivo ROS study of HPPH, OLA and HPPH-OLA; (A) In-vivo image (B) Microscopic image of tumor tissue (C) Fluorescence intensity of tumor tissue; Data represent mean \pm SD. **** p value < 0.0001 and *** p value < 0.001 compared with the control group	103-104
21	Figure 5.13: Tunnel assay for HPPH, OLA and HPPH-OLA; Data represent mean \pm SD. **** p value < 0.0001 and *** p value < 0.001 compared with the control group	104-105

22	Figure 5.14: Histochemical analysis for HPPH, OLA and HPPH-OLA using H&E staining	105
23	Figure 5.15: Mean plasma concentration–time profiles of (A) OLA (30 mg/kg) and (B)HPPH (5 mg/kg) after i.v. administration of OLA and HPPH alone and their combination to Balb/c mice	106
24	Figure 5.16: ¹ H NMR spectra of the Biotin-PEG-PLGA	108
25	Figure 5.17: ¹ H NMR of Linoleic acid-ss-TPP	108
26	Figure 5.18: Mass analysis of Linoleic acid-ss-TPP using LC-MS/MS	109
27	Figure 5.19: QbD based design space; A) Particle size B) Entrapment efficiency C) Desirability, D) Over lay Plot	112
28	Figure 5.20: Physicochemical characterization of HPPH loaded LPHNs: (A) Particle size (B) Zeta Potential (C) TEM image of Biotin@HPPH-LPHNs (D) SEM image of Bt@HPPH-LPHNs	113
29	Figure 5.21: In vitro release study of HPPH, HPPH-LPHNs and Biotin@HPPH-LPHNs in pH 7.4 and pH5.4	115-116
30	Figure 5.22: DSC thermogram of HPPH and its LPHNs (Blank LPHNs, HPPH-LPHNs and Biotin@HPPH-LPHNs)	116
31	Figure 5.23: SOSG analysis of HPPH and its LPHNs	117
32	Figure 5.24: Storage stability study of HPPH loaded LPHNs; A) Particle size; B) PDI	118
33	Figure 5.25: In vitro cytotoxicity Study of HPPH and its LPHNs (pure HPPH, HPPH-LPHNs, and Biotin@HPPH-LPHNs)	119
34	Figure 5.26: In vitro cellular uptake assay of HPPH loaded LPHNs (pure HPPH, HPPH-LPHNs, and Biotin@HPPH-LPHNs)	120
35	Figure 5.27: In-vitro ROS HPPH and its LPHNs (pure HPPH, HPPH-LPHNs, and Biotin@HPPH-LPHNs)	121
36	Figure 5.28: Apoptosis analysis of HPPH and its LPHNs	122
37	Figure 5.29: Hemolysis study of HPPH and its LPHNs	122
38	Figure 5.30: In vivo pharmacokinetic study of HPPH and its LPHNs	123
39	Figure 5.31: In vivo biodistribution study of HPPH loaded LPHNs (A) Time-dependent fluorescence images of tumor-bearing BALB/c mice after i.v. administration; (B) Graph representing the fluorescence intensity for the region of interest; (C) Ex vivo fluorescence images of major organs and tumor excised at 24 h post-injection; (D) Mean fluorescent intensity of fluorescence probe tagged formulations in tumors and organs.	125
40	Figure 5.32: Safety evaluation study of HPPH loaded LPHNs	126
41	Figure 5.33: Morphological Characterization of OLA loaded LPHNs (A) Sample of St/Biotin@OLA-LPHNs; (B) Particle size of non-lyophilized samples, i.e., OLA-LPHNs (red), St@OLA-LPHNs(black), St/Biotin@OLA-LPHNs St/Biotin@OLA-LPHNs(blue); (C) SEM image of St/Biotin@OLA-LPHNs;	128

	(D) Zeta potential of OLA-LPHNs (red), St@OLA-LPHNs (black), St/Biotin@OLA-LPHNs (blue)	
42	Figure 5.34: In vitro release study of free OLA, OLA-LPHNs, St@OLA-LPHNs and Biotin/St@OLA-LPHNs in pH 7.4 and pH 5.4	130
43	Figure 5.35: Physical state characterization of OLA and its LPHNs; (A) DSC thermogram and (B) IR spectra of pure drug (OLA) and OLA loaded LPHNs (Targeted cationic Blank-LPHNs and OLA loaded LPHNs).	131-132
44	Figure 5.36: Storage Stability study of lyophilized OLA loaded LPHNs at two different conditions, i.e., 4 °C/65% RH and 25 °C/60% RH (3 months duration)	133
45	Figure 5.37 In vitro cytotoxic effect of different concentration of free drug (OLA), OLA-LPHNs (St@OLA-LPHNs and St/Biotin@OLA-LPHNs; Control represents media control (green color), non-cationic blank LPHNs (violet color), non-targeted cationic blank LPHNs (blue color) and targeted cationic blank LPHNs	134
46	Figure 5.38: In vitro cellular uptake of the coumarin-6 loaded LPHNs (C6-LPHNs, St@C6-LPHNs and Biotin/St@C6-LPHNs) estimated using confocal microscopy at 525 nm	134
47	Figure 5.39: Apoptotic assay study in 4T1 cells for pure OLA, OLA-LPHNs, St@OLA-LPHNs and Biotin/St@OLA-LPHNs	135
48	Figure 5.40: Blood compatibility study for pure OLA, OLA-LPHNs, St@OLA-LPHNs and Biotin/St@OLA-LPHNs using RBCs cells.	136
49	Figure 5.41: In vivo pharmacokinetic study of pure OLA, OLA-LPHNs and St@OLA-LPHNs and St/Biotin@OLA-LPHNs St/Biotin@OLA-LPHNs.	136
50	Figure 5.42: In vivo biodistribution study of OLA co-loaded LPHNs (A) Time-dependent fluorescence images of tumor-bearing BALB/c mice after i.v. administration; (B) Graph representing the fluorescence intensity for the region of interest; (C) Ex vivo fluorescence images of major organs and tumor excised at 36 h post-injection; (D) Mean fluorescent intensity of fluorescence probe tagged formulations in tumors and organs	138
51	Figure 5.43: Safety evaluation studies of various organs (i.e., heart, kidney, liver, lungs, spleen) using H&E staining	139
52	Figure 5.44: Morphological evaluation of HPPH and OLA co-loaded LPHNs; (A) SEM of Biotin-ss-TPP@HPPH/OLA-LPHNs; (B) Particle size of Biotin-ss-TPP@HPPH/OLA-LPHNs; (C) Zeta Potential of Biotin-ss-TPP@HPPH/OLA-LPHNs; (D) Sample for Biotin-ss-TPP@HPPH/OLA-LPHNs	140
53	Figure 5.45: In vitro release of HPPH and OLA co-loaded LPHNs at 7.4 and pH 5.4	142-143
54	Figure 5.46: In vitro SOSG measurement of HPPH and OLA co-loaded LPHNs	144
55	Figure 5.47: Storage stability study of HPPH and OLA co-loaded LPHNs	144-145
56	Figure 5.48: Dose-response effect and cytotoxicity study of HPPH and OLA co-loaded LPHNs;(A) cytotoxicity of HPPH and OLA (B)Combination index for	146

	HPPH and OLA solution (C) Combination index for Biotin@HPPH/OLA-LPHNs(D) Combination index for Biotin-ss-TPP@ HPPH/OLA-LPHNs	
57	Figure 5.49: In vitro cellular and mitochondrial uptake analysis of HPPH and OLA co-loaded LPHNs (HPPH, OLA, HPPH-OLA, Biotin@HPPH/OLA-LPHNs and Biotin-ss-TPP@HPPH/OLA-LPHNs)	147
58	Figure 5.50: Apoptosis Analysis of HPPH and OLA co-loaded LPHNs (HPPH-OLA, Biotin@HPPH/OLA-LPHNs and Biotin-ss-TPP@HPPH/OLA-LPHNs)	148
59	Figure 5.51: In-vitro ROS of HPPH and OLA co-loaded LPHNs (HPPH-OLA, Biotin@HPPH/OLA-LPHNs and Biotin-ss-TPP@HPPH/OLA-LPHNs)	149
60	Figure 5.52: Hemolysis study of HPPH and OLA co-loaded LPHNs; Data represent mean \pm SD. **** p value < 0.0001 and *** p value < 0.001 compared with the control group	149
61	Figure 5.53: In vivo pharmacokinetic study of HPPH and OLA co-loaded LPHNs (HPPH-OLA, Biotin@HPPH/OLA-LPHNs and Biotin-ss-TPP@HPPH/OLA-LPHNs)	150
62	Figure 5.54: Biodistribution study of HPPH and OLA co-loaded LPHNs; (A) Time-dependent fluorescence images of tumor-bearing BALB/c mice after i.v. administration; (B) Graph representing the fluorescence intensity for the region of interest; (C) Ex vivo fluorescence images of major organs and tumor excised at 24 h post-injection; (D) Mean fluorescent intensity of fluorescence probe tagged formulations in tumors and organs.	151-152
63	Figure 5.55: In-vivo efficacy study of HPPH and OLA co-loaded LPHNs	153
64	Figure 5.56: Luminescence intensity of HPPH, OLA, HPPH-OLA, Biotin@HPPH/OLA-LPHNs and Biotin-ss-TPP@HPPH/OLA-LPHNs	154
65	Figure 5.57: In vivo ROS of HPPH and OLA co-loaded LPHNs; Data represent mean \pm SD. **** p value < 0.0001 and *** p value < 0.001 compared with the control group and ** p value < 0.05 compared with the control group	155
66	Figure 5.58: Tunnel assay of HPPH and OLA co-loaded LPHNs; Data represent mean \pm SD. **** p value < 0.0001 compared with the control group	156
67	Figure 5.59: Histochemical analysis of HPPH and OLA co-loaded LPHNs (HPPH, OLA, HPPH-OLA, Biotin@HPPH/OLA-LPHNs and Biotin-ss-TPP@HPPH/OLA-LPHNs) using HE staining	157

Abstract

Background

Triple-negative breast cancer (TNBC) is an aggressive type of heterogeneous breast cancer which is known for the absence of estrogen, progesterone, and human epidermal growth factor 2 receptors (HER2). TNBC has the tendency of early relapse and metastatic spreading toward the lungs, liver, and central nervous system, as well as a poor prognosis. The risk of TNBC is higher in certain ethnic groups, such as Latin, African, and African-American women, as well as women with breast cancer 1 (BRCA1) gene mutations. As per the American cancer society, TNBC accounts for about 10-15% of all breast cancer cases with its most prevalence in young women whereas in Indian population, it comprises approx. 25-30% of total cases. According to classification based on molecular and morphological characterization invasive ductal carcinomas account for around 90% of TNBC cases, while lobular, apocrine, adenoid cystic, and metaplastic carcinomas account for the rest. Despite sharing the triple negative phenotype, the prognosis of different types of breast cancer is distinct. Further, based on gene expression profile, TNBC is classified into six subtypes i.e., Basal-like 1 & 2, Immunomodulatory, Luminal androgen receptor, Mesenchymal, and Mesenchymal stem-like. TNBC's diversity in terms of gene expression and the variety of genetic events usually results in distinct responses to therapy which further complicates its therapeutic management.

In recent past, in order to identify novel molecular target, research in the area of finding molecular pathways and identifying biomarkers have been done substantially. However, despite significant amount of research, till date ideal treatment approach has not been identified. The selection for TNBC treatment depends on the origin of cancer and its development, stage of progression as well as its molecular site. In the late twentieth century, for the management of TNBC, various conventional therapeutic approaches, including surgery, adjuvant chemotherapy and radiation therapy have been tried. The current treatment approach for TNBC is either individual use of selective anticancer drugs or along with surgery or radiotherapy. The chemotherapeutic approach involves the use of anticancer agents belonging to classes such as anthracyclines, platinum compounds, and taxanes. Although, various conventional therapeutic approaches are already established, but still there is an unmet need pertaining to the treatment as these conventional therapy approaches have several limitations, including non-selective targeting, resistance due to efflux transporters, and severe systemic toxicities such as mucositis, thrombocytopenia, alopecia etc. Since then, newer targeted therapy

approaches have been researched extensively, which includes, targeting DNA repair pathways, cell cycle retardation, inhibiting poly ADP-ribose polymerase (PARP) enzyme, anti-angiogenesis therapy, immunotherapy. Further, photodynamic therapy (PDT) and radiation therapy also provides a practicable approach to boost the therapeutic effectiveness.

Among these therapies, in the recent past, PDT is getting much attention as it is a localized and non-invasive treatment method that has undergone exploration for potential benefits in cancer therapy. This therapy is utilizing a photosensitizer and exposure to a particular wavelength of light that can generate reactive oxygen species (ROS) through light activation. The photosensitizer i.e., 2-[1-hexyloxyethyl]-2-devinyl pyropheophorbide-a (HPPH) is a second-generation, lipophilic, chlorin-based small molecule; is initially injected in the bloodstream, which is then absorbed and further deposited into the cancer cells. This photosensitizer accumulates in these cells, and on exposure to a particular wavelength of light, generate ROS which can eventually kill cancer cell. HPPH is currently under phase I/II clinical trials for different cancer types including esophageal, neck, head cancer, and breast cancer. However, HPPH has certain limitations which includes aggregation in physiological condition, quick photobleaching, low solubility, poor pharmacokinetics, limited cellular uptake into the target cells, and phototoxic side effects including DNA damage to the normal cell. Moreover, PDT is impeded by the action of a nuclear enzyme i.e., PARP which is involved in the repair of DNA by binding to specific location of single-strand damage on the DNA molecule, and in turn, facilitating the repair process. These PARP family enzymes are involved in the process of poly-ADP-ribosylation (PARylation), whereby they transfer ADP-ribose units from NAD⁺ to proteins that serve as substrates. This process facilitates the repair of DNA single-strand breaks (SSBR) via base excision repair (BER). Along with that, the clinical challenges i.e., development of resistance to PDT might be facilitated if the tumour tissue is not rapidly eradicated during the first PDT sessions. This poses a challenge to the effectiveness of the treatment, mostly due to the activation of cellular redox defenses and repair mechanisms. The precise mechanism behind PDT resistance remains elusive; nevertheless, in vitro experiments have shown that resistance may arise through activation of the PARP damage-repair signaling pathway. Hence, the inhibition of PARP may possibly augment the PDT response. Therefore, the co-administration of a PARP inhibitor (PARPi) along with PDT may exert a synergistic or additive role in the killing of tumour cells. Amongst all the PARPi, Olaparib (OLA) is one of the US-FDA approved drug for breast cancer with or without a BRCA1/2 mutation which acts by inhibiting DNA synthesis and ROS induced apoptosis. It is important to mention that OLA

have not only the capacity to induce the inactivation of PARP but also to effectively sequester PARP at the specific location of DNA damage, ultimately culminating in cellular death. While, OLA might possibly be encouraging the efficiency of PDT but it has certain major limitations in effective clinical translation. These includes less aqueous solubility, stability issue in biological system along with the poor pharmacokinetic profile (low bioavailability, low biological half-life, etc.). Further, these overall drawbacks of both HPPH and OLA can be circumvented by the employment of advanced targeted drug delivery system for the effective management of TNBC.

In the field of advanced drug delivery, nanomedicines are one of the finest tools that has emerged in the past couple of decades, having the potential to fight against severe, difficult-to-manage diseases like cancer, particularly due to its advantage of enhanced permeability and retention effect (EPR). Researchers are considering the option of nanomedicine for combinational therapy or as a multidrug delivery system in case of cancer so as to employ several advantages such as improving the pharmacokinetic profile, decreasing the systemic toxicity related to free drug, and having a synergistic pharmacological effect when two different class of drug employed and co-administered. Considering all the nanocarrier system, a lipid-polymer hybrid nano-carriers (LPHNs) is a promising delivery approach for the hydrophobic therapeutic molecules. These hybrid systems deliver combinational benefits of lipids as well as polymers such as good loading capacity, better release profile, biomimetic system, and superior therapeutics. Hence, it provides an efficient tool in the management of TNBC. Moreover, due to the absence of surface receptors i.e., ER, PR and HER2 protein in TNBC, makes it difficult for conventional LPHNs to target the tumor cells. These limitations can be effectively addressed by the surface modification with certain chemical-based ligand or molecular targeted biomarker such as Biotin, Trans-Activator of Transcription protein, Folic acid, and Triphenylphosphine (TPP).

Therefore, in the present research work, we have designed a LPHNs system to deliver HPPH and OLA for the therapeutic management of TNBC. For its fabrication, we have used amphiphilic co-polymer (PEG-PLGA) and Lipid (SPC100, DC₈₉PC and linoleic acid), Stearylamine and Polyvinyl alcohol (PVA). Besides, to improve the targetability of LPHNs, multi-functional surface modification was carried out using biotin, disulfide bond and TPP. These ligands can provide better response as it can directly induce intracellular ROS production at the mitochondrial site, leading to cancer cell death. Finally, the present research work was

carried out in adherence to the following major objectives. (i) *To investigate the therapeutic potential and pharmacokinetic studies of HPPH and Olaparib-alone and in combination using in vitro and in vivo studies;* (ii) *To improve the efficacy, circumvent pharmacokinetic limitations of HPPH and Olaparib by developing tumor targeted lipid-polymer hybrid nanoparticles;* (iii) *To develop and characterize HPPH and Olaparib co-loaded tumor targeted lipid-polymer hybrid nanoparticle and evaluate its therapeutic efficacy, pharmacokinetic and biodistribution advantages in TNBC condition.*

Methodology and results

In-vitro and in-vivo experiments were carried out to explore the therapeutic potentials of HPPH and Olaparib alone & in combination using 4T1 cell line and TNBC bearing mice model. Primarily, the cytotoxicity study was conducted using MTT assay on the 4T1 cell line. The IC₅₀ of HPPH and OLA was found to be ~10 μM and ~ 60 μM and no significant morphological changes were observed in the 4T1 cell line. Moreover, co-administration of HPPH and OLA showed the combination index value below 0.9 (46.27% of cell viability at the dose 4/24 μM of HPPH/OLA), indicating the possible synergistic effect. Based on the cytotoxicity result, we have proceeded to in vivo experiments. The Balb/c mice were injected with TNBC cell line (luc-4T1 cell line) with a cell count of 2x10⁶ in PBS exactly at mammary pad through a disposable syringe. The developed TNBC orthotopic murine models was confirmed by bioimaging system (IVIS® Lumina III, PerkinElmer, USA). Afterward, HPPH (Dose 5mg/kg.bw), OLA (Dose 30mg/kg.bw) and in combination of HPPH with OLA were administered in TNBC bearing Balb/c mice. A substantial enhancement (p<0.001) in the tumor suppression and enhanced apoptosis cell death pathway was observed when compared to diseased animal. Moreover, to check the pharmacokinetic profile and interaction between HPPH and OLA, pharmacokinetic studies of HPPH, OLA and in combination of HPPH and OLA was performed in Balb/C mice. The pharmacokinetic results confirmed short plasma half-life (t_{1/2}) i.e., 5.74±3.35 h for OLA, while plasma half-life of HPPH was found to be 15 h. The result also showed a high-rate of elimination and high clearance in case of OLA. Further, the pharmacokinetic data for combination of HPPH and OLA (HPPH-OLA) suggested the HPPH-OLA did not find any significant pharmacokinetic interaction after administration in animal. Therefore, to circumvent the problems associated with poor pharmacokinetic and pharmacodynamic of HPPH and OLA, a site specific-LPHNs were fabricated and biologically evaluated using Balb/c mice model.

Firstly, Biotin-PEG-PLGA was synthesized using amide coupling and was confirmed by ¹H-

NMR. HPPH loaded lipid polymer hybrid nanoparticles (LPHNs) were formulated using a single emulsification followed by solvent evaporation method. For the preparation of HPPH loaded LPHNs, the excipients such as DC₈₉PC, PEG-PLGA/Biotin-PEG-PLGA and linoleic acid was used for the organic phase, while PVA solution was used as aqueous phase. Further, to optimize the LPHNs, the effect of independent parameters (i.e., concentration of PVA solution and amount of DC₈₉PC) on response parameters (i.e., Particle Size and % Entrapment efficiency) were studied using the Central Composite Design (CCD) based response surface methodology via DOE approach. The comparative analysis of physiochemical properties such as average Particle size (PS), Polydispersity index (PDI) and zeta potential of the optimized LPHNs with fresh and after freeze drying were studied. HPPH-LPHNs showed an average PS of 152 nm with a PDI value of 0.217 and -0.2 mV Zeta potential. Due to incorporation of Biotin-PEG-PLGA instead of non-surface engineered polymer i.e., PEG-PLGA, the avg. PS was slightly increased to 156 nm with the PDI of 0.208. Further, this surface engineered polymer also showed minor change in surface charge from -0.2 mV to 1.16mV. Then after, the lyophilization of LPHNs was performed using different cryoprotectant to improve its storage stability. The lyophilized LPHNs with 10% PEG 4000 showed good result as all the physiochemical parameters were nearly unchanged compared to fresh LPHNs. The morphological evaluation of LPHNs was carried out using SEM analysis. The data revealed that the developed LPHNs were spherical with uniform distribution. The % Entrapment efficiency(%EE) of HPPH-LPHNs was found to be approx. 67.34.%, whereas Biotin@HPPH-LPHNs showed approx. 66.23 % which indicates substantial cargo potential of the designed LPHNs systems. The release profile of HPPH encapsulated LPHNs (HPPH-LPHNs and Biotin@HPPH-LPHNs) and pure HPPH was performed using dialysis bag method. The release profile of pure HPPH described complete drug release from the dialysis bag within 12 h. Whereas HPPH encapsulated LPHNs followed a biphasic release pattern i.e., 20% CDR from both the LPHNs (HPPH-LPHNs and Biotin@HPPH-LPHNs) in first 4 h and remaining 40% was released till 72 h. This indicates that the designed LPHNs can provide initial burst release followed by a sustained release system. The DSC thermogram of free HPPH showed melting peak at 205°C. In case of LPHNs, the melting point peak was not observed at 205°C that indicates encapsulation of HPPH in nanocarrier system. The stability of lyophilized LPHNs was characterized with two different storage condition i.e., 4 °C/65% RH and 25 °C/60% RH for 90 days to understand the shelf life of the LPHNs. The results indicated that LPHNs was stable at both the condition as no significant changes were observed on avg. PS, PDI and %EE in comparison to fresh nanocarriers. The singlet-oxygen-generating potential of HPPH and its

LPHNs was detected by the Singlet Oxygen Sensor Green (SOSG) assay at the excitation wavelength of 494 nm. Notably, the fluorescence intensity of HPPH was significantly reduced due to encapsulation of HPPH in nanocarrier, the $^1\text{O}_2$ generation ability of both nanocarrier (HPPH-LPHNs and Biotin@HPPH-LPHNs) was ~60 % relative to that of pure HPPH. Although, singlet oxygen generation is the key for ROS production in cancer cell. In spite of that, production of ROS also depends upon cellular uptake of the HPPH. Therefore, it can be compensated. The in vitro cytotoxicity was studied using MTT assay in 4T1 breast cancer cells with following treatment of free HPPH, HPPH-LPHNs, Biotin@HPPH-LPHNs and Blank-LPHNs. The IC₅₀ values of Biotin@HPPH-LPHNs, HPPH-LPHNs and pure HPPH was found to be 3.9 μM , 8.8 μM and 10 μM respectively. On the other hand, the developed blank LPHNs showed no cytotoxicity. The cellular uptake of HPPH loaded LPHNs was performed by using confocal microscopy. The fluorescence intensity was analyzed for 4h and 8h. The intensity of Biotin@HPPH-LPHNs was stronger than HPPH-LPHNs at both the time interval. The intracellular ROS generation was studied using a fluorescence probe, 2',7'-dichlorofluorescein diacetate (DCFH-DA). Notably, the intracellular ROS level of Biotin@HPPH-LPHNs was higher than that of HPPH-LPHNs and pure HPPH which is evident by higher color intensity of DCFH-DA in case of Biotin@HPPH-LPHNs. The cell apoptosis of pure HPPH and its LPHNs was studied using an Annexin V-FITC apoptosis detection kit. The apoptotic ratio of pure HPPH, HPPH-LPHNs were 4% and 8%, while Biotin@HPPH-LPHNs exhibited 52% apoptotic ratio which is highest apoptotic ratio than that of other groups. Hence, the above-mentioned cellular results provide substantial evidence related to enhanced invitro tumour mediated activity via apoptosis. Hemolysis studies showed that Biotin@HPPH-LPHNs has less hemolytic index in comparison to HPPH-LPHNs and pure HPPH. This indicates Biotin@HPPH-LPHNs is highly biocompatible for animal study. The in-vivo pharmacokinetics of HPPH encapsulated LPHNs and pure HPPH were carried out at dose of 5mg/kg.bw in Balb/c mice. Further, the comparative pharmacokinetic parameter of pure HPPH and its LPHNs were studied via non-compartmental analysis (NCA) using WinNonlin software version 6.3(Certara, USA). The resultant LPHNs showed improved pharmacokinetics of HPPH as compared to free drug (HPPH). The area under curve was found to be 116647.50 \pm 22067.11 h*ng/mL and 123354.60 \pm 26533.07 h*ng/mL for HPPH-LPHNs and Biotin@HPPH-LPHNs respectively which was higher in comparison to pure HPPH i.e., 72575.11 \pm 9169.30 h*ng/mL. In addition, the plasma half-life, $t_{1/2}$ (h) of both LPHNs (Biotin@HPPH-LPHNs and HPPH-LPHNs) was approx. 30h which is 2-fold time higher when compared to pure HPPH solution (15.15h). Moreover, to evaluate the biodistribution of LPHNs, dye loaded LPHNs (Di-LPHNs

and Biotin@DiI-LPHNs) was prepared and administered to tumor bearing Balb/c mice for both in-vivo and ex-vivo fluorescence imaging study. The results showed greater tumor accumulation with Biotin@DiI-LPHNs for a longer period in comparison to DiI-LPHNs which is 1.2-fold times. A safety study was carried out in the BALB/c mice as per OECD guidelines to evaluate the toxicity of LPHNs. No toxicity was observed in pure HPPH and HPPH loaded LPHNs, indicating that fabricated LPHNs for HPPH is biocompatible.

In the same way, the LPHNs for OLA (i.e., OLA-LPHNs, St@OLA-LPHNs and Biotin/St@OLA-LPHNs) was fabricated using emulsification followed by solvent evaporation method. The OLA loaded LPHNs (both lyophilized and non-lyophilized LPHNs) were characterized with respect to PS, PDI, zeta potential, shape, %EE and % DL. All the OLA encapsulated LPHNs showed the particles size less than 150 nm with narrow PDI (~ 0.21). The zeta potential for the OLA-LPHNs were found to be ~ 0.4 mV for both lyophilized and non-lyophilized samples, while zeta potential of St@OLA-LPHNs and St/Biotin@OLA-LPHNs was much higher, i.e., ~ 28 mV. The % EE was found in the range of 56-67% with % DL value of ~9% for all OLA loaded LPHNs. Additionally, SEM image showed that OLA loaded LPHNs were nano-metric in size with spherical shape which matches with result of DLS analysis. It has also been observed that LPHNs were less aggregated with enhanced stability. The release study was performed using dialysis bag method in two different pH conditions, that is 5.4 and 7.4. The OLA encapsulated LPHNs showed approx. 40% drug release within first 4 h, while remaining 60% of release was completed in 48 h. In case of pure OLA, complete release was attained within 2 h. Moreover, the IR spectra of the pure drug, targeted cationic blank LPHNs, OLA-LPHNs, St@OLA-LPHNs and St/Biotin@OLA-LPHNs were studied. The major characteristic peak in IR spectra for pure drug was observed at 3186.12 cm^{-1} due to N-H stretching, 1631 cm^{-1} due to C=O aromatic stretching and 1407 cm^{-1} due to C-H bending. While drug loaded nanoparticles, the peak intensity was found to be low when compared to the pure drug. Further, the DSC analysis was also studied for pure OLA, targeted cationic blank LPHNs, OLA-LPHNs, St@OLA-LPHNs and St/Biotin@OLA-LPHNs. A sharp melting point peak at 210.63 °C was observed for OLA whereas, no melting point peak in OLA loaded LPHNs was observed at 210.63 °C. Both DSC and IR results confirmed that OLA is completely encapsulated in the LPHNs. The stability of lyophilized nanocarrier was characterized for 3 months with two different storage conditions i.e., 4 °C/65% RH and 25 °C/60% RH. From their results, it was observed that the stability samples with both storage condition showed no significant changes in PDI, PS and %EE as compared to the fresh batch. The *in vitro* cytotoxicity was studied using MTT assay in 4T1 breast cancer cells, following

treatment of OLA, OLA-LPHNs, St@OLA-LPHNs, St/Biotin@OLA-LPHNs and blank nanoparticle. Based on the % cell viability data obtained after 48 h. period, IC₅₀ value was calculated and it was 7.3 μ M, 26.76 μ M, 29.69 μ M and 60 μ M for St/Biotin@OLA-LPHNs, St@OLA-LPHNs, OLA-LPHNs, and OLA, respectively. Further, the cellular uptake of LPHNs was performed in 4T1 cell line using coumarin-6(C6) which is commonly employed for uptake studies of nanoparticle. The fluorescence intensity of C6 loaded LPHNs (C6-LPHNs, St@C6-LPHNs and St/Biotin@C6-LPHNs) was estimated using confocal microscopy at 525 nm. The results suggested that Biotin/St@OLA-LPHNs revealed more cellular uptake compared to pure OLA, C6/OLA-LPHNs, and St@C6/OLA-LPHNs as it showed more fluorescence intensity. Apoptosis assay was also performed in 4T1 cell line using flow cytometry. The cell line was treated with pure OLA and OLA loaded LPHNs based on the dose calculated using IC₅₀ value. The apoptotic cell death in OLA solution was 9% whereas resulting LPHNs i.e., OLA-LPHNs, St@OLA-LPHNs and Biotin@OLA-LPHNs unveiled 13.83%, 20.7 % and 72.1% respectively. Hemolysis of pure OLA and its LPHNs was performed using RBCs of mice. The pure OLA and its LPHNs (OLA-LPHNs, St@OLA-LPHNs and Biotin@OLA-LPHNs) showed hemolytic index of approx. 1.5% which indicates that nanocarriers are safe and biocompatible for in-vivo evaluation. The pharmacokinetics study was carried out in Balb/C mice at 30mg/kg.bw via i.v. route of administration . The AUC was found to be greater in St/Biotin@OLA-LPHNs (i.e., 14824.27 \pm 2094.51 h*ng/ml) in comparison of free drug (5149.59 \pm 1050.38 h.*ng/ml). Other pharmacokinetic parameters i.e., elimination rate constant (Ke) of LPHNs was significantly lower than that of free OLA (0.18 \pm 0.16 h⁻¹). Furthermore, a short biological half-life was observed and the value was found to be 5.74 \pm 0.3.35 h in case of pure OLA whereas, for OLA-LPHNs, St@OLA-LPHNs and St/Biotin@OLA-LPHNs, values were 12.85 \pm 4.8, 15.46 \pm 0.12, 17.50 \pm 1.42 h. respectively. Moreover, to evaluate the biodistribution of LPHNs, DiI loaded LPHNs (DiI-LPHNs, Biotin@DiI-LPHNs and St/Biotin@DiI-LPHNs) was prepared and administered to tumor bearing Balb/c mice for both in-vivo and ex-vivo fluorescence imaging study. The results showed greater tumor accumulation with St/Biotin@DiI-LPHNs for a longer period in comparison to DiI-LPHNs which is 3-fold times. The safety evaluation for the developed OLA loaded LPHNs were carried out in the BALB/c mice. No toxicity was observed in the treated group when compared to control group, indicating OLA loaded LPHNs to be biocompatible and safe.

In addition, co-encapsulated HPPH and OLA in LPHNs were also formulated by single emulsification method using the stearylamine, Biotin-PEG-PLGA, linoleic acid-ss-TTP/Linoleic acid and PVA. Further, the designed nanocarrier was subjected to physiochemical

characterization. It was observed that the PS was found in between the range of 100-200 nm which is in line with SEM analysis and further, the FE-SEM data representing the spherical morphology of the particle with uniform size distribution across nanocarrier systems. PDI and Zeta potential was 0.201 ± 0.5 and 27.1 ± 0.2 mV for Biotin@HPPH/OLA-LPHNs and 0.203 ± 0.1 and 26.3 ± 0.3 mV for Biotin-ss-TPP@HPPH/OLA-LPHNs respectively, indicating a narrow distribution without particle aggregation. The release profile of the free drug and LPHNs was performed using dialysis bag method. The drug loaded nanoparticle exhibited a burst release followed by controlled release pattern which could provide a better residence time of drug in biological system. Moreover, the SOSG study indicates Biotin-ss-TPP@HPPH/OLA-LPHNs showed slightly less fluorescence intensity when compared to pure HPPH i.e., ~3% less fluorescence intensity than pure HPPH. Despite the singlet generation ability of Biotin-ss-TPP@HPPH/OLA-LPHNs, production of ROS also depends upon its intracellular uptake. Thus, it can be compensated. The cytotoxicity of HPPH and Olaparib co-encapsulated LPHNs were studied in 4T1 cell line. The result suggested that Biotin-ss-TPP@HPPH/OLA-LPHNs showed 14.47% cell death at combination dose of 4 μ M and 24 μ M for HPPH and OLA respectively, while Biotin @HPPH-OLA-LPHNs and pure combination of HPPH and Olaparib showed 28.80 % and 46.27% cell death respectively. Blank LPHNs did not show any significant change in the cell viability at concentration of 100 μ g/ml. The cellular uptake of LPHNs was performed by using a hydrophobic dye i.e., coumarin-6. The fluorescence intensity of Biotin-ss-TPP@HPPH/OLA-LPHNs was stronger than Biotin@HPPH/OLA-LPHNs. Further, to evaluate mitochondrial penetration of nanocarrier, Mito-tracker (Red) was also used. The Mito tracker fluorescence intensity of Biotin-ss-TPP@HPPH/OLA-LPHNs was stronger when compared to Biotin@HPPH/OLA-LPHNs. The result suggests surface modification of LPHNs with TPP and disulfide bond may enhance the drug accumulation in mitochondrial site. The intracellular ROS generation was studied using a fluorescence probe, 2',7'-dichlorofluorescein diacetate (DCFH-DA). Notably. the intracellular ROS level of Biotin-ss-TPP@HPPH/OLA-LPHNs was higher than Biotin@HPPH/OLA-LPHNs and pure HPPH/OLA as it shows the higher color intensity of DCFH-DA in case of Biotin-ss-TPP@HPPH/OLA-LPHNs. The pure HPPH-OLA and, Biotin@HPPH/OLA-LPHNs were 16.15% and 19% of apoptotic ratio, while Biotin-ss-TPP@HPPH/OLA-LPHNs exhibited 37.74% of apoptotic ratio. Moreover, the resultant HPPH and OLA encapsulated LPHNs showed improved pharmacokinetics as compared to free drug. The biodistribution of Biotin@DiI-LPHNs and Biotin-ss-TPP@DiI-LPHNs was carried out in tumor bearing Balb/c mice. The results showed a greater tumor accumulation with Biotin-ss-TPP@DiI-LPHNs in

comparison to Biotin@DiI-LPHNs which is 1.8-fold times higher. The in-vivo efficacy was assessed in Luciferin tagged 4T1 tumor bearing animal using an in vivo imaging technique with the IVIS® Lumina III, PerkinElmer, USA. On days 1,3, 6, and 10 of the treatment periods, all the animals in each group (HPPH, OLA, HPPH/OLA, Biotin@HPPH/OLA-LPHNs and Biotin-ss-TPP@HPPH/OLA-LPHNs) were examined for tumor growth. Notably, the result suggested Biotin-ss-TPP@HPPH/OLA-LPHNs treated animal showed significant tumor suppression when compared to combination of HPPH and OLA and Biotin@HPPH/OLA-LPHNs. Further, Biotin-ss-TPP@HPPH-OLA LPHNs treated animal group showed a higher intensity of ROS generation compared to other group i.e., HPPH, OLA, HPPH-OLA and Biotin@HPPH/OLA-LPHNs. It might be due to better penetration of drug loaded nanoparticle in mitochondrial site of tumour tissue. The tunnel assay also suggested higher apoptotic response of Biotin-ss-TPP@ HPPH/OLA-LPHNs (exhibits 2.1-fold time apoptotic ratio) in comparison to combination of pure HPPH and OLA. Also, histochemical analysis was performed for all the above-mentioned group using H&E staining. No toxicity was observed in vital organ, which may be due to effective drug encapsulation into the nanocarriers system. In conclusion, the fabricated Biotin-ss-TPP@HPPH/OLA-LPHNs has shown stronger anti-tumor activity and a greater clinical therapeutic potential for the management of TNBC.

Summary and conclusion

- Our research work confirmed that both HPPH and OLA are effective against TNBC. Moreover, their combination has also confirmed synergistic response against TNBC. Therefore, it could pave the way for facilitating further clinical translation avenue.
- To the best of our knowledge, for the first time, a surface modified lipid-polymer hybrid nanocarrier system for an effective targeted delivery of HPPH and OLA was fabricated. Also, developed nanocarrier system for HPPH and OLA-alone and its combination, significantly circumvented the pharmacokinetic problem including short half-life, high elimination rate, and biological instability.
- The bio-distribution of surface modified LPHNs of co-encapsulated HPPH and Olaparib has been carried out in 4T1 mouse model which showed enhanced drug accumulation in tumor site i.e., Biotin-ss-TPP@HPPH/OLA-LPHNs showed approx. 4-fold times better penetration when compared to Biotin@HPPH/OLA-LPHNs. Thus, it is evident that Biotin-ss-TPP@HPPH/OLA-LPHNs delivered both HPPH and OLA selectively to TNBC tissue that could minimize the toxicity.
- Moreover, Biotin-ss-TPP@HPPH/OLA-LPHNs showed significant tumor suppression

activity when compared with free drug and non-targeted nanocarrier system. There was no toxicity observed with these two drugs loaded LPHNs.

- Therefore, succinctly, our work demonstrated that this surface modified LPHNs based therapeutic strategies could be utilized for HPPH and Olaparib with improved target specific biodistribution leading to enhanced anti-tumor efficacy against TNBC along with reduced toxicity.



INTRODUCTION



1. Introduction

1.1. Background

Cancer is the major cause of mortality across the world, resulted due to the mutation of oncogene and inactivation of tumor suppressive gene. On a global scale, 7.6 million deaths are caused by cancer annually, representing 13% of all deaths worldwide. According to WHO, it is arising due to various factors including ageing population, genetic disposition [1,2]. Among all types of cancer, breast cancer is the most prevalent cause of death and has high mortality and morbidity rates. It can affect both men and women, but it is significantly more common in women [3,4]. In 2020, it was reported that about 252,710 new cases have been diagnosed as breast cancer among all the women, and 42,170 new cases will be expected that may increase the risk of death due to breast cancer [5].

On the basis of histological and molecular characteristics, clinically the breast cancers is classified into five subtypes including, Triple negative breast cancer (TNBC), Luminal A, Luminal B, and HER2-enriched (HER2+), and normal like and basal-like. Among all type of breast cancer, TNBC may account 15% which is an aggressive cancer and don't have ER, PR and HER expression. Further, TNBC is characterized by elevation in mitotic count, stromal lymphocyte response and high ratio of nucleus: cytoplasm. Moreover, according to current molecular and morphological studies, invasive ductal carcinomas account for around 90% of TNBC cases, while lobular, apocrine, adenoid cystic, and metaplastic carcinomas account for the rest. TNBC is commonly diagnosed in young women and the risk of TNBC is higher in certain ethnic groups, such as Latin, African, and African-American women, as well as women with breast cancer 1 (*BRCA1*) gene mutations. Additionally, molecular heterogeneity, BRCA mutation, early relapse and metastatic spreading toward the lungs, liver, and central nervous system may contribute to therapeutic failure, poor prognosis and its management[6,7]. Overall, TNBC is an aggressive form of cancer which is having very poor survival rates along with high risk of chemotherapeutic resistance.

Further, in development of therapeutic intervention for TNBC, a critical diagnosis is needed. Although the diagnosis is based on the imaging technique including, ultrasound mammography, immuno-histochemistry, palpation, magnetic resonance imaging (MRI) and ultrasonography. But, the absence of cancer biomarkers (ER, PR and HER), faces the clinical challenge for early diagnosis. Therefore, the discovery of specific biomarkers should be explored for TNBC which would surely enhance the diagnosis process, as well as provide aid for the development of targeted therapeutics [8,9].

Furthermore, the selection of the treatment for TNBC depends on its cell origin, development and stage of progression including mutation (spreading to lymph node)[10,11]. The absence of a particular molecular target is a vital clinical challenge for the management of TNBC patients. In the late twentieth century, for the management of TNBC, various conventional therapeutic approaches, including surgery, adjuvant chemotherapy and radiation therapy have been used to manage it. The current treatment approach for TNBC is either individual use of selective anticancer drugs or along with surgery or radiotherapy[12]. The chemotherapeutic approach involves the use of anticancer agents belonging to different classes of drug such as anthracyclines, platinum compounds, and taxanes derivative and immunomodulating agent[13]. However, the clinical therapeutic approaches have several limitations, including non-selective targeting, resistance due to efflux transporters, and severe systemic toxicities such as mucositis, thrombocytopenia and alopecia[13]. Therefore, still there is an unmet need to explore newer therapeutic approaches that may pave the way for effective clinical management of TNBC. Moreover, the pathophysiological process and mechanism involved in TNBC are different in comparison to other breast cancer and complexes that may pose a greater risk for the chemotherapeutic failure and development of resistance during its treatment[14]. Presently, researchers are focusing to understand and to explore the molecular pathway that are involved in the pathogenesis and progression of TNBC.

1.2. Pathophysiology and mechanism involved in TNBC

Although, the pathogenesis is not so far clear but numerous risk factors including genetic predisposition and environmental toxins have been identified that are involved in the development of cancer. Exposure of exogenous and endogenous hormone secretion, genetic mutations and ionization radiation in DNA repair genes are also well-known factors that contribute to breast cancer development. Further, due to the absence of the ER, PR and HER2-gene expression, TNBC becomes more aggressive[15][16]. Also, the frequent mutation of Tp53 and BRCA gene have been confirmed that may increase the levels of tumor-infiltrating lymphocytes (TILs) and inactivation of apoptosis cell death pathway that eventually leads to development of TNBC[17]. Furthermore, recent study stated that TNBC also occurs due to the overexpression of EGFR, thereby stimulating the high proliferation through AKT and MAPK signaling, resulting in increased rates of DNA aberrations, and possibly defective DNA repair pathways[18]. Although, the mechanism involved in TNBC is not so far very clear but the possible pathological alteration in TNBC progression has been shown in Figure 1.1. which

emphasizes the various pathological mechanism that have a crucial role in TNBC including BRCA1/2(breast cancer type 1and 2gene) gene mutation.

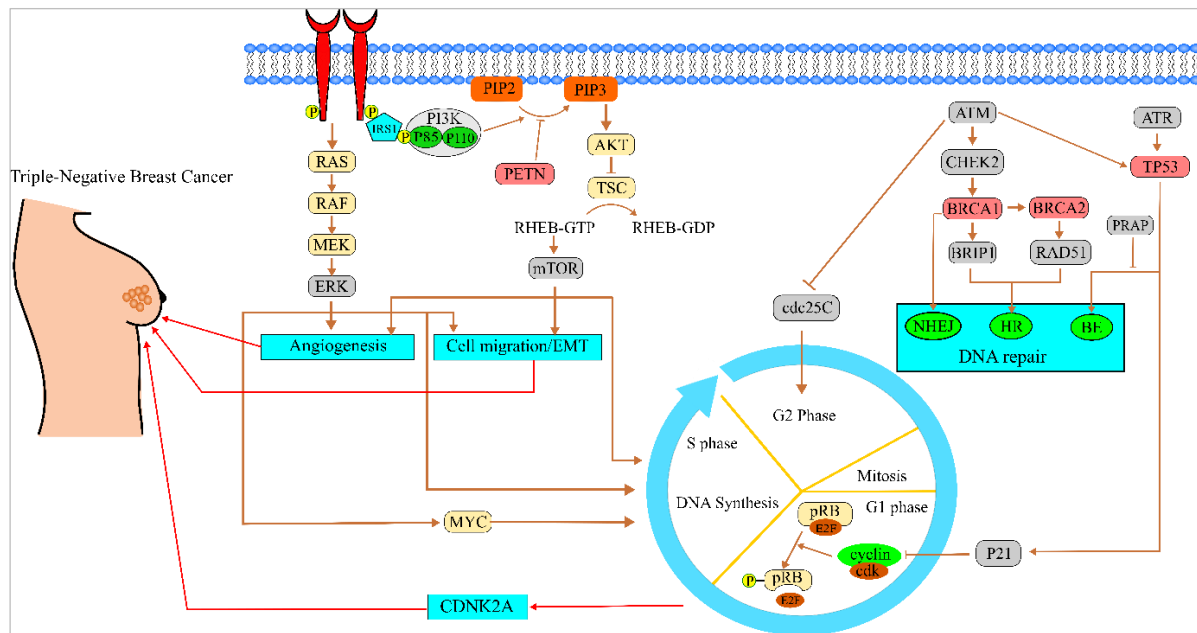


Figure 1.1: Pathogenesis of triple negative breast cancer ;Adopted from ref.[19]

1.2.1. Epidermal Growth Factor Receptor (EGFR) and TNBC

The Epidermal Growth Factor Receptor (EGFR) belongs to the category of tyrosine kinase receptors. Numerous studies indicate elevated expression of EGFR in various mutated and aberrant epithelial cancers, such as lung and breast cancer. Specifically, within the different subtypes of breast cancer, EGFR is frequently present in aggressive inflammatory and triple-negative breast cancer, constituting approximately 89% of triple-negative breast cancer cases[18,20,21].

The signaling at the membrane involves the interaction of ligands like transforming growth factor alpha (TGF- α) or epidermal growth factor (EGF) with the EGFR receptor. This interaction results in the formation of receptor dimers and the autophosphorylation of tyrosine residues located on the intracellular domain. Consequently, this activation initiates downstream signaling pathways, including PI3K/AKT/mTOR and Ras/Raf/MEK/ERK cascades, ultimately triggering various cellular responses such as cell adhesion, differentiation, proliferation, survival, migration, and extracellular matrix (ECM) construction. Mutations in the PI3K, AKT, and mTOR pathways, involving alterations in proto-oncogenes or tumor suppressor genes, can contribute to the development of cancer[22].

Overexpression of EGFR in TNBC allows cells to evade the normal regulatory mechanisms that induce apoptosis. This resistance to cell death contributes to the survival and persistence of cancer cells, promoting tumor aggressiveness[18]. Moreover, the heightened expression of EGFR results in the generation of pro-angiogenic substances such as VEGF (vascular endothelial growth factor) and bFGF (basic fibroblast growth factor). These substances stimulate angiogenesis by encouraging endothelial cells proliferation and migration, which serve as the foundation for blood vessels formation [23]. Additionally, in TNBC, EGFR signaling promotes the expression of matrix metalloproteinases (MMPs), enzymes that destroy the extracellular matrix. MMPs promote the remodeling of the tissue around blood arteries, hence promoting angiogenesis and subsequently leading to TNBC aggression[24].

Additionally, a recent investigation uncovers a notable positive feedback loop linking the Epidermal Growth Factor Receptor (EGFR) pathway and Kindlin-2. The activation of EGFR, potentially by ligands like EGF, leads to the increased expression of Kindlin-2 through the EGFR/PI3K signaling pathway. Upon elevation, Kindlin-2 attaches to the EGFR kinase domain, enhancing the stability of the EGFR protein and facilitating EGF-induced cell migration. Importantly, Kindlin-2 hinders EGFR degradation by reducing EGFR ubiquitination. This intricate molecular interplay establishes a reciprocal relationship between EGFR and Kindlin-2, contributing to the enhanced migratory phenotype and potentially other aggressive characteristics in TNBC [25].

Furthermore, recent molecular studies suggest that the EGFR signaling pathway and ECM molecules are mutually regulated in tumor cells, affecting ECM stiffness, angiogenesis, survival, adhesion, migration, and metastasis. Overproduction of tumor-promoting ECM components, such as glycoproteins and proteoglycans, enhances EGFR activation and loss of PTEN, promoting tumorigenesis progression [26].

In addition to tumor progression, EGFR is also primarily involved metabolic reprogramming. EGFR has a major role in metabolic reprogramming in addition to tumor growth. Specifically, the increase in Hexokinase 2 expression, responsible for initiating glycolysis, and the suppression of Pyruvate Kinase Muscle isoenzyme 2 activity, which concludes glucose metabolism are triggered by Epidermal Growth Factor (EGF). This stimulation fosters aerobic glycolysis and results in the accumulation of metabolic intermediates. The elevated levels of F1,6BP through this process, coupled with increased extracellular lactate, contribute to larger tumor sizes in vivo, as well as heightened proliferation, metastasis, and evasion of the immune response[27].

Apart from the above-mentioned cellular functions, recent studies have revealed that EGFR and its downstream regulators also controls epithelial-mesenchymal transition (EMT) and tumour invasion. EMT is a process through which a cell converts from a polarized epithelial phenotype to a mesenchymal fibroblastoid phenotype. EMT plays an important role in formation of healthy mammary gland, but on EGFR dysregulation, it plays major role in tumour progression. EMT leads to transcriptional reprogramming of cells. Because of its significant role in EMT, EGFR may be a crucial target for preventing tumour spread[28,29]. Furthermore, the intricate molecular landscape of triple-negative breast cancer (TNBC) extends beyond EGFR, with the dysregulation of key signaling pathways amplifying the aggressiveness of this subtype. The cascade of events initiated by EGFR overexpression seamlessly integrates with the intricate signaling network governed by PI3K/Akt/mTOR. This convergence underscores the complexity of TNBC pathogenesis, where the synergistic activation of multiple signaling pathways fuels tumorigenesis.

1.2.2. PI3K/AKT and mTOR signalling pathway and TNBC

The PI3K/AKT/mTOR (PAM) pathway plays a crucial role as an intracellular mechanism that oversees cell growth, migration, proliferation, transcription, survival, metabolism, and regulation. [30]. Numerous epidemiological and in vivo investigations have confirmed the participation of the PI3K/AKT signaling pathway in the advancement of diverse human tumors. Additionally, it serves as a pivotal element in regulating both tumor angiogenesis and the metastasis of tumor cells. Activation of the PI3K signaling pathway is initiated through the binding of ligands or growth factors to various membrane-associated receptor tyrosine kinases (RTKs), including HER2 proteins and IGF-1 receptors. [31]. Activation of the receptor tyrosine kinases (RTKs) leads to the recruitment of the p85 subunit, causing a subsequent change in conformation that allows the p110 subunit to catalyze the phosphorylation of PIP2 (4,5-phosphoinositide) into PIP3 (3,4,5-phosphoinositide). PIP3 acts as a crucial secondary messenger, governing growth, cell proliferation, and survival signaling through the AKT pathway. [31]. Moreover, the regulation of survival signaling through PIP3 is restrained by dephosphorylation mediated by tumor suppressors such as p53 and lipid phosphatase (PTEN). PTEN counteracts this process by dephosphorylating PIP3, thereby hindering the activation of AKT. Additionally, any modification or mutation in PIK3CA and genes with tumor-suppressive functions has the potential to induce genetic instability and contribute to the onset of tumorigenesis[32].

Moreover, the serine-threonine protein kinase AKT, comprising three isoforms (AKT1, AKT2, and AKT3), undergoes stimulation through PI3K phosphorylation, playing a role in the regulation of tumor growth and angiogenesis. In the PI3K signaling pathway, the formation of PIP3 results in the recruitment of AKT, which then binds to PDK1 (phosphoinositide-dependent kinase 1) through their pleckstrin homology (PH) domains. Subsequently, PDK1 phosphorylates AKT at the kinase domain, specifically at Thr 308 in AKT1, for its activation. Full activation of AKT requires phosphorylation within the carboxyl-terminal regulatory domain (Ser 473 in AKT1) by PDK2. Once activated, AKT translocates to the cytoplasm and nucleus, where it phosphorylates, activates, or inhibits numerous downstream targets, regulating various cellular functions, including angiogenesis. The enforced expression of active forms of PI3K/Akt augments the formation of sprouting vessels, inducing angiogenesis.[33]. Activation of Akt also impacts the mammalian target of rapamycin (mTOR), a protein kinase present in two complexes - mTOR Complex 1 (mTORC1) and mTOR Complex 2 (mTORC2). Akt triggers the activation of mTORC1 by suppressing the tuberous sclerosis complex (TSC), which acts as a negative regulator of mTORC1.

mTOR is a protein kinase that plays a role in cell proliferation, metabolism, and regulation. Excessive activation of the mammalian target of rapamycin (mTOR) signaling pathway often stems from mutations in upstream genes, including proto-oncogenes and tumor suppressor genes like PIK3CA and p53. The hyperactivation of mTOR in cancer primarily occurs through two distinct mechanisms. Firstly, abnormal mTOR signaling arises from mutations in upstream genes, involving loss-of-function mutations in suppressor genes and gain-of-function mutations in oncogenes. Secondly, mutations in the mTOR components, namely mTORC1 and mTORC2, contribute to hyperactivation. Additionally, the loss of function of tumor suppressor genes such as PTEN, TSC1/TSC2, and Serine Threonine Kinase 11 (STK11) has been implicated in activating mTOR, potentially playing a role in cancer development and progression. Furthermore, mTOR signaling predominantly promotes proliferation and metabolism in tumor initiation and progression by dysregulating downstream substrates of mTORC1 (E-BP1/eIF-4E). Besides mTORC1 activity, mTORC2 participates in the hyperphosphorylation of AKT and mTORC1, stimulated by growth factors (e.g., glucose and insulin), and further suppresses apoptotic activity, leading to increased survival of cancer cells[34].

Furthermore, the activation of the PI3K/AKT and mTOR pathways can occur independently of hypoxia, induced by various factors like chemokines and growth factors. These factors bind to receptors such as receptor tyrosine kinases, G protein-coupled receptors, and alarmin receptors on the cell surface, potentially triggering the activation of HIF-1 α [35]. Moreover, within cancer cells, alterations in epigenetics and acquired mutations affecting the components of these pathways result in the loss of functions associated with tumor suppressors (ING4, p53, PTEN) and the acquisition of functions linked to oncogenes (Ras, Raf, Src, mTOR, and Myc). These changes contribute to uncontrolled growth of cancer cells.[36]. Hence, the PI3K/AKT and mTOR pathway is believed to have a significant role in the process of malignant transformation and is being explored as a promising molecular target for the development of therapeutic agents aimed at treating TNBC.

1.2.3. BRCA1/2 gene mutation in TNBC

BRCA1 and BRCA2 (breast cancer type 1 and 2) are tumor suppressor genes, primarily found in the breast and various female organs' tissues. Their main functions include participating in the repair of DNA damage or eliminating cells if the DNA cannot be adequately repaired[37]. Moreover, BRCA1 operates within the DNA damage signaling pathway, aiding in DNA repair through diverse recombination pathways like homologous recombination (HR), nucleotide-excision repair (NER), and potentially non-homologous end-joining (NHEJ) DNA repair pathways[38]. Conversely, BRCA2 plays a vital role in controlling the activity of the RAD51 protein, which promotes the DNA repair process within the homologous recombination (HR) pathway. This involvement encompasses the activation of subsequent recovery pathways, DNA synthesis, and the resolution of DNA[39]. Nevertheless, mutations in BRCA lead to the destabilization of tightly regulated cellular processes. Specifically, mutations in BRCA1/2 disturb the homologous recombination (HR)-mediated DNA damage repair process, forcing cells to resort to alternative error-prone repair pathways. Over time, this reliance on alternative pathways can result in the accumulation of multiple mutations, ultimately triggering carcinogenesis[40]. The mutation in the BRCA gene prompts the repair of DNA double-strand breaks through mutagenic mechanisms rather than homologous recombination. This shift results in genetic instability, fostering the development of triple-negative breast cancer (TNBC)[41].

Recent studies shows that mainly BRCA1 mutation carriers are linked with TNBC. Although ~ 5% of all breast cancer cases have BRCA1/2 mutations, TNBC patients have higher mutation

rates. As a matter of fact, out of total breast cancer cases, 65% of BRCA1 mutation carriers and 23% of BRCA2 carriers are conforming in TNBC[42]. Furthermore, several studies stated that mutation in BRCA shows a lack of the C-terminal second BRCA1 C-terminal (BRCT) domain that may reduce p53-mediated transcriptional activation, subsequently causing uncontrolled cell proliferation. This evidence suggests the interplay between BRCA and p53 transcription[43].

1.2.4. Tumour suppressive gene -p53 gene mutation and TNBC

The p53 gene functions as a tumor suppressor gene (TSG), overseeing cell cycle regulation, cell proliferation, DNA repair, and the initiation of cell death through apoptosis. Recently, triple-negative breast cancer (TNBC) has been associated with elevated endoplasmic reticulum stress, potentially stemming from TP53 mutations. The TP53 mutation is the most commonly altered gene in cancer, detected in 80% of all cases of TNBC[44]. Moreover, missense mutations in TP53 result in the production of a mutant p53 protein that demonstrates reduced susceptibility to degradation compared to the wild-type (wt) p53. This leads to the overexpression of the mutant p53 protein in triple-negative breast cancer (TNBC)[45]. The overexpression then triggers cytogenetic changes, genetic instability, and an elevated probability of experiencing loss of heterozygosity[46]. The mutant p53 gene also contributes to evading apoptosis by interacting with other members of the p53 family, such as p63 and p73, thereby suppressing their tumor suppressive functions. These p53 mutations impede apoptosis by inhibiting the expression of BCL2-modifying factor through heightened AKT signaling and diminishing the transcriptional activity of p73[47]. Mutant p53 is implicated in heightening tumor aggressiveness and promoting metastasis by disrupting various mechanisms. One such example is the stabilization of the mutant p53 protein facilitated by Rab coupling protein-mediated secretion of Hsp90, which enhances cell invasion and metastasis in triple-negative breast cancer (TNBC)[48]. Further, SC Linn et al reported that the p53 mutation has been also identified as a potential contributor of chemoresistance in TNBC via upregulating the expression of multidrug resistance gene 1(ABCB1). These evidences suggest a key role of p53 gene mutation in the development of TNBC which can be a target for therapeutic intervention[49].

Apart from that, the intricate link between ATM (ataxia telangiectasia mutated), ATR (ataxia telangiectasia and Rad3-related), and TP53 (tumor protein 53) forms a critical axis in the pathogenesis of triple-negative breast cancer (TNBC). These three key players are integral

components of the DNA damage response (DDR), orchestrating a finely tuned system to maintain genomic stability[50]. ATM and ATR act as sensors of DNA damage, responding to double-strand breaks and replication stress, respectively. Upon activation, both kinases phosphorylate TP53, leading to its stabilization and subsequent activation[51]. TP53, in turn, functions as a central regulator, driving cellular responses such as cell cycle arrest, DNA repair, and apoptosis. In TNBC, the dysregulation of ATM, ATR, and TP53 contributes to genomic instability, a hallmark of this aggressive breast cancer subtype. Aberrations in these pathways compromise the cell's ability to repair damaged DNA properly, fostering the accumulation of genetic alterations that fuel TNBC pathogenesis[52].

Furthermore, several studies demonstrated that mutation in P53 or inactivation causes stimulation of the PI3K/AKT pathway which cause hyperactivation of mTOR via AMPK- β 1 and TSC2, leads to development of cancer cell growth and metastasis of cancer. This evidence suggests the interplay between p53 and PI3K/AKT and mTOR mutation[53].

Beyond the complex effects of TP-53, retinoblastoma protein (Rb1), another protector of cellular integrity, becomes a significant component in the intricate molecular environment of TNBC. Rb1 and TP-53 interact in a dynamic progression and disruptions to one of their roles combine to encourage unchecked cell proliferation.

1.2.5. Rb1 pathway and TNBC

The retinoblastoma protein (Rb1), a tumour suppressor gene serves as a critical regulator of the cell cycle exerting control over the transition from the G1 to S phase[54]. In its active, hypophosphorylated state, Rb1 acts as a checkpoint guardian, binding and inhibiting the activity of cyclin-dependent kinases (CDKs)[55]. This inhibition prevents the phosphorylation of Rb1 and maintains its association with the transcription factor E2F, thereby suppressing the expression of genes essential for DNA synthesis and cell cycle progression[56]. As cells receive signals to proliferate, various cyclin-CDK complexes are activated, leading to the phosphorylation and inactivation of Rb1. This release of E2F allows for the transcription of genes necessary for S phase entry and progression[57]. In cancer cells, overexpression of Cyclin-E, activate CDK2 which cause up-regulation of CDNK2 that encourages the inactivation of suppressor gene RB1, which blocks the senescence in apoptosis pathways [58]. The amplified expression of CDNK2A and related CDNK2's complex permits evading the

cell-cycle regulatory checks in the RB1 pathways and allows progression into the G1/S phase. Hence, it leads to high expression of cellular proliferation and growth[59].

Furthermore, several studies also reported the tumor suppression mechanisms orchestrated by the retinoblastoma protein (Rb1) that are multifaceted, contributing significantly to the prevention of uncontrolled cell growth and tumorigenesis[54]. One primary mechanism involves Rb1's ability to induce cellular senescence, a state of irreversible cell cycle arrest. In response to various stress signals, active, hypophosphorylated Rb1 restricts cell cycle progression, halting cells in the G1 phase[60]. Furthermore, Rb1 promotes apoptosis, the programmed cell death, as a safeguard against the survival of cells with damaged DNA or aberrant proliferation signals. This pro-apoptotic function is mediated through the regulation of Bcl-2 family proteins and interactions with apoptotic pathways [56]. The interplay between Rb1 and the p53 tumor suppressor pathway further amplifies these tumor-suppressive effects, forming a robust defense mechanism against the emergence of cancerous cells[55]. Dysregulation or loss of Rb1 function dismantles these safeguards, allowing for unbridled cell growth and contributing to the development and progression of various cancers, including triple-negative breast cancer (TNBC)[61].

The retinoblastoma protein (Rb1) undergoes various alterations in triple-negative breast cancer (TNBC), contributing to the dysregulation of critical cellular processes. Genetic and epigenetic changes in Rb1 are prevalent in TNBC, including mutations, deletions, and methylation alterations. These alterations disrupt the normal functioning of Rb1 as a tumor suppressor, leading to the loss of its inhibitory control over the cell cycle[62]. Mutations in the Rb1 gene can render the protein non-functional, while deletions may result in a partial or complete loss of Rb1[63]. Epigenetic modifications, such as hypermethylation of the Rb1 promoter region, can silence its expression, further contributing to Rb1 inactivation[64]. The cumulative effect of these alterations in TNBC is the promotion of uncontrolled cell proliferation, a hallmark of cancer. Thus, targeting RB1 pathway can be strategy to manage the TNBC.

1.3. Therapeutic approach for the management of TNBC

In the current era, the medical practitioners /clinicians are facing challenges in the therapeutic management of TNBC due to its aggressiveness[65]. The treatment of tumors has progressed from surgery to the use of targeted X-rays with or without chemotherapeutic agent. The selection of the treatment for TNBC depends on the origin of cancer development, cancer type, and molecular site, as well as the stage of progression[66]. The most commonly used treatment

approaches such as chemotherapy, surgery, and radiotherapy are which discussed in detail below.

1.3.1. Chemotherapy in TNBC

Chemotherapeutic drugs are well-established therapeutic approaches for various cancer treatments. They work biologically by interfering with cellular pathways, stopping tumor progression by impairing tumor cells' ability to proliferate and induction of apoptosis. The clinical therapeutic class of drug for TNBC are alkylating agents, antimetabolites, mitotic inhibitors, and topoisomerase inhibitors[67].It is believed that TNBC is sensitive to neoadjuvant chemotherapy. However, chemo-resistance is a serious problem associate with neoadjuvant chemotherapy, with up to 90% of drug failures in metastatic TNBC. Moreover, there is a possibility of relapse within first five year of neoadjuvant treatment. A study was reported by Alvaro Moreno-Aspitia et al., with neoadjuvant treatment of anthracycline–taxane chemotherapy. Their findings demonstrated that the combination of anthracycline–taxane showed better treatment against TNBC, unfortunately, by the time the disease recurs, the resistance was developed for this therapeutic regimen due to the upregulation of ABC transporters (Pgp transporter). Thus, it is vital to select the proper regimen to improve its prognosis. In addition to chemoresistance, systemic toxicity due to non-specific targeting, poor bioavailability restricts the chemotherapeutics in the management of TNBC[68,69]. Moreover, chemotherapy kills the quickly growing cells in the bone marrow that leads to leucopenia, anemia and thrombocytopenia. Further, due to use of high-dose chemotherapy, there is a chance of the development of oral and or gastrointestinal mucositis, leading to ulcerations pain anorexia, weight loss, anemia, fatigue, and chances of sepsis formation. Additionally, chemotherapy is primarily utilized in combination with surgery to treat cancer. Chemotherapy-based drugs are often administered to patients before or after surgery to improve the therapeutic effectiveness. Based on the therapeutic utilization, it is classified into two types i.e., adjuvant therapy, after surgery and Neoadjuvant therapy i.e., before surgery[70].

1.3.2. Surgery in TNBC

Surgery is a well-established traditional technique used to treat cancer without any preventable tissue damage. Surgery offers minimal damage to the surrounding tissues over radiation therapy and chemotherapy. There are two types of surgical processes involved in TNBC, i.e., lumpectomy and mastectomy. In the case of lumpectomy, only the part of the breast having cancer along with the surrounding normal tissue was removed. While in mastectomy the entire

breast is removed. Studies have shown lumpectomy to give better loco-regional recurrence-free survival (LRRFS), disease-free survival (DFS), and overall survival (OS) compared to mastectomy[12,71]. It has been reported that the combination of breast-conserving surgery with postoperative radiotherapy improves the overall survival and breast cancer-specific survival (BCSS) compared to total mastectomy TNBC patients. Although surgery is a better option, it also has certain limitations, including post-operative pain, numbness and tingling, damage to neighboring normal tissues, side effects associated with breathing and heart problem due to use of general anesthesia, lymphedema, and nosocomial infections along with influencing the lifestyle of the patient[72].

1.3.3. Radiation Therapy in TNBC

Generally, after mastectomy or conservation breast surgery (CBS), radiotherapy is given as it can improve loco-regional control in breast cancer. In addition to this, reports exhibit BRCA1 mutation leading to high sensitivity to radiation. It has been reported that removal of occult BRCA1 deficient tumor foci from the breast and surrounding tissue can occur if CBS is followed by radiotherapy, leading to a decreased locoregional recurrence[73–75]. The limitations of radiation in the treatment of triple-negative breast cancer (TNBC) are mostly attributed to the presence of related toxicities and the absence of established treatment protocols. A significant constraint associated with this particular kind of radiation is to the financial implications stemming from the use of intricate apparatus and advanced technologies[73–75].

1.4. Challenges in diagnosis and treatment of TNBC

The morphological and molecular findings suggest that TNBC is a highly aggressive and heterogenous malignant disease. Thus, diagnosis of TNBC is complex due to lack of ER, PR and HER2 protein. Till date, IHC analysis of biopsy samples is the only suitable technique for TNBC diagnosis which follows the critical examination of patient in clinical practice. However, IHC is dependent upon imaging encompassing a mammogram which sometimes gives either false- positive or false negative results affecting the treatment of the patient. Further, molecular imaging techniques using targeting ligands may be a promising approach for the early detection of tumors in TNBC[76,77]. This strategy is predominantly associated with the utilization of an adequate targeting ligand. Thus, it is very crucial to identify suitable targets expressed in early stages of tumour growth before developing any targeting agents. Taken all together, biomarkers involved in molecular imaging techniques for TNBC diagnosis,

still needs to be validated before claiming their clinical application. Additionally, problems associated with molecular imaging techniques includes high production costs of biomarker, variability in biodistribution and degradation of biomarker. Thus, these problems need to be overcome before these strategies can be translated to clinical practice[76,77].

In TNBC patients, chemotherapy is the only therapeutic option apart from surgery and radiotherapy that has shown some effectiveness at early stages. However, these therapeutic approaches have several clinical limitations such as non-selective targeting, side effects, and chronic toxicities[78]. Additionally, resistance in chemotherapeutic drugs like taxanes and anthracyclines pose clinical challenge due to presence of efflux transporters i.e., P-gp efflux transporter. On the other hand, the poor outcomes associated with TNBC due to lack of surface receptor, endocrine therapies such as selective estrogen receptor modulators (SERMs) and aromatase inhibitors, or anti-HER2 targeted monoclonal antibody treatments like trastuzumab are ineffective in treating TNBC[79].

Moreover, the tumor microenvironment (TME) is a critical factor that supports in development of TNBC. The tumor proliferation, angiogenesis, anti-apoptosis pathways, suppression of immune system, and check point related to immune system in TNBC are inherently associated with TME. Amplification of tumor cells proliferation induces hypoxia, with consequent reprogramming of cancer cells in the TME. Due to reprogramming, tumor cells and its TME frequently familiarize to the new conditions and promote tumor growth[76,80,81]. Further, the reciprocal communication between tumor cells and stromal cells as well as immune cells induces changes in the cellular components of TME, which influences cancer cells to metastasis. In addition to metastasis, TME also induces the transition of epithelial cells to TNBC stem cells. The interactions between these cells in TME nurture several biological events that support cancer growth, invasion and angiogenesis. This evidently shows that TME is biggest challenges for the management of TNBC. Therefore, there is a unmet of need new strategy to tackle the aggressiveness of TNBC[76,80,81].

Since then, newer targeted therapy approaches have been researched extensively, which includes, targeting DNA repair pathways, cell cycle retardation, inhibiting poly ADP-ribose polymerase (PARP) enzyme, anti-angiogenesis therapy, immunotherapy. Further, photodynamic therapy (PDT) and radiation therapy may possibly provide a practical approach to boost the therapeutic effectiveness for the management of TNBC.

1.5. Photodynamic therapy

Photodynamic therapy (PDT) has emerged as a minimally invasive therapeutic method that has garnered significant interest in recent years as a novel approach to cancer treatment. It involves the induction of cytotoxic oxygen species by the photoexcitation of photosensitizer molecules, ultimately resulting in cellular demise[82]. In contrast to traditional treatment techniques, photodynamic therapy (PDT) exhibits enhanced selectivity towards tumour cells, owing to the preferential localization of photosensitizers inside tumour lesions and the precise irradiation of these lesions with light. There are many photosensitizers available for PDT. Based on chemical structure, these are classified into porphyrins, chlorins and dyes. The example of various photosensitizers is aminolaevulinic acid (ALA), Silicon Phthalocyanine Pc 4, m-tetrahydroxyphenylchlorin (mTHPC), chlorin e6 etc. Among them, chlorin based photosensitizer like Chlorin e6, Puritytin, HPPH are mostly used in diagnosis and biomedical application due to its easy biosynthesis, high production and reduced side effect[83].

The photosensitizer i.e., 2-[1-hexyloxyethyl]-2-devinyl pyropheophorbide-a (HPPH) is a second-generation, lipophilic, chlorin-based small molecule; is initially injected in the bloodstream, which is then absorbed and further deposited into the cancer cells. This photosensitizer accumulates in these cells, and on exposure to a particular wavelength of light, generate ROS which can eventually kill cancer cell. HPPH is currently under phase I/II clinical trials for different cancer types including esophageal, neck, head cancer, and breast cancer[84]. Nevertheless, HPPH also has some severe limitations including aggregation of the therapeutic agent, photostability against quick photobleaching, less aqueous solubility and poor pharmacokinetics, and phototoxic side effects which are severe obstacle against clinical translation for this drug[84]. Moreover, like other therapeutic modalities, PDT has several drawbacks and restrictions. This may cause photosensitivity with long exposure of laser light. The effectiveness of the treatment is reliant on the precision with which the tumour is irradiated with light. The oxygenation of tissues is essential for the photodynamic effect. With the technologies that we have now, treating metastatic cancer is quite challenging. When considering PDT as a potential form of therapy, the precision of the irradiation of light to the target tissue is the single most critical factor to consider. Due to the poor penetration of visible light into the tissue, it is challenging to treat deep tumour since these tumour are not readily accessible without the assistance of surgical procedures[85,86]. Therefore, researchers are more focusing on development of novel formulation to overcome the above-mentioned issue.

1.6. Poly (ADP-ribose) polymerase (PARP) inhibitor

Poly (ADP-ribose) polymerase (PARP) inhibitor is another promising new therapeutic approach which has already been tried in cancer therapy. These are acting by inhibiting ribosylation of the target protein by transfer of ADP ribose from NAD⁺, which plays an essential role in DNA repair. Till date, Olaparib (OLA) and Talozoparib are the two PARPi agent which has been approved by US-FDA for management of different subtypes of breast cancer. Moreover, the meta-analysis data showed no statistically significant difference between olaparib and Talazoparib in terms of efficacy, safety, and acceptability, which means that the two FDA-approved single-agent PARPi have similar efficacy, safety, and acceptability when used for treating patients with advanced breast cancer[87,88].

Olaparib is a highly selective PARP inhibitor with significant anti-tumor activity is used in breast cancer with or without a BRCA1/2 mutation which has been used for treatment of various cancers, specifically ovarian and breast cancer. It can kill cancer cell via inhibiting DNA synthesis or ROS induced apoptosis. However, it is also associated with several limitations such as lack of targeting a tumour tissue, poor bioavailability (12-17%), shorter biological half-life (6-12 h), in vivo stability, and toxicity. Moreover, with the passage of time during the treatment some cancer cells might develop resistance to PARP inhibitors which can subsequently affect the effectiveness of the therapy. Along with above limitations, side effects such as fatigue, vomiting and anaemia, also generate greater hindrances against its clinical translation [89,90]. Therefore, researchers are more focusing on development of better delivery approach or combination strategy to overcome the above-mentioned issue.

1.7. Possible mechanism involved in modulation PDT via PARP inhibition

PDT has considerable potential as a viable approach for treating malignant tumors due to its notable selectivity. Colocalizing light, oxygen, and photosensitizer produce a significant quantity of reactive oxygen species (ROS) when excited by a laser at a specific wavelength. This phenomenon can cause DNA damage and effectively eradicate cancer cells[91,92]. Nevertheless, the repair mechanism shown by tumour cells and the poor immune response they elicit constraints on the further advancement of PDT. Further, PDT is impeded by the action of a nuclear enzyme i.e., PARP which is involved in the repair of DNA by binding to specific location of single-strand damage on the DNA molecule, and in turn, facilitating the repair process. These PARP family enzymes are involved in the process of poly-ADP-ribosylation (PARylation), whereby they transfer ADP-ribose units from NAD⁺ to proteins that serve as

substrates. This process facilitates the repair of DNA single-strand breaks (SSBR) via base excision repair (BER). Along with that, the clinical challenges i.e., development of resistance to PDT might be facilitated if the tumour tissue is not rapidly eradicated during the first PDT sessions[93,94]. This poses a challenge to the effectiveness of the treatment, mostly due to the activation of cellular redox defenses and repair mechanisms. The precise mechanism behind PDT resistance remains elusive; nevertheless, in vitro experiments have shown that resistance may arise through activation of the PARP damage-repair signaling pathway. Hence, the inhibition of PARP may possibly augment the PDT response[93,95].

Although, the PDT and its combination with PARPi showed various advantages against TNBC, but these are also associated with few limitations such as less aqueous solubility, stability issue in biological system along with the poor pharmacokinetic profile (low bioavailability, low biological half-life, etc.). Thus, these overall drawbacks can be circumvented by the employment of advanced targeted drug delivery system for the effective management of TNBC.

1.8. Emerging Nanotechnology Based Delivery Approaches toward TNBC Treatment

Nanotechnology is one of the finest tools that has emerged in the past couple of decades, having the potential to fight against severe, difficult-to-manage diseases like cancer. Biomedical sciences have seen the evolution of nanotechnology in targeting cancer, via various approaches in order to have a robust and targeted delivery of diagnostics and therapeutics. Researchers are considering the option of nanomedicine for combinational therapy or as a multidrug delivering system, in case of cancer so as to employ several advantages such as improving the pharmacokinetic profile, decreasing the free drug toxicity, and having a synergistic pharmacological effect of the drugs employed[96]. Other advantages offered by the nano systems are improved therapeutic index, with an increase in localization of the drug in the blood, decreased off-target secondary pharmacological effects, with increased localized targeted action in tumor cells. The employment of nanoparticles with primary purpose targeted delivery is based on the characteristic features of the nanoparticles including, average nanoparticulate size, uniformity, surface potential as well as drug loading capacity. The specific advantages offered by nanoparticles can be attributed to the increased large surface area to volume ratio of nanocarriers[97,98]. Furthermore, the entrapment or loading of drugs in or onto the nanocarriers, has increased the chances of efficient targeting of the tumor cells via the use of single drug molecules or via combination therapy. The nanomedicines are required to be

explored more, in targeting the TNBC, as it's already known that TNBC lacks ER, PR, and HER2 receptors on their membrane. The absence of these receptors makes it difficult for conventional drug systems to target the tumor cells. As a consequence, nanotherapeutics is looked upon as an emerging non-conventional approach in targeting TNBC[97,98]. Various nanoparticle systems consisting of Liposomes, Micelles, Dendrimers, Solid-lipid Nanoparticles, Polymeric Nanoparticles, Gold Nanoparticles etc. and their details are shown Figure 3. The adoption of nano systems in targeting cancer is increased, as it increases the permeation and localization of the drug.

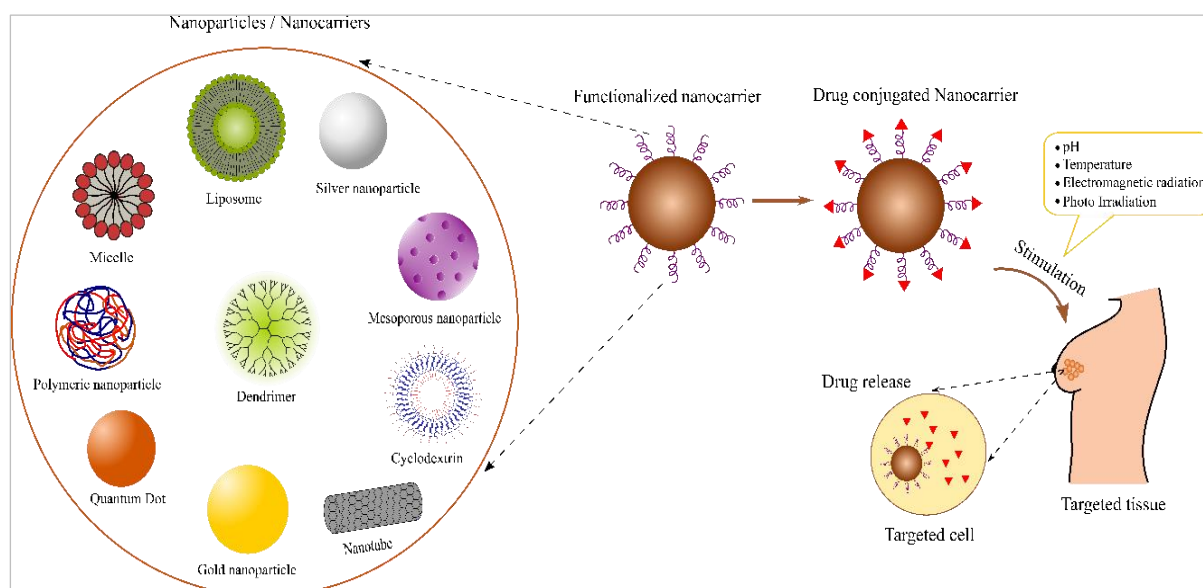


Figure 1.2. Different types of nanoparticles used in treatment of TNBC ;Adopted from the ref.[74]

1.9. Surface engineered ligands used to target TNBC

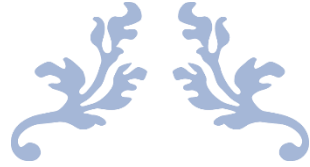
All the conventional based nano therapy options for cancer treatment have prominent side effects, mainly because of the absence of specificity. Most often, the site of administration will be far from the site of action such that there is a great chance for drug accumulation and toxicity of anti-cancer drugs. Therefore, novel strategies have been developed to better deal with tumors and further complement present traditional therapies. Also, it has attracted the scientific community to study more on delivering the drugs to a specific site using nanocarriers to avoid unwanted toxic effects via targeted nano drug delivery systems. Several reports stated that modifying the surface properties such as molecular size, surface charge, and physicochemical properties of nanoparticles can improve their in vivo stability, biocompatibility, and drug delivery capacity[99]. As a result, scientists are interested in studying the surface modification of nanoparticles to learn more about the targeted delivery of anti-cancer medications. The

surface of nanoparticles can be attached with small molecules (dyes or drugs) as well as large biomolecules (polymers, peptides, or ligands). Coating nanoparticles with small molecules is an effective way to change the surface charge, hydrophobicity, and stability, all of which are essential features for regulating the cellular absorption of nanoparticles[100]. In addition, modification of nanoparticle surfaces such as attaching specific ligands that are complementary to the receptors which are overexpressed in breast cancer will show good efficacy in treatment. There are few surfaces modified nanoparticle, their target site and ligand with respect to TNBC was mentioned in the table 1.1.

Table-1.1. Different therapeutic approaches for TNBC

Target	Ligand	Drugs	Delivery system	Therapeutic outcome	Reference
Transferrin receptor	Transferrin	Benzoporphyrin derivative of mono acid	Polymeric nanoparticles	Exhibited the highest photo triggered in-vivo cytotoxicity	[101]
Folic acid receptor	Folic acid	Diallyl trisulfide	Solid Lipid Nanoparticles	Higher cellular internalization and efficient Bcl2 protein downregulation with improved in-vivo anticancer efficacy	[102]
		Quercetin	Nickel oxide (NiO) nanoparticles	Reduced cytotoxicity and good biocompatibility along with appreciable anti-cancer activity	[103]
Mucin (MUC1)	Aptamers	Navitoclax	Mesoporous silica nanoparticles	Effectively induce apoptosis, overcoming navitoclax resistance	[104]
Biotin receptor	Biotin, vitamins	Methotrexate	Biotin-PEG conjugated nanogels (Biotin-PEG-CMPEI)	Lowered tumor volume and mortality rate and had less lung metastasis and glomerular damage	[105]
CD44 receptor	HA	Tirapazamine	Mesoporous Ia3d silica nanoparticles	Improved in-vivo antitumor activity	[106]
		Triptolide	Core-shell nanoparticles	Suppression of cell proliferation and higher efficacy in shrinking tumor size and blocking lung metastasis	[107]
EGFR	Growth factors	Paclitaxel, Piperine	Liposomes	Enhanced cellular uptake and improved anticancer efficacy	[108]
		Curcumin	Lipidic nanoparticles	Retardation of tumor growth and tumor volume ultimately, enhance the anticancer activity	[109]

Taken all together, research evidence disclosed that the mutation in BRCA gene and abnormal activity of PARP enzyme may eventually leads to TNBC. Therefore, PDT and PARP inhibitor (PARPi) can be the two promising strategies to treat the TNBC. In this research work, we have used HPPH as Photosensitizer for PDT therapy to eradicate the tumor cell via ROS mediated pathway and further, also used Olaparib, a selective PARP inhibitor which can enhance the ROS base apoptosis for cancer cell death. We also evaluate if any possibility of therapeutic synergistic effect or additive effect with combination of these two drugs for TNBC treatment as PARPi works to resolve the problem associate with PDT resistance. In spite of the advantage of HPPH and OLA, these two molecules have certain limitations including low solubility, poor pharmacokinetics, limited cellular uptake into the target cells, and clinical side effects including DNA damage to the normal cell. Hence, to overcome the pharmacokinetic and pharmacodynamic issue along with adverse events associated with these two drugs; a tumor targeted drug delivery system will be a possible approach to minimize the toxicity and increased efficacy. Therefore, in the current research, we have developed a lipid-polymer hybrid system which have been surface factionalized with a biotin to impart better efficacy via increasing the site-specific accumulation of HPPH and OLA. Additionally, we also aimed to evaluate if any synergist antitumoral efficacy exist between these two drugs against TNBC. Finally, we also developed a co-encapsulated the HPPH and OLA LPHNs which is decorated with 2-different class chemical ligand (i.e., mitochondrial targeting ligand, ROS inducing moiety and Biotin receptor targeting) as multifunctional tumor targeted nanocarrier to improve the therapeutic efficacy at the site of tumor along with to minimize toxicity if any exists in comparison with the pure drug on TNBC.



LITERATURE REVIEW



2. Literature Review

2.1. Triple-negative breast cancer and its prevalence

Triple-negative breast cancer (TNBC) is a highly aggressive sub-type of breast cancer that lacks the expression of three important receptors i.e. estrogen receptor, progesterone receptor, and human epidermal growth factor 2 receptor (HER2) found on the surface of breast cancer cells [40]. It is characterized by highly aggressive behavior, increased invasiveness, and demonstrating a propensity for early recurrence and metastatic spreading toward the nearby organs along with poor prognosis [110,111]. TNBC is more common in certain ethnic groups, including Hispanic descent, Africans, and African-American women, as well as individuals with mutations in the breast cancer 1 (BRCA1) gene [112,113]. African American women have a higher likelihood of developing TNBC compared to Caucasians, indicating that the germline genetic background plays a significant role in the transcriptional program and tumor differentiation [114]. This particular form of breast cancer is most commonly found in young women, constituting 15-20% of all diagnosed cases of breast cancer [113,115,116]. Indeed, over 85% of breast cancers that arise in individuals with a BRCA1 germline pathogenic variant exhibit a triple-negative phenotypic expression. Additionally, 11% to 19% of patients diagnosed with triple-negative breast cancer carry either BRCA1 germline or somatic mutations [117]. Recent molecular and histological studies (**Table 2.1**) suggest that the majority of TNBC cases are characterized by invasive ductal carcinomas, constituting approximately 90% of instances. The remaining cases involve lobular, adenoid cystic, apocrine, and metaplastic carcinomas [115,118].

Although they share the phenotypic expression of TNBC, each class has a distinct prognosis. Additionally, TNBC is categorized into six subtypes (Mesenchymal, Mesenchymal stem-like, Basal-like 1&2, Immunomodulatory, and Luminal androgen receptor) according to their gene expression profiles [21]. A study by Burstein et al. suggested four subtypes of TNBC including, luminal androgen receptor, mesenchymal, basal-like immune-suppressed, and basal-like immune-activated [119]. In recent studies, researchers have explored the diversity of gene expression and various genetic events in TNBC. The wide-ranging characteristics of TNBC, leads to varied responses to treatments, suggesting the need for further subdivision from a therapeutic standpoint. Identifying specific molecular markers for TNBC subtypes would

undoubtedly improve the diagnostic process and contribute to the development of predictive biomarkers and targeted therapeutic approaches [66,120].

Table 2.1: Histologic Types of TNBCs and their essential genetic features/potential molecular targets; Adopted with permission from ref.[121]

Histological Grade of TNBCs	Histological type	Essential genetic features/Molecular targets
Low Grade	Adenoid-Cystic Carcinoma	MTB/MYBL1 activation
	Secretory Carcinoma	ETV6-NTRK3
	Various other salivary gland-like tumors including, polymorphous carcinoma, mucoepidermoid carcinoma, and adenomyoepithelioma	<ul style="list-style-type: none"> • Mucoepidermoid carcinoma-MAML2 rearrangements • Polymorphous carcinoma-PRKD gene rearrangement • Adenomyoepithelioma -PIK3CA
	Low-Grade Adenosquamous Metaplastic Breast Carcinoma	PIK3CA mutations, lack of TP53 mutations
	Solid Papillary Carcinoma with Reverse Polarity refers to a type of BC that exhibits characteristics resembling the tall cell variant of papillary thyroid neoplasms.	PIK3CA and IDH2 R172 hotspot mutations
High Grade	Apocrine Carcinoma	PIK3CA pathway mutations, AR expression,
	Medullary carcinoma	Correlation with IM intrinsic molecular subtype
	Metaplastic Carcinoma	TP53 mutations, PI3K and WNT pathways, MSL and claudin-low genetic similarities, epithelial-to-mesenchymal transition markers
	Invasive ductal carcinoma NOS	TP53, BRCA1

2.2. Prognostic role of BRCA Mutation in TNBC

Normal mammary gland development is a critical function of BRCA1 and the gene is needed to translate ER-negative cells to ER-positive cells. BRCA1 and BRCA2 are of significance in the homologous recombination process of all the DNA repair actions, important in repairing the breaks in DNA double-strand. The tumor suppression mechanisms of these proteins are via homology-directed repair (HDR), responsible for repairing damage to DNA thus inhibiting tumorigenesis. Homologous recombination (HR) utilizes a section of DNA possessing high sequence identity like the identical sister chromatid for copying and replacing the damaged sequence in repairing lesions[39].

The cancer-suppressive effect of BRCA1 is closely linked to its role in maintaining genetic stability. In order to restore impaired DNA, the hyperphosphorylated BRCA1 protein translocate to replication sites and recruits numerous protein complexes capable of recognizing and repairing damaged DNA and initiating cell-cycle checkpoints, thereby controlling cell survival[122].

In brief, the cellular response to DNA damage involves the activation of BRCA, which subsequently induces the homologous recombination (HR) pathway initiation. During the HR-mediated Double Strand Break (DSB) repair, the ends of the DSB are cleaved, resulting in the generation of 3' single-stranded DNA tails. These tails are then coated with Replication Protein A (RPA). Subsequently, the recombinase protein RAD51 displaces RPA and takes place on the single-stranded DNA tails. RAD51 is an indispensable protein in the HR repair mechanism. It plays a vital role in facilitating the subsequent steps of the repair process, including the activation of the downstream recovery pathway, DNA synthesis, and the resolution of DNA. This series of events ultimately leads to the completion of the repair process[123]. The BRCA1-BARD1 complex plays a crucial role in this biological process by directly engaging with the RAD51 protein to facilitate DNA invasion in homologous recombination (HR). This interaction enhances the ability of RAD51 to grab homologous double-stranded DNA, leading to the assembly of the synaptic complex and the formation of the displacement loop (D-loop)[124]. On the other hand, BRCA2 plays a crucial role in regulating the function of RAD51 protein that stimulate DNA repair process in HR pathway including the activation of the downstream recovery pathway, DNA synthesis, and the resolution of DNA[125].

However, cells in absence of BRCA genes are not capable of repairing breaks in double-strand DNA by HR. Reduced DNA repair efficiency is seen due to mutations and/or function loss in the two genes thus increasing the expansion of cancer cells. Since, normal mammary gland development is a critical function of BRCA1 and the gene is needed to convert ER-negative cells to ER-positive cells, the reduced DNA repair efficiency leads to an elevation in the risk of developing breast cancer by five to six-fold time and is the main cause underlying cancer disposition in carriers of BRCA mutations[126]. Mutations in the BRCA1 gene, often exhibit an association with hereditary breast and ovarian malignancies. Loss of heterozygosity of BRCA1 gene is often seen in high-grade breast cancers, as 75% of female breast cancer patients with TNBC phenotype have BRCA1 mutation[127]. The potential alternative processes that contribute to BRCA-1 faulty genotypes, including BRCA1 hypermethylation, germline

mutation, and gene deletion, have been clearly well understood but BRCA1 protein stability regulation remains inadequately known[128].

In the same way, in normal physiology, BRCA1 plays a significant role in the initiation of apoptosis. Primarily, it acts on subcellular location i.e., alternating between the cytoplasm and nucleus, critically influences the apoptotic pathway. The subcellular location of BRCA1 is influenced by various proteins, such as BARD1 and BRAP2, which exert significant regulatory functions. BARD1 facilitates the translocation of BRCA1 into the nucleus by concealing the nuclear export signal (NES), whereas BRAP2 facilitates the retention of molecules in the cytoplasm[129]. The induction of apoptosis is reliant on BRCA1 and occurs as a consequence of the disruption of the BRCA1-BARD1 complex, leading to the accumulation of BRCA1 in the cytoplasm. The protein BRCA1 undergoes many posttranslational changes, including phosphorylation and sumoylation, which have the potential to impact its subcellular distribution and functional properties[130]. The BRCA1 protein exhibits localization inside several cellular compartments, including centrosomes, mitochondria, and the endoplasmic reticulum. It also interacts with proteins such as Bcl2 and inositol 1,4,5-trisphosphate receptors (IP3Rs), implying its participation in many apoptotic pathways[130]. In a DNA cell with impaired integrity, BRCA1 can induce cellular demise through a p53-independent mechanism. This process involves the translocation of BRCA1 from the nucleus to the cytoplasm, where it initiates signaling cascades such as Ras-MEKK4-JNK and Fas. Activating these pathways ultimately leads to cell death by activating caspase 8, an enzyme with molecular properties akin to scissors that cleave cellular components, culminating in cell demise[130]. However, mutations in p53 and BRCA1 genes have been shown to impair the mobility of BRCA1, thereby impacting its apoptotic functionality. The BRCA1 gene functions as a regulatory protein within the cellular environment, akin to a traffic controller. It determines whether cells should persist in their growth or undergo cessation and apoptosis. The regulation occurs through its translocation across distinct cellular compartments. When the movement of BRCA1 is impaired, its functionality may be compromised, potentially contributing to cancer development[130].

2.3. Challenges towards management of TNBC

2.3.1. Tumour microenvironment and its role in tumorigenesis

The tumor microenvironment (TME) is a critical factor that supports in development of TNBC. The tumor proliferation, angiogenesis, anti-apoptosis pathways, suppression of immune

system, and check point related to immune system in TNBC are inherently associated with TME[131]. The increased proliferation of tumor cells leads to hypoxia, promoting reprogramming of cancer cells within tumor Microenvironment (TME). This reprogramming often results in the adaptation of both tumor cells and their TME to the altered conditions, subsequently facilitating tumor growth. Based on the TME, various numerous mechanisms of tumorigenesis and disease progression have been identified[131]. Different cytokines and inflammatory mediators are secreted by cancer associated fibroblasts (CAF) that promote the proliferation and invasiveness of tumor cells [131]. It has been found that CAF has a significant role in TNBC progression mediated by activating TGF- β pathway [131]. Furthermore, in TNBC, a notable abundance of tumor-infiltrating lymphocytes (TIL) is observed, attributed to somatic mutations. The tumor-infiltrating lymphocytes mainly consists of T-cells such as CD4+ helper T cells, CD8+ cytotoxic T cells, and CD4+ regulatory T cells. Elevated TIL levels are recognized as marker for comprehensive pathological response in TNBC patients. Notably, cancers with higher TILs tend to be estrogen receptor negative [132].

Moreover, the bidirectional communication between stromal cells and tumor cells, along with immune cells, triggers alterations in the cellular makeup of the tumor microenvironment (TME), ultimately promoting cancer cells to undergo metastasis. In addition to metastasis, TME also facilitates the transformation of epithelial cells into TNBC stem cells. The interplay among these cells within the TME fosters various biological processes that sustain the growth, invasion, and angiogenesis of cancer. For instance, T-cells play a role in modulating the immune response during the early phases of cancer. Nevertheless, their engagement with tumor cells and formation of regulatory T cells (Tregs) contribute to the increased aggressiveness and development of cancer [133,134]. These Treg cells release TGF- β , and IL-10 cytokines, suppressing the overall immune system. It was observed that they inhibit cellular contact by expressing CTLA-4 (cytotoxic T-lymphocyte-associated antigen 4), preventing its detection by tumor cells [135]. Furthermore, tumor-associated macrophages (TAMs) are natural immune effector cells attracted to tumor tissues, playing a role in fostering tumor growth and metastasis. They achieve this by facilitating angiogenesis, generating factors that break down stromal tissue and suppressing adaptive immunity. Additionally, TAMs diminish the tumor's responsiveness to chemotherapy. Robust clinical evidence indicates that a high concentration of TAMs in tumor tissues is associated with an unfavorable prognosis for TNBC and an elevated risk of metastasis. These evidences show that TME is biggest challenges for the

management of TNBC. Therefore, there is an unmet need of a new strategy to tackle the aggressiveness of TNBC[136].

2.3.2. 2.4.2. Lack of efficient chemotherapeutic drugs in the management

A significant challenge in TNBC management is the poor prognosis as it is attributed to the absence of surface receptors. Present chemotherapy strategies for TNBC involve the use of taxanes, platinum compounds and anthracyclines. The prevailing initial treatment approach for TNBC often combines anthracyclines and taxane, followed by capecitabine upon progression. While these standard agents demonstrate efficacy in a subset of early TNBC patients exhibiting chemosensitivity, individuals with advanced disease typically exhibit a limited response to current chemotherapeutic drugs [137]. Despite positive responses to conventional chemotherapy protocols, there is a subsequent observation of swift disease progression in many cases. The emergence of resistance to chemotherapy is a significant factor contributing to the metastasis and recurrence of cancer in TNBC patients. Reports indicate that the presence of heterogeneity and chemo-resistant cancer stem cells (CSCs) may be accountable for the chemotherapy resistance seen in TNBC patients, leading to metastasis and tumor recurrence, ultimately resulting in high mortality rates. The absence of a clinically effective and molecularly targeted therapy has created a notable treatment gap, emphasizing the urgent need for the identification of new molecular targets and targeted agents for TNBC patients [67].

2.3.3. Biological barrier involved towards TNBC

Despite the availability of the promising chemotherapeutic agents, the delivery of these agents to the tumor cells remains one of the major hurdles for the effective therapeutic activity. The drug delivery carrier needs to overcome the various therapeutic barriers. The major effect shown by these biological barriers are short blood circulation time, poor accumulation and penetration in tumor tissues, low cellular uptake, poor organelle uptake[138]. While nanocarriers provide numerous benefits, researchers continue to grapple with challenge of overcoming both physicochemical and biological barriers [138]. Upon entering the bloodstream, nanocarriers experience adsorption of plasma proteins, apolipoproteins and immunoglobulins, resulting in the formation of protein corona, a process referred to as opsonization. Phagocytes subsequently uptake these nanocarriers bound to the protein corona, leading to their clearance from the body. This clearance primarily occurs in organs such as liver, lymph nodes and spleen [138]. To reach the tumor site, the nanocarrier must traverse the endothelial layer of blood vessels. This endothelial layer consists of a glycocalyx and

proteoglycan layer that directs the entry of solutes and macromolecules. The long continuous, fenestrated nature of endothelium serves as a barrier for the nanocarrier [139,140]. The non-uniformity of endothelial gaps in tumor blood vessels creates an uneven distribution of nanocarriers within the tissue. Nanocarrier accumulation in tumor tissue is influenced by perfusion, which is also heterogeneous, contributing to an irregular distribution. Additionally, the interstitial tumor matrix acts as a barrier for nanocarriers that do not extravasate into the tumor tissue [141]. Extravasation has been identified as reliant on the hemodynamics of nanocarriers, though further investigation is required to fully understand its impact. The subsequent barrier is the TME, where the interstitial space is composed of collagen, proteins, glycosaminoglycans and fibers. Tumor tissue exhibit a higher collagen content compared to normal tissues, rendering the extracellular matrix (ECM) exceptionally rigid and restricting the entry of nanocarriers into tumor cells [140]. Hypoxic core and interstitial fluid pressure are additional factors influencing the distribution of nanocarriers within tumor tissue. Moreover, for nanocarriers to penetrate the nucleus and exert their effects, they must traverse the cell membrane. The internalization of nanoparticles occurs through endocytosis. If nanocarriers are taken up by endosomes and phagosomes associated with the phagocytic and clathrin-mediated endocytic pathway, they reach the lysosomes. However, in certain instances, caveolin-mediated endocytosis had been observed to bypass lysosomes. This particular endocytic pathway is utilized by nanocarriers when their surface is functionalized with albumin, cholesterol or folic acid [139,142]. In a conducted meta-analysis study, it was approximated that the targeting of nanocarriers to the highly enhanced permeability and retention region (EPR) of the tumor is below 1%. This low efficiency is ascribed to physiological obstacles, including cellular barriers, endothelial barriers, clearance by the mononuclear phagocyte system (MPS) and challenges related to endosomal escape [141].

2.4. Novel therapeutic approaches against TNBC

The conventional chemotherapy regimen demonstrates efficacy in the early stages of TNBC but their effectiveness diminishes significantly in advanced stages [30]. Traditional therapeutic approaches have limitations like adverse side effects, limited specificity and chronic toxicities. Additionally, efflux transporters, including the P-gp efflux transporter glycoprotein, pose challenges for anti-cancer drugs like anthracyclines and taxanes [143]. The inadequate targeting, unfavorable prognosis and drug resistance observed with conventional medications for TNBC have spurred scientists' interest in the exploration and development of novel targeted

therapeutics. The suboptimal results linked with TNBC can be attributed to the absence of efficient targeted therapies commonly employed for treating ER+/PR+ and HER2+ breast cancer subtypes. Due to the limited or absent expression of ER, PR, and HER2 receptors, endocrine treatments like aromatase inhibitors and SERMs (selective estrogen receptor modulators), as well as anti-HER2 targeted monoclonal antibody therapies like trastuzumab, prove ineffective in addressing the TNBC. Consequently, standard cytotoxic chemotherapy remains the fundamental approach for systemic therapy in TNBC [144]. Various well-known novel treatment strategies are briefly described in figure 2.2.

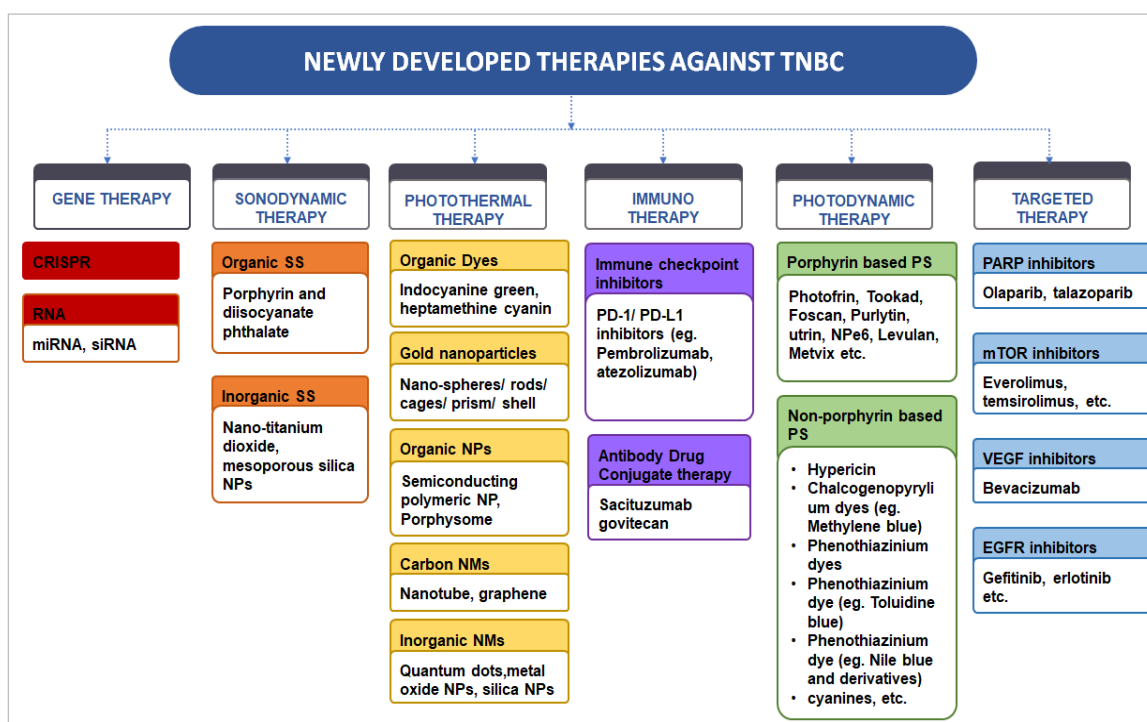


Figure 2.1. Pictorial representation of different novel therapies against TNBC (Adopted from the ref.[19])

2.4.1. VEGF Inhibitor

Vascular endothelial growth factor-A (VEGF) is identified as the primary angiogenic factor in human cancers. Its role involves stimulating angiogenesis, invasion, and enhancing vascular permeability. VEGF facilitates vascular development and angiogenesis in 30-60% of TNBC by binding to the VEGF receptor family member 2 (VEGFR-2) (58,59). VEGF function as a growth factor ligand, binding to tyrosine kinase receptors, namely VEGFR-1 and VEGFR-2, located on endothelial cells. Elevated levels of VEGF expression are correlated with unfavorable clinical outcomes in numerous solid tumors, indicating a potential prognostic marker for disease progression. In a research investigation, it was noted that mutant p53, in conjunction with SWI/SNF, triggers the upregulation of VEGFR-2 expression. Consequently,

targeting mutant p53 could be a viable approach for treating breast cancer. Additionally, JAK2/STAT3, recruited by VEGFR-2, can be targeted to deactivate MYC and SOX2 in breast cancer stem cells [138]. In a recent investigation, conducted by Zhiwen Xu et al., a monoclonal antibody named aNRP2-10 was developed to specifically hinder the binding of VEGF to NRP2. This antibody demonstrated antitumor efficacy without inducing toxicity. The researchers assessed the impact of aNRP2-10 in a TNBC animal model and observed that it was able to inhibit cancer stem cell function and epithelial-to mesenchymal transition. Furthermore, aNRP2-10 sensitized cell lines, organoids, and xenografts to chemotherapy while impeding metastasis by promoting the differentiation of cancer stem cells to a state that is more receptive to chemotherapy and less prone to metastasis. These findings support the rationale for initiating clinical trials aimed at enhancing the response of patients with aggressive tumors to chemotherapy through the use of this monoclonal antibody.

2.4.2. EGFR Inhibitors

The epidermal growth factor receptor (EGFR), a crucial tyrosine kinase receptor within the ErbB family, orchestrates a spectrum of cellular functions encompassing proliferation, differentiation, angiogenesis, metastasis, and the modulation of apoptosis pathways, thereby conferring protection against cell death [139][141]. EGFR serves as a focal point for targeted inventions, including tyrosine kinase inhibitors like gefitinib and monoclonal antibodies such as cetuximab. Remarkably, a synergistic impact emerges when combining gefitinib with docetaxel and carboplatin. Diverse monoclonal antibodies strategically target EGFRs through varied mechanisms, including ligand-receptor blockade, inhibition of dimerization, and disruption of cell survival signaling pathways. This multifaceted approach undergoes the potential for innovative strategies in harnessing EGFR-targeted therapies for enhanced efficacy in cancer treatment. [142]

The antibody-drug conjugate targeting EGFR in TNBC exhibits superior benefits compared to treatments involving solely the antibody or chemotherapy alone. This approach effectively addresses tumor cell proliferation and impedes DNA repair through modulation of both cell and nuclear membranes. Its distinct advantage lies in its selectivity, as it spares normal tissues, thereby minimizing undesirable effects. Additionally, this conjugate facilitates the precise delivery of small molecules, enhancing its therapeutic efficacy (64). In another study, Yingnan Si et al. developed an antibody drug conjugate (ADC) i.e., anti-EGFR- Mertansine using Sulfo-SMCC as linker and evaluated its efficacy and pharmacokinetics in TNBC animal model. It

was found that ADC significantly reduced the tumor growth, and also showed a high circulation stability, ultimately it enhances the pharmacokinetic with longer biological half-life. Therefore, this evidence suggested that the anti-EGFR ADC has great potential against TNBC.

2.4.3. PARP Inhibitors

PARP functions as a crucial protein for initiating and recognizing damage in DNA, specifically for single-strand breaks (SSB). When inhibited, PARP leads to the accumulation of SSBs, consequently triggering the formation of double-strand breaks (DSB). In the realm of innovative oral anticancer drugs, PARP inhibitors exhibit significant promise in the treatment of TNBC, particularly in cases involving BRCA mutations [12]. Currently, there are numerous PARP inhibitors available including veliparib, talizumab, niraparib, olaparib, and rucaparib [67]. Recent studies have proven the efficacy of PARP inhibitors in patients with BRCA linked TNBC. PARP inhibitors have been demonstrated to enhance the characteristics of both anti-tumor and pro-tumor macrophages by reprogramming glucose and lipid metabolism through the sterol regulatory element-binding protein 1 (SREBF1, SREBP1) pathway. Consequently, when PARP inhibitors are coupled with antibodies targeting the colony-stimulating factor 1 receptor (CSF1R), there is a substantial augmentation in both innate and adaptive immune responses [13]. Since that time, there have been noteworthy strides in comprehending the mechanisms that enhance tumor sensitivity to PARP inhibitors, leading to the broader application of PARPi in the treatment of various cancer types (38). Till date, Olaparib (OLA) and Talozoparib are the two PARP agent which have been approved by US-FDA has been approved for management of various subtypes of breast cancer (39). These work by inhibiting ribosylation of the target protein by modulating the transfer of ADP ribose from NAD⁺, which plays an vital role in DNA repair [145].

2.4.4. mTOR inhibitors

In the pathophysiology of TNBC, the activation of mTOR plays a pivotal role in various functions that contribute to carcinogenesis. This pathway involves the targeting of AKT, PI3K or both PI3K and mTOR [67]. While addressing both mTOR and PI3K can enhance efficacy, it also raises concerns about increased toxicity. The pivotal functions of the PI3K/AKT/mTOR (PAM) pathway encompasses cell proliferation, survival, migration and metabolism, with its involvement in malignant cell transformation being a subject of investigation. Ipatasertib, a pan AKT inhibitor targeting phosphorylated AKT, has demonstrated synergistic effects when combined with paclitaxel in preclinical studies. Another

small molecular AKT inhibitor, capivasertib, exhibits activity even in models with alterations in PIK3CA, PTEN and AKT [146]. Additionally, Cretella et al. have highlighted the increased anti-tumor efficacy of CDK4/6 inhibitors by combining mTOR inhibitors with impaired glucose metabolism. Their findings suggest superior efficacy in combining palbocicib and mTOR inhibitors, although further preclinical and clinical studies are necessary to validate these results [147].

2.4.5. Immunotherapy

The aggressive nature of TNBC has spurred the development of targeted immunotherapies. Unlike other subtypes of breast cancer, TNBC has been identified as immunogenic, prompting researchers to explore methods to enhance the host's immune system. TNBC's immunogenic characteristics encompass an increased mutational burden, increased quantities of TIL and elevated expression of programmed death-ligand 1 (PD-L1). The augmented immunogenic mutations prompt tumor cells to generate novel antigens. Existing immunotherapy approaches for eradicating tumor cells include cancer vaccines, immune checkpoint blockades like PD-1/PD-L1 inhibitors and CTLA-4 inhibitors, induction of cytotoxic T-lymphocytes, adoptive cell transfer-based therapy, and the modification of the tumor microenvironment to bolster cytotoxic T lymphocyte activity [148],[149]. Furthermore, Immune Checkpoint inhibitors (ICI) represent a promising frontier in immunotherapy. These cell surface membrane proteins, such as the programmed cell death-1 (PD-1) receptor found on T-cells, belong to the B7 family of checkpoints. Tumour cells express PD-L1, which binds to the PD-1 receptor on T-cells, leading to T-cell inactivation and impeding the immune system's ability to destroy tumors. Researchers have developed various anti-PD-1 antibodies and therapeutic antibodies targeting PD-L1 to disrupt immune regulatory checkpoints. These antibodies activate anti-tumor immune responses by blocking these receptors; preventing T-cell inactivation [150][151]. ICI has opened new avenues in the treatment of TNBC, with several agents undergoing clinical trials. For instance, anti-CTLA-4 mAbs (Ipilimumab) and anti-PD-1 mAbs (atezolizumab, avelumab, durvalumab) have shown promising initial results, but comprehensive clinical trials are essential to establish response rates and assess the long term efficacy of ICIs [152]. J.A. Kagihra et al. successfully developed Nab-paclitaxel and atezolizumab for treating PDL-1 positive metastatic TNBC, a combination that received approval from the FDA and enhanced progression-free survival in TNBC patients [153]. CTLA-4, also known as CD152, is widely expressed in CD8⁺, CD4⁺, FOXP3⁺ and NK cells, playing a regulatory role in T-cell mediated

immune responses. It associates with B7-1 (CD80) and B7-2 (CD-86) ligands on antigen-presenting cells, negatively regulating T-cell activation and suppressing T-cell dependent immune responses. Agents that block CTLA-4 and activate T-cell dependent immune responses have been developed by scientists, although it has been reported that CTLA-4 inhibitors may have more side effects compared to PD-1 inhibitors. Ipilimumab was the first CTLA-4 inhibitor used for melanoma, and Tremelimumab and Ipilimumab are currently under investigation for breast cancer. Researchers have explored other immune checkpoint targets, including BTLA, VISTA, TIM3, LAG3 and CD47 [151],[11]

2.4.6. Gene Therapy

The use of microRNAs (miRNAs) and small interfering RNAs (siRNAs) to silence genes is an evolving and swiftly advancing strategy in the treatment of cancer [154]. This method is employed for both diagnostic and therapeutic objectives (theranostics). The siRNA delivery system has the potential to incorporate imaging agents, such as dextran-coated superparamagnetic nanosized particles, enabling non-invasive real-time visualization of siRNA delivery to the tumor through magnetic resonance imaging (MRI). The use of siRNA labeling in delivery can also assist in monitoring and predicting therapeutic outcome [155]. The effective delivery of siRNA poses a significant challenge due to its susceptibility to degradation by nucleases, and its negative charge make cellular localization challenging [154]. In the study by Alshaer et al. developed nanoparticles guided by aptamers, aiming to target CD-44 in TNBC. The core of these nanoparticles comprised a siRNA-protamine complex, while the shell incorporated an aptamer ligand designed for the specific targeting of CD-44 cells. The outcomes demonstrated that this formulation displayed anti-tumor activity [156]. MicroRNAs (miRNAs) play a pivotal role in the initiation and progression of TNBC, suggesting their potential as diagnostic biomarkers [157]. Generally, tumor cells exhibit a downregulation of miRNAs, although certain miRNAs experience upregulation [158]. Notably, miRNA558 is overexpressed and the cluster miR-17/92, miR-106b, miR-200 family (miR-200a, miR-200b, and miR-200c), miR-155 and miR-21 are highly expressed. In TNBC with lymph node metastasis, analysis of lymph node tissues revealed the expression of six miRNAs: miR-627, miR-125a-5P, let-7g, miR-424, miR-579, and miR-101 [31]. A reported study demonstrated that combination of Orlistat-loaded nanoparticles along with doxorubicin or antisense-miR-21-loaded NPs significantly enhanced the apoptotic impact compared to treatments involving alone doxorubicin, antisense-miR-21-loaded NPs, orlistat-loaded NPs, or free orlistat [159].

2.4.7. PDT

PDT therapy involves photosensitizers, light activatable molecules, near IR light, and oxygen. It comprises of two phases: administration of photosensitizer and light radiation. The incubation period lies between these two stages determining the location of the photosensitizer release, affecting therapy efficacy [79][160]. The photosensitizer is distributed in both normal and tumor cells. However, normal cells eliminate it, whereas tumor cells accumulate it because of morphological changes in tumor cells including impaired vasculature and lymphatic drainage in the tumor cells [161]. Hence, it prevents photosensitizers elimination and leading to tumour cell destruction through increased level ROS which is produced upon activation of photosensitizer to triplet-state and then transferring its energy to molecular oxygen [162]. Near-IR illumination of photosensitizers results in the absorption of photons, forming an unstable singlet stage. This unstable state is stabilized by returning to the ground state through fluorescence or internal conversion. This aids in understanding of the pharmacokinetic profile of photosensitizers in the body. The excited singlet state can also experience intersystem crossing and cause the destruction of tumor tissue through either type 1 or type 2 reactions. Type 1 reactions involve electron or hydrogen abstraction from amino acids or guanine in nucleic acid or NADPH, resulting in a radical anion that donates electrons to oxygen, producing a superoxide anion radical. Type 2 reactions transfer energy to molecular oxygen, resulting in singlet oxygen, a ROS. The type of reaction depends on oxygen, substrate concentration, and photosensitizer type. Type 2 reactions are more prevalent due to higher energy transfer rates [163],[164].

PDT represents a promising treatment strategy for TNBC due to its marginal invasiveness, precise controllability and high accuracy. It is used to treat various cancers, including breast, head and neck, lung, esophageal, oral, and laryngeal cancers. PDT destroys tumor cells via three mechanisms depending on the location of the photosensitizer: direct cell death, targeting vascular effects, and immune reactions. Cell death mechanisms encompasses apoptosis, necrosis, and autophagy, while the other two mechanisms include targeting vascular effects and eliciting immune reactions. Apoptosis occurs when the photosensitizer accumulates in the mitochondria, increasing permeability and releasing cytochrome c, which is an essential factor to activate the caspase-mediated apoptotic pathway. Following PDT damage, released cathepsins induce the cleavage of the proapoptotic protein Bid into t-Bid, leading to the release of cytochrome c and initiation of intrinsic apoptosis. NPe6 has been identified to demonstrate this mechanism. In instances where damage is extensive enough to impair apoptotic pathways

and the photosensitizer is situated in the plasma membrane, necrosis becomes prevalent, resulting in the release of intracellular materials outside the cell and triggering inflammation [163], [165], [166] [167].

Autophagy, a protective mechanism, is induced with low PDT damage to cells. Nevertheless, if the lysosome undergoes damage, the protective capacity of autophagy is surpassed, resulting in cell death. Porphyrins with negative charges, such as phenothiazinium methylene blue, NPe6, were observed to concentrate in the lysosome. Lysosome damage triggers apoptosis and necrosis. In certain cells damaged by PDT, necroptosis is also initiated due to imbalance in intracellular and extracellular homeostasis, influenced by RIPK3 and RIPK1. PDT induces cell damage, leading to both apoptosis and necrosis and the release of DAMPs (damage associated membrane proteins). These DAMPs consist of calreticulin, arachidonic acid, HSP70 and ATP. Tumor antigens bind to heat shock proteins and engage with toll like receptors, activating APC (antigen presenting cells). These cells then present antigen to CD4 helper T-cells, activating cytotoxic CD8+ cells and resulting in the destruction of tumor cells. The destruction of tumors induced by PDT bypasses the resistance mechanisms displayed by tumor cells [164],[167]. In a study, Sun et al. fabricated a multifunctional cationic porphyrin-grafted microbubble carrying HIF 1 alpha siRNA and administered it through ultrasound targeted PDT for treating TNBC. The siHIF cationic porphyrins were transformed into nanoparticles within the body, leading to the specific accumulation of siRNA and porphyrin in cancer tissue. The researchers concluded that this therapeutic approach proves effective in management of TNBC [168].

2.5. Exploiting synthetic lethality of PARP enzyme in TNBC

Poly (ADP-ribose) polymerases (PARPs) are a group of enzymes consisting of at least 18 members. Although distinct genes express these enzymes, they exhibit similarity in a conserved catalytic domain[169]. These enzymes can facilitate the catalysis of ADP-ribose transfer to specific proteins. PARP1 is the most well-studied constituent within this particular family, whereas PARP2 has a tight association with PARP1, sharing a catalytic domain with a 69% similarity[170]. PARP1 and PARP2 play an essential role in the repair of DNA damage, while other members of this protein family are engaged in a variety of cellular activity, such as, cell apoptosis, cell differentiation and proliferation, chromatin functions, and maintenance of genomic integrity[169].

In response to DNA damage PARP is activated along with other DNA-sensing molecules such as DNA-PK, ATM, and p53. The activation of PARP-1 is initiated by DNA breaks, leading to

the breakdown of NAD⁺(nicotinamide adenine dinucleotide) into ADP-ribose and nicotinamide. The ADP-ribose molecule undergoes a series of consecutive additions, forming complex and branched chains denoted as poly (ADP-ribose) (PAR). The aforementioned chains form covalent bonds with acceptor proteins, including histones, DNA repair proteins and PARP-1, establishing an interconnected system around DNA breaks. The PAR structures, which possess a negative charge, function as a structural scaffold that facilitates the recruitment of vital proteins involved in SSBR (single-strand break repair) and BER (base excision repair)[171].

When DNA strand breaks occur, PARP rapidly interacts with them and undergoes self-modification. Consequently, the result is the generation of elongated and branching poly(ADP-ribose) polymers on certain proteins, mainly on the PARP enzyme itself. The aforementioned procedure utilizes NAD⁺ as a substrate and thereby reducing cellular NAD⁺. The altered poly (ADP-ribose) polymerase (PARP), which has an electronegative charge, subsequently dissociates from the ends of the DNA. The process of detachment plays a crucial role in enabling the advancement of DNA repair processes, hence facilitating the efficient restoration of damaged DNA[172].

Since, in TNBC with BRCA1/BRCA2 mutation, tumor cells lack homologous recombination pathway which control the repair of double-strand breaks of DNA. Therefore, the tumor cells become dependent on alternative repair pathways, including PARP-mediated repair. Inhibition of PARP enzyme can lead to accumulation of SSB (single-strand breaks), which progresses to DSB(double-strand breaks) on DNA replication and subsequently on accumulation can lead to genomic instability and tumor cell death[131].

2.6. Role of HPPH and Olaparib in management of TNBC

2.6.1. Photosensitizer: 2-[1-Hexyloxyethyl]-2-devinyl pyropheophorbide-a (HPPH)

PDT is a therapeutic modality based on the principles of photochemistry that has emerged as a minimally invasive method garnering significant attention in recent years as a new therapeutic approach for cancer management [173]. PDT involves the generation of cytotoxic reactive oxygen species through photoexcitation of photosensitizer molecules by specific wavelength of visible light, subsequently resulting in cellular death [174].

In current clinical practices, various photosensitizer molecules, including first-generation photosensitizers like hematoporphyrin derivatives (HpD) and photofrin, a purified form of HpD and second-generation photosensitizer like benzoporphyrin, purpurines, texaphyrins,

protoporphyrin, phthalocyanines, naphthalocyanines and HPPH are in use. Among these HPPH is preferred over other photosensitizers due to its preferential accumulation in tumor cells, ideal absorption and emission properties in the near-infrared region, high efficiency in generating cytotoxic molecules, and long-lasting effects [175]. HPPH (2-[1-Hexyloxyethyl]-2-devinyl pyropheophorbide) -a chlorin -based, lipophilic and second-generation photosensitizer. Photochlor is being developed as a possible therapeutic option for the management of oesophageal cancer. The administration of the substance occurs through the intravenous method. Following intravenous treatment, HPPH has a specific tendency to concentrate inside the cytoplasm of malignant or pre-cancerous cells. The application of laser light induces a photodynamic interaction between HPPH and oxygen, leading to the production of singlet oxygen and cytotoxic free radicals. Consequently, cell death is triggered by the mechanism of free radical-mediated cytotoxicity. Furthermore, this particular treatment is being researched for its potential application in managing SCC (squamous cell carcinoma) of the oral cavity, recurrent SCC of the neck and head, invasive cancer of the oropharynx and larynx, breast cancer, squamous non-small cell lung cancer, adenocarcinoma in Barrett's oesophagus, and basal cell cancer.

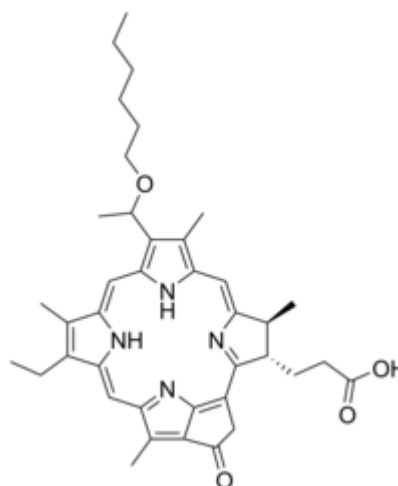
Physiochemical Properties of HPPH

IUPAC Name : 2-1-hexyloxyethyl-2-devinyl pyropheophorbide-a

CAS Registry Number : 149402-51-7

Empirical Formula : C₃₉H₄₈N₄O₄

Structure :



Molecular Weight : 636.837 g·mol⁻¹

Therapeutic Class : Second- Generation Photosensitizer

Appearance : Black solid powder

Solubility	: Soluble in DMSO, not in water
Partition Coefficient (LogP)	: 5.6
Proprietary Name	: Photochlor
Marketed as	: Powder

Limitations associated with HPPH

HPPH has certain limitations including, photoinstability, quick photobleaching, less aqueous solubility, poor pharmacokinetics, and phototoxicity which are severe obstacles against clinical translation of this drug. Therefore, researchers are focusing more on development of novel formulation to overcome the above-mentioned limitations.

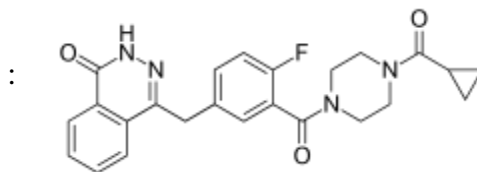
2.6.2. OLA: A selective PARP (Poly (ADP-ribose) polymerase) inhibitor

PARPi (PARP inhibitors) are the novel cancer drugs approved for their precise targeting of the DNA damage response in cancers with BRCA1/2 mutations. It is a highly selective PARP inhibitor, explicitly targeting PARP1 and PARP2. Commercially, it is known as Lynparza, is indicated for treating cancers linked with BRCA gene mutations, with significant anti-tumor activity used in breast cancer with or without a BRCA1/2 mutation which has been used for treatment of various cancers, specifically ovarian and breast cancer. It can kill cancer cells via inhibiting DNA synthesis or ROS induced apoptosis cell death mechanism [176]. The PARP family plays crucial roles in various cellular processes such as transcription regulation, control cell death mechanism and the DNA damage response. PARP1 possesses poly (ADP-ribose) activity and when activated by DNA damage, adds branched PAR chains to facilitate the recruitment of other repair proteins to promote the repair of DNA ssb [177].

Properties of OLA

IUPAC Name	: 4-[[3-[4-(cyclopropanecarbonyl)piperazine-1-carbonyl]-4-fluorophenyl]methyl]-2H-phthalazin-1-one
CAS Registry Number	: 763113-22-0
Empirical Formula	: C ₂₄ H ₂₃ FN ₄ O ₃

Structure



Molecular Weight	: 434.5 g/mol
Therapeutic Class	: Antineoplastic Agent
Appearance	: White to pale yellow crystalline powder
Solubility	: 0.1 mg/mL in aqueous media. Poorly soluble and pH independent
Melting Point	: 206°C
pKa	: 12.07
Partition Coefficient (LogP)	: 1.49
BCS Classification	: Class IV
Proprietary Name	: Lynparza
Marketed as	: 100 mg, 150 mg film-coated tablets. And 50 mg capsules.

Therapeutic Indications of OLA

- The use of OLA is recommended for treating elderly women patients who have been identified with advanced fallopian tube, primary peritoneal or epithelial ovarian cancer. These patients must have either confirmed or suspected detrimental somatic or germline BRCA mutations, and must also be in a state of partially or complete response to platinum-based chemotherapy [178].
- OLA is advised for adult patients dealing with high-risk early breast cancer, exhibiting deleterious or presumed detrimental gBRCAm HER2 negative status. It is recommended for those individuals who have undergone neoadjuvant or adjuvant chemotherapy [179].
- OLA is authorized for the maintenance therapy of adult patients with metastatic pancreatic adenocarcinoma characterized by deleterious or suspected deleterious gBRCAm provided their condition shows no progression after completing at least 16 weeks of initial platinum-based chemotherapy [180].
- The FDA has granted approval for the use of OLA as a kind of maintenance therapy in adult individuals with advanced pancreatic adenocarcinoma. This approval is specifically for patients whose illness has not shown progression for a minimum of 16

weeks after first treatment with a platinum-based chemotherapy regimen. Additionally, these patients must possess deleterious or suspected harmful hereditary BRCA-mutations [10].

Limitations associated with OLA

Olaparib is a promising drug in improving therapeutic outcomes for cancer patients but several limitations are also associated with OLA such as lack of targeting a tumour site, poor bioavailability (12-17%), shorter biological half-life (6-10 h), in vivo instability, and toxicity. Moreover, with the passage of time during the treatment some cancer cells might develop resistance to PARP inhibitors which can subsequently affect the effectiveness of the therapy. Along with above limitations, side effects such as nausea, fatigue, vomiting and anaemia, also generate greater hindrances against its clinical translation. Therefore, researchers are focusing more on development of better delivery approaches to overcome the above-mentioned limitations.

2.6.3. Modulation of PDT action via inhibition PARP enzyme

As already mentioned earlier, PDT has great potential as a viable approach for treating tumor cells due to its notable selectivity. Colocalizing light, oxygen, and photosensitizer produce a significant quantity of reactive oxygen species (ROS) when excited by a laser at a specific wavelength. This phenomenon can cause DNA damage and effectively eradicate cancer cells [181]. However, the repair mechanism shown by tumour cells constraints on the further advancement of photodynamic therapy (PDT) [182]. PDT is impeded by the action of PARP enzyme which is involved in the repair process of DNA by binding to the specific location of single-strand damage on the DNA molecule. These PARP family enzymes have intricacy in the process of PARylation (poly-ADP-ribosylation), whereby they transfer ADP-ribose units from NAD⁺ to proteins that serve as substrates. This process facilitates the repair of DNA SSBs through BER (base excision repair). Administration of PARP inhibitors along with PDT play a synergistic role in the death of the tumour cells as the inhibition of PARP enzyme results in the accumulation of DSBs on DNA replication. Subsequently, this process promotes genomic instability and triggers death in tumour cells [183]. Additionally, it is important to mention that PARP inhibitors have the capacity to induce the inactivation of PARP as well as to effectively sequester PARP at the specific location of DNA damage, ultimately culminating in cellular death [184]. In the absence of adequate repair mechanisms, SSBs can develop into DSBs that are harmful to the cell. The repair of these DSBs necessitates the involvement of BRCA1/2 proteins, which facilitate the homologous recombination (HR) pathways for repair.

Further, the efficacy of PARP inhibitors in producing synthetic lethality is credited to the absence of homologous recombination mechanisms in BRCA-mutated cancer cells [185]. Consequently, the combination of photodynamic treatment (PDT) along with poly (ADP-ribose) polymerase (PARP) has the potential to significantly increase the therapeutic efficacy of PDT. This synergistic approach would intensify DNA damage and hamper the regenerative capacity of tumour cells. Moreover, the development of resistance to photodynamic therapy (PDT) might be facilitated if the tumour tissue is not rapidly eradicated during the first PDT sessions. This poses a challenge to the effectiveness of the treatment, mostly due to the activation of cellular redox defenses and repair mechanisms. The precise mechanism behind photodynamic therapy (PDT) resistance remains elusive; nevertheless, *in vitro* experiments have shown that resistance may arise through activation of the poly (ADP-ribose) polymerase (PARP) damage-repair signaling pathway [186]. Additionally, photodynamic therapy (PDT) not only cause direct harm to the DNA of tumour cells but also to initiate a process known as immunogenic cell death (ICD). In brief, death of the tumor cells triggered by photodynamic therapy have the potential to synthesize a group of death signaling molecules such as DAMPs (damage-associated molecular patterns). These damage-associated molecular patterns can attract APCs (antigen-presenting cells) to engulf and break down tumour cell antigens. This process triggers the activation of T lymphocytes, leading to an immunological response against the tumour [187]. On the other hand, after the administration of PARP inhibitors, elevation in cytoplasmic DNA levels is observed. Increased levels of cytoplasmic DNA, in turn, trigger the activation of the cGAS-STING (cyclic guanosine monophosphate-adenosine monophosphate synthase-interferon gene stimulator) pathway, leading to a sequence of interconnected biochemical responses. These responses lead to the generation of type I interferon as well as other immune mediators. These immune mediators together with DAMPs attract and stimulate APCs to eliminate cancer cells. Hence, the PARP inhibitors play the crucial role to enhance the effectiveness of photodynamic therapy (PDT).

2.7.Role of nanomedicine in TNBC treatment

As mentioned in the earlier section, there has been significant research is going on in developing new therapeutic molecules for the treatment of the TNBC. However, delivering these molecules to the target cells are another challenging as most of these molecules lacks specificity. Being a cytotoxic agent, delivery of these molecules to the normal cells leads to the various side effects. Further, for the optimum therapeutic effect, these drugs need to be

delivered to the target site in the desired rate along with desired pharmacokinetic profile. Over the period of time various drug delivery systems has been developed for the efficient delivery of these chemotherapeutic molecules. Nano-scale delivery carriers not only showed the promising means of efficient delivery of these molecules but also addresses various limitations which has been associated with the chemotherapeutic agents. Nano carriers offer several advantages particularly in the management of cancer, which includes:

- The nanoscale (usually in the range of 1 to 200 nm), showed the increased selectivity towards cancer cells in comparison with normal cells due to the EPR (enhanced permeability and retention) effect. It has been well established that, the tumor cells display increased permeability in their blood vessels due to structural and membranal deformations. This feature provides the selective advantage for the nano scaled carriers to selectively accumulate in the tumor cells compared to the normal cells [143].
- Nano carriers improved therapeutic index by reducing the drug distribution to non-targeted organs and overall distribution in targeted tumor cells, thereby enhancing the overall treatment efficacy [144]
- Nano carriers can be formulated from the polymeric, lipidic or hybrid biomaterials, which provides the further advantages of modulating the property of the nanocarrier system as per the characteristics of the molecules [138],[188]
- The targeting moiety can be efficiently designed in the nano carrier systems for the targeting delivery [140].

2.8. Lipid-Polymer Hybrid nanoparticle: a hybrid strategy for drug delivery

LPHNs are a new class of hybrid lipid-polymer nano-carriers which combines and encompasses more benefits than individual lipidic as well as polymeric systems, including increased drug loading, biomimetic system, superior therapeutics and better release profile. These systems on the basis of structure are classified into four classes: polymer-caged liposomes, monolithic, biomimetic lipid-polymer nanoparticles and core-shell. Polymer-caged liposomes are formed by anchoring polymers on the surface of liposomes. They are primarily used in drug delivery, vaccine adjuvants, gene delivery, RNAi, and diagnostic agent delivery. Researchers are interested in their applicability for both small molecules (chemotherapeutics) and macromolecules (proteins, peptides, and vaccines) due to their unique characteristics. In a monolithic system, polymeric matrix consists of evenly distributed lipids, which together form a core for the loading of hydrophobic molecules. Biomimetic lipid-polymer nanoparticles, also

knowns as erythrocyte membrane-camouflaged nanoparticles are composed of RBC's membrane coated onto the polymeric core. Core-shell type hybrid systems, lipids are layered on polymeric core to generate lipid shells that encircle the polymeric core. These kinds of systems are also altered so that lipids are used to create a central hollow core, which is surrounded by a polymeric shell and then a lipid shell. [139].

Each component of LPHNs has their own unique benefits and importance which can be further improved by controlling the composition of each layer for the required pharmaceutical purposes. The single or multiple lipid layer not only provides sustained drug delivery but also prevents the outward diffusion and burst release of drug which can occur with the polymeric nanoparticles [141]. Additionally, the lipid coating can encapsulate hydrophobic drugs and help drugs pass across the biological barrier, which is frequently a significant barrier to medication delivery to the target site [142]. On the other hand, a core shell structure provides supplementary benefits to the polymeric nanoparticles. A polymeric core can encapsulate hydrophilic drugs and provides mechanical strength, high structural integrity and controlled release advantages to the LPHNs [189]. Furthermore, the outer layer of LPHNs can be surface engineered with ligands or antibodies which helps in recognizing and binding to specific cell, minimizing off target side effects and subsequently enhances efficacy and bioavailability of drugs. Owing to their property to encapsulate both hydrophobic and hydrophilic drugs resulting in increased drug loading capacity and make LPHNs an interesting nano-carrier system [19].

2.9. Surface engineered active targeting moiety for the management of TNBC

2.9.1. Biotin receptor targeting ligands in TNBC

Actively targeted delivery of anticancer drug and photosensitizer is governed by the recognition of the type of receptor expressed on to the surface of breast cancer cells. Receptor-mediated drug delivery approach serves as an important therapeutic strategy in the area of active targeting for delivering actives selectively to cancer cells resulting in improved suppression of tumor growth in comparison to non-targeted drug delivery. Adopting such a tumor-selective strategy could be very helpful in reducing the off-target cytotoxicity associated with the non-selective distribution of chemotherapeutic agents to normal healthy tissues, thereby eliminating unnecessary exposure to normal cells resulting into their lower IC₅₀ values and enhance the therapeutic potential. Amongst various types of receptors overexpressed on breast cancer cells, folate receptor, biotin receptor, transferrin, ICAM1 and EGFR receptors are commonly present with triple-negative breast cancer (TNBC) [12]. Several findings suggested that amongst all the receptor, biotin is showing highly expression due to necessary

for nucleic acids and DNA synthesis. Further, biotin and its substituents are an essential component and required in large quantities for the biosynthesis of amino acid, nucleotides and methylated substances in rapidly proliferating cells. Apart from breast cancers, including ovarian, lung and colorectal. Thus, biotin can be used as a promising targeting site for selective accumulation of actives in cancer cells. For achieving active targeting, functionalized onto the surface of the nanocarrier system. Further, it was hypothesized that coupling this active targeting approach with combination therapy using gene and the cytotoxic drug might serve as a promising approach for effective management of breast cancer, especially, TNBC.

In a study Nosrati et al., prepared the biotin targeted nanoparticle for artemisinin for treatment of breast cancer. The formulation was tested in a TNBC cancer cell line (4T1) mice model, resulting in a significant this formulation significantly increases the accumulation of substances in the tumour and reduction in tumor volume on treatment with biotin decorated micelle compared to non-targeted nanoformulation or free drugs [67]. Furthermore, in another study Mehdizadeh et al. developed a biotin modified PLGA for SN-38 for the treatment of cancer. Results suggested that there was a rapid and selective uptake of biotin decorated PLGA nanoparticle in the cancer cells with enhanced in-vitro tumor activity [13].

2.9.2. Mitochondrial active targeting ligand – triphenylphosphine (TPP) in TNBC

In biological system, mitochondria take part a vital role in the cell's ability to regulate to the changing microenvironments and any pathological changes related to its functions, causing severe array of illnesses, including cancer, diabetes, obesity, atherosclerosis etc. Further, in tumor cell, mitochondria involve in various metabolic pathways such as glucose, glutamine and FA oxidation, for the development and progression of cell. Hence, its dysfunction has been recognized as a possible therapeutic target for TNBC therapy. Now a days, considering all the active targeting strategy, mitochondrial targeting is becoming an evolving field of TNBC management due to promising its outcomes. This targeting strategy provide less adverse effects by preventing its action in non-targeted sites. There are several chemical entities providing mitochondrial targeting such as TPP, pyridinium, or cationic peptides etc. Among all, TPP is the most commonly used as a chemical mitochondrial targeting signal, because it not only non-toxic nature to normal fibroblasts, but also potentially target the CSC propagation. In a research study, Zhang and colleagues created a theranostic system with mitochondrial targeting and aggregation-induced emission (AIE), enabling both targeted imaging and treatment for cancer. They found developed system offering enhanced ROS production against the HeLa and MDA-MB-231 cell line. Also, they observed, combination cancer therapies guided by imaging,

without the need for traditional drug conjugation, which could gain advantages from multifunctional systems that are less prone to developing drug resistance. Therefore, these results suggested that TPP-targeted theranostic system would increase the ROS production and enhanced cancer cell death than the unconjugated nanoparticle.

Taken all together, in order to develop a novel therapy in management of TNBC, the functional status of DNA repair mechanisms has to be taken into account. BRCA1/2 gene is involved in repairing DNA double-strand breaks and mutations in this gene has strong associations with TNBC. BRCA1/2 gene mutation causes faulty DNA repair and subsequently leads to error prone DNA replication, which in turn is believed to be a possible cause of TNBC. Basically, major mechanisms involved in DNA repair includes Non-homologous end joining (NHEJ), Base Excision Repair (BER), Nucleotide exchange repair (NER), Mismatch repair (MMR) and Homologous recombination (HR). These major DNA repair pathways exhibits overlapping function in their mechanisms, which play a crucial role in maintaining the genomic stability even when a defect in either one of these pathways exists. Therefore, TNBC shows resistance mechanisms due to the presence of these alternative DNA repair pathways. Further, among all the novel, PDT can be promising therapeutic strategy to treat the TNBC.

Photodynamic therapy, which is being invested in preclinical and clinical studies has shown potential advantages in TNBC by selectively targeting and killing tumor cells with minimal invasiveness and limited systemic toxicity. In PDT, tumor cells when exposed to light of specific wavelength in the presence of oxygen and photosensitizer induced the generation of reactive oxygen species. The generated ROS led to DNA single-strand breaks. However, if the tumor cells are not eradicated in the first PDT session itself, the repair mechanism shown by PARP enzyme via base excision repair serves hindrance on the further advancement of PDT. Evidence suggests that the inhibition of PARP enzyme by PARP inhibitor not only sequesters PARP at the DNA damage location but also play a synergistic role in facilitating the death of the tumor cells. Therefore, we have used HPPH as a photosensitizer molecule and OLA mediated PARP inhibition to see if there is enhancement in ROS generation and this synergistic combination can overcome the PDT resistance shown by the tumor cells in TNBC. In this research work, we have used HPPH as Photosensitizer for PDT therapy to eradicate the tumor cell via ROS mediated pathway and further, also used Olaparib, a selective PARP inhibitor which can enhance the ROS base apoptosis for cancer cell death. We also evaluated if any possibility of therapeutic synergistic effect or additive effect with combination of these two

drugs for TNBC treatment as PARPi works to resolve the problem associated with PDT resistance. In spite of the advantage of HPPH and OLA, these two molecules have certain limitations including low solubility, poor pharmacokinetics, limited cellular uptake into the target cells, and clinical side effects including DNA damage to the normal cell. Hence, to overcome the pharmacokinetic and pharmacodynamic issues along with adverse events associated with these two drugs; a tumor-targeted drug delivery system will be a possible approach to minimize the toxicity and increase efficacy.

Therefore, in the current research, we have employed a lipid-polymer hybrid nanoparticulate system which is surface-fractionalized with a biotin to impart better efficacy via increasing the site-specific accumulation of HPPH and OLA. Additionally, we also aimed to evaluate if any synergistic antitumoral efficacy exists between these two drugs against TNBC. Finally, we also developed a co-encapsulated HPPH and OLA LPHNs which is decorated with 2-different class chemical ligands (i.e., mitochondrial targeting ligand, and Biotin receptor targeting) to improve the therapeutic efficacy along with minimum toxicity.



GAP IN EXSISTING RESEARCH AND OBJECTIVES



Gaps in existing research and hypothesis

3.1. The Gap in Existing Research

Several studies stated that lack of expression of surface receptor such as ER, PR or HER2 proteins leads to development of TNBC. The majority of TNBC cases is because of mutation in BRCA. In spite of several therapeutic strategies, an effective management for complete recovery from TNBC seems to be far away. Till date, only available therapies for TNBC are chemotherapy but it has several limitations like non-selective targeting, resistance issue due to efflux transporter and severe systemic toxicity. Hence, research has moved forward to find novel drugs to counter chemoresistance and decrease the risks associated with anti-cancer drugs. Thus, discovering new therapeutic approach is an unmet need for efficient clinical management of TNBC.

In this regard, HPPH (PDT) is getting much attention as it is a localized and non-invasive treatment method that has undergone exploration for potential benefits in cancer therapy. This photosensitizer (HPPH) accumulates in cancer cell and on an exposure to a particular wavelength of light, generate reactive oxygen species (ROS) which can eventually kill cancer cell. However, HPPH has certain limitations which includes aggregation in physiological condition, quick photobleaching, low solubility, limited cellular uptake into the target cells, and phototoxic side effects including DNA damage to the normal cell. Along with that, the clinical challenges i.e., development of resistance to PDT might be facilitated if the tumour tissue is not rapidly eradicated during the first PDT sessions. This poses a challenge to the effectiveness of the treatment, mostly due to the activation of cellular redox defenses and repair mechanisms. The precise mechanism behind PDT resistance remains elusive; nevertheless, in vitro experiments have shown that resistance may arise through activation of the PARP damage-repair signaling pathway. Hence, the inhibition of PARP may possibly augment the PDT response. Therefore, the co-administration of a PARP inhibitor (PARPi) along with PDT may exert a synergistic or additive role in the killing of tumour cells. Amongst all the PARPi, Olaparib (OLA) is one of the US-FDA approved drug for breast cancer with or without a BRCA1/2 mutation which acts by inhibiting DNA synthesis and ROS induced apoptosis. it is important to mention that OLA have not only the capacity to induce the inactivation of PARP but also to effectively sequester PARP at the specific location of DNA damage, ultimately culminating in cellular death. While, OLA might be possibly encouraging the efficiency of PDT but it has certain major limitations in effective clinical translation. These includes less aqueous solubility, stability issue in biological system along with the poor pharmacokinetic profile (low bioavailability, low biological half-life, etc.). Further, these overall drawbacks of

both HPPH and OLA can be circumvented by the employment of advanced targeted drug delivery system for the effective management of TNBC. Therefore, there is an unmet need of development novel therapeutic strategies to improve the drug availability at tumor site and alternatively which can encourage anti-tumor activity. On this basis, the surface modified active targeted nanocarrier systems signifies a promising strategy for enhancing the delivery and efficacy of HPPH and OLA. Furthermore, their combination approach i.e., co-delivery of HPPH and OLA may synergies their therapeutic benefits. However, still there is still a significant gap in the research regarding the optimal formulation and design of nanocarrier systems for efficient HPPH delivery for the management TNBC.

3.2. Objectives of the proposed research

On basis of identified gaps in the existing research, the present research work was focused on preparation and evaluation of nano-based platform i.e., surface modified lipid-polymer hybrid nanoparticles (LPHNs) for delivery of HPPH, OLA and their combination of HPPH and OLA for the efficient management of TNBC. The objective of the proposed research was categorized and prioritized into the areas that require further investigation and development.

Objective 1: To investigate the therapeutic potential and pharmacokinetic studies of HPPH and OLA-alone and in combination using in vitro and in vivo studies

Objective 2: To improve the efficacy, biodistribution and circumvent pharmacokinetic limitations of HPPH and OLA by developing tumor targeted lipid-polymer hybrid nanoparticles

Objective 3: To develop and characterize HPPH and OLA co-loaded tumor targeted lipid-polymer hybrid nanoparticle and evaluate its therapeutic efficacy, pharmacokinetic and biodistribution advantages in TNBC condition.



MATERIALS AND METHODS



4. Materials and Methods

4.1. Materials used for the Experiments

4.1.1. *In vitro* Cell line

4T1 tumour cell lines were procured from National Centre for Cell Science (NCCS), Pune, India. Further, the cell line was cultured in DMEM/F12 (Dulbecco's Modified Eagle's Medium/ Ham's F-12) which contains 10% fetal bovine serum (FBS) and 1ml/L of antibiotics (penicillin - streptomycin) solution. After 70% confluency, cells were passaged in above mentioned media and incubated at 37°C and 5% CO₂.

4.1.2. *Animals*

All experimental animals (Balb/c; females; 4-6 weeks; 20–30 g) were obtained from the central animal facility, BITS-Pilani, Pilani campus, India (417/PO/ReBi/2001/CPCSEA) to conduct the in-vivo study. The animals were housed in polyacrylic cage under optimized conditions (2 h light/dark cycle, 22 ± 1°C with 60% relative humidity) with normal feed and purified water ad libitum at the central animal facility. All in-vivo experiments were conducted as per Institutional Animal Ethic Committee (IAEC) guidelines of BITS-Pilani, Pilani campus, Rajasthan, India (Approved protocol number: IAEC/RES/23/09).

4.1.3. *Chemicals and reagents*

HPPH was obtained as a gift sample from Chemical Biology Laboratory, NCI-NIH Frederick, MD, USA. OLA was provided by Cipla Pharmaceutical Pvt. Ltd. (Mumbai, India) as a generous gift sample. The solvent and reagents including HPLC/LC-MS/MS grade methanol, acetonitrile, dichloromethane, Glacial acetic acid and ammonium acetate were purchased from Merck, Limited, Mumbai, India. 1, 2-bis (10, 12 tricosadiynoyl)-sn-glycero-3-phosphocholine (DC₈₉PC) was procured from Avanti® Polar Lipids, USA. NH₂-PEG-PLGA (Mn. 10-15 kDa) and Stearylamine were obtained from Sigma-Aldrich, Mumbai, India. Nitrocellulose Membrane Filter (0.22µm) was acquired from Merck Limited (Mumbai, India). Milli-Q water (Deionized) was collected from in-house Millipore Direct-Q ultra-pure water system (Millipore, Bedford, USA). All other chemicals were acquired with an analytical standard grade from authorized vendor.

4.1.4. Instrument / Equipment used

All the instruments /equipment used in the present research work were mentioned in Table. 4.1.

Table 4.1: List of instruments/ equipment with manufacturer's name used to conduct the experiments.

Instrument / Equipment name	Manufacture's/ Company name
Ultrasonic microtip processor	: Vibra-Cell™, Sonics®, USA
Magnetic stirrer with a hot plate and temperature controller	: Tarsons, India or Remi, India
Rota vacuum evaporator	: Rotavapor R210, Buchi, Switzerland
Ultrasonic bath sonicator	: Toshiba, India
Temperature-controlled centrifuge	: Eppendorf biotech company, Germany
Ultra-centrifuge, Freezer (-20 °C, -80 °C), CO ₂ incubator, Biosafety cabinet	: Thermo Scientific, USA
Triad Freeze Dry System	: Labconco, USA
Malvern Zetasizer, nanoZS	: Malvern, UK
Field emission Scanning microscope	: FEI limited, USA
Confocal Laser Scanning Microscope	: Carl Zeiss
High Resolution-Transmission	: Technai FEI, USA
Inverted microscope	: Zeiss, India
Microplate reader	: Bio Tek ELXS0, Epoch
UV spectrophotometer	: UV-1800 Shimadzu, Japan
Bruker alpha-one FTIR	: Bruker Optik, Germany
DSC-60 plus	: Shimadzu, Kyoto, Japan
Centrifuge	: Eppendorf
ELISA Plate reader	: Bio Tek, Agilent, USA
High-performance liquid chromatography	: Shimadzu, Kyoto, Japan
Liquid chromatography-mass spectrometry	: Waters Corporation, USA

4.1.5. Software used

All the software used in the research work were mentioned in Table. 4.2.

Table 4.2: List of software used to conduct the experiments

Software	Company Name
Origin	: Origin Lab Corporation, USA
Phoenix Win Nolin	: Certera™ Pharsight, USA
Graph Pad Prism	: Dotmatics, California
Flow Cytometry	: Beckman Coulter Life Sciences, USA

Methods

4.2. Analytical development for estimation of HPPH using RP-HPLC

4.2.1. Instrumentation and Chromatographic condition

The analytical method development was performed using a RP-HPLC system (Shimadzu LC-2010HT HPLC, Japan). The data acquisition and the data integration were recorded using Lab

solution software (Shimadzu Corporation, Japan). The chromatographic separation of HPPH was done at ambient temperature using two different columns i.e., Durashell C18 (250×4.6 mm i.d., 5 µm particle size) column and X Bridge™ Shield RP 18 (50×4.6 mm i.d, 5 µm particle size) column. Furthermore, elution systems of analytes were done with the two mobile phase of ACN–ammonium acetate buffer (pH: 4.0) and sodium phosphate buffer (pH: 4.0) in an isocratic mode with a ratio of 80:20 (v/v) at a flow rate of 1 mL/min for the analysis. The analyte was monitored at 406 nm. The sample temperature for this method was maintained at ambient temperature(25°C) and 20 µL of injection volume was kept for the sample analysis.

4.2.2 Preparation of stock and working standard solution

Primary stock solutions of 1 mg/mL HPPH were prepared in ACN. The aliquots of the reference compound were taken from primary stock solutions with suitable dilution by using diluent i.e., ACN to obtain the final calibration standard of 50-2000 ng/mL of HPPH. Further, quality control (QC) samples at four different concentrations (75 ng/mL as LQC, 300 ng/mL as MQC 1, 900 ng/mL as MQC 2, and 1800 ng/mL as HQC) were also separately made in four replicates, independent of the calibration standards. Quality control standard and unknown samples were determined by using the calibration curve to obtain the concentrations of the respective analytes. The standard solutions were analyzed and chromatograms were recorded using LC solution software[190].

4.2.3 Method validation of HPPH

All the validation parameter such as system suitability test, selectivity, specificity, linearity, accuracy, precision, sensitivity and robustness were conducted as per the International Conference on Harmonization (ICH) guidelines Q2 (R1)[190,191].

4.2.3.1 System suitability test

This system suitability test was applied to ensure the instrument suitability for the chromatographic conditions. This study was performed using six injections of specific standard solutions of standard (MQC 2: 900 ng/mL). The obtained chromatograms were used for the calculation of different system suitability parameters such as peak symmetry, % relative standard deviation (% RSD), resolution, and theoretical plates. Moreover, the specificity of HPPH was also performed to verify different parameters like column efficiency, resolution, retention time, and peak tailing of the chromatographic system[190–192].

4.2.3.2 Specificity

The specificity study for the developed method was studied by examining HPPH in the presence of different excipients such as lipid, polymer, surfactant and or solvents. Briefly,

Blank NP were prepared and added to the solvent (Acetonitrile,) containing a known amount of HPPH. The above sample was vortexed properly for 10 min and centrifuged with $5018\times g$ for 10 min. Afterward, supernatant was analyzed using the developed RP-HPLC-UV method for HPPH[193].

4.2.3.3 Linearity and range

The linearity for HPPH was performed with six times at different concentration points including 50, 100, 200, 400, 800, 1000, 1500 and 2000 ng/mL. The peak area response of all the concentrations were recorded and calibration curves were plotted between the peak area response versus concentration[194,195].

4.2.3.4 Accuracy and precision

Accuracy and precision (intra-batch and inter-batch) of the developed method were performed within five days at four different quality control levels of concentration i.e., lower quality control (LQC), medium quality control 1 (MQC 1), medium quality control 2 (MQC 2), and high-quality control (HQC) of HPPH. The accuracy and precision were calculated in terms of %RSD and %bias as per the analytical regulatory guidelines[193,196,197].

4.2.3.5 Sensitivity

Based on signal-to-noise ratio (S/N) of the response of an analyte, LOD and LOQ was calculated for the determination of sensitivity of HPPH. According to ICH Q2 (R1) guidelines, the S/N ratio should be greater than 3 for the limit of detection (LOD) and greater than 10 for the lower limit of quantification (LOQ).

4.2.3.6 Robustness

The three different parameters including the effect of flow rate, the effect of mobile phase ratio, and pH of the buffer were used for the determination of robustness of method[198,199]. Moreover, the effect of flow rate was studied at 0.8 mL/min and 1.2 mL/min instead of 1.0 mL/min. The effect of mobile phase composition was assessed at (ACN: 10 mM ammonium acetate: 85:15 v/v) and (ACN:10 mM ammonium acetate 75:25, v/v) instead of (ACN:10 mM ammonium acetate 80:20, v/v). Consequently, pH was also determined with two different values (3.8 and 4.2) instead of the optimized value i.e., pH 4.0 at the flow rate of 1 mL/min. The %RSD of robustness testing under these conditions was calculated as per regulatory guidelines[192].

4.2.3.7 Stability studies of the developed analytical method

The stability of the HPPH was studied by exposing the sample to different storage conditions. Stability studies were performed with different conditions such as bench-top stability (7 hr.),

auto-sampler stability (24 hr.), short-term stability (14 days), stock solution stability (10 days), and long-term storage (180 days) for HPPH as per the international standard analytical guideline. These studies were conducted in three replicates at four different QC levels (LQC, MQC1, MQC2, and HQC). All stability studies were compared against a freshly prepared calibration curve [190–192].

4.2.3.8 Forced degradation studies

A standard drug solution of 1 mg/mL was prepared by adding 5 mg of the drug into 5 mL of ACN. Further, aliquots of 500 ng/mL of HPPH were prepared from standard stock solution using ACN as the diluent and used for forced degradation studies. In brief, a drug solution of 500 ng/mL of HPPH was dissolved into 1 mL of the 1N HCl and the same procedure was also followed for 1N NaOH. Then both the solution was incubated for 1.5 h in a rotary shaker under ambient conditions and evaluated for acidic and alkaline degradation. For the oxidative study of HPPH, 30% w/v of hydrogen peroxide (1 mL) was added to 1 mL of 500 ng/mL of HPPH and further, the sample was incubated for 15 min at ambient temperature. For thermal degradation, the drug solution was exposed to 80° C for 5 h in a hot air oven. Similarly, the stock solution was exposed to direct sunlight for 20 h as per the photo-degradation study as described elsewhere[200–203]. The analysis was performed in three replicates of each sample. All the samples were analyzed using developed RP-HPLC-UV method, and the data was recorded using LC solution software[197,204,205].

4.3 Analytical Method for estimation of OLA using RP-HPLC

4.3.1 Instrumentation and Chromatographic Condition

A simple, and reliable method for OLA was developed using Shimadzu RP-HPLC system coupled with an autosampler and PDA detector was utilized for the analysis. Chromatographically, the elution was achieved on Water Xbridge™ RP-18 column (4.6 x 50 mm). Furthermore, elution systems of analytes are done with the mobile phase of acetonitrile–ammonium acetate buffer in an isocratic mode with a ratio of 30:70 (v/v) at a flow rate of 1 mL/min for the analysis. The analyte was monitored at 269 nm. The sample temperature for this method was maintained at ambient temperature (25° C) and 20 µL of injection volume was kept for the sample analysis. Initially, the baseline correction in RP-HPLC system was performed by equilibration of system for 20 min before analysis of the samples. The mixture of methanol and water (50:50) was utilized as rinsing of solution. All the data acquisition, recording, interpretation and reporting were done by LC solution software (version 1.22 SP1).

4.3.2 Preparation of stock solution, calibration standards and quality control samples

A primary stock solution at concentration of 1 mg/mL was prepared for OLA by dissolving 1 mg of OLA in 1 mL of HPLC grade methanol. Further, the calibration range 50-2000ng/mL was prepared with 8 different point of calibration standard i.e., 50,100,200,400,800,1000,1500 and 2000 ng/mL were prepared from primary sock solution with appropriate dilution. Likewise, five different quality control samples (QC sample) were also prepared from primary stock solution i.e., 50 ng/mL for LLOQ, 75 ng/mL for LQC, and 300 ng/mL for MQC1, 900 ng/mL for MQC2 and 1800 ng/mL for HQC[192].

4.3.3 Method validation of OLA

The assay validation for developed method was done as per the ICH Q2 (R1) guidelines. The various parameters of validation such as specificity, selectivity, accuracy, precision, robustness and stability were studied below[206].

4.3.3.1 Specificity

The Specificity was carried out at MQC2 level in presences of different excipient which were utilized during fabrication of nanoparticle[192,206,207].

4.3.3.2 System suitability Test

System suitability test was performed at six repeat injection at MQC2 level. The system performance was verified as per guideline with respect to various system-based parameters such as tailing factor, theoretical plate numbers and HETP[208].

4.3.3.3 Calibration curve and linearity

The linearity for OLA was carried out for a range of 50-2000 µg/mL. The calibration curve was plotted between calibration standards concentration (µg/mL) on X-axis against peak area response (mAU) on Y-axis, expressed by the equation $y = mx + c$, where m is slope and c is intercept[209–212].

4.3.3.4 Accuracy and precision

Both intra-day and inter-day analysis was performed for accuracy and precision with five different QC level (LLOQ, LQC, MQC1, MQC2, and HQC), in four replicates. For the data interpretation, %Bias was utilized for expression of accuracy. Whereas %RSD were utilized to describe the precision respectively. According to standard guidelines, accuracy and precision said to be pass, if both % bias and % RSD fall within the range of $\pm 2\%$ [200,209–212].

4.3.3.5 Sensitivity: Limit of detection (LOD) and limit of quantitation (LOQ)

The sensitivity of OLA was expressed in term of LOD and LOQ. Based on the S/N ratio, these two parameters was calculated as per ICH Q2(R1) guidelines. As per the guidelines, the LOD

should be 3 times higher S/N ratio and LOQ should be 10 times higher than signal to noise ratio, respectively[190,191,213].

4.3.3.6 Robustness

The robustness was carried out with three parameters i.e., slight change in pH, flow rate and mobile phase composition[190,191,213]. For pH, there are two different pH i.e., 4 and 4.4 was performed against pH 4.2 Likewise; in case of flow rate, two different flow rates i.e., 1.2, and 0.8 mL/min was used at mobile phase composition ACN: 10mM ammonium acetate of ratio 30:70 (% v/v). Likewise, another parameter i.e., instead of 60:40 ratio of mobile phase, samples were analyzed at two different mobile phase composition (ACN:10mM ammonium acetate pH 4.2 (% v/v) i.e., 25:75, and 35:65, respectively at flow rate of 1.0 mL/min.

4.3.3.7 Stability studies

The stability of the OLA was studied by exposing the sample to different storage conditions. Stability studies were performed with different conditions such as bench-top stability(7hr), auto-sampler stability(24hr), short-term stability (14 days), stock solution stability (10 days), and long-term storage (180 days) for OLA as per the international standard analytical guideline. These studies were conducted in three replicates at four different QC levels (LQC, MQC1, MQC2, and HQC). All stability studies were compared against a freshly prepared calibration curve. As per the ICH Q2 (R1) guideline, the acceptance criteria of the stability sample should be within the ± 2 %RSD[214].

4.4. Simultaneous analytical method development and validation for HPPH and OLA using LC-MS/MS

4.4.1 Instrumentation and Chromatographic condition

The sample analysis was conducted using the UPLC-MS/MS system (Waters, USA) The Instrument control, peak detection, and integration were carried out using Mass lynx software. The chromatographic separation was attained using BEH LC column (Dim. 150*3, particle size: 2.6 μ) and mobile phase mixture consisted of Acetonitrile: Methanol: 5mM Ammonium acetate with 0.1 % formic acid (85:10:05, v/v) at a flow rate of 0.350 mL/min. Injection volume was kept 10 μ L. Rinsing solution of methanol: water (50:50) was used. The sample temperature for this method was maintained at 25 °C and injection volume was 20 μ L respectively.

4.4.2 Preparation of stock and working standard solution

Primary stock solutions of 1mg/mL HPPH and OLA were prepared in acetonitrile. Aliquots of HPPH and OLA were taken from primary stock solutions with suitable dilution by using mobile phase to obtain final concentrations of 1-200 ng/mL of HPPH and OLA. Likewise, four

different quality control samples (QC sample) were prepared from primary stock solution i.e., 2 ng/mL for LQC, 15 ng/mL for MQC1, 90 ng/mL for MQC2, and 180 ng/mL for HQC[195].

4.4.3 Method validation

All the method validation parameters such as accuracy, linearity, precision, detection limit, quantification limit and robustness were validated as per the International Conference on Harmonization (ICH) guidelines Q2(R1) [198].

4.4.3.1 System suitability

This system suitability test was conducted to ensure whether the instrumentation facility is suitable for analysis or not. This assay was executed for six repeat injections at MQC level for both HPPH and OLA. The peak area response and retention time of the both compounds were recorded. As per the guidelines, the %RSD should be less than 1% for retention time (RT) and 2.0% for area response of OLA and HPPH[190,191,195].

4.4.3.2 Linearity and range

The linearity for both HPPH and OLA was performed in the range of 1.56-200ng/ ml. The calibration curves were plotted using Area response against calibration standard concentration. Thereafter, regression equation and correlation coefficient were obtained from the calibration curve[190,209,215,216].

4.4.3.3 Accuracy and precision

Accuracy and precision (Intra- and inter analysis) of the developed method were carried out at four different levels of concentration i.e., LQC, MQC1, MQC2 and HQC. Both accuracy and precision were expressed in %Bias and %RSD respectively as per the analytical regulatory guidelines[190,209,215,216].

4.4.3.4 Sensitivity

Based on signal to noise ratio (S/N) of the response of an analytes, sensitivity was calculated and expressed in term of limit of detection (LOD) and limit of quantification (LOQ). As per the guidelines, LOD should be three-time greater of S/N ratio and similarly, LOQ should be 10 time greater from S/N value[209,215].

4.4.3.5 Robustness

The robustness analysis of this developed method was done at 4-QC level for 4 replicates by two different analysts. The %RSD of robustness testing under these conditions was calculated as per regulatory guidelines.

4.4.3.6 Stability studies

The stability of the both OLA and HPPH was studied by different storage conditions. Briefly, Stability studies sample were subjected to six parameter such as bench-top stability(7hr), auto-sampler stability(24hr), short-term stability (14 days), stock solution stability (10 days), and long-term storage (180 days) for HPPH and OLA as per the international standard analytical guideline. These were conducted for four different QC levels (LQC, MQC1, MQC2, and HQC) in triplicate manner. All stability parameter were compared against a freshly prepared calibration curve. As per the guideline, the acceptance criteria of the stability sample should be within the ± 2 %RSD[190].

4.5 LC-MS/MS based simultaneous bioanalytical method of HPPH and OLA using mice plasma

4.5.1 Instrumentation and chromatographic condition

The analysis was performed using the UPLC-MS/MS system (Waters, USA), coupled with Waters UPLC and Xevo TQD MS system. Further, the bioanalytical method for HPPH and OLA were developed using UPLC-MS/MS (ACQUITY UPLCTM H Class, Waters, Manchester, UK). A Xevo TQD tandem quadrupole mass spectrometer coupled with an orthogonal Z-spray TM electrospray ionization (ESI) source was employed for analysis of these two analytes. The Mass Lynx 4.1 software was utilised for Instrument control, peak detection and integration. The chromatographic separation was attained in ACQUITY UPLC®BEH Shield RP column (150mm*2.1, 1.7 μ m IDM) with the mobile phase mixture consisting of Acetonitrile: Methanol: 0.1% Formic acid in 5mM Ammonium acetate (87:10:03, v/v) at an isocratic flow rate of 0.350 mL/min.

4.5.2 Calibration standard and quality control sample preparation

A primary stock solution of HPPH and OLA were prepared individually in methanol/ACN at concentration 1 mg/ml for CS and QC sample as well. Further, standard working solutions were prepared by serial dilution with diluent (mobile phase). A mixed working solution of 5 μ g/mL of OLA and HPPH was prepared by diluting the standard working solution with pooled mice plasma (spiked 2%) to obtain the desired concentration of 1, 3, 10, 20, 40, 80, 160 and 320ng/ml for the calibration standard. In the same way, five different QCs sample such as LLOQ, LQC, MQC1, MQC2 and HQC was also prepared at the 1.05ng/ml, 2ng/ml, 50 ng/ml,100ng/ml and 300ng/ml respectively. Further, a stock solution of 1mg/ml of docetaxel was prepared using methanol and further, a fix concentration of 200ng/ml was used as internal

standard for bioanalysis. All the stock solution prepared was stored at -20°C till further use[217].

4.5.3 Collection of plasma

The blood was collected from Balb/c mice via retro-orbital plexus and transferred into an anticoagulant (10% K₂EDTA) containing 15 mL disposable tubes. Further, it was centrifuged at 10,000 rpm for 10 minutes. The supernatant plasma was collected and stored at -80°C till further analysis.

4.5.4 Sample processing and optimization

The sample processing was carried out using different extraction techniques such as protein precipitation (PPE), Solid Phase Extraction (SPE) and Liquid-liquid extraction (LLE). In protein precipitation technique, we have used organic solvent like methanol, acetonitrile, and sodium sulphate for the extraction. Furthermore, in liquid-liquid extraction, we have tried with solvent like n-hexane, ethyl acetate, diethyl ether and TBME. Finally, liquid-liquid extraction method with diethyl ether was selected for the sample preparation as it shows no matrix interference with high recovery. Briefly, 94 µL of pooled mice plasma, 2 µL of specific analytes and 2 µL of IS (Docetaxel) was spiked and vortexed for 5 min on vortexer (Spinix Tarsons, India), then 1.8 µL of diethyl ether was added, again vortexed for 8 min and subsequently centrifuged for 10 min at 7000 rpm on the centrifuge. The supernatant (1.6mL) was transferred to the 1.5 mL Eppendorf tube and evaporated to dryness under a nitrogen dryer. The residue was reconstituted in 100 µL of the reconstitution solvent (Methanol) and 10 µL was injected onto LC-MS/MS. Likewise, the same procedure was followed for Blank and treated plasma sample. The Concentration of analytes in plasma i.e., treated plasma sample was calculated from standard calibration curve (1-320 ng/mL).

4.5.5 Bioanalytical method validation for HPPH and OLA

The developed bioanalytical method for both OLA and HPPH was validated as per US-FDA guidelines in terms of different parameters such as system suitability, selectivity, sensitivity, linearity, accuracy, precision, matrix effect, carryover effect, dilution integrity, and stability [217,218]. A brief detail related to different validation parameters have been shown below.

4.5.5.1 System suitability

The system suitability test was estimated using six injections of sample at MQC1 level (100 ng/mL) The % RSD for the area ratio response (Drug/IS) and the retention time was observed. As per the regulatory guidelines, the %RSD should be less than 1% for retention time (RT) and 2.0% for area ratio of OLA and HPPH[219,220].

4.5.5.2 Selectivity

For the selectivity analysis, six lots of different pooled plasma i.e., four normal plasma, one hemolytic plasma, and one lipoemic plasma were selected and spiked with drug combination and IS. According to US-FDA guidelines, the method was considered to be specific and selective when there is no interference peak of the endogenous matrix at the analyte and IS retention time (RT), and the mean response of analytes in blank plasma should be less than 20% of LLOQ response and less than 5% of the mean response at of IS[217–220].

4.5.5.3 Carry over effect

The carryover effect was performed by analyzing the sample set of plasma blank, ULOQ, and LLOQ. As per the guidelines, plasma blank sample after ULOQ sample should be within $\pm 20\%$ of LLOQ[221,222].

4.5.5.4 Calibration curve and linearity range

The calibration curve was performed at eight different standard concentration with linearity ranging from 1-320ng/ml. The calibration equation was calculated by plotting a graph between peak area ratio response and calibration standard concentration. As per guidelines, at least 70% of calibration standards should fall on the acceptance limit of $\pm 15\%$ RSD (for LLOQ, $\pm 20\%$ CV acceptance criteria) of its nominal value[221,223].

4.5.5.5 Accuracy and precision

Both Intra-day and inter-day were performed with six replicates of Five different concentrations (LLOQ, LQC, MQC1, MQC2 HQC) for accuracy and precision. The accuracy and precision should be expressed in term of %RSD and %Bias as per guidelines[223].

4.5.5.6 Matrix effect

The matrix effect was performed to evaluate the interferences of biometrics with respect to ion suppression and ion enhancement. Three sets of QC samples (LQC, MQC1, MQC2 and HQC) were analyzed. The matrix effect is said to be passed if %RSD of QC sample was within $\pm 15\%$ of true concentration[224].

4.5.5.7 Dilution integrity

The dilution integrity was performed at 4 times higher than the ULOQ concentration. Briefly, the analytes concentration of 1200 ng/mL was processed in mice blank plasma. Further, processed samples were estimated against freshly calibration curve. The dilution integrity assay is said to be passed if, the value of %RSD and % Bias are within $\pm 15\%$ from the nominal value [225]

4.5.5.8 Robustness

The robustness of this developed method was performed with 4-QC level (LQC, MQC1, MQC2, and HQC) against different operators as per international standard guidelines[226,227].

4.5.5.9 Stability studies

The stability study was performed for both OLA and HPPH at six replicates with four as per the guidelines with respect to five different conditions i.e. Bench-top(7hr) Autosampler stability(24hr), short-term stability (14 days), freeze-thaw cycles (4-cycle; 48hr) and long-term stability (180 days). All the stability samples were processed and quantified against calibration curve and the obtained was compared with the peak area ratio response of freshly prepared QC samples. The study is said to be passed if % RSD of QCs sample will meet within the acceptance limit i.e., $\pm 15\%$ from the true concentration[228].

4.6 Synthesis and characterization of amphiphilic polymer and mitochondrial targeted lipid

4.6.1 Synthesis and characterisation of Biotin-PEG-PLGA

The carboxylic group of the biotin was activated using DCC and NHS as per previously reported method with slight modification [229]. The activated biotin, i.e., Biotin-NHS was further used for the conjugation to NH_2 -PEG-PLGA. The Biotin-PEG-PLGA copolymer was synthesized by conjugation of Biotin-NHS and NH_2 -PEG-PLGA (Figure 1).

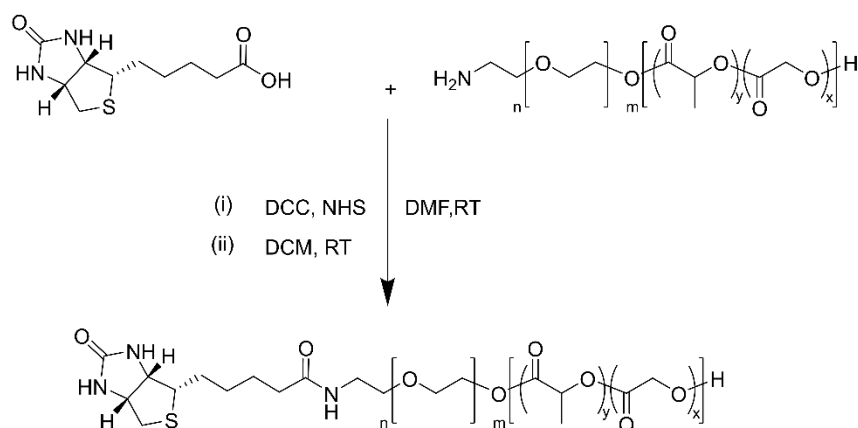


Figure 4.1: Synthesis scheme for Biotin-PEG-PLGA

In brief, NH₂-PEG-PLGA (400 mg, 0.008 mmol) was dissolved in 3 ml of DCM and added to activated Biotin (Biotin-NHS) solution. The reaction was kept for 48hr at room temperature under stirring. The product was collected and purified using chilled diethyl. The solvent was removed *in vacuo*. White-yellowish powder product was obtained.

4.6.2 Synthesis and characterisation of of Linoleic acid-ss-TPP

The novel *Linoleic acid-ss-TPP* was synthesized in two steps based on EDC/NHS coupling. Cysteamine hydrochloride (5mmol, 1.126 mg) was reacted with linoleic acid (1mmol, 333 μ L) in the presence of 1-ethyl-3-(3-dimethylaminopropyl)carbodiimide/*N*-hydroxysuccinimide(EDC/NHS)(5mmol,955mg/575.45mg) and triethylamine (TEA) (28 μ L), taking dimethylformamide (DMF) as solvent under inert conditions to get **R01**, which was further reacted with triphenyl phosphine (TPP) to get **R02** using similar conditions as shown in **FIG. 4** wherein (a) = Room temperature, 48h, EDC/NHS, DMF, TEA. **R02** denotes linoleic acid-ss-TPP. Further the final product was characterized using H-NMR and LC-MS/MS.

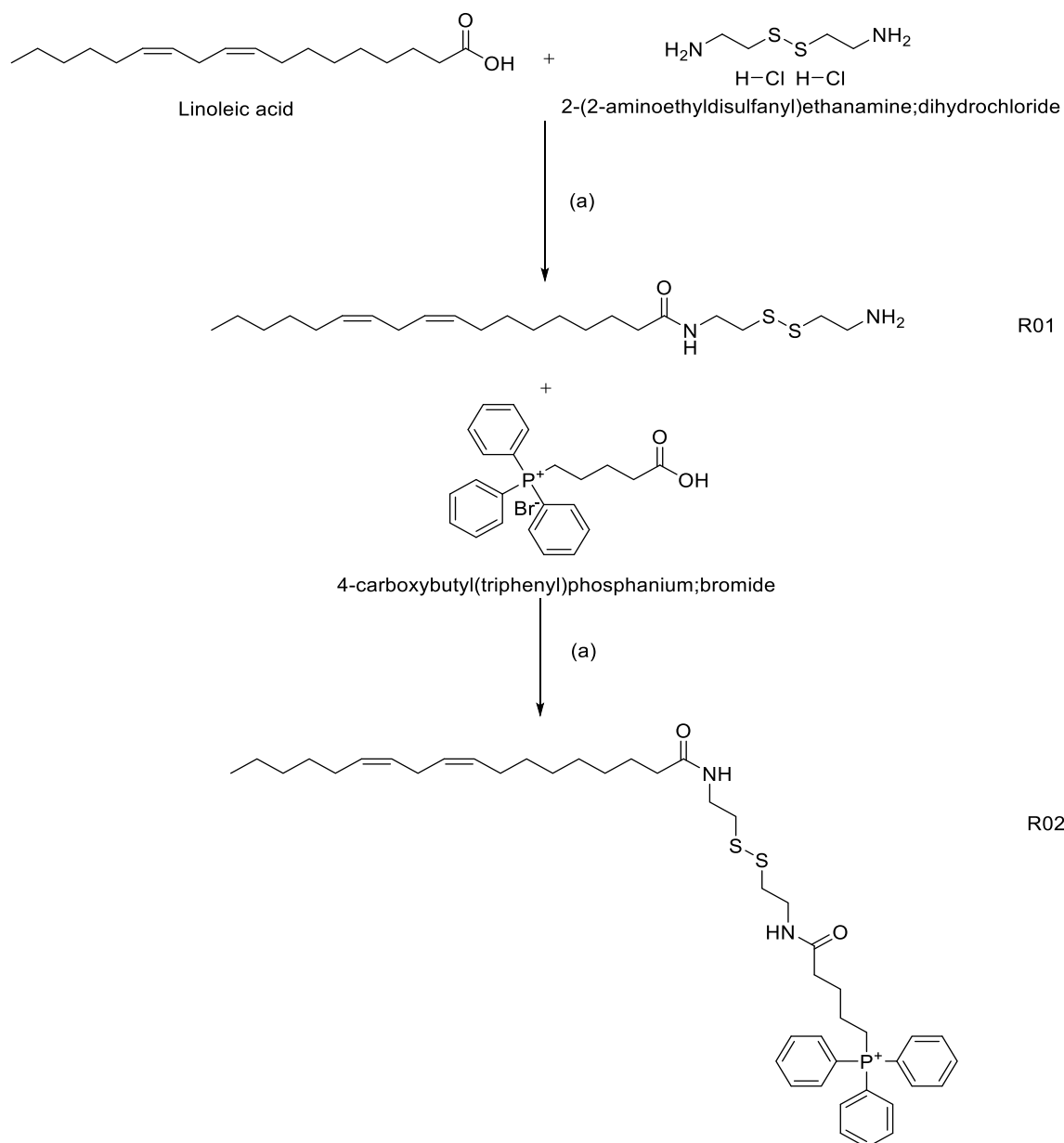


Figure 4.2: Synthesis scheme for Linoleic acid-ss-TPP

4.7. In-vitro cell culture study

4.7.1 In-vitro cytotoxic studies of HPPH and OLA on 4T1 cell line

The MTT 3-(4, 5-dimethylthiazol-2-yl)-2,5-diphenyltetrazolium Bromide) assay was carried out to study the cytotoxicity of HPPH and OLA. Briefly, after reaching the 75% confluency, 4T1 cells were trypsinised with trypsin EDTA solution and further seeded into 96-well plate with the cell count of 5×10^3 / each well. The cells were exposed to treatment with different pure HPPH concentrations (i.e., 1.5 μ M, 2.5 μ M, 5 μ M, 7.5 μ M, 10 μ M and 20 μ M). The HPPH treated group was irradiated with laser light of 650 nm for 20 minutes (60 mW power over 5mm diameter circular exposure, equiv. to approx. 03 W/cm²). Likewise, the different concentration

i.e., 10 μM, 20 μM, 30 μM, 45 μM, 60 μM and 120 μM was followed for OLA. Afterwards, all the treated groups were incubated for 48 hr. The MTT assay was conducted and optical density was calculated at 570 nm wavelength, using a microplate reader (Multiskan# Thermo scientific). The study was repeated for three times with two individual experiments [190]. The following equation was used to calculate cell viability as a percentage of the control wells.

$$\% \text{ Cell viability} = \frac{\text{O.D of treated cells}}{\text{O.D of control (without treatment)}} \times 100 \dots \text{Eq1}$$

4.7.2. Estimation of combination index (CI) of HPPH and OLA

The cytotoxicity study was performed using 3-(4, 5-dimethylthiazol-2-yl)-2,5-diphenyltetrazolium Bromide assay (MTT Assay). In brief, 4T1 cells were seeded at a density of 5000 cells/ well in 96-well plate. The cells were subjected to treatment with different concentrations of combination of HPPH and OLA combination solution (2/12, 4/24, 6/36, 8/48, 10/60 μM). Subsequently, MTT reagent was added to cells and further incubated for 6 hr at 37°C. The media was removed and 200 μL of DMSO was added to each well. Further, the samples (n=3) were analyzed by ELISA Plate reader (Biotek Synergy H1) at 570 nm [230]. Cell viability was estimated using the following equation 1.

Further, combined beneficial effect of HPPH and OLA on 4T1 cancer cell viability was evaluated using the Chou–Talalay method [231]. The combination index (CI) was calculated using compusyn software which is based on Chou Talalay et. al. . The CI equation is as follows:

$$\text{CI} = D_{\text{HP}}/D_{\text{xHP}} + D_{\text{OL}}/D_{\text{xOL}} \dots \text{Eq2}$$

where, D_{HP} is the dose of HPPH in combination to achieve x% inhibition and D_{OL} is of HPPH in combination to achieve x% inhibition. whereas D_{HPx} and D_{OLx} in the denominator represent doses of compounds (HPPH and OLA) to achieve x% inhibition when present alone. If CI values of <1, =1 and >1 indicate synergism effect, additive effect and antagonism effect in combined drug action respectively. In our experiments, the relationship between drug concentration and decreased cell viability (IC_{10-50}) was calculated, and a CI–Fa plot are presented.

4.7.3. Apoptosis Analysis

The apoptotic assay for HPPH and OLA and in combination of HPPH and OLA and their LPHNs was analyzed using Dead cell apoptosis kit with Alexa Fluor 488-Annexin-FITC Conjugate by flow cytometry as per the manufacturer's protocol (Invitrogen protocol). In brief, 4T1 were seeded in 6-well plate (1×10^6 cells/well). After 24 h incubation, the media was removed and washed with PBS. Afterwards, cells were treated with free HPPH and its LPHNs at their IC₅₀ concentrations (obtained from the cytotoxicity study). Subsequently, the HPPH treated plate was irradiated with PDT laser (Omega Laser) with light dose of 650 nm for 20 minutes (60 mW power over 5mm diameter circular exposure, equiv. to approx. 03 W/cm²) and incubated for 48 hr. The treated cells were subject to trypsinization and harvested in PBS. Later, the cells were collected by centrifugation for 6 min at 1500 rpm. Afterward, the all the treated cells were redispersed with 1X binding buffer and subsequently, stained with apoptotic assay dye i.e., Annexin V-FITC (2 μ L) and Propidium iodide (5 μ L). Further, it was incubated for 5 min and samples were analyzed under flow cytometer (Beckman Coulter). The data were recorded using Cyt Expert software[230,232].

4.8. In-vivo efficacy study in 4T1 bearing Balb/c mice

4.8.1. Development of Orthotopic 4T1 bearing breast cancer model using 4T1-Luc cells

For this *in vivo* animal study experiment, 4T1-Luc cells were cultured in RPMI media as per ATCC guidelines. Following a seven-day quarantine period, the animals were subcutaneously injected with 2 million cell lines diluted in 100 μ L of sterile PBS into the mammary pads of female Balb/c mice in order to implant tumors. After 17 days post-injection of the cells, tumor sign was observed in all the animals. The tumor volume was measured using digital vernier caliper and calculated using the formula: Tumour volume = [(length \times width²)/2]. 20 animals. The tumour was further confirmed by *in vivo* imaging technique (IVIS® Lumina III, PerkinElmer, USA)[233,234].

4.8.2. Treatment of HPPH and OLA in 4T1 bearing breast cancer model

Once the tumor volume reached 80 mm³, the animals were divided into four groups as in mentioned in the Table 4.3 to check the anti-tumour effect of HPPH and OLA. The treatment was administered to the animal daily until 10 days. Body weights and tumor volumes were recorded every alternate day. The HPPH and OLA was administered intravenously at the dose of 5mg/kg.bw and 30mg/kg.bw respectively through tail vein. After every treatment, all the animals were exposed to the laser of wavelength 650nm for 20 min. The survival timing, body weight and change in behavior of all the animals were recorded during the study period.

Further, after completion of the experiment, all the animals were sacrificed and the tumors were removed. Further, the parameters like tumor volume, animal body and survival rate of the animal were examined.

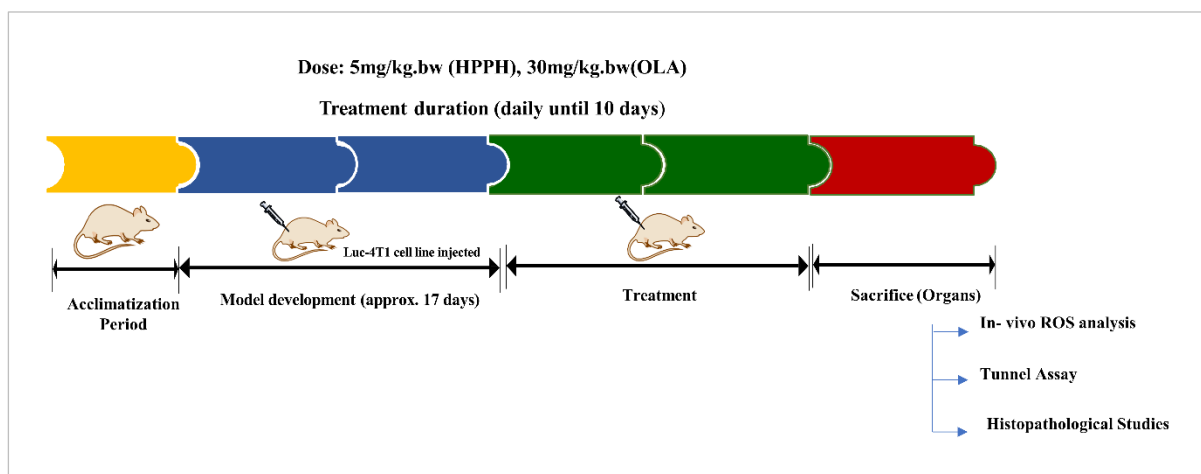


Figure 4.3: Experimental schedule of animal model development and treatment

4.8.3 Bioluminescence image analysis in the treated 4T1-Luc tumor bearing mouse model

In order to conduct bioluminescence analysis, the tumor growth was evaluated at regular intervals using an *in vivo* imaging technique (IVIS® Lumina III, PerkinElmer, USA). In brief, all the study animals were anesthetized and afterwards, 100 µL of Luciferin D dye at the dose of 100 mg/kg was injected to animals intraperitoneally. Further, Mice were positioned inside the imaging facility after 2 min of Luciferin D administration. During the treatment period, all the animals were examined for tumor growth, and images for the all the treated group were captured via bioimaging facility. The region of interest has been chosen around the tumor, and the bioluminescence signals were analyzed in the units of photons/sec/cm²/sr (maximum photons per second per centimeter square per steradian). After completion of experiment, the animals were sacrificed, and vital organs along with the tumour tissue were isolated and stored in tissue freezing media at -80 °C till further evaluation[90].

Table 4.3: Experimental design for the screening of HPPH and OLA and in combination of HPPH and OLA and their LPHNs in 4T1 bearing Balb/c mice

Animal Group	Treatment used
Group 1:	Normal diet, (Disease Control)
Group 2:	4T1 bearing Balb/c mice, administered with pure HPPH (Dose: 5mg/kg, i.v.)
Group 3:	4T1 bearing Balb/c mice, administered with pure OLA (Dose :30mg/kg, i.v.)
Group 4:	4T1 bearing Balb/c mice, administered with pure HPPH (Dose: 5mg/kg, i.v.) and OLA (Dose: 30mg/kg, i.v.)
Group 5	4T1 bearing Balb/c mice, administered with Biotin@HPPH/OLA-LPHNs (Dose: 5mg/kg for HPPH and 30mg/kg for OLA; i.v.)
Group 6:	4T1 bearing Balb/c mice, administered with Biotin-ss-TPP@HPPH/OLA-LPHNs (Dose: 5mg/kg for HPPH and 30mg/kg for OLA; i.v.)

4.8.4 Assessment of in-vivo reactive oxygen species (ROS) generation

To evaluate the ROS generation ability of the HPPH and OLA, DCFH-DA probe was used. Briefly, the Mice were anesthetized (n = 5) and 50 μ L of DCFH-DA (25 μ M) was injected intratumorally on the last day of treatment. The bioimaging was carried out via IVIS® Lumina III, PerkinElmer, USA. The fluorescence intensity [(p/sec/cm²/sr)/ μ W/cm²] was analyzed. The tumors were removed surgically after 30 minutes. The tumor sections were studied under a fluorescence microscope under the FITC channel (ex/em = 495/519 nm). The fluorescence intensities were recorded using *Image J* software[90].

4.8.5 Terminal deoxynucleotidyl transferase dUTP nick end labeling (TUNEL) assay on tumor tissue sections

Using a cryotome (Leica Biosystems, Germany), the frozen tumor sections in the OCT media were cryo-sectioned to a thickness of 5 μ m. The tumor tissues, along with the terminal deoxynucleotidyl transferase (TdT) enzyme and 4% paraformaldehyde, were kept at 37 °C. The TUNEL reaction mixture was added to the fixed tissue slides and kept in the dark, humid environment at 37 °C for another hour. Also, they were stained with DAPI for 5 minutes after being washed three times with 1X PBS. The slides were photographed using a fluorescence microscope. The images were processed and analyzed using *Image J* software[90].

4.8.6 Histological evaluation of the tumor cryosections by H&E staining assay

An immunohistochemical examination was carried out for all the groups (Table 4.3) for both organs and the tumor sections. Tissue sections of 5 μ m thickness were mounted on glass slides and treated with xylene and ethyl alcohol (100% - 30%), then followed by washing with 1X PBS and water. The nuclei and cytoplasm were stained with hematoxylin and eosin, respectively. After that, the tissue sections were dehydrated with ethyl alcohol (30%-100%), followed by a xylene wash. Finally, the sections were mounted with mounting fluid and examined under a fluorescence microscope at 20X magnification[90].

4.9 In vivo pharmacokinetic study

In-vivo pharmacokinetic study was conducted in Balb/c Mice. The single dose of 5 mg/kg.bw and 30mg/kg.bw of free HPPH and OLA respectively were administered to the animal through i.v. route. An aliquot of 200 μ L of blood samples were collected in K₂EDTA containing tube from animal at predetermined time interval. Further, the blood sample was centrifuged at 13,000 rpm (g) for 12 min at 4 °C. The plasma was collected and stored at -80° C till the analysis. Further the sample were analyzed by validated LC-MS/MS method. The obtained

plasma concentration was subjected to non-compartmental pharmacokinetic analysis using WinNonlin software version 6.3 (Certara, USA). Statistically significant differences were assumed at $P < 0.05$ [217,218].

4.10 Safety Evaluation of HPPH and OLA

The sub chronic toxicity study was conducted in BALB/c mice (4-6 week; average body weight 25-30g). Briefly, the animals were acclimatized for 7 days and divided into three groups, each consisting of five Balb/c mice (Table 4.10). HPPH and OLA were administered to the Balb/C mice intravenously at the dose of 5 mg/kg.bw and 30mg/kg.bw respectively. Afterwards, the drugs (HPPH and OLA) were administered intravenously into the tail vein of animals at the above-mentioned dose. Subsequently, HPPH treated group was irradiated with the laser light at 650 nm for 20 minutes after administration. In the similar way, the control group was treated with normal saline. After 21 days of treatment, all the animals were sacrificed. All the vital organ such as liver, kidney, heart, spleen, lungs and blood sample of different groups were collected. Based on the OECD guidelines, The collected organs were subjected to H&E analysis.

Table 4.4: Experimental design for the safety study of HPPH with nanocarrier systems in 4T1 bearing Balb/c mice

Animal Group	Treatment used
Group 1:	Normal diet, (Saline 100 μ L; Control)
Group 2:	4T1 bearing Balb/c mice, administered with pure HPPH (Dose: 5mg/kg, i.v.)
Group 3:	4T1 bearing Balb/c mice, administered with pure OLA (Dose :30mg/kg, i.v.)

4.11. Development and optimization and characterization of HPPH loaded LPHNs

4.11.1 Fabrication of LPHNs for HPPH

The HPPH loaded LPHNs was prepared by single step emulsification followed by solvent evaporation method with slight modification [235,236]. In brief, DC₈₉PC, NH₂-PEG-PLGA, Linoleic and HPPH were dissolved in dichloromethane to obtained organic phase. Subsequently, the aqueous phase was also prepared by using acidified 1.5% PVA (pH5.5) to avoid degradation of the HPPH. Afterwards, the organic phase was added dropwise to the aqueous phase under probe sonication at 25 % amplitude with pulse mode (25 sec on and 10 sec off) for 3.50 min. The organic phase was later removed using Buchi Rotary evaporator® at 30° C for 20 min to obtain nanoparticles and further subjected to centrifugation to remove the un-entrapped HPPH. In the same way, Blank-LPHNs were fabricated using above mentioned method without incorporation of drug. In the same ways, Biotin@HPPH-LPHNs was

formulated by substituting NH₂-PEG-PLGA with Biotin-PEG-PLGA in the above-mentioned method.

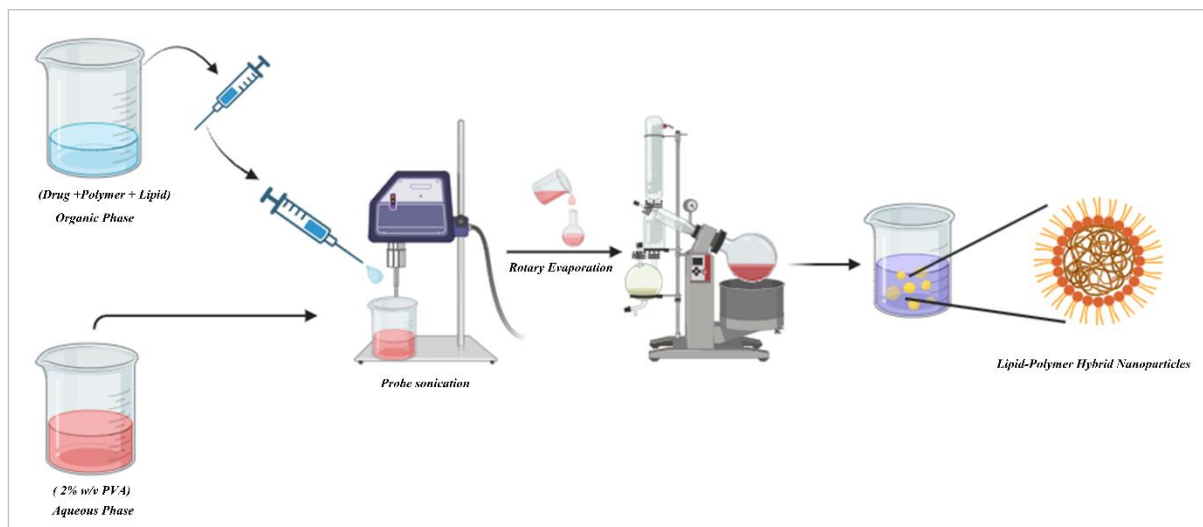


Figure 4.4: Schematic representation of LPHNs preparation procedure

4.11.2 Optimization: Experimental design study for Nanoparticle

In order to determine the critical LPHNs formulation and process factor, preliminary trials were conducted. These factors like surfactant concentration, polymer concentration, volume of aqueous phase and Lipid content plays a crucial role in alteration of various physiochemical properties of nanocarrier such as particle size, zeta potential, entrapment efficiency and drug loading. Additionally, the parameters like the volumes of organic phase, sonication time and amount of linoleic acid, were kept constant during the data optimization. Additionally, the parameters like amount of drug (1mg) and total lipid (5mg) and amount of polymer (4 mg) were kept constant in all formulations. In prior to further optimization, Central Composite Designs (CCD) by Design-Expert software (Version 7.3, Stat-Ease, Inc., Minnesota, USA) was implemented[237]. Finally, the two independent variables (i.e., Amount of Phospholipid (DC₈₉PC) and surfactant concentration) and two dependent variables (particle size and Entrapment Efficiency) were screened for the optimization. The low value and high value were selected based on the literature and their range of variable was shown in table 4.5.

Table 4.5: Variable used in CCD response surface design

Independent variable	Factor	Unit	Type	Applied Level	
				Low	High
X1	PVA	% w/v	Numerical	1	2
X2	DC ₈₉ PC	mg	Numerical	3.5	4.0
Dependent variable		Unit	Constraints		
Y1	Entrapment efficiency	%	-	Maximum	
Y2	Particle Size	nm	-	Minimum	

The 3D surface plots were utilized to study the relationship and interaction between the independent variables and dependent variables. The analysis of variance (ANOVA) with test (p-value < 0.05) was performed to estimate the significance of the variables on the responses. Further, the acceptability the model was checked by observing the R² and adjusted R². The optimized formulation was done on the basis of the higher encapsulation efficiency of drug and the smaller particle size.

4.11.3 Characterization Of HPPH loaded LPHNs

4.11.3.1 Measurement of Particle shape , size, PDI and Surface charge

The mean diameter, PDI and zeta potential were determined using a by dynamic light scattering using Zetasizer (Malvern Nano ZS) with back scattering angle of 173° at 25 °C. In prior to analysis, the HPPH loaded LPHNs was diluted with deionized water. Further, the shape of LPHNs was examined using FEI scanning electron microscope (FEI-SEM) (Hillsboro, Washington).

4.11.3.2 Determination of %EE and %DL

The %EE and %DL of HPPH form LPHNs was estimated using RP-HPLC. Briefly, HPPH was extracted from prepared LPHNs by diluting formulation with Acetonitrile followed by bath sonication at 70° C. Further, the sample centrifuged for 20 min at 22658× g. The supernatant was analyzed by this validated HPLC method to estimate the content of HPPH. Further, the following equation was used to calculate the %Entrapment efficiency and % Drug loading.

$$\% \text{Entrapment efficiency} = \frac{\text{Amount of HPPH in LPHNs}}{\text{Initial amount of HPPH taken}} \times 100$$

$$\% \text{Drug Loading} = \frac{\text{Amount of HPPH entrapped in LPHNs}}{\text{Total weight of LPHNs}} \times 100$$

4.11.3.3 Freeze drying

The freeze drying of HPPH loaded LPHNs were carried out in Lyophiliser (Free Zone Triad® Benchtop Freeze Dryers, Labconco, MO, USA) to enhance its storage stability. In brief, four different cryoprotectants including sucrose, mannitol, trehalose, and PEG4000 were added to the prepared nanoparticles with three different concentrations (2.5%, 5% and 10 % w/w) and later, the sample were transfer to Lyophiliser. Finally, lyophilized nanoparticle powders were reconstituted with Milli-Q water, and further, subjected to physiochemical characterization such as particle size, PDI, and entrapment efficiency.

4.11.3.4 In vitro drug release

In vitro drug release study was performed using a dialysis membrane technique[238]. In brief, 1ml of LPHNs containing HPPH (100µg/mL) was taken into dialysis membrane (MWCO12 kDa; Himedia, India) and immersed into release medium (phosphate-buffered saline with 5% (v/v) Tween80 and 5% PEG 400 and 2% IPA; pH 7.4 & 5.4) and incubated at 37°C and shaken at 100 rpm. Based on the predetermined time intervals, the release samples were withdrawn from the sink and was replaced with fresh release media. Further, the collected sample were filtered with 0.22 µm syringe filter and analyzed using validated RP-HPLC method. In the same ways, pure HPPH solution was also studied as above-mentioned method.

4.11.3.5. Physical state characterisation (DSC)

In order to understand the thermal behavior, DSC analysis was performed for pure HPPH and lyophilized LPHNs (Blank nanoparticle, HPPH-LPHNs, Bt@OLA-LPHNs) was studied using a DSC apparatus (DSC-60 Instrument, Shimadzu, Tokyo, Japan). Briefly, accurately 3mg of samples were weighed and cramped with aluminum pans. Then after, samples were transfer to DSC apparatus and analysis was carried out by heating from room temperature to 300 °C at a rate of 5 °C/ min under nitrogen environment. Finally, thermogram was recorded for all the samples using DSC 60A software.

4.11.4. Stability study of LPHNs

To understand the storage condition, the colloidal stability studies of LPHNs was performed at two different room ($25 \pm 1^\circ\text{C}$) and refrigeration ($4 \pm 2^\circ\text{C}$) temperature for 90 days. Briefly, the prepared LPHNs were stored in amber glass and based on pre-determined time (0.5,1,3,7,15,30 and 90 days), sample was removed and subjected to physiochemical parameter analysis and all the data were recorded.

4.11.5. Measurement of Singlet oxygen generation

The analysis of Singlet oxygen generation was carried out using SOSG dye. Briefly, the pure HPPH and HPPH loaded LPHNs (HPPH-LPHNs and Biotin@HPPH-LPHNs) at the concentration of 5 µM were irradiated at 650 nm using a laser system. The SOSG dye solution (1.0 µM) was prepared in 2% methanol in deionized water. Further, fluorescence intensity of SOSG dye was recorded using Plate reader (Synergy II microplate reader, Bio Tek, VT) at excitation wavelength of 494 nm. The singlet oxygen generation of LPHNs was evaluated by the SOSG fluorescence intensity compared with control samples.

4.11.6 In-vitro cell studies for HPPH loaded LPHNs

4.11.6.1. Cytotoxic studies on 4T1 cell line

The MTT 3-(4, 5-dimethylthiazol-2-yl)-2,5-diphenyltetrazolium Bromide) assay was carried out for HPPH and HPPH loaded LPHNs (HPPH-LPHNs and Biotin@HPPH-LPHNs) in accordance with the same protocol as mentioned in section 4.7.1. Except, the experiment was subjected to treatment with concentration i.e., 2 μ M, 3.9 μ M, 7.8 μ M, 10 μ M, 31.25 μ M, 62.5 μ M and 125 μ M for HPPH and its LPHNs.

4.11.6.2. Cellular Uptake of HPPH loaded LPHNs

The cellular uptake of nanocarrier (HPPH-LPHNs and Biotin@HPPH-LPHNs) was evaluated using confocal microscopy in 4T1 cells. Briefly, the cells were seeded six-well plate (1×10^5 cells/well) and kept it for 24 h at 37 °C. Afterward, 30 μ L of HPPH-LPHNs (HPPH-LPHNs and Biotin@HPPH-LPHNs) were treated to each well. Subsequently, all the treated group was irradiated with laser light of 650 nm for 20 minutes (60 mW power over 5mm diameter circular exposure, equiv. to approx. 03 W/cm²). Further, the treated plate was subjected to incubation at 37 °C for 4 and 8 h, after that media was removed and trypsinised to get suspended cell monolayer. The transfection of the HPPH and nanocarrier was observed using confocal microscopy at 525 nm.

4.11.6.3. Measurement of reactive oxygen species (ROS) of HPPH loaded LPHNs

The ROS generation assay was performed using 2', 7'-Dichlorofluorescein diacetates (DCFH-DA). Briefly, the cells were seeded in a 6-well plate at a density of 1×10^5 cells/well and incubated for 24 hr. Further, cells were exposed to treatment of pure HPPH and HPPH loaded LPHNs and irradiated with laser light of 650 nm for 20 minutes (60 mW power over 5mm diameter circular exposure, equiv. to approx. 03 W/cm²). Further, all the treated group was subjected to incubation for 12hr. After incubation, the treated cells were washed two times with PBS. All the treated group (pure HPPH, HPPH-LPHNs and Biotin@HPPH-LPHNs) were expose to 10 μ M of DCFDA for 30 min at 37 °C. The fluorescence intensity was monitored at an excitation wavelength of 485 nm and an emission wavelength of 530 nm using confocal microscopy (Zeiss, USA).

4.11.6.4. Apoptosis Analysis of HPPH loaded LPHNs

The apoptotic assay for HPPH and their LPHNs (HPPH-LPHNs and Biotin@HPPH-LPHNs) was analyzed using Dead cell apoptosis kit with Alexa Fluor 488-Annexin-FITC Conjugate by flow cytometry as per the manufacturer's protocol (Invitrogen protocol) in accordance with the same protocol as mentioned in section 4.7.3.

4.11.7. Hemolysis study of HPPH loaded LPHNs

The hemolysis was studied by analyzing hemoglobin content in the supernatant of the centrifuged RBC suspension. In brief, RBCs were collected from Balb/c mice blood by centrifuging the blood sample at 1000 rpm in 3 min. After collection, the RBCs was washed with normal saline to obtained a colorless supernatant. The free HPPH and HPPH loaded LPHNs (HPPH-LPHNs and Biotin@HPPH-LPHNs) at different concentration of HPPH (500, 250,125,62.5,31.56 and 15 μ g/mL) were added to processed RBCs solution and incubated for 30 min at 37 ° C. The incubated sample was centrifuged for 25 min at 1500 rpm. The supernatants were collected and analyzed by using plate reader at 540 nm to calculate the hemolysis. Likewise, positive control and negative control were also processed.

4.11.8. In-vivo experiment for HPPH loaded LPHNs

4.11.8.1 Pharmacokinetic study

The in-vivo (pharmacokinetic, biodistribution and toxicity) studies were performed as mentioned in the section 4.9. All results were expressed as mean \pm standard error mean (S.E.M.). The experimental data were analyzed using a graph pad with a one-way analysis of variance (ANOVA) followed by Tukey's test at a defined significant level of $p < 0.05$.

4.11.8.2 In-vivo biodistribution study

After 7 days quarantine period, the female Balb/c mice were inoculated subcutaneously with 2 million cells (4T1 cell line) suspended in 100 μ L of sterile PBS into the mammary pad for tumor implantation. Once the tumor sign was observed and tumor volume reached 350 mm³, this biodistribution study was performed. In vivo fluorescent imaging with fluorescent markers was used to provide visible, time-dependent nanoparticle biodistribution imaging. To assess the distribution and tumor accumulation of LPHNs, Tumor-bearing mice were divided into two groups of three mice each for the in vivo distribution of LPHNs. Further, DiI-loaded LPHNs have been fabricated and administered to the Balb/C mice through the tail vein. Subsequently, in vivo fluorescent imaging was performed using an IVIS® Lumina III, PerkinElmer, USA. To monitor the tumor accumulation of DiI-loaded LPHNs, mice were continuously anesthetized with O₂ and 2% isoflurane and the tumor accumulation profile of DiI-loaded LPHNs was evaluated at different time points (0.5,1,3,6,12 and 24h) using the IVIS imaging system. For ex-vivo imaging, animals were sacrificed and the perfused organs like tumor, heart, liver, kidney, lung, and spleen was isolated. These organs were also imaged using IVIS® Lumina III, PerkinElmer, USA.

4.11.8.3 Safety evaluation of HPPH Loaded LPHNs

The in-vivo toxicity studies for HPPH loaded LPHNs (HPPH-LPHNs and Biotin@HPPH-LPHNs) were performed in accordance with the same protocol as mentioned in section 4.10.

4.12. Development and Evaluation of OLA loaded LPHNs

4.12.1 Fabrication of OLA loaded LPHNs

The OLA loaded LPHNs was fabricated using emulsification followed by solvent evaporation method with slight modification[239–241]. Briefly, for fabrication of non-cationic nanoparticle (OLA-LPHNs), organic phase was prepared using the phospholipid SPC-100, polymer (NH₂-PEG-PLGA, MW: 10-15 kDa) and OLA with a wt. ratio 4:5:1 i.e., 8mg,10mg and 2mg respectively in DCM. Further, organic phase was gently added dropwise into the aqueous phase i.e., 2% (w/v) of PVA solution using 2mL syringe under continuous stirring. The prepared emulsion was further sonicated for 3.20 min at 25 % amplitude with pulse mode (30 sec on and 10 sec off) using Probe Sonicator (IKA, Mumbai, India). Afterwards, the organic solvent was removed *in vacuo* using Buchi Rotoevaporator® at 40° C for 20 min to obtain nanoparticle suspension. The obtained suspension was centrifuged at 20000 rpm for 30 min to remove the non-encapsulated drug.

Further, the non-targeted cationic nanoparticle (St@OLA-LPHNs) was prepared using stearylamine. In this preparation, 0.5 mg of stearylamine was added to the organic phase followed by same procedure as used for the fabrication of OLA-LPHNs. In the similar manner, targeted cationic nanoparticle (St/Biotin@OLA-LPHNs) was prepared using copolymer Biotin-PEG-PLGA, instead of PEG-PLGA. In the similar way, three blank nanoparticles (Blank-LPHNs: non-cationic, non-targeted cationic and targeted cationic blank) were also formulated.

4.12.3. Characterisation of OLA loaded LPHNs

4.12.3.1. Morphological evaluation: Size, PDI, Zeta Potential and Shape

The morphological analysis of parameters such as size, polydispersity index (PDI), and Zeta potential of nanoparticles were estimated using Zetasizer (Malvern Nano ZS) at a scattering angle of 173°. The surface topography of nanoparticle was studied by using field emission scanning electron microscopy (FESEM, Quorum Q150 T ES, Quorum technologies Ltd, UK). In brief, the diluted nanoparticle suspension was placed on the coverslip and kept into a vacuum dryer till complete dryness. Further, Nanoparticle containing coverslip was mounted on a

double faced sticky tape followed by gold coating using sputter coater unit (Quorum Q150 T ES, Quorum technologies Ltd, UK) and the coated sample was subjected to topographical screening [242].

4.12.3.2. Entrapment efficiency(%EE) and Drug Loading(%DL)

The entrapment efficiency and drug loading of formulated OLA-LPHNs were calculated by estimating the trapped amount of OLA in nanoparticles. In brief, OLA was extracted from formulated nanoparticles using methanol with suitable dilution followed by bath sonication at 65°C for 30 min. The sample was then cooled and centrifuged at 21,000 rpm for 20 min. The supernatant was collected and analyzed using a developed RP-HPLC method. Entrapment efficiency (%) and drug loading (%) was calculated using the following equations.

$$\% \text{ Entrapment Efficiency} = \frac{\text{Amount of OLA in LPHNs}}{\text{Initial amount of OLA taken}} \times 100 \dots \text{Eq.2}$$

$$\% \text{ Drug Loading} = \frac{\text{Amount of OLA in LPHNs}}{\text{Initial amount of Exipient and OLA taken}} \times 100 \dots \text{Eq.3}$$

4.12.3.3. Freeze drying of OLA loaded LPHNs

The formulated LPHNs were subjected to lyophilization. In brief, the cryoprotectants such as mannitol, trehalose, sucrose and PEG-4000 were treated to the formulated nanoparticles (OLA-LPHNs, St@OLA-LPHNs and St/Biotin@OLA-LPHNs) with three different concentrations (i.e., 2.5% w/v, 5% w/v and 10 % w/v). Afterward, the treated samples were kept under freeze-drying using Lyophiliser (Free Zone Triad® Benchtop Freeze Dryers, Labconco, MO, USA) for the period of 24hr. Finally, for the characterization of the obtained lyophilized powder samples, they were reconstituted with deionized water. The characterization parameters such as particle size, PDI, Zeta potential, entrapment efficiency and drug loading of nanoparticles were estimated.

4.12.3.4. In vitro release study of OLA loaded LPHNs

The in-vitro release study was conducted using dialysis method. The study was performed using 1% w/w tween 80 and 2% ethanol in phosphate buffer saline as release media at two different pH, i.e., 5.4 and 7.4. In the first step, the dialysis bag was placed into the prepared release media for 24h prior to the experiment. The sample amount equivalent to 500 µg /mL of OLA and OLA loaded nanoparticle (OLA-LPHNs, St@OLA-LPHNs and St/Biotin@OLA-LPHNs) were placed in dialysis bag containing 30 mL of release media. Subsequently, the 1mL of aliquots of sample were withdrawn at pre-determined time points (0.25, 0.5, 1, 2, 4, 8, 12, 24, and 48 h) for 48 h from the release media and replaced with release media at each time

point to maintain sink condition. This study was performed three times and collected samples were estimated using a developed HPLC method. The release profile for both OLA and OLA loaded nanoparticle were plotted between % drug release vs. Time [243].

4.12.3.5. Physical state characterisation

Attenuated total reflection-IR (ATR-IR)

Drug-excipient interaction study was studied using ATIR spectroscopy (Bruker, USA)). All samples including OLA and lyophilized nanoparticles (Targeted cationic blank nanoparticle, OLA-LPHNs, St@OLA-LPHNs and St/Biotin@OLA-LPHNs) were scanned from 4000 to 400 cm^{-1} . The recorded IR Spectrum was subjected to analysis for all sample and compared with pure OLA spectrum.

Differential scanning calorimetry (DSC)

To evaluate the physical state of samples, DSC analysis was carried out for pure OLA and lyophilized nanoparticle (targeted cationic blank nanoparticle, OLA-LPHNs, St@OLA-LPHNs and St/Biotin@OLA-LPHNs) using a DSC apparatus (DSC-60 Instrument, Shimadzu, Tokyo, Japan). The samples were heated at a rate of 5 $^{\circ}\text{C}/\text{min}$ from room temperature to 300 $^{\circ}\text{C}$ under nitrogen environment. Finally, thermogram was recorded for all the samples using DSC 60A software.

4.12.3.6. Stability study of LPHNs

The stability studies for lyophilized nanoparticles (OLA-LPHNs, St@OLA-LPHNs and St/Biotin@OLA-LPHNs) were performed as per the previously reported method [244]. In brief, the lyophilized nanoparticles were stored at two different temperature conditions i.e., ambient temperature ($25 \pm 1^{\circ}\text{C}$) and cold temperature ($4 \pm 2^{\circ}\text{C}$) for 90 days. The samples were characterized for particle size, PDI and % EE subsequently, stability sample was compared with freshly prepared nanoparticle

4.12.4. In-vitro cell culture study for OLA loaded LPHNs

4.12.4.1. Cytotoxic studies on 4T1 cell line

The cytotoxicity study for OLA loaded LPHNs (OLA-LPHNs, St@OLA-LPHNs and St/Biotin@OLA-LPHNs) was performed using 3-(4, 5-dimethylthiazol-2-yl)-2,5-diphenyltetrazolium Bromide assay (MTT Assay) in accordance with the same protocol as mentioned in section 4.7.1.

4.12.4.2. Cellular Uptake of OLA loaded LPHNs

The cellular uptake evaluation was carried out using coumarin-6 (C6) for LPHNs (C6-LPHNs, St@C6-LPHNs and St/Biotin@C6-LPHNs) in accordance with the same protocol as mentioned in section.4.11.6.2

4.12.4.3 Apoptosis analysis of OLA loaded LPHNs

The apoptotic assay for OLA and their LPHNs (OLA-LPHNs, St@OLA-LPHNs and St/Biotin@OLA-LPHNs) was analyzed using Dead cell apoptosis kit with Alexa Fluor 488-Annexin-FITC Conjugate by flow cytometry as per the manufacturer's protocol (Invitrogen protocol) in accordance with the same protocol as mentioned in section.4.7.3

4.12.5. Hemolysis Study of OLA loaded LPHNs

Hemolysis was studied by estimating hemoglobin content in the supernatant of the centrifuged RBC suspension as per the previously reported method[245]. In brief, RBCs were collected from Mice blood via centrifugation at 1000 rpm for 3 min. Further, the RBCs was subjected to washing with normal saline to obtain a colorless supernatant. The free OLA and OLA loaded LPHNs (OLA-LPHNs, St@OLA-LPHNs and St/Biotin@OLA-LPHNs) were added to normal saline RBCs at the concentration of 900 µg/250µL and incubated for 30 min at 37 ° C. The incubated samples were centrifuged for at 1500 rpm for 25 min. The supernatants were collected and analyzed using plate reader (Biotek Synergy H1) at 540 nm to calculate the % hemolysis. In the similar way, positive control and negative control were also processed.

4.12.6. In vivo animal study for OLA loaded LPHNs

4.12.6.1. Pharmacokinetic study

The in-vivo pharmacokinetic studies for pure OLA and OLA loaded LPHNs (OLA-LPHNs, St@OLA-LPHNs and St/Biotin@OLA-LPHNs) were performed as per same protocol mentioned in the section 4.9. All results were expressed as mean ± standard deviation. The experimental data were analyzed using a graph pad with a one-way analysis of variance (ANOVA) followed by Tukey's test at a defined significant level of $p < 0.05$.

4.12.6.2 In vivo imaging and biodistribution analysis

After 7 days quarantine period, the female Balb/c mice were inoculated subcutaneously with 2million cells (4T1 cell line) suspended in 100 µL of sterile PBS into the mammary pad for tumor implantation. Once the tumor sign was observed and tumor volume reached 350 mm³, this biodistribution study was performed. In vivo fluorescent imaging with fluorescent markers was used to provide visible, time-dependent nanoparticle biodistribution imaging.

To assess

the distribution and tumor accumulation of LPHNs, Tumor-bearing mice were divided into two groups of three mice each for the in vivo distribution of LPHNs. Further, DiI-loaded LPHNs have been fabricated and administered to the Balb/C mice through the tail vein. Subsequently, In vivo fluorescent imaging was performed using an IVIS® Lumina III, PerkinElmer, USA[246]. To monitor the tumor accumulation of DiI-loaded LPHNs, mice were continuously anesthetized with O₂ and 2% isoflurane and the tumor accumulation profile of DiI-loaded LPHNs was evaluated at different time points (0,1,3,6,12, 24 and 36 h) using the IVIS imaging system. For ex-vivo imaging, animals were sacrificed and the perfused organs like tumor, heart, liver, kidney, lung, and spleen was isolated. These organs were also imaged using IVIS® Lumina III, PerkinElmer, USA[246].

All results were expressed as mean \pm standard deviation (Mean \pm SD). The experimental data were analyzed using a graph pad with a one-way analysis of variance (ANOVA) followed by Tukey's test at a defined significant level of $p < 0.05$.

4.12.6.3 Safety evaluation

The in-vivo toxicity studies for OLA loaded LPHNs (OLA-LPHNs, St@OLA-LPHNs and St/Biotin@OLA-LPHNs) were performed in accordance with the same protocol as mentioned in section 4.10.

4.13. Development and characterization of HPPH and OLA co-encapsulated LPHNs

4.13.1. Preparation of HPPH and OLA co-encapsulated LPHNs

The co-encapsulate HPPH and OLA LPHNs was prepared by emulsification followed by solvent evaporation with slight modification[247]. Briefly, HPPH and OLA and Biotin-PEG-PLGA and linoleic acid was dissolved in DCM/EtOH (500 μ L) was added to 3 mL of purified water containing acidified 2%w/v PVA. Subsequently, the mixture was sonicated at 25% amplitude for 3 min (Pulse on 30 sec and Pulse off 10sec) using a probe Sonicator (Sonics Vibra cell™, Newtown, CT, USA). It was then kept on stirring overnight at RT to remove DCM/EtOH, resulting in the formation of nanoparticles (Biotin@HPPH/OLA-LPHNs). Afterwards, Biotin@HPPH/OLA-LPHNs suspension was centrifuged at 5000 rpm for 5 min to remove untrapped drug or larger particles as a pellet. In the same ways, Biotin-ss-TPP@HPPH/OLA-LPHNs was prepared using linoleic acid-ss-TPP, instead of linoleic acid. Further Blank nanoparticle (Biotin-ss-TPP@LPHNs) was also prepared without using drug.

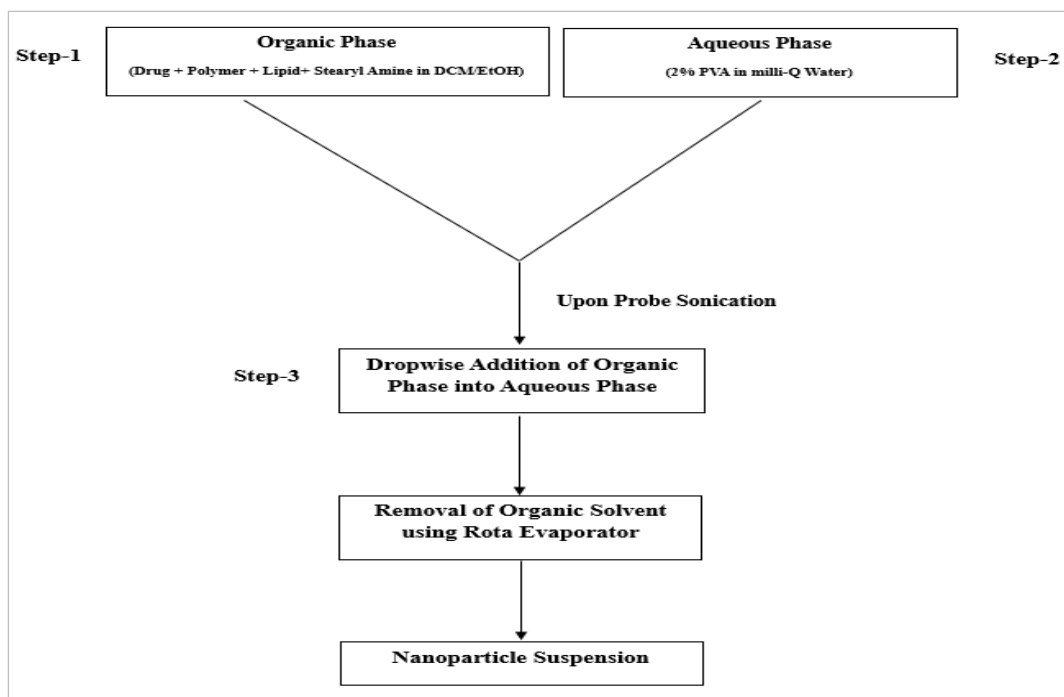


Figure 4.5: Schematic representation of HPPH and OLA co-loaded LPHNs

4.13.2. Characterization of co-encapsulated HPPH and OLA loaded LPHNs

4.13.2.1 Morphological Evaluation: Size Particle, PDI, Shape and Zeta Potential

The particle size, polydispersity index (PDI) and zeta potential of the obtained LPHNs (Biotin@HPPH/OLA-LPHNs and Biotin-ss-TPP@HPPH/OLA-LPHNs) were determined by dynamic light scattering technique using a Malvern Zetasizer (Malvern Nano ZS) [190,191].

To characterize the surface topography, LPHNs were visualized using field emission scanning electron microscopy (FEISEM). Briefly, the sample was placed on a coverslip and dried in a vacuum dryer until complete dryness. Further, a coverslip containing Nanoparticle was mounted on a double faced sticky tape followed by Gold coating using sputter coater unit (Quorum Q150 T ES, Quorum technologies Ltd, UK) and the coated sample was subjected to topographical screening [242].

4.13.2.2 Determination of %EE and %DL

The %EE and %DL of HPPH and OLA from LPHNs was estimated using LC-MS/MS. Briefly, HPPH was extracted from prepared LPHNs using destructive method. The supernatant was analyzed by this validated HPLC method to estimate the content of HPPH and OLA. Further, the following equation was used to calculate the %Entrapment efficiency and % Drug loading.

$$\% \text{Entrapment efficiency} = \frac{\text{Amount of HPPH and OLA in LPHNs}}{\text{Initial amount of HPPH taken}} \times 100$$

$$\%Drug\ Loading = \frac{Amount\ of\ HPPH\ and\ OLA\ entrapped\ in\ LPHNs}{Total\ weight\ of\ LPHNs} \times 100$$

4.13.2.3 Freeze Drying of HPPH and OLA co-loaded LPHNs

The HPPH and OLA co-loaded LPHNs were subjected to lyophilization with different cryoprotectants (Mannitol, Trehalose, Sucrose and PEG 4000). The freeze drying of HPPH and OLA co-loaded LPHNs were performed in accordance with the same protocol as mentioned in section 4.12.3.4.

4.13.2.4 In-vitro release profile

The in-vitro release study of LPHNs was performed using a cellulose dialysis bag diffusion technique. In brief, the free HPPH-OLA (100µg/mL of HPPH and 600 µg/mL of OLA) or eq. amount of their nanoparticles were placed into dialysis bag (12 kDa cut-off; SnakeSkin® Dialysis Tubing, Thermo Fischer Scientific). The end of the dialysis bag was sealed and were subsequently placed in 30 mL of release media (10mM phosphate buffer saline pH 7.4 & pH 5.4 containing 10% w/v tween 80, 2% w/v IPA and 5% v/v PEG 400; pH 7.4 & pH 5.4) to maintain the sink condition. The experiment was performed under continuous vibration rate of 100 rpm at 37°C in an incubator. At a predetermined time, intervals, i.e., 0.25, 0.5, 1, 2, 4, 8, 12, 24, 48 and 72 hr., 2ml of release samples were collected regularly, and replaced with an equivalent amount of freshly prepared release media at each time point. The amount of released drug was determined using LC-MS/MS method, and cumulative release was plotted against time.

4.13.3 Stability study of nanoparticles

To evaluate the stability, the lyophilized LPHNs (Biotin@HPPH/OLA-LPHNs and Biotin-ss-TPP@HPPH/OLA-LPHNs) were divided into two groups and subjected to stability studies for 90 days under two different temperature conditions i.e., ambient temperature (25 ± 1°C) and cold temperature (4 ± 2°C). The stability of LPHNs was determined by assessing its physical properties such as Particle Size, PDI, Zeta Potential and Entrapment Efficiency at definite time intervals, only after reconstituting the lyophilized LPHNs with milli-Q water under gentle agitation [244].

4.13.4. In-vitro cytotoxic studies on 4T1 cell line

4.13.4.1. Estimation of combination index (CI) of HPPH and OLA co-loaded LPHNs

The cytotoxicity study for HPPH and OLA co-encapsulated LPHNs (Biotin@HPPH/OLA-LPHNs and Biotin-ss-TPP@HPPH/OLA-LPHNs) was performed using 3-(4, 5-

dimethylthiazol-2-yl)-2,5-diphenyltetrazolium Bromide assay (MTT Assay) in accordance to the same protocol as mentioned in the section 4.7.2.

4.13.4.2. Cellular uptake of HPPH and OLA co-loaded LPHNs

For the cellular uptake evaluation, 4T1 were seeded in a six-well plate (1×10^6 cells/well) and kept it for 24 h at 37 °C in carbon dioxide incubator. Afterward, the uptake of LPHNs was studied using a coumarin-6(C6) which is commonly employed for uptake studies of nanoparticles. 30 μ L of C6 and C6 loaded LPHNs (Biotin@C6-LPHNs and Biotin-ss-TPP@C6-HPPH) were administered to each well. Further, mitochondrial penetration of nanocarrier was also studied using Mito-Traker (Invitrogen). Further, the treated plate was subjected to incubation at 37 °C for 4h and 12 h, after that media was removed and trypsinised to get suspended cell monolayer. The transfection HPPH and OLA coloaded LPHNs (Biotin@C6-LPHNs and Biotin-ss-TPP@C6-HPPH) was estimated using confocal microscopy at 525 nm[230].

4.13.4.3. Apoptosis Analysis of HPPH and OLA co-loaded LPHNs

The apoptotic assay for combination of pure HPPH and OLA and their LPHNs (Biotin@HPPH/OLA-LPHNs and Biotin-ss-TPP@HPPH/OLA-LPHNs) was analyzed using Dead cell apoptosis kit with Alexa Fluor 488-Annexin-FITC Conjugate by flow cytometry as per the manufacturer's protocol (Invitrogen protocol) in accordance with the same protocol as mentioned in section.4.7.3

4.13.4.4. In-vitro ROS generation Assay

The in-vitro for HPPH-OLA and their LPHNs (OLA-LPHNs, Biotin-ss-TPP@HPPH/OLA-LPHNs and Biotin @HPPH/OLA-LPHNs) was analyzed using DCFH-DA fluorescence's probe, in accordance with the same protocol as mentioned in section.4.11.6.3

4.13.4.5. Hemolysis Study of HPPH-OLA loaded LPHNs

Hemolysis was studied by estimating hemoglobin content in the supernatant of the centrifuged RBC suspension as per the previously reported method[245]. In brief, RBCs were collected from Mice blood via centrifugation at 1000 rpm for 3 min. Further, the RBCs was subjected to washing with normal saline to obtain a colorless supernatant. The free HPPH-OLA and its LPHNs (Biotin@ HPPH/OLA-LPHNs and Biotin-ss-TPP@HPPH/OLA-LPHNs) were added to normal saline RBCs at combination of 150 and 900 μ g/200 μ L for HPPH and OLA respectively and incubated for 30 min at 37 °C. The incubated samples were centrifuged for at 1500 rpm for 25 min. The supernatants were collected and analyzed using plate reader (Biotek

Synergy H1) at 540 nm to calculate the % hemolysis. In the similar way, positive control and negative control were also processed.

4.13.6. In vivo animal studies HPPH and OLA co-loaded LPHNs

The in-vivo (pharmacodynamics, pharmacokinetic, toxicity and biodistribution) studies for HPPH and OLA co-encapsulated LPHNs (Biotin@HPPH/OLA-LPHNs and Biotin-ss-TPP@HPPH/OLA-LPHNs) were performed as mentioned in the section 4.8, 4.9, 4.10 and 4.12.5.2 respectively. All results were expressed as mean \pm standard deviation (SD). The experimental data were analyzed using a graph pad with a one-way analysis of variance (ANOVA) followed by Tukey's test at a defined significant level of $p < 0.05$



RESULTS



5. Results

5.1. Analytical method development and Validation of HPPH using RP-HPLC

5.1.1. Method development

The RP-HPLC-based method was performed by Shimadzu HPLC with UV-Visible detector. Chromatographically, two different columns including Durashell C18 and Waters X bridge RP18 were used for the separation of the analyte. From the initial screening process, separation of HPPH on Durashell C18 with Mobile phase (acetonitrile and sodium phosphate buffer pH 4.2; 80:20) showed delayed retention time i.e., at 17.3 min with interference. While, Elution on Waters Xbridge RP18 column with mobile phase (acetonitrile and sodium phosphate buffer pH 4.2; 80:20), exhibited the retention time at 4.7 min with noise interference.

Table 5.1: Chromatographic condition for HPPH

Chromatographic Parameter	Optimized condition for HPPH
System	Shimadzu HPLC (LC-2010HT, Shimadzu Corporation, Japan)
Column	Waters X Bridge™ Shield RP 18 (50 × 4.6 mm i.d., 5 μm)
Injection volume	20 μL
Linearity range	50-2000 ng/MI
R ² value	0.999
Mobile phase	Acetonitrile: Ammonium acetate pH 4.2 (80:20)
Oven Temperature	Ambient temperature(30°C)
Wavelength	406 nm

Thereafter, Waters Xbridge RP18 column was selected because of the good properties including separation efficiency, lower tailing factor, a high number of the theoretical plate and shortest retention time when compared to Durashell C18 column. Moreover, two buffer systems including ammonium acetate, and phosphate buffer with pH 4.0 were also used for chromatographic screening. Finally, it was observed that ammonium acetate with pH 4.0 showed clear baseline and symmetric peaks compared to other buffer systems. The chromatographic condition and chromatogram were shown in Table 5.1 and Figure 5.1 respectively.

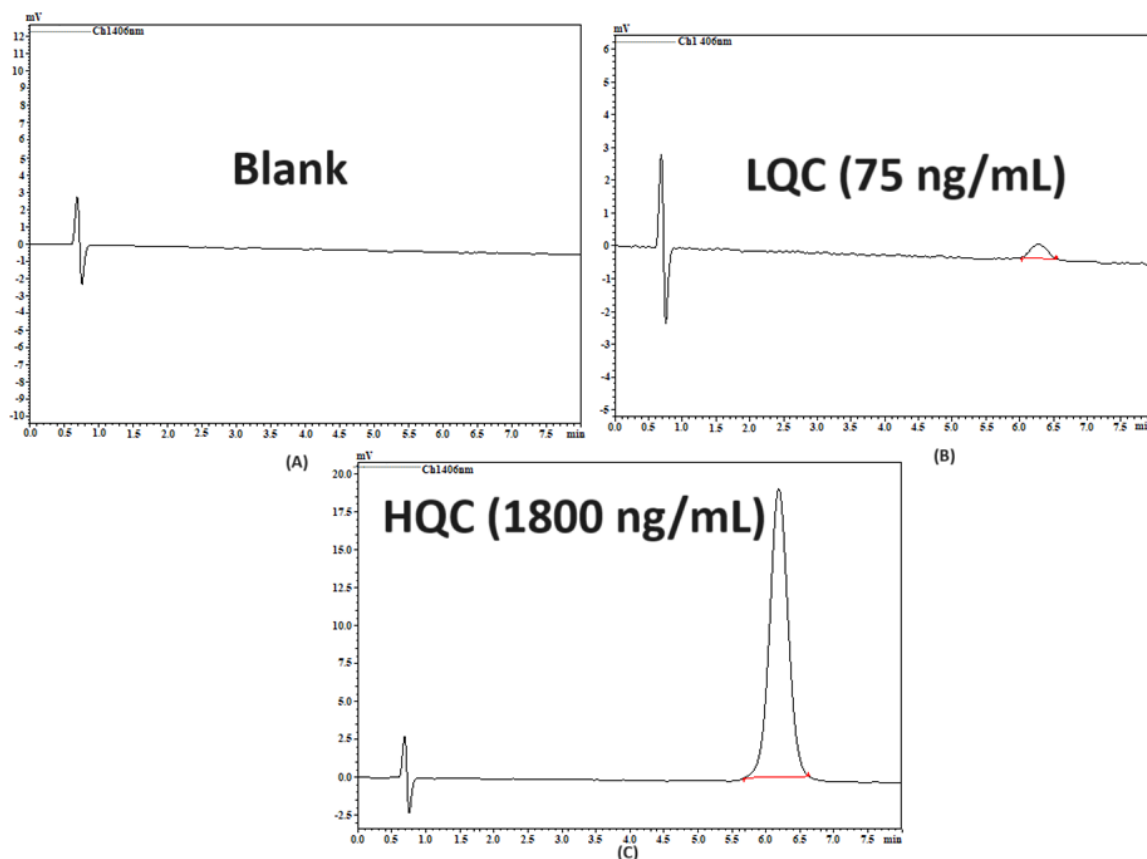


Figure 5.1: Chromatogram of HPPH; A) Blank, B) LQC, C) HQC

5.1.2. Method validation Parameters

5.1.2.1. System suitability

System suitability test was performed as per ICH Q2 R1 guideline. This was expressed in terms of retention time, HETP, theoretical plate and tailing factor. From the result, these values were found to be 6.2 min for RT, 47.04 for HETP, 3188 for theoretical plate and 1.080 for tailing factor, respectively. A good and suitable performance of the system was indicated by the results of the system suitability test. The parameters with respect to system suitability of standard solution were within the limits which indicated a degree of acceptability.

5.1.2.2. Specificity

The specificity of developed method was checked by analysing of the amount of HPPH in its lipid-polymeric nanoparticle without any interference from the excipients. The specificity result was revealed in term of %recovery and obtained value for HPPH was $99.90 \pm 1.10\%$. The obtained result indicated that there was no obstruct from the different excipients used in the carrier system and suggested that the developed method was highly specific to HPPH.

5.1.2.3. Linearity and range

The linearity was conducted with six injections of calibration points. The calibration curve equation was $y = 179.81x - 639.66$. From the data, the calibration curves displayed a linear relationship over a range of 50-2000 ng/mL for HPPH with an R^2 value of 0.999.

5.1.2.4. Accuracy and precision

Accuracy and precision with respect to intra-day and inter-day were calculated at four different quality control levels i.e., LOQ, MQC1, MQC2, and HQC with four sets of samples. All the results of accuracy and precision were shown in Table 5.2. The obtained results meet the acceptance criteria as per guidelines and exhibited the accuracy and highly reproducible nature of the method.

Table 5.2: Accuracy and precision of HPPH

Levels	Nominal Conc. (ng/mL)	Intra-day		Inter-day	
		%RSD	%Bias	%RSD	%Bias
LQC	75	1.40	-1.06	1.69	0.87
MQC1	300	1.12	-0.26	1.67	1.08
MQC2	900	0.12	1.21	1.22	1.10
HQC	1800	0.07	0.43	1.69	1.28

5.1.2.5. Sensitivity

The LOD and LOQ were calculated using the S/N ratio of response of analyte and their value was found to be 14.03 ng/mL for LOD and 42.80 ng/mL for LOQ respectively. This indicated the developed method was highly sensitive.

5.1.2.6. Robustness

Robustness of developed RP-HPLC method was conducted using three different conditions i.e. flow rate, pH, mobile phase ratio and %RSD were calculated at MQC 2. The data were shown in Table 5.3 which was within the acceptance limit as per ICH Q2 R1. The results indicated that HPPH was not disturbed by minor deviation in process parameters, such as flow rate and mobile phase ratio and the area response of HPPH remained the same. Hence, the method was highly robust and can be used for routine analysis.

Table 5.3: Robustness of HPPH

Parameter	Level	Nominal Value (ng/mL)	Observed Value (ng/mL) (Mean \pm SD)	%RSD
Flow rate (mL/min)	0.8	900	917.33 \pm 9.44	1.02
	1	900	907.87 \pm 3.84	0.42
	1.2	900	899.35 \pm 9.24	1.02
	4.2	900	896.71 \pm 1.73	0.19
	4.0	900	909.73 \pm 11.26	1.23
pH	3.8	900	917.33 \pm 14.33	1.56

	75:25	900	915.48±12.85	1.40
Mobile phase	80:20	900	909.55±10.48	1.15
(ACN : AA)	85:15	900	896.45±0.48	0.05

ACN: Acetonitrile; AA: 10mM Ammonium Acetate Buffer pH 4.2

5.1.2.7. Stability

The stability studies including benchtop, short term, auto-sampler, long term, and the stock solution were performed under different conditions with different environments. Both stock solution stability (10 days) and long-term stability (180 days) studies were performed at -20° C. Short-term stability and auto-sampler stability studies were performed at 4° C with four QC concentrations for 14 days and 24 h respectively. Similarly, a bench-top stability study was conducted at room temperature for 7 hr. The stability study of HPPH was determined based on the peak areas and retention time compared to the freshly prepared solution of QC samples. The %RSD among these samples was calculated. For HPPH, the %RSD was found to be less than 2%. The analytes were found to be stable at different temperature conditions. The representative data were shown in Table 5.4.

Table 5.4: Different Stability studies of HPPH

Exercise	Level	Nominal Conc. (ng/mL)	%RSD	%Bias
Stock solution Stability (10 days)	LQC	75	1.89	-1.45
	MQC1	300	1.15	-0.94
	MQC2	900	0.27	1.66
	HQC	1800	0.79	1.27
Autosampler Stability (24 hr.)	LQC	75	1.25	0.44
	MQC1	300	1.05	-0.38
	MQC2	900	0.26	1.98
	HQC	1800	0.83	1.26
Benchtop Stability (7 hr.)	LQC	75	1.79	-0.51
	MQC1	300	1.10	-0.99
	MQC2	900	0.10	1.83
	HQC	1800	0.70	0.86
Short term Stability (14days)	LQC	75	0.77	1.43
	MQC1	300	0.53	-0.05
	MQC2	900	1.23	0.97
	HQC	1800	1.35	1.70
Long term Stability (180 days)	LQC	75	1.39	-1.25
	MQC1	300	0.56	-0.99
	MQC2	900	0.10	1.83
	HQC	1800	0.93	1.07

5.1.2.8. Forced degradation studies of drug

Different forced degradation studies of HPPH were performed under different conditions such as basic, acidic, oxidative, light, and thermal. From the results, it was shown that HPPH was highly sensitive to alkali and subsequently resulted in its degradation. While, HPPH was comparatively stable under acidic, oxidative, photolytic, and thermal stress. For oxidation,

HPPH was affected by oxidation stress degradation studies using hydrogen peroxide. Only 0.02% of the drug was degraded which indicated that HPPH was stable under oxidative stress. Further, HPPH in alkaline medium i.e., treated with 1N NaOH showed 98.98% degradation after five minutes of incubation. This degradation may be due to the precipitation of HPPH in a basic environment. Consequently, the acidic study of HPPH was revealed that there was no degradation of the drug in acidic interaction. The hydrolysis in acidic conditions was lower than hydrolysis in alkaline conditions. Photolytic studies showed that less than 1% of HPPH i.e., 0.23% was degraded in sunlight treatment. Subsequently, the thermal study showed that there was no degradation of HPPH in 80° C. The representative chromatograms of the forced degradation study of HPPH were depicted in Figure 5.2. From this study, it can be revealed that the developed method was highly selective indicating i.e., the developed method can detect and differentiate the impurity peaks in the sample matrix. This could be utilized during formulation development for the investigation of impurity generation.

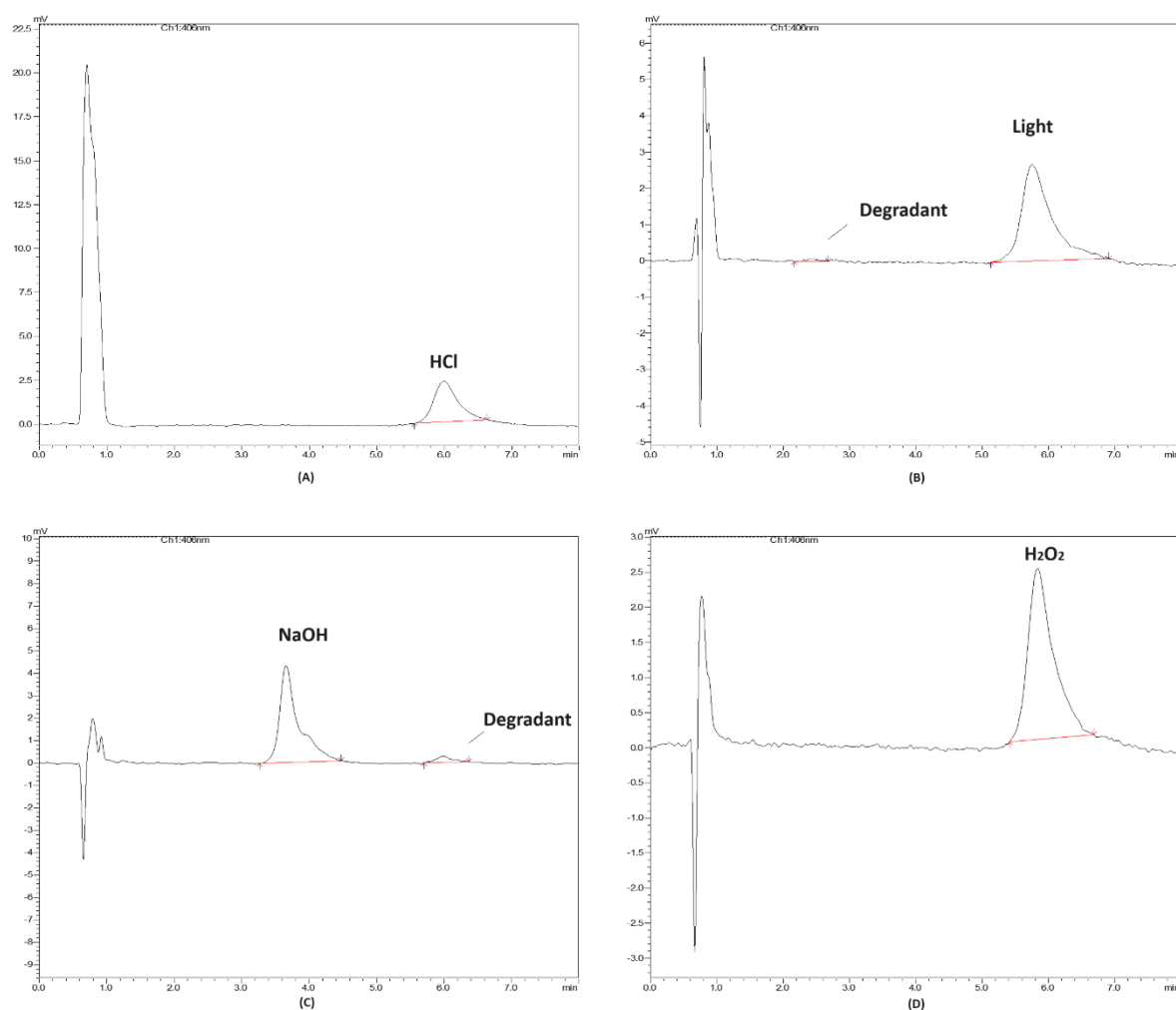


Figure 5.2: Force degradation study of HPPH

5.2. Analytical method development and validation of OLA by RP-HPLC

5.2.1. Method development

The RP-HPLC-based method was done with Shimadzu HPLC with UV-Visible detector. Chromatographically, Waters X bridge RP18 were used for the separation of the analyte. The OLA elution was carried out with mobile phase mixture (acetonitrile and Ammonium acetate pH 4.2; ratio 30:70), exhibited the retention time at 3.7 min with noise interference.

Table 5.5: Chromatographic condition for OLA

Chromatographic Parameter	Optimized condition for OLA
System	Shimadzu HPLC (LC-2010HT, Shimadzu Corporation, Japan)
Column	Waters X Bridge™ Shield RP 18 (50 × 4.6 mm i.d., 5 μm)
Injection volume	20 μL
Linearity range	50-2000 ng/mL
R2 value	0.992
Mobile phase	Acetonitrile: Ammonium acetate pH 4.0 (30:70)
Oven Temperature	Ambient temperature(30°C)
Wavelength	269 nm

Finally, it was observed that ammonium acetate with pH 4.0 showed clear baseline and symmetric peaks. The chromatographic condition and chromatogram were shown in Table 5.5 and Figure 5.3 respectively.

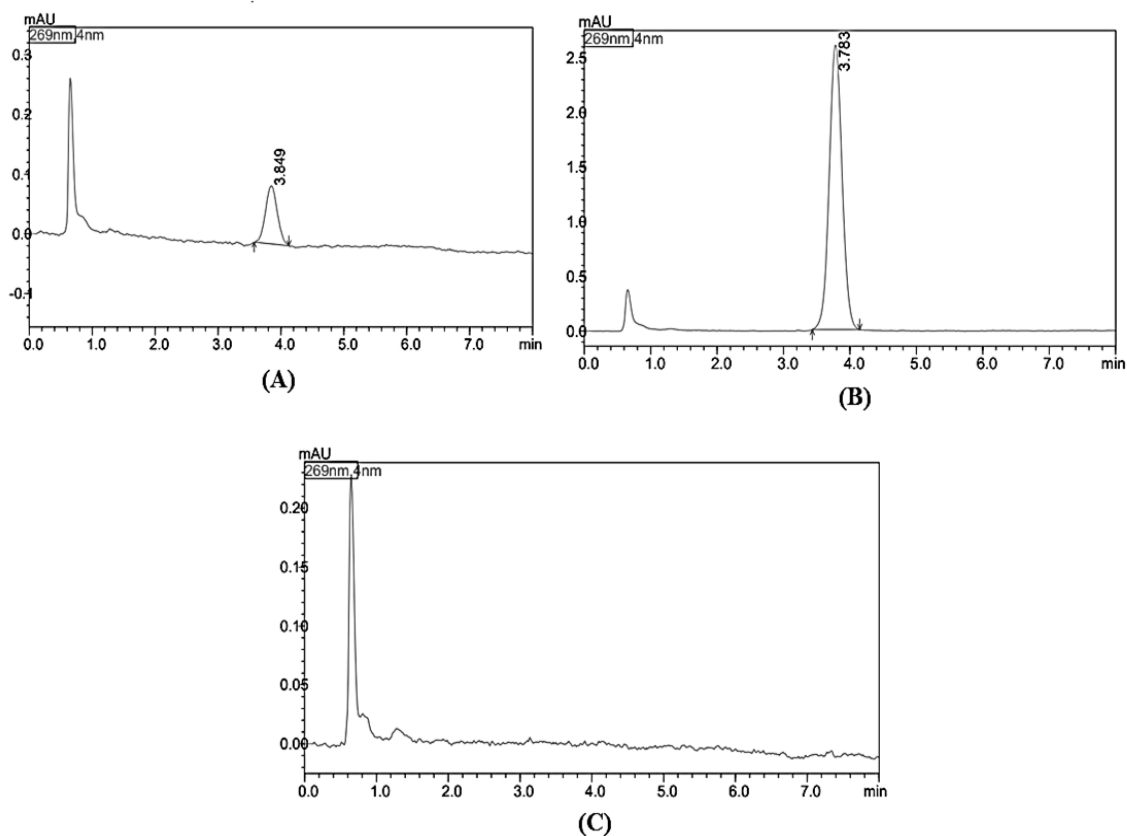


Figure 5.3: Chromatogram of OLA; A) LQC (75ng/mL); B) HQC 1800ng/mL; C) Blank

5.2.2. Validation Parameters

Assay validation of the method was performed on the basis of various parameters including accuracy, precision, specificity, system suitability and stability as per the guidelines.

5.2.2.1. Specificity

The specificity of developed methods for OLA were assessed with MQC level by spiking the mobile phase with different excipients utilized in nano-formulation. It was observed that there is no interference with analytes retention time which indicated that method was highly specific drugs.

5.2.2.2. System suitability

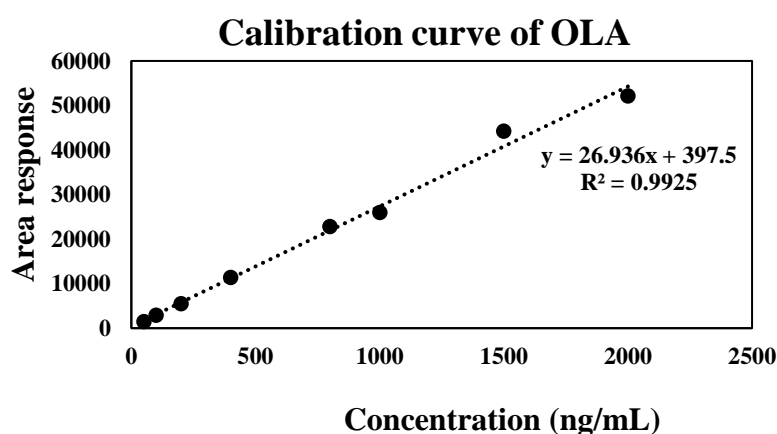
The System suitability of developed method was carried out using six replicates of the injection of QC level (MQC2). All the result suggested that the instrument facility is highly efficient for analysis. The representative values of system suitability were shown in the table 5.6.

Table 5.6: System Suitability Parameter of OLA

Parameters	Acceptance limit	OLA
Tailing factor	<1.5	1.011
Theoretical plate	>2000	3820.0
HETP	-	36.55

5.2.2.3. Calibration curve and Linearity

The developed method was validated with eight calibration standard concentration over a linearity range of 50-2000ng/mL. The obtained result indicated that observed linearity was successfully fitted calibration range with R^2 value of 0.992. The representative calibration curves with standard calibration equation were depicted in Figure 5.11.

**Figure 5.4: Calibration curve and standard calibration equation of OLA**

5.2.2.4. Accuracy and precision

Accuracy and precision of developed method were accessed with five different QC level i.e., LLOQ, LOQ, MQC, MQC2 and HQC in 4 replicates. Both % Bias and % RSD were found within the range of $\pm 2\%$ that indicates developed method was highly accurate and précised. The obtained data for both accuracy and precision were revealed in Tables 5.7.

Table 5.7: Accuracy and precision of OLA

Levels	Nominal Conc. (ng/mL)	Intra-day		Inter-day	
		%RSD	%Bias	%RSD	%Bias
LLOQ	50	1.73	-0.94	0.66	-1.26
LQC	75	1.72	1.65	2.68	0.00
MQC1	300	1.99	-1.05	0.88	-0.95
MQC2	900	1.99	0.52	0.22	0.55
HQC	1800	1.87	-0.10	0.04	-0.11

5.2.2.5.Sensitivity: LOD and LOQ

Based on S/N ratio, LOD and LOQ values was 16.27 ng/mL and 48.2 ng/mL. Hence, the data indicates that method is highly sensitive to perform the desired assay of OLA.

5.2.2.6.Robustness

The developed methods were subjected to robustness analysis using three parameters viz. flow rate, pH and mobile phase composition at MQC2 level. The obtained data for robustness were mentioned in table 5.8. It was indicated that % RSD were found within the acceptance criteria limit. Therefore, the developed method is said to be highly robust and can be utilized in routine analysis.

Table 5.8: Robustness of analytical method of OLA

Parameter	Level	Nominal Value (ng/mL)	Observed Value(ng/mL) (Mean \pm SD)	%RSD
Flow rate (mL/min)	0.8	900	907.17 \pm 4.97	0.55
	1	900	901.48 \pm 16.73	1.86
	1.2	900	895.70 \pm 23.84	2.66
pH	4.4	900	899.50 \pm 9.47	1.05
	4.2	900	901.97 \pm 6.81	0.76
	4.0	900	906.92 \pm 2.29	0.25
Mobile Phase (ACN: AA)	25:75	900	905.68 \pm 1.32	0.15
	30:70	900	902.47 \pm 0.19	0.02
	35:65	900	884.65 \pm 1.44	0.16

ACN: Acetonitrile; AA: Ammonium Acetate Buffer;

5.2.2.7.Stability

The stability studies including benchtop, short term, auto-sampler, long term, and the stock solution were performed under different conditions with different environments. Both stock solution (10 days) and long-term stability (180 days) studies were performed at -20° C. Short-term stability and auto-sampler stability studies were performed at 4° C with four QC concentrations for 14 days and 24 hrs respectively. Similarly, a bench-top stability study was conducted at room temperature for 7 hrs. The stability study of OLA was determined based on the peak areas and retention time compared to the freshly prepared solution of QC samples. The %RSD among these samples was calculated. For OLA, the %RSD was found to be less than 2%. The analytes were found to be stable at different temperature conditions. The representative data are shown in Table 5.9.

Table 5.9: Different Stability studies of OLA

Exercise	Level	Nominal Conc. (ng/mL)	%RSD	%Bias
Stock solution Stability (10 days)	LQC	75	1.66	-0.50
	MQC1	300	2.68	0.00
	MQC2	900	0.90	-0.94
	HQC	1800	0.28	0.47
Autosampler Stability (24 hr.)	LQC	75	1.65	-0.45
	MQC1	300	0.47	-1.34
	MQC2	900	1.13	-1.77
	HQC	1800	0.23	0.54
Benchtop Stability(7hr.)	LQC	75	1.25	-1.54
	MQC1	300	0.52	-1.51
	MQC2	900	0.92	-0.89
	HQC	1800	0.14	0.45
Short term Stability (14 days)	LQC	75	0.63	-1.31
	MQC1	300	0.44	1.64
	MQC2	900	0.88	-0.95
	HQC	1800	0.15	0.63
Long term Stability (180 days)	LQC	75	0.95	-1.04
	MQC1	300	0.21	-1.52
	MQC2	900	1.03	-0.81
	HQC	1800	0.29	0.59

5.3. Simultaneous analytical method development and validation of HPPH and OLA by LC-MS/MS

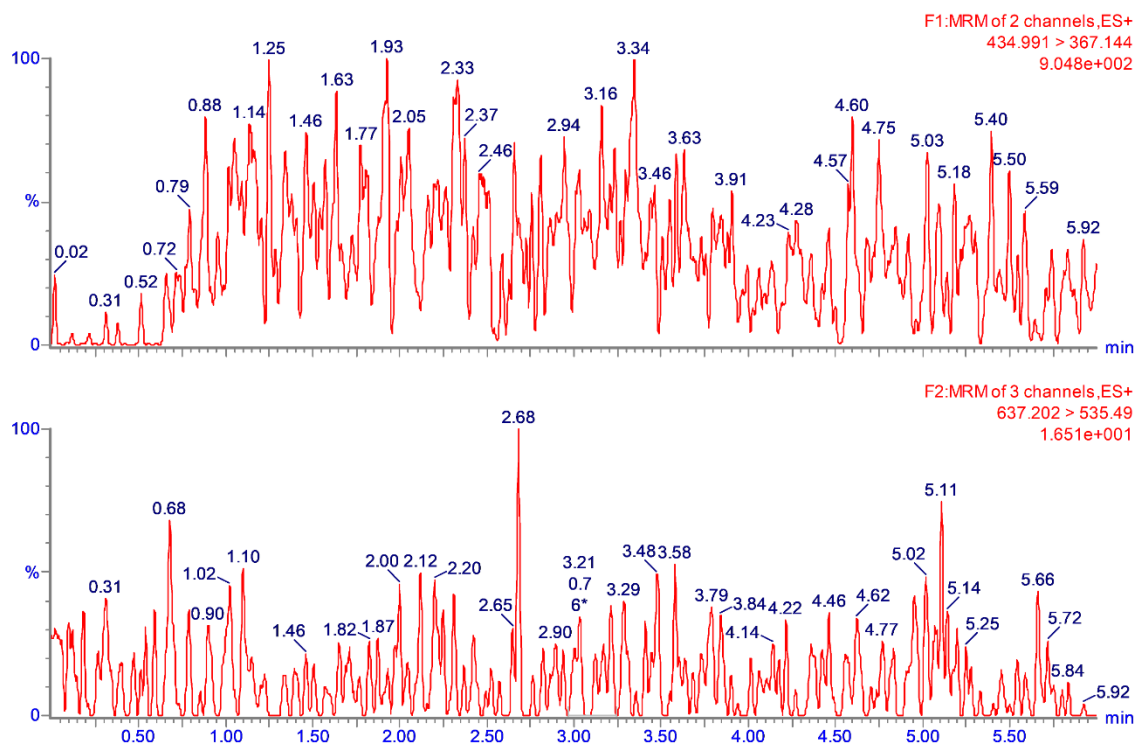
5.3.1. Method Development

The analytical method in mice plasma was developed for both OLA and HPPH using LC-MS/MS with Acquity UPLC® BEH C18 column (150 mm × 2.1 mm i.d, 1.7 μm particle size) and mobile phase mixture of 0.1 % formic acid in 10mM Ammonium Acetate, Acetonitrile, Methanol with the ratio of 5:85:10 at a flow rate of 0.350 mL/min. The analysis of OLA and HPPH was done by ESI positive mode. The transitions m/z 637.99 → 267.14, and m/z 434.99 → 367.14 was obtained for HPPH and OLA respectively. The representative chromatographic condition was depicted in table 5.10.

Table 5.10: Chromatographic condition of HPPH-OLA

Chromatographic Parameter	Optimized condition
LC-MS/MS system	Waters ACQUITY UPLC® system (Waters Corporation, Milford, MA, USA)
Column	Waters UPLC® BEH C18 (2.1 × 50 mm, 1.7 μm)
Column oven temperature	40 °C
Mobile Phase	Acetonitrile: Methanol: 0.1% Formic Acid in AA: 85:10:05 (Isocratic)
Flow rate	0.350 mL/min
Injection volume	10 μL
Linearity	1.56-200 ng/mL (HPPH and OLA)
Run Time	6.00 Min.

Injection volume was kept 10 μ L. Total analysis time of single injection was 5 min. Besides, a two step liquid-liquid extraction by using diethyl ether was employed for sample extraction. The retention time of HPPH and OLA were about 3.1 min and 1.05min respectively. The representative MRM are depicted in figure 5.5.



(A)

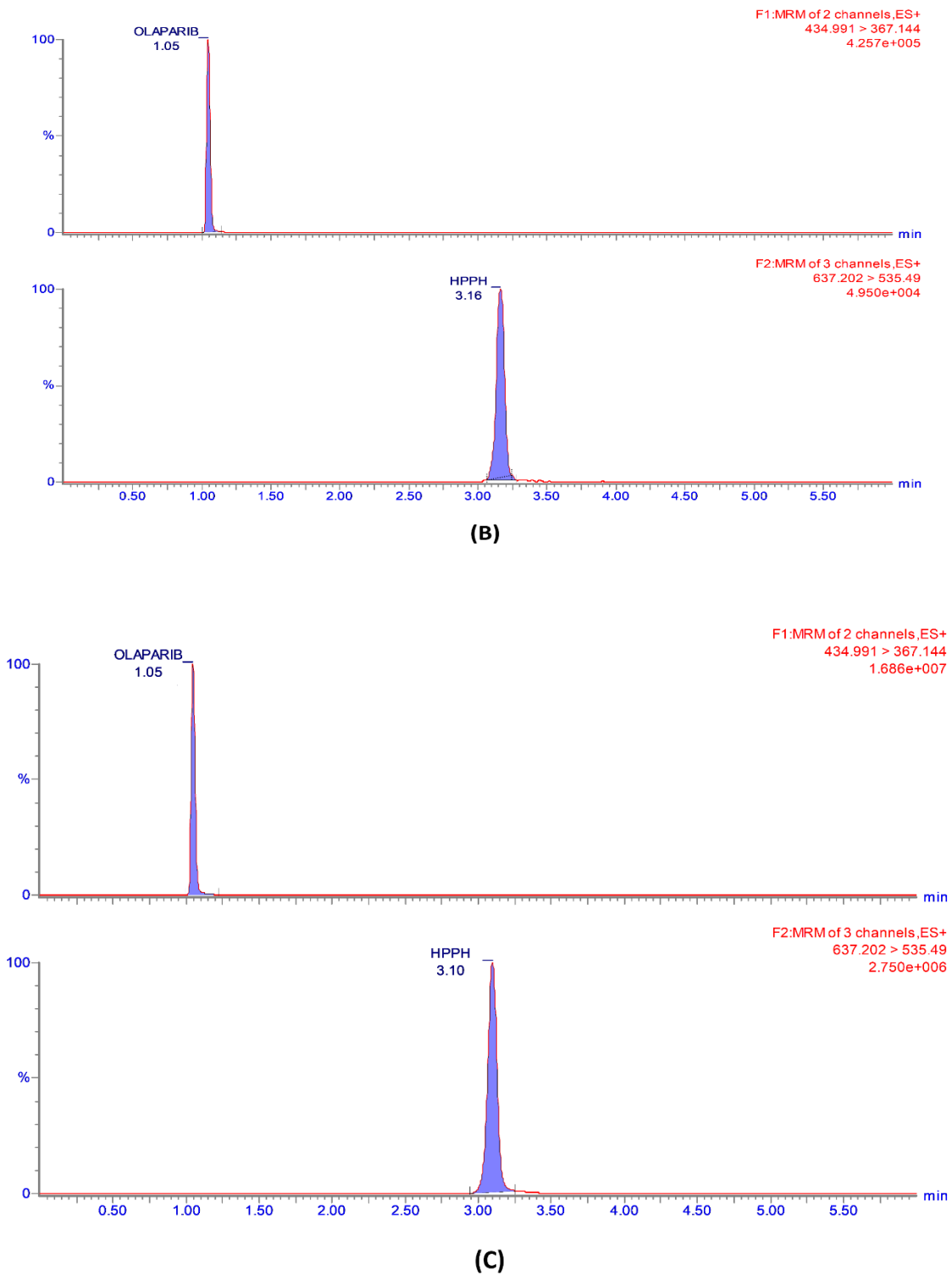


Figure 5.5: MRM based simultaneous chromatogram of HPPH and OLA; A) Blank; B) LQC (2ng/mL);C) MQC (90ng/mL); D)HQC (180ng/mL)

5.3.2. Method validation

5.3.2.1. System suitability

The results of the system suitability indicates that instrumentation has shown good performance of the system. The system suitability parameters of standard solution were found to be within the limits.

5.3.2.2. Linearity and Calibration curve

The calibration curves were exposed with a good linear relationship over a range of 1.56-200 ng/ml for HPPH and OLA. The results for the linearity of the calibration curve were validated by the regression coefficient (R^2) which is given in Table 5.11.

Table 5.11: Standard calibration curves equation and correlation coefficients of HPPH and OLA

Analytes	Standard curve equation	R2 value
HPPH	$y = 1600.03x + 697.53$	0.993
OLA	$y = 1012.1x + 614.13$	0.993

5.3.2.3. Accuracy and Precision

Accuracy and precision (intra- and inter-batch) were determined at four different levels i.e., LOQ, MQC, MQC2 and HQC in 4 replicates manner; the representative data was depicted in Table 5.12. The result suggested that accuracy and precision of both OLA and HPPH were fall on acceptance criteria as per analytical guidelines. hence, it can say to be the developed methods is highly accurate and reproducible.

Table 5.12: Accuracy and Precision of HPPH and OLA

Drugs	Level	Nominal Concentration (ng/mL)	Intra day		Inter day	
			% RSD	% Bias	% RSD	% Bias
HPPH	LQC	2	0.68	-1.81	1.73	0.75
	MQC	15	0.48	1.92	1.72	1.54
	MQC2	90	1.95	-1.29	1.99	0.81
	HQC	180	1.09	-0.05	1.87	1.54
OLA	LQC	2	1.38	-1.98	1.83	0.65
	MQC	15	0.46	1.96	1.93	1.40
	MQC2	90	1.99	-1.10	1.99	0.79
	HQC	180	1.13	-0.02	1.86	1.55

5.3.2.4. Sensitivity: LOD and LOQ

The sensitivity was were established using the S/N ratio parameter as per the analytical guidelines. The LOD value were found to be 300 pg/mL and 1.02 ng/mL for OLA and HPPH respectively. Likewise, the obtained LOQ was 250 pg/mL and 1.05 ng/mL for OLA and HPPH

respectively. Hence, this data shown that the developed simultaneous method was highly sensitive for analysis.

5.3.2.5. Robustness

The obtained data revealed that the developed method was met acceptance criteria i.e., all area response fall on % RSD value ± 2 . Thus, the method is said to be a robust and the results are shown in Table 5.13.

Table 5.13: Robustness (Different Analyst) HPPH and OLA

Drug	Level	Concentration (ng/ml)	%RSD	%Bias
HPPH	LQC	2	1.38	-1.98
	MQC	15	0.46	1.96
	MQC2	90	1.99	-1.10
	HQC	180	1.13	-0.02
OLA	LQC	2	1.83	0.65
	MQC	15	1.93	1.40
	MQC2	90	1.99	0.79
	HQC	180	1.86	1.55

5.3.2.6. Stability

Based on regulatory guidelines, the stability studies for the developed method were executed in terms of bench-top, short term, auto-sampler, long term, and the stock solution. The stability study of OLA and HPPH was determined with respect to %RSD and % Bias compared to the freshly prepared solution of QC samples. The obtained data suggested that %RSD and %Bias of this simultaneous method of OLA and HPPH was within 2%. Both the analytes were shown to be stable with respect to different stability studies. The obtained result for different stability were mentioned in Table 5.14.

Table 5.14: Stability studies of HPPH and OLA

Stability	QC Sample	Level	HPPH		OLA	
			%RSD	%Bias	%RSD	%Bias
Autosampler Stability (24 hr.)	LQC	2	0.85	-1.98	1.51	-2.05
	MQC	15	0.41	1.97	0.08	1.50
	MQC2	90	1.95	-1.28	1.99	0.72
	HQC	180	1.09	-0.05	1.88	1.53
Bench-Top Stability (7 hr.)	LQC	2	1.44	-1.65	1.95	0.44
	MQC	15	0.45	1.95	0.93	-1.51
	MQC2	90	1.99	-1.24	0.70	-1.87
	HQC	180	1.10	-0.02	1.90	1.56
Freeze-Thaw Stability (3-cycle,48hr.)	LQC	2	0.85	-1.98	1.73	0.75
	MQC	15	0.33	2.01	1.72	1.54

	MQC2	90	1.95	-1.29	1.99	0.58
	HQC	180	1.09	0.05	1.88	1.53
Short-term Stability (14 days)	LQC	2	1.69	1.81	1.73	0.75
	MQC	15	0.21	2.06	1.73	1.40
	MQC2	90	1.94	-1.29	1.99	0.81
	HQC	180	1.15	-0.23	1.96	1.43
Long-term Stability (180 days)	LQC	2	0.68	-1.81	1.73	0.75
	MQC	15	0.43	1.84	0.56	-2.06
	MQC2	90	1.92	-1.27	1.98	0.64
	HQC	180	1.09	-0.04	1.90	1.54

5.4. Bioanalytical method development and validation of HPPH and OLA using LC-MS

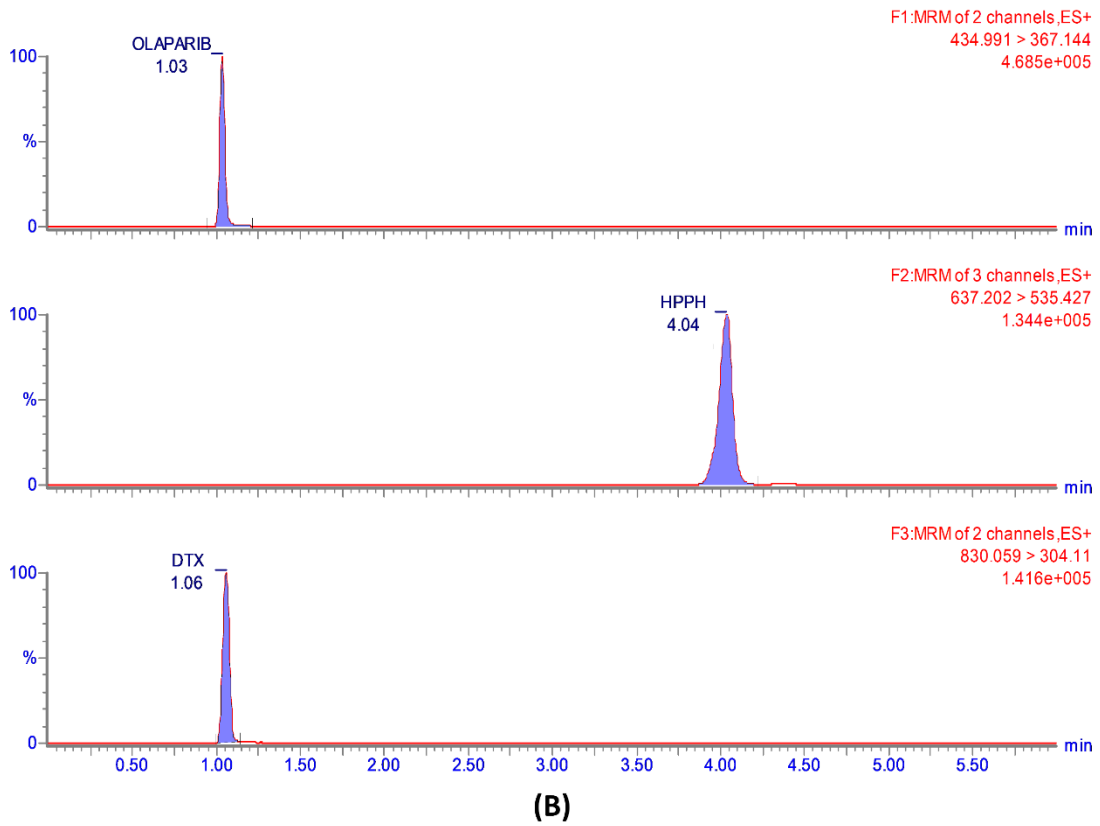
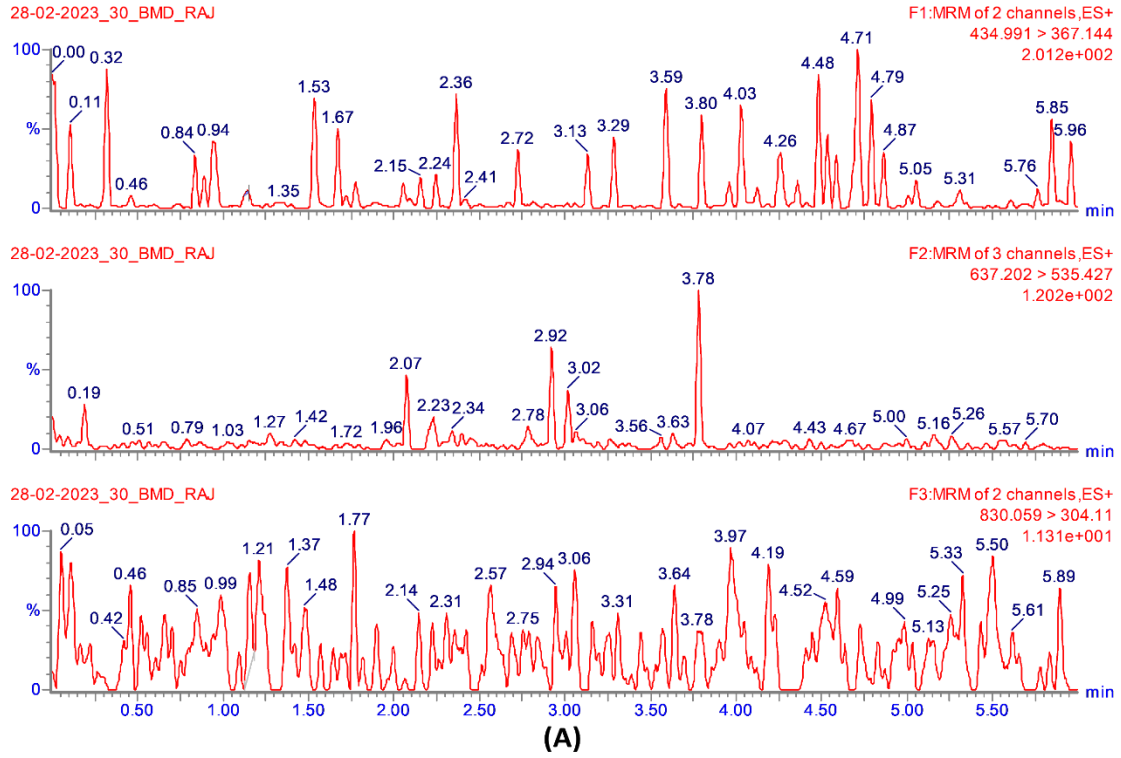
5.4.1. Method development

The bioanalytical method in mice plasma was developed for both OLA and HPPH using LC-MS/MS with Acquity UPLC®BEH C18 column (150 mm × 2.1 mm i.d, 1.7 μM particle size) and mobile phase mixture of 0.1 % formic acid in 10mM Ammonium Acetate, Acetonitrile, Methanol with the ratio of 7:83:10 at a flow rate of 0.350 mL/min. The analysis of OLA and HPPH was done by ESI positive mode. Docetaxel was selected as internal standard. The transitions m/z 637.99 → 267.14, m/z 434.99 → 367.14 and m/z 830.059 → 304.11 was obtained for HPPH, OLA and Docetaxel (IS) respectively. The representative table was depicted in table 5.15.

Table 5.15: Optimization of chromatographic condition of HPPH-OLA (Mice plasma)

Chromatographic Parameter	Optimized condition
LC-MS/MS system	Waters ACQUITY UPLC® system (Waters Corporation, Milford, MA, USA)
Column	ACQUITY UPLC®BEH Shield RP column (150mm*2.1, 1.7μm IDM)
Column oven temperature	40 °C
Mobile Phase	Acetonitrile:Methanol: 0.1% Formic Acid in AA :: 83:10:07 (Isocratic)
Flow rate	0.350 mL/min
Injection volume	10μL
Linearity	1-320 ng/mL (HPPH and OLA)
Run Time	6.00 Min.

The injection volume was kept 10 μL. The total analysis time for single injection was 5 min. Besides, a single step liquid-liquid extraction was employed using diethyl ether for sample processing. The retention time of HPPH, OLA and Docetaxel (IS) were 4.04 min , 1.03 min and 1.05 min respectively. The representative MRM were depicted in figure 5.6.



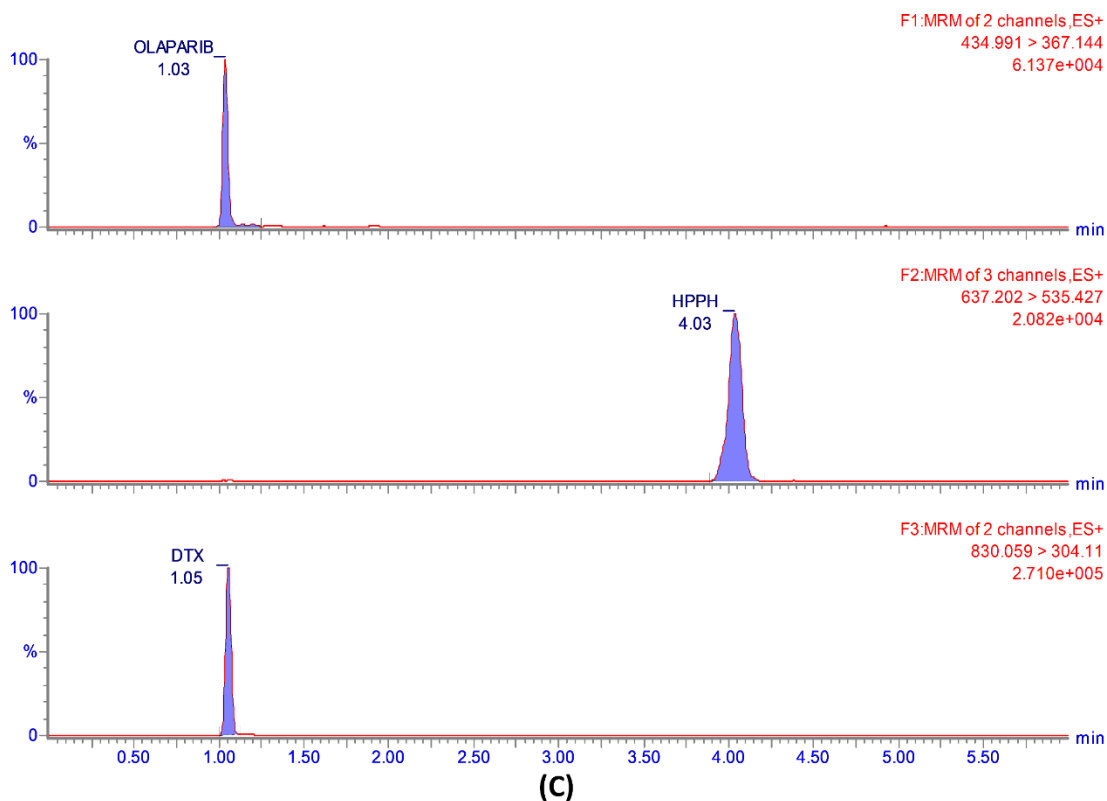


Figure 5.6: MRM based simultaneous chromatogram for HPPH and OLA; A) Blank; B) LQC (2ng/mL); C)HQC (300ng/mL)

5.4.2. Assay Validation for HPPH and OLA in mice Plasma

5.4.2.1. System suitability

The system suitability test was performed at MQC2 (100 ng/mL) level for six repeat injections. The % CV of the retention times and peak area response of both analytes and IS were within the acceptance limit i.e., 2% and 5% CV, respectively which was confirmed that the developed method was suitable for analysis.

5.4.2.2. Selectivity

The selective study was performed with six different pooled plasma. The obtained selectivity data for both OLA and HPPH indicated that plasma matrix showed no significant interference at retention time. The MRM based chromatograms representation of blank plasma and LLOQ was depicted in figure 5.6.

5.4.2.3. Carry-over effect

The carry-over results suggested that no enhancement in the peak area ratio response was observed in blank samples after the ULOQ at retention times.

5.4.2.4. Calibration Curve and Linearity

The calibration curves were linear over the concentration range of 1–320 ng/mL for both HPPH and OLA which is given in the table 5.16.

Table 5.16: Standard calibration curves equation and correlation coefficients of HPPH-OLA(Plasma)

Drug	Standard curve equation	R2 value
HPPH	$y = 0.0333x - 0.0063$	0.998
OLA	$y = 0.0314x - 0.0182$	0.993

The calibration model was fitted on basis of the analysis of the data by linear regression with and without intercepts ($y=mx+c$ and $y=mx$) and weighting factors ($1/x^2$). The lowest concentration with RSD < 20% was taken as LLOQ and was shown to be 1.05ng/mL. The representative calibration curve is shown in the Figure 5.7.

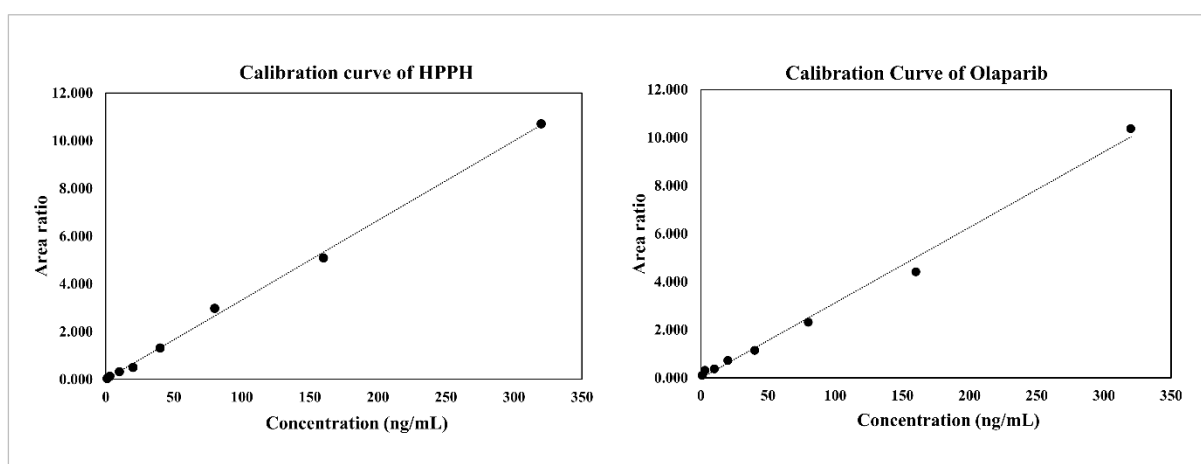


Figure 5.7: Calibration curve of HPPH and OLA

5.4.2.5. Sensitivity: Lower limit of detection (LOD) and Lower limit of quantification (LOQ)

In this method, LOD for HPPH was 0.280 ng.mL^{-1} and 0.330 ng.mL^{-1} for OLA which was calculated based on S/N ratio ≥ 3 . In the same manner, LLOQ was found to be 1.05 ng ml^{-1} for both HPPH and OLA which was exhibited on the basis of S/N ratio ≥ 10 . Moreover, LLOQ was estimated accurately and precisely as per international standard guidelines.

5.4.2.6. Matrix effect

The obtained results indicated that there is no significant interference of biometrics for all QC sample (table 5.17).

Table 5.17: Matrix effect of HPPH-OLA(Plasma)

Drug	Level	Nominal Concentration (ng/ml)	Calculated concentration (ng/ml)	%RSD
HPPH	LQC	2	1.97± 0.13	6.55
	MQC1	50	48.08± 6.60	13.73
	MQC2	100	104.63± 5.48	5.24
	HQC	300	286.54 ± 19.16	6.69
OLA	LQC	2	1.99 ± 0.10	4.77
	MQC1	50	55.76 ± 2.51	4.50
	MQC2	100	87.18 ± 3.13	3.59
	HQC	300	307.03 ± 16.67	5.43

5.4.2.7. Precision and accuracy of HPPH-OLA(Plasma)

The precision and accuracy of six replicates at five different concentrations (LLOQ, LQC, MQC1, MQC2 and HQC) were performed and the value was found within the acceptable criteria of 85-115%. The results of inter-day and intra-day accuracy and precision are illustrated in the table 5.18.

Table 5.18: Accuracy and Precision of HPPH and OLA(Plasma)

Drugs	Level	Nominal Concentration (ng/mL)	Intra day		Inter day	
			% RSD	% Bias	% RSD	% Bias
HPPH	LLOQ	1.05	1.53	15.51	14.53	-8.87
	LQC	2	11.58	-7.04	11.32	4.55
	MQC1	50	13.64	-4.22	6.70	-10.57
	MQC2	100	3.95	2.73	3.51	9.26
	HQC	300	6.50	-4.49	5.26	0.54
OLA	LLOQ	1.05	11.72	-14.47	2.71	-7.13
	LQC	2	5.49	-4.00	1.37	-3.47
	MQC1	50	6.10	10.02	6.24	10.26
	MQC2	100	4.50	-13.77	4.49	-13.71
	HQC	300	5.07	1.91	4.86	1.67

5.4.2.8. Dilution integrity

The dilution integrity was performed at 1200 ng. mL⁻¹ for both HPPH and OLA i.e., four times higher than ULOQ. The obtained results were demonstrated that the accuracy value (% recovery) of HPPH and OLA was found to be 102.31 ± 3.92 and 99.56± 2.34 respectively. The results of dilution integrity indicated that % recovery met the acceptance criteria.

5.4.2.9. Robustness

The robustness results against different analyst indicated that the precision and accuracy value were within acceptance criteria i.e., ±15% (%RSD and %Bias) for all QCs which were depicted in the table 5.19.

Table 5.19: Robustness against different analyst of HPPH and OLA(Plasma)

Drug	Level	Concentration (ng/ml)	%RSD	%Bias
HPPH	LQC	2	6.02	-1.80
	MQC1	50	13.95	-4.03
	MQC2	100	5.24	4.63
	HQC	300	6.27	-4.17
OLA	LQC	2	4.86	-3.47
	MQC1	50	5.86	10.26
	MQC2	100	4.57	-13.88
	HQC	300	5.13	1.99

5.4.2.10. Stability studies

According to US-FDA, the different stability studies (Autosampler, Bench-top, Freeze-thaw, Short-term and Long-term) were carried out at four different QC sample. As shown on Table 5.20, the data suggested that both the compounds (OLA and HPPH) were within the acceptance criteria as per the US-FDA guideline.

Table 5.20: Stability studies of HPPH and OLA(Plasma)

Stability	QC Sample	Level	HPPH %RSD	%Bias	OLA %RSD	%Bias
Autosampler Stability (24 hr.)	LQC	2	2.22	10.93	0.65	-3.48
	MQC1	50	7.75	-6.87	4.76	0.62
	MQC2	100	4.29	10.80	3.06	-11.06
	HQC	300	5.17	0.72	3.52	-11.18
Bench-Top Stability (7 hr.)	LQC	2	2.90	3.96	2.43	-2.42
	MQC1	50	8.99	-7.43	8.57	-1.51
	MQC2	100	4.97	11.29	4.78	-2.24
	HQC	300	8.01	-1.36	4.84	-10.47
Freeze-Thaw Stability (3-cycle,48hr.)	LQC	2	3.84	8.48	6.07	-0.29
	MQC1	50	10.25	-5.10	2.28	6.33
	MQC2	100	2.69	7.16	5.62	-14.77
	HQC	300	5.35	0.56	3.94	-11.17
Short-term Stability (14 days)	LQC	2	5.28	8.23	3.37	-1.88
	MQC1	50	6.49	-8.32	6.80	2.74
	MQC2	100	2.43	9.95	1.39	-7.95
	HQC	300	3.37	0.17	4.03	-11.53
Long-term Stability (180 days)	LQC	2	1.28	14.24	1.16	-4.54
	MQC1	50	9.19	-5.42	4.43	4.89
	MQC2	100	5.59	5.15	7.28	-14.83
	HQC	300	2.45	-1.02	3.68	-4.09

5.5. In-vitro cell culture study to explore the therapeutic potential of HPPH and OLA

5.5.1. Invitro cytotoxicity test of HPPH and OLA

The MTT assay was performed with different concentrations of HPPH to estimate cell viability. MTT is based on colorimetric analysis which quantify the reduction of yellow MTT by mitochondrial enzyme i.e., succinate dehydrogenase. Based on the MTT results data, 50% of cell death (IC₅₀) was observed at the dose 9.90 μ M after 48 h (Figure 5.8).

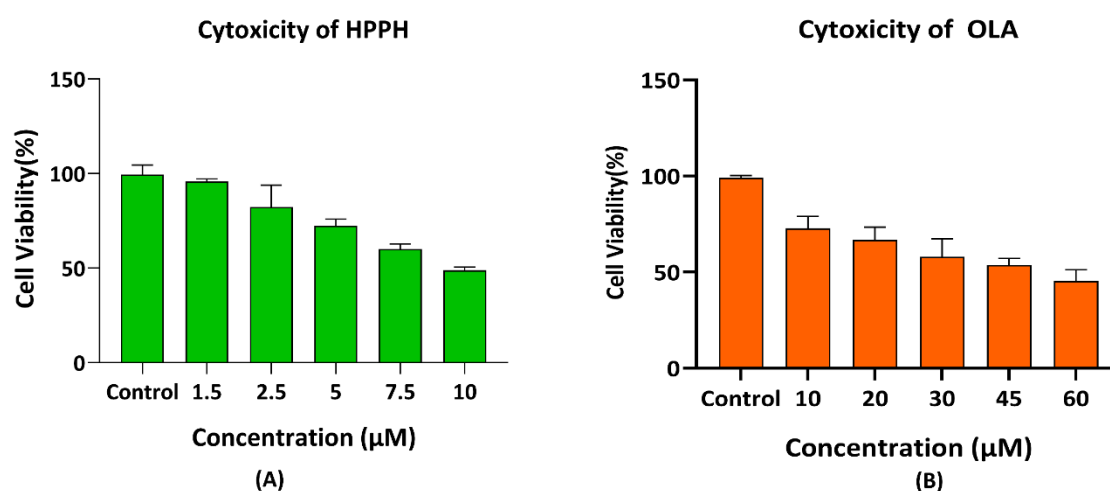


Figure 5.8: MTT assay of HPPH and OLA

In the same way, the MTT assay was performed for OLA with different concentrations to estimate cell viability. Based on the MTT results data of OLA, 50% of cell death (IC₅₀) was observed at the dose 59.8 μ M after 48 hr. and no significant morphological changes were observed in the 4T1 cell line (figure 5.8).

5.5.2. Evaluation of HPPH and OLA synergy

The synergistic effect of combining HPPH and OLA (HPPH-OLA) was studied in 4T1 cell line based on the IC₅₀ value of HPPH and OLA (Fixed combination with a ratio 1:6). The HPPH-OLA showed greater cytotoxicity when compared with HPPH and OLA- alone. The combination index of HPPH-OLA is less than 0.9 which indicated a strong synergy between HPPH and OLA in 4T1 cell line. The figure 5.9. shows the results of a dose-response effect and cytotoxicity study where (A) shows cytotoxicity of combination of HPPH and OLA (B) Combination index plot for HPPH-OLA. The cell viability of HPPH-OLA showed 46.27% cell viability at the HPPH/OLA combination dose of 4 μ M /24 μ M as shown in figure 5.9.

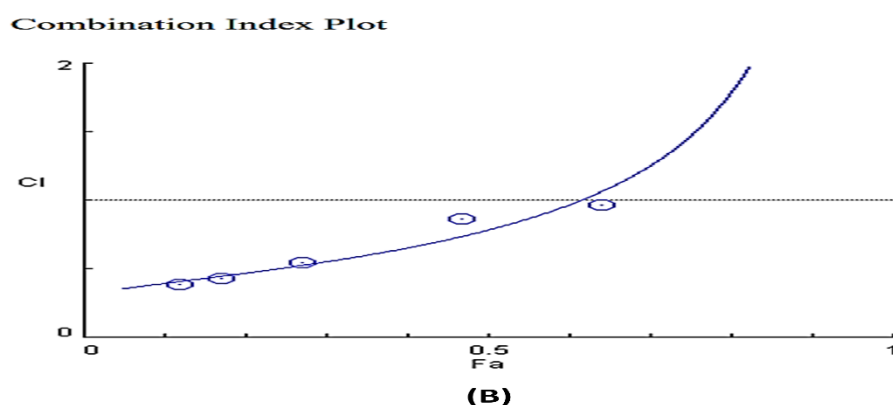
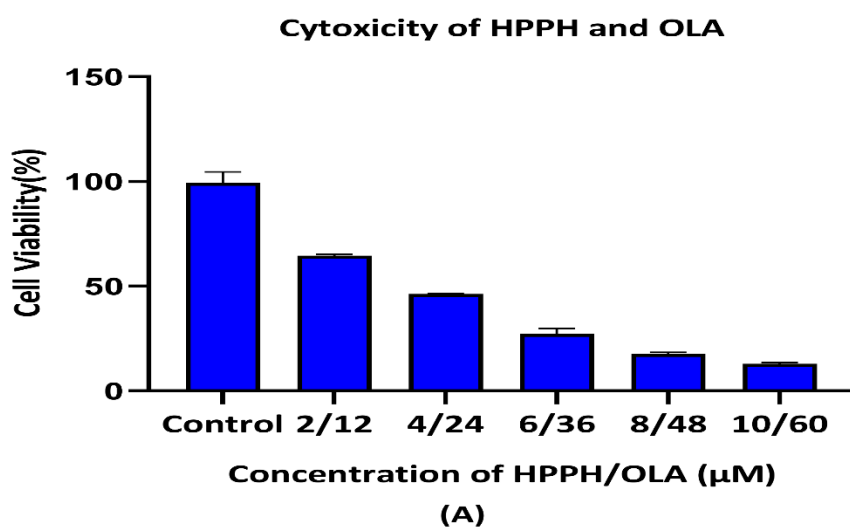


Figure 5.9: Dose-response effect and cytotoxicity study; (A) cytotoxicity of combination of HPPH and OLA (B) Combination index plot for HPPH-OLA

5.5.3. *In vivo* efficacy study of HPPH and OLA

The *in-vivo* efficacy was assessed in Luciferin tagged 4T1 (luc-4T1) tumor bearing animal model using an *in vivo* imaging technique with the IVIS® Lumina III, PerkinElmer, USA. The treatment was carried out for 10 days with daily administration of drug. The HPPH and OLA was administered intravenously at the dose of 5mg/kg.bw and 30mg/kg.bw respectively through tail vein. After every treatment, all the animals were exposed to laser light at 650nm for 20min. The survival timing, body weight and change in behavior of all the animals were recorded during the study period. On days 0, 3, 6, and 10 of the treatment periods, all the animals in each group i.e., HPPH, OLA and HPPH-OLA were examined for tumor growth, and body weight of the animal and their value were recorded. The body weight of all the group animal showed similar to the control group (figure 5.10 A). As shown in figure 5.11., the

luminescence intensity and in vivo imaging from treatment Day 0 to Day 10 was recorded for each group of animals i.e., Control, HPPH, OLA and HPPH-OLA. The result showed HPPH-OLA treated group has greater tumor suppression when compared to other treatment and control group which was further confirmed by measuring the tumor volume by vernier caliper (figure 5.10 B).

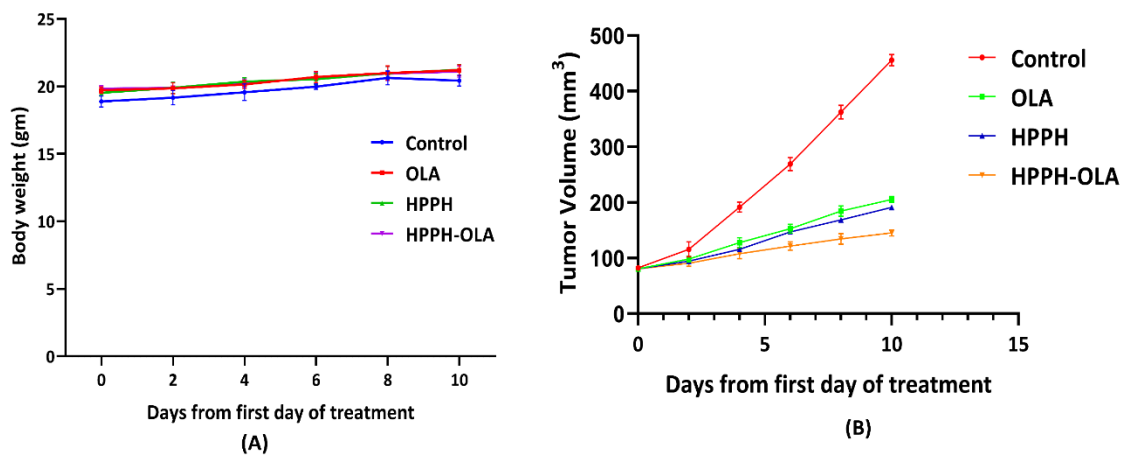
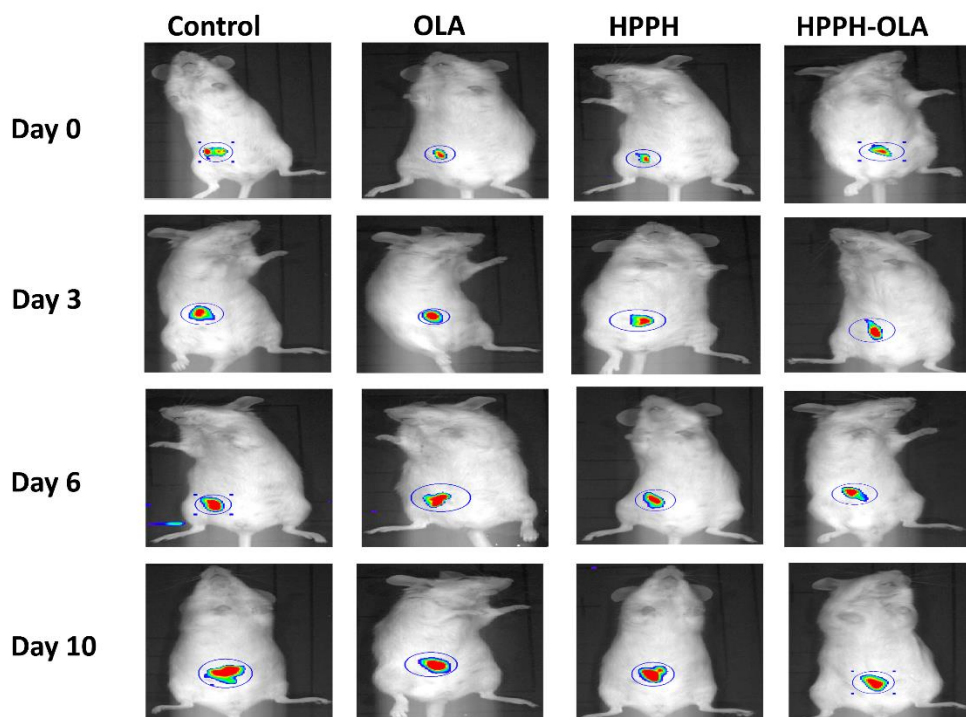


Figure 5.10: Body weight and tumour volume of each animal group i.e., Control, HPPH, OLA and HPPH-OLA



(A)

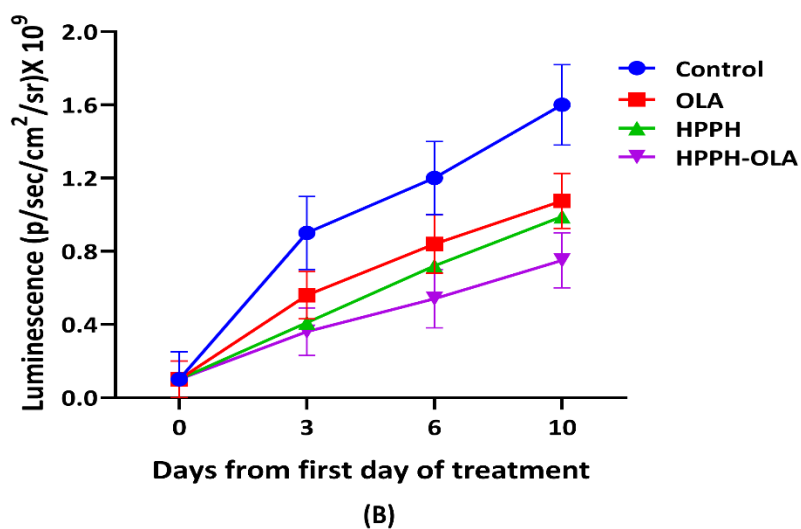
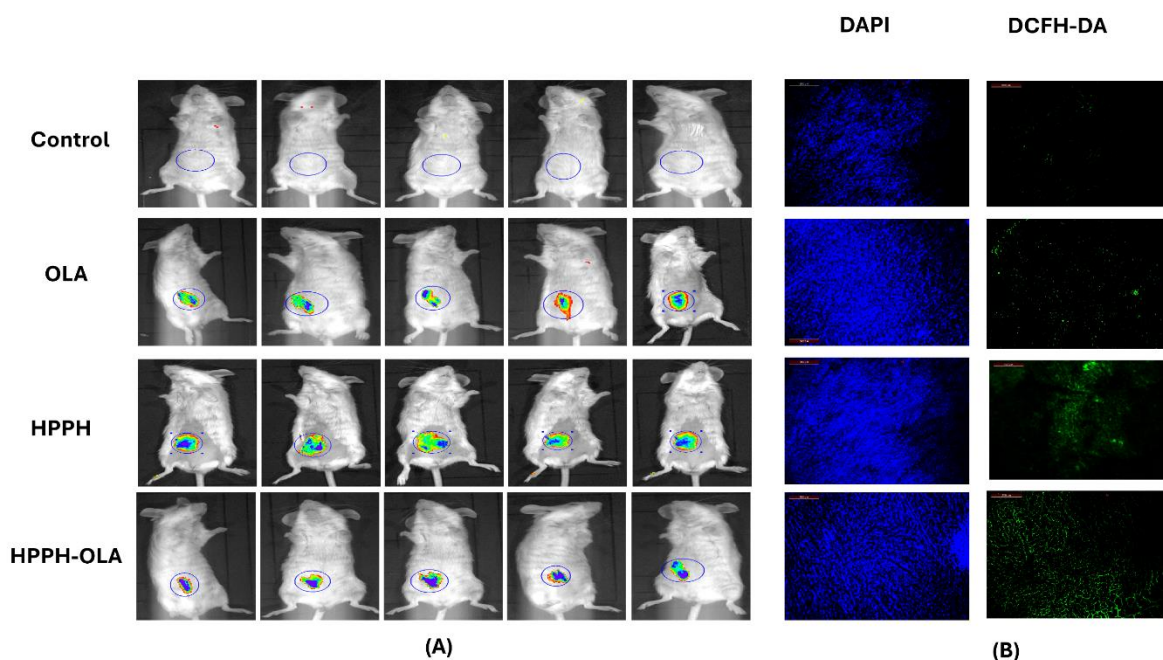


Figure 5.11: Luminescence imaging and intensity of each animal group i.e., control, HPPH, OLA and HPPH-OLA

In-vivo ROS generation was also studied using DCFH-DA fluorescence probe. As shown in figure 5.12, the study confirmed that the treatment group i.e., OLA, HPPH and HPPH-OLA were able to induce ROS in tumor bearing animal.



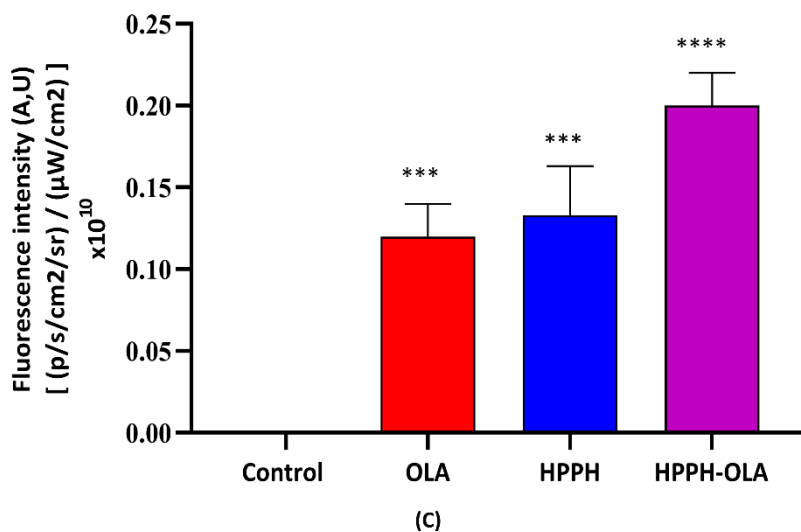
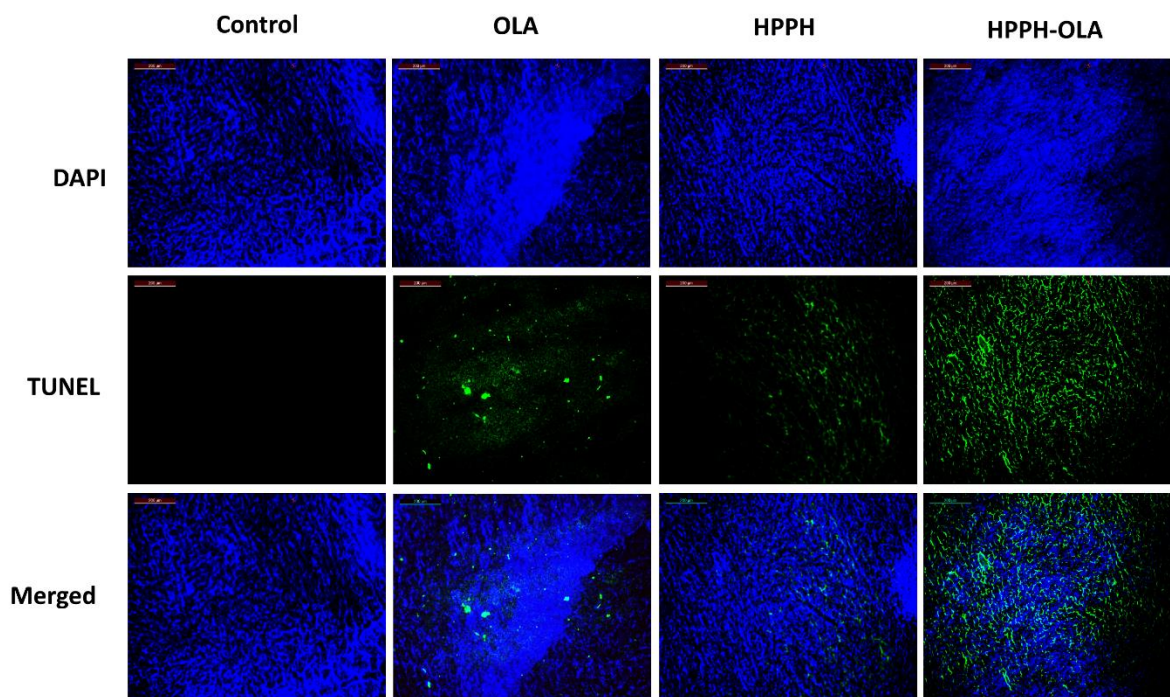


Figure 5.12: In vivo ROS study of HPPH, OLA and HPPH-OLA;(A) In-vivo image (B)Microscopic image of tumor tissue(C) Fluorescence intensity of tumor tissue; Data represent mean \pm SD. **** p value < 0.0001 and *** p value < 0.001 compared with the control group

Moreover, tumor and organ tissue were collected from all the groups (control, HPPH, OLA and HPPH-OLA) and subjected to sectioning by microtome which were further used for histological analysis and tunnel assay. The tunnel assay as shown in figure 5.13 suggested that OLA, HPPH and HPPH-OLA showed apoptotic ratio of 15.5%, 21.3% and 30.5% respectively as compared to control.



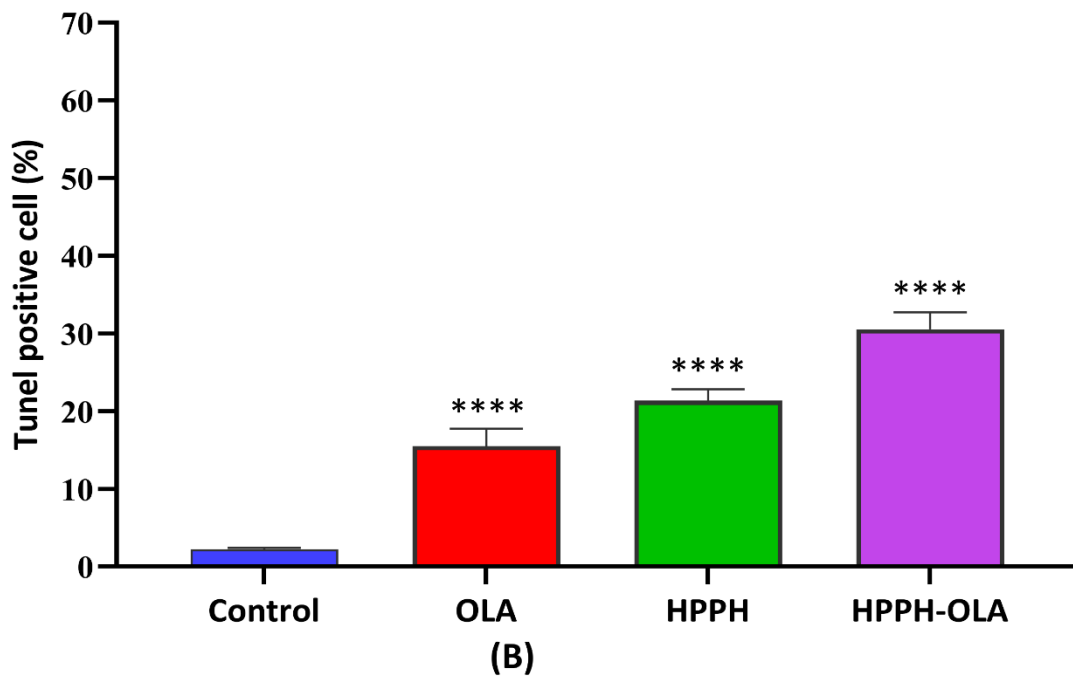


Figure 5.13: TUNEL assay for HPPH, OLA and HPPH-OLA; Data represent mean \pm SD. **** p value < 0.0001 and *** p value < 0.001 compared with the control group

Also, histochemical analysis, as shown in figure 5.14, was performed for all the above-mentioned groups/entities using hematoxylin and eosin (H&E) dye, which revealed that no toxicity was observed in vital organs of all the treated groups.

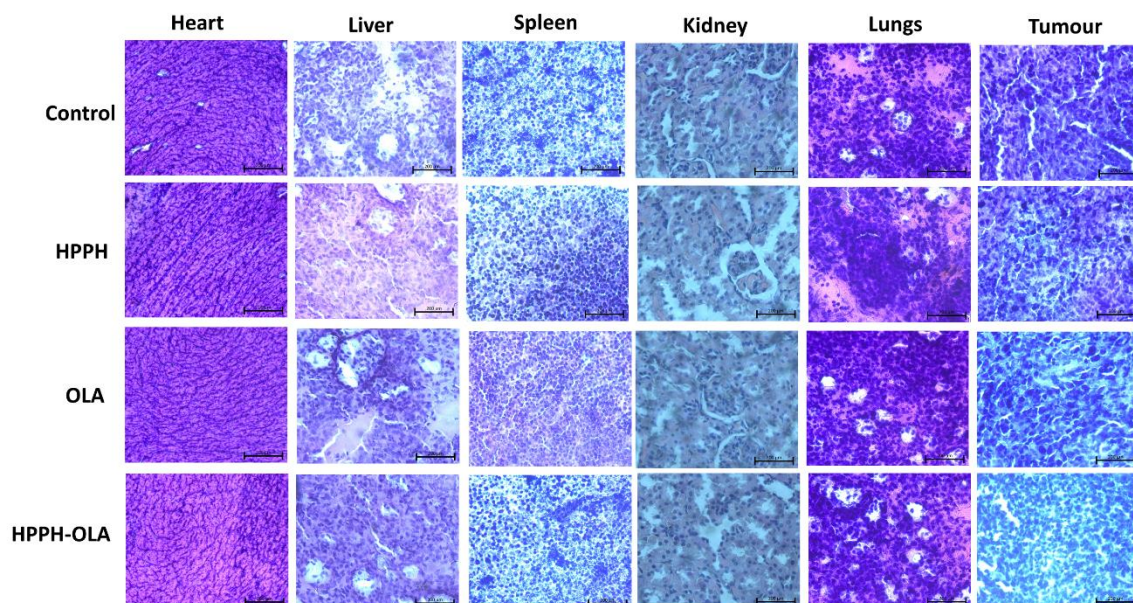


Figure 5.14: Histochemical analysis for HPPH, OLA and HPPH-OLA using H&E staining

5.6. In-vivo pharmacokinetic study

The validated LC-MS/MS based simultaneous method for HPPH and OLA was successfully utilized for the estimation of their concentration in mice plasma after intravenous administration at the dose of 5mg/kg.bw (HPPH) and OLA (30 mg/kg.bw) respectively. The mean plasma concentration-time profile of HPPH, OLA and combination of HPPH and OLA was determined for up to 24 hr. which is shown in the figure 5.15. Further, a non-compartmental analysis method (NCA) was employed for the evaluation of all the pharmacokinetic parameters for HPPH(Alone), OLA (Alone) and their combination (HPPH/OLA) via WinNonlin software version 8.3 (Certara, USA).

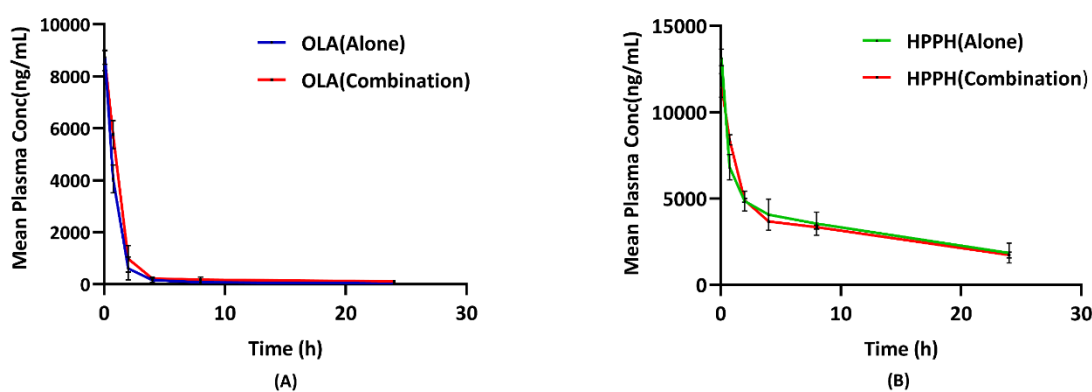


Figure 5.15: Mean plasma concentration–time profiles of (A) OLA (30 mg/kg) and (B)HPPH (5 mg/kg) after i.v. administration of OLA and HPPH alone and their combination to Balb/c mice

The C_0 was found to be 13858.28 ± 2179.87 ng/mL, 10745.31 ± 1318.78 ng/mL, 9350.89 ± 1675.39 ng/mL and 8806.09 ± 323.51 ng/mL for HPPH (Alone), HPPH (Combination), OLA(Alone) and OLA (Combination) respectively. All the other parameters like AUC, biological half-life ($t_{1/2}$), rate of elimination (K_e) etc. were depicted and shown in table no 5.21. The data showed no significant difference in between the pharmacokinetic parameters of alone drugs (HPPH and OLA) with its combination administration of both HPPH and OLA(HPPH-OLA). Moreover, the pharmacokinetic results confirmed short plasma half-life ($t_{1/2}$) i.e., 15.15 ± 2.76 h and 5.74 ± 3.35 h for HPPH and OLA respectively. The result also showed a high-rate of elimination in case of OLA. Further, the pharmacokinetic profile of HPPH-OLA suggested the combination of HPPH and OLA as no significant pharmacokinetic interaction was found after administration in animal (Table 5.21).

Table 5.21: In vivo pharmacokinetic parameter of HPPH, OLA and their combination (n=5, Mean \pm SD)

Parameter	Unit	OLA(A)	HPPH(A)	OLA(C)	HPPH(C)
C ₀	ng/mL	9350.89 \pm 1675.39	13858.28 \pm 2179.87	8806.09 \pm 323.51	10745.31 \pm 1318.78
T _{max}	h	0.08 \pm 0.00	0.08 \pm 0.00	0.08 \pm 0	0.08 \pm 0.00
AUC _{last}	h*ng/mL	5149.59 \pm 1050.38	72575.11 \pm 9169.30	5698.76 \pm 213.20	73964.45 \pm 466.24
Vd _{obs}	mL/kg	50778.67 \pm 33690.97	1049.30 \pm 236.37	46443.17 \pm 1494.14	1041.42 \pm 4.44
Cl _{obs}	mL/h/kg	5781.59 \pm 1086.37	47.79 \pm 2.61	4847.79 \pm 133.72	46.08 \pm 0.20
K _e	1/h	0.18 \pm 0.16	0.05 \pm 0.01	0.12 \pm 0.00	0.04 \pm 0.00
T _{1/2}	h	5.74 \pm 3.35	15.15 \pm 2.76	5.34 \pm 0.04	15.66 \pm 0.002

A: Alone; C: Combination;

Based on the in-vitro and in-vivo results, it was confirmed that both HPPH and OLA can provide therapeutical benefit against TNBC. Along with that, there were certain limitations i.e.; poor pharmacokinetic and pharmacodynamic associated with the HPPH and OLA. Therefore, we further planned to circumvent the observed problems and also to improve the site-specific accumulation of the HPPH and OLA using a surface modified targeted nano drug delivery systems, which were developed and biologically evaluated.

5.7. Synthesis and characterization of targeted co-polymer and lipid molecules

5.7.1. Synthesis and characterization of Biotin-PEG-PLGA

The synthesis of Biotin-PEG-PLGA block copolymer was performed by activating the -COOH group of biotins using DCC and NHS and then covalent conjugation to the amine group of NH₂-PEG-PLGA was carried out as shown in the Fig. 4.1. The Biotin-PEG-PLGA product was confirmed by ¹H NMR (CDCl₃, 400MHz) spectroscopy (Figure 5.16). The presence of sharp peak at 3.8 ppm corresponding to -CH₂- groups of PEG. The presence of 5.2 ppm corresponds to the presence of -CH- of lactide group. The presence of 1.5 ppm peak corresponds to the -CH₃ of lactide group. The presence of 4.8 ppm corresponds to the -CH₂- of glycolide group. The presence of peaks between 2-3 ppm corresponds to biotin group.

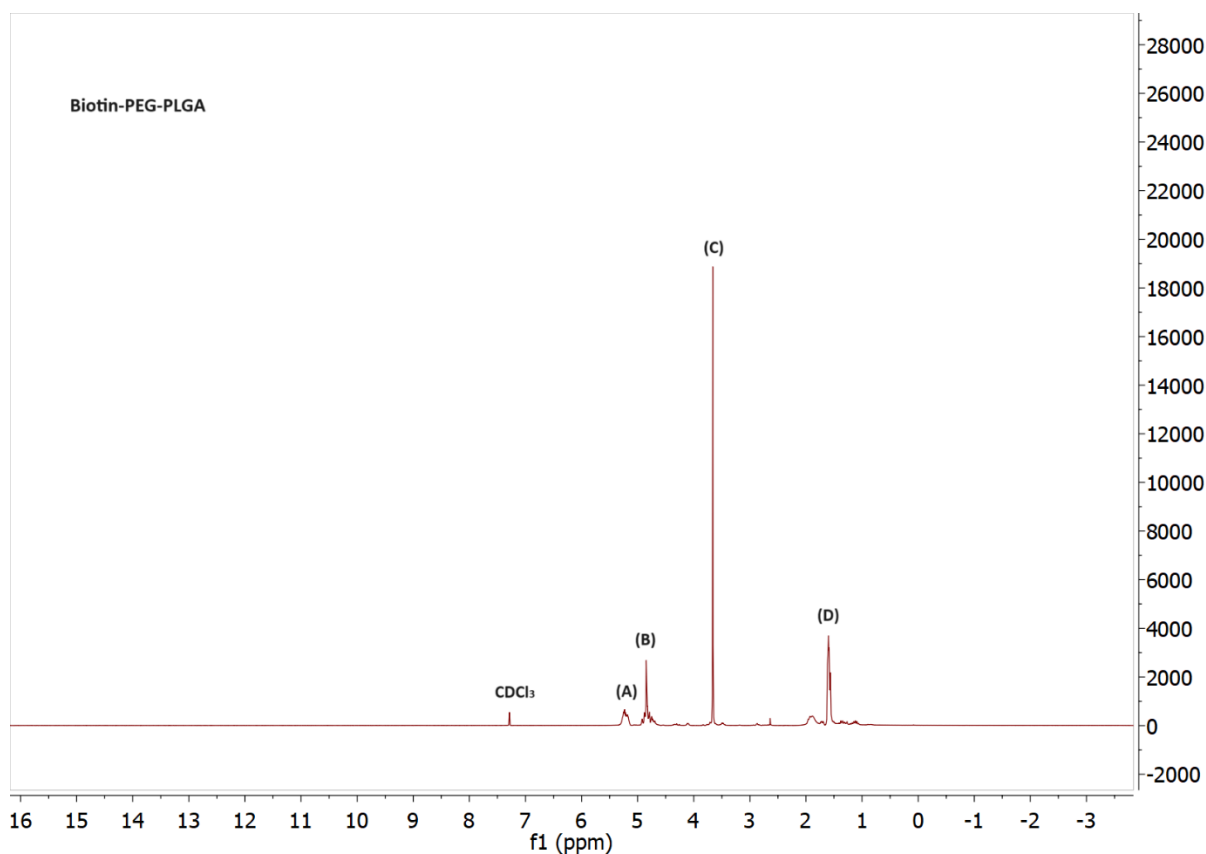


Figure 5.16: ¹H NMR spectra of the Biotin-PEG-PLGA

5.7.2. Synthesis of linoleic acid-ss-TPP

The novel *Linoleic acid-ss-TPP* was synthesized using EDC/NHS coupling. The product was confirmed by Proton NMR and LC-MS/MS. The details related to NMR and Mass result shown below (Fig.5.17 and 5.18).

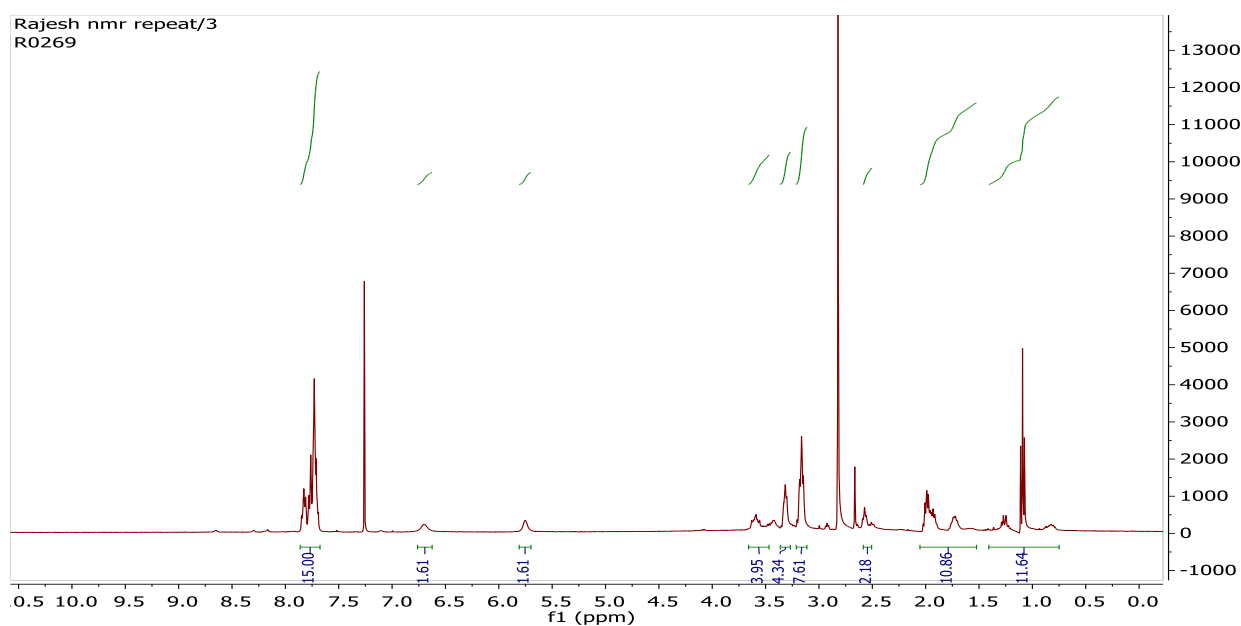


Figure 5.17: ¹H NMR of Linoleic acid-ss-TPP

^1H NMR (400 MHz, Chloroform-*d*) δ 7.89–7.70 (m, 15H), 6.72 (s, 2H), 5.78 (s, 2H), 3.68–3.49 (m, 4H), 3.33 (d, $J = 6.1$ Hz, 4H), 3.24–3.12 (m, 8H), 2.61–2.53 (m, 2H), 2.08 – 1.55 (m, 11H), 1.43 – 0.77 (m, 12H). LCMS (+ESI): m/z calculated for $\text{C}_{45}\text{H}_{64}\text{N}_2\text{O}_2\text{PS}_2^+$ 760.11 found 761.55(M+H)

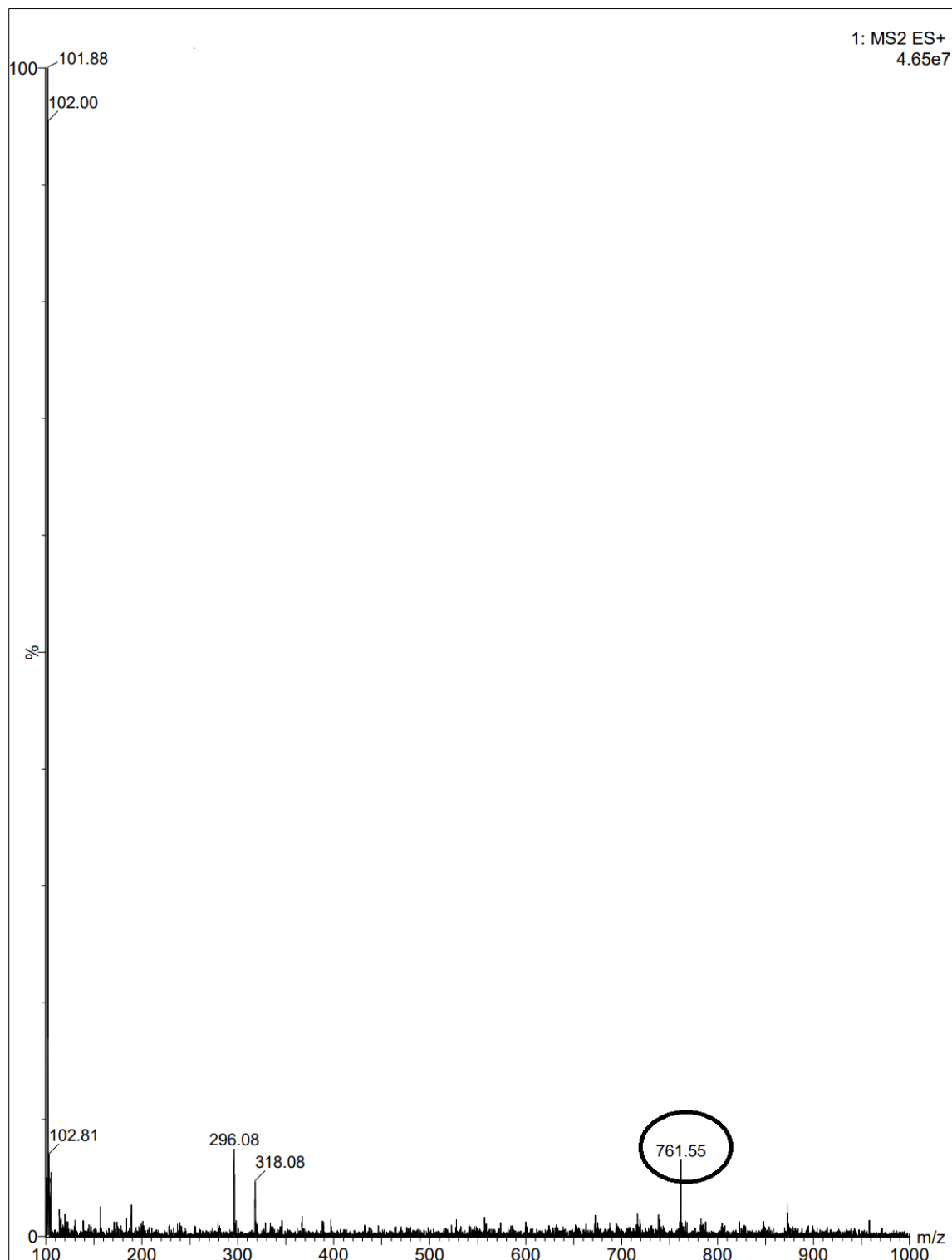


Figure 5.18: Mass analysis of Linoleic acid-ss-TPP using LC-MS/MS

5.8. Fabrication, Optimisation and Characterization of HPPH-Loaded LPHNs

5.8.1. Fabrication of HPPH loaded LPHNs

The HPPH loaded LPHNs were fabricated using different excipients PEG-PLGA/Biotin PEG-PLGA, DC₈₉PC, and Linoleic acid via emulsification followed by solvent evaporation method. Here, PEG-PLGA is FDA approved amphiphilic co-polymer used in long term drug delivery application due to its slow diffusion and nontoxic in nature. Along with that PEG behaves like a capping agent and act as a shield for growing nanoparticle. Therefore, the particle can't expand after certain extent. In addition, DC₈₉PC is a phospholipid that contains a light triggering moiety in the structural backbone which could enhance the light activation of HPPH. Further, linoleic acid is an unsaturated fatty acid which can trigger ROS generation that could accelerate the Photodynamic activity of HPPH in biological systems.

5.8.2. DOE based Optimization of LPHNs

The optimization of LPHNs was conducted by QbD approach using DOE and response surface methodology (RSM). According to RSM strategy, the experimental runs were carried out to investigate the impact of independent variables (PVA concentration in %w/v and Amount of DC₈₉PC in mg) on the dependent variable (%EE and Particle size) with the experimental conditions which is utilized for optimization of highly acceptable nanocarrier. Table 5.22 depicted the data of the experimental trials

Table 5.22: CCD based experimental runs and their corresponded responses.

Std	Run	Factor 1 (X1) PVA (%)	Factor 2(X2) DC ₈₉ PC (mg)	Response 2(Y2) EE (%)	Response 1(Y1) Particle size(nm)
1	7	1	3.5	15	345
2	4	2	3.5	65	155
3	6	1	4	11	320
4	8	2	4	86	170
5	5	1	3.75	23	340
6	1	2	3.75	64	150
7	3	1.5	3.5	52	215
8	9	1.5	4	76	198
9	10	1.5	3.75	50	205
10	2	1.5	3.75	48	212

To study the interaction between dependent variable with independent variable and understand the magnitude of the impact of critical factor, the analysis of variance (ANOVA) was performed. Further, the ANOVA based statistical data for dependent factor % EE is depicted in Table 5.23. A Linear model Eq. was obtained for %EE which is shown below

Equation 1

$$\text{Entrapment efficiency (Y}_1\text{)} = 49 + 27.67X_1 + 6.83X_2$$

Where Y_1 is the predicted %EE and X_1 and X_2 are the PVA concentration and amount of DC₈₉PC, respectively. The Table 5.23, indicates the obtained model was found to be highly significant with value $p < 0.05$. The obtained coefficient of determination (R^2) and adjusted R^2 were 0.83 and 0.78, respectively which lies under acceptance criteria as the difference is very less. It is suggested that this predicted ANOVA can explain 95% variability in the response. Additionally, it can also explain the efficiency of the model to predict the response (%EE).

Table 5.23: The analysis of variances for %EE as the response (Y1)

Source	Sum of Squares	df	Mean Square	F-value	p-value	
Model	4872.83	2	2436.42	17.17	0.0020	significant
X1-PVA	4592.67	1	4592.67	32.37	0.0007	
X2-DC ₈₉ PC	280.17	1	280.17	1.97	0.2027	
Residual	993.17	7	141.88			
Lack of Fit	991.17	6	165.19	82.60	0.0840	not significant
Pure Error	2.00	1	2.00			
Cor Total	5866.00	9				
R²	0.8307					
Adjusted R²	0.7823					

In similar manner, the ANOVA results for response Y_2 i.e. particle size is displayed in Table 5.24 and also provide a quadratic second-order polynomial which is displayed below.

$$\text{Particle Size (Y}_2\text{)} = 207.21 - 88.33X_1 - 4.50X_2 + 10.00X_1.X_2 + 39.07X_1^2 + 0.5714X_2^2$$

Table 5.24: The analysis of variances for particle size as the response (Y2)

Source	Sum of Squares	df	Mean Square	F-value	p-value	
Model	51020.60	5	10204.12	187.74	< 0.0001	significant
X1-PVA	46816.67	1	46816.67	861.37	< 0.0001	
X2-DC ₈₉ PC	121.50	1	121.50	2.24	0.2092	
X1*X2	400.00	1	400.00	7.36	0.0534	
X1 ²	3562.01	1	3562.01	65.54	0.0013	
X2 ²	0.7619	1	0.7619	0.0140	0.9115	
Residual	217.40	4	54.35			
Lack of Fit	192.90	3	64.30	2.62	0.4193	not significant
Pure Error	24.50	1	24.50			
Cor Total	51238.00	9				
R²	0.9958					
Adjusted R²	0.9905					

Where Y_2 is the predicted response of particle size and X_1 and X_2 are PVA concentration and amount of DC₈₉PC respectively. The statistical result (ANOVA) suggested that the p-value of model is less than 0.05 and considered to be significant, whereas the lack fit of the model is

not significant ($p > 0.05$), which further strengthened the reliability of the models. The coefficient of determination (R^2) and adjusted R^2 were found to be 0.99 and 0.99, respectively. It indicates the high closeness between R^2 and adjusted R^2 which ensured that the efficiency and predictability of the model to estimate the particle size by the optimized method.

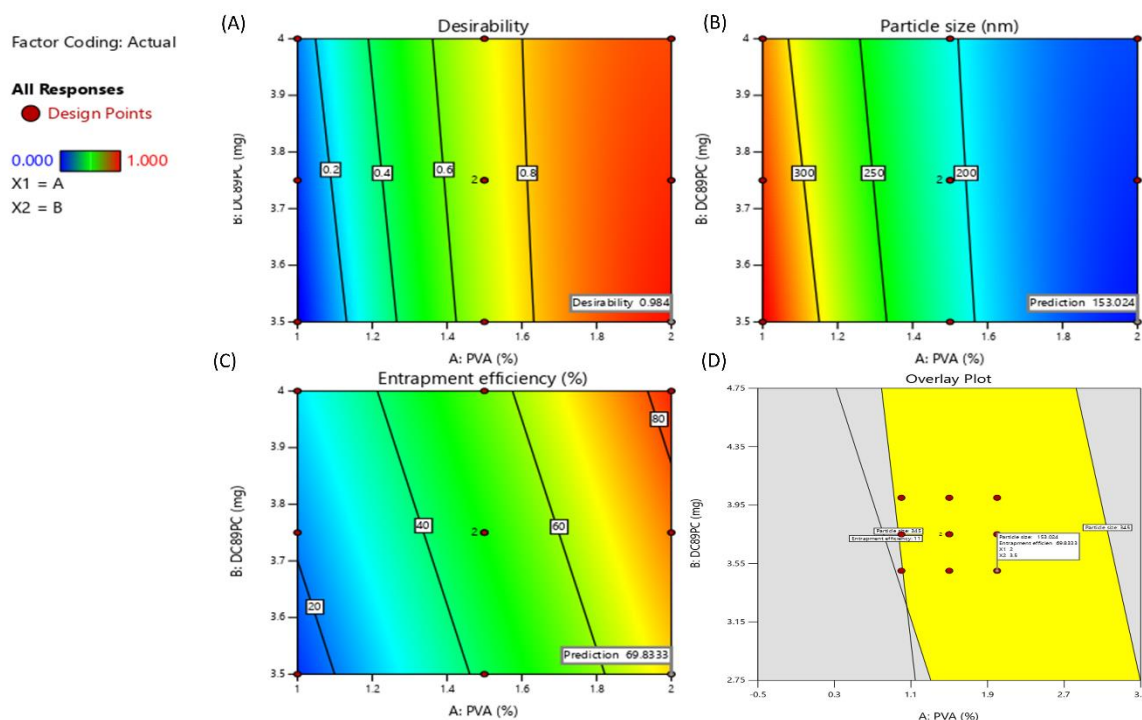


Figure 5.19: QbD based design space; A) Desirability B) Particle Size C) Entrapment Efficiency D) Overlay Plot

Further, the 2D response surface plot of both the response i.e., %EE and particle size of LPHNs is depicted in Figure 5.19. It was shown that %EE was enhanced by increasing both the independent variable i.e., amount of DC₈₉PC and PVA concentration. Moreover, an increase in the amount of DC₈₉PC enhanced the % EE which could be due to hydrophobic nature of HPPH and DC₈₉PC and alternatively, HPPH penetrates more into nanocarrier system [41].

As shown in the Fig. 5.19(B), enhancement in the PVA concentration led to a decrease in particle size. On the other hand, increase in the amount of phospholipid (DC₈₉PC) also showed decrease in the particle size of LPHNs.

In order to validate the RSM model, the obtained experimental values of dependent variable i.e., particle size and %EE were compared with predicted response value from the design. The results are shown in the table 5.25. According to data, there is a rational relationship between the observed and predicted amounts for the %EE and particle size, which shows the suitability

of the optimization procedure in developing HPPH loaded LPHNs and adequacy of models which is depicted in Fig 5.19. A&D.

Table 5.25: Predicted and experimental values of the responses obtained at optimum conditions

Independent variable	Optimized amount	Dependent variable	Predicted amount	Observed amount	Prediction error (%)
X1 DC ₈₉ PC	3.5mg	Y1 PS	153	152	0.65
X2 PVA	2%	Y2 %EE	69	67.34	3.85

5.8.3. Physicochemical characterization of HPPH loaded LPHNs

The comparative analysis of physiochemical properties such as mean particle size, PDI and zeta potential of the optimized LPHNs are depicted in Table 5.26. HPPH-LPHNs showed an average particle size of about 152 nm with a PDI value of 0.217 and -0.2mV Zeta potential. Due to incorporation of Biotin-PEG-PLGA instead of non-surface engineered amphiphilic copolymer i.e., PEG-PLGA, the avg. particle was slightly increased to 156 nm with the PDI of 0.208 which is non-significant.

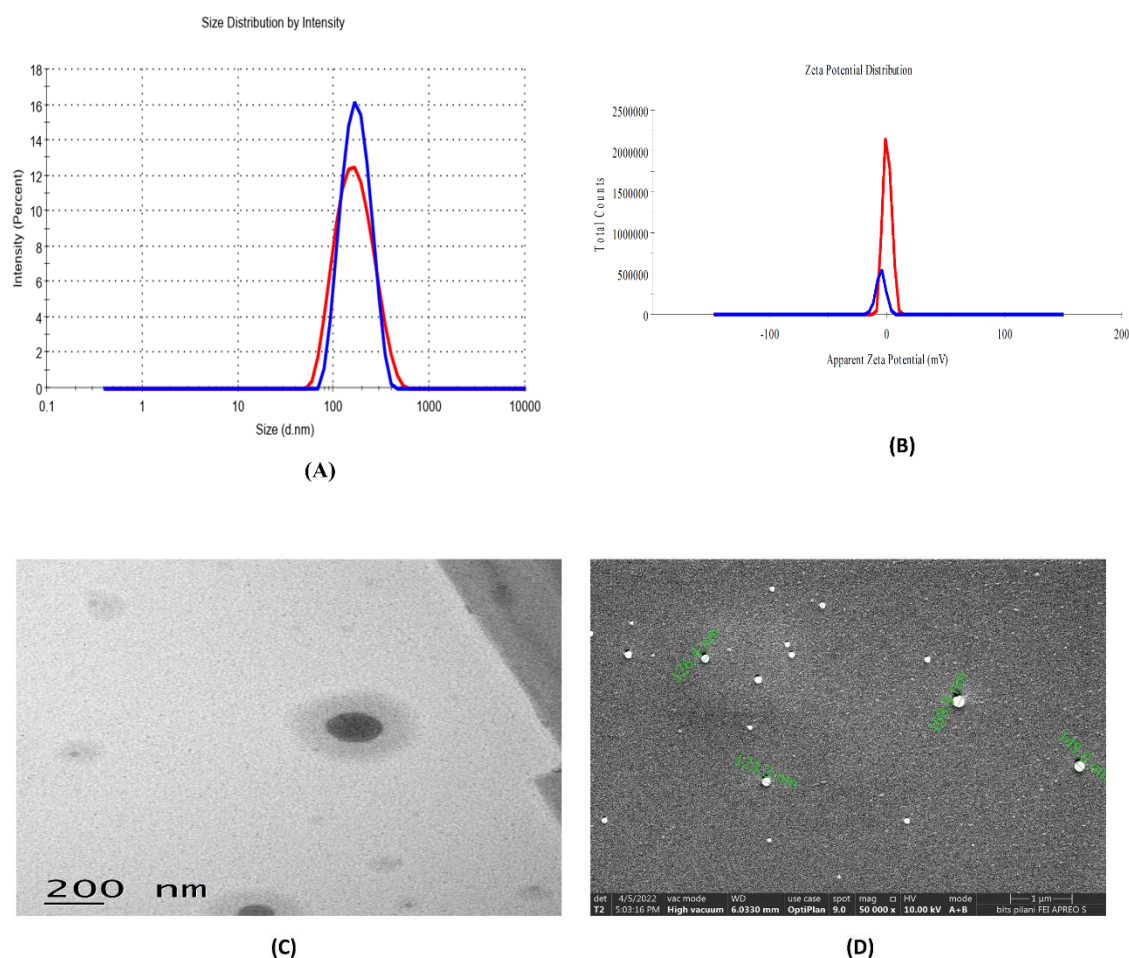


Figure 5.20: Physicochemical characterization of HPPH loaded LPHNs: (A) Particle size (B) Zeta Potential (C) TEM image of Biotin@HPPH-LPHNs (D) SEM image of Biotin@HPPH-LPHNs

Further, this Surface engineered polymer (Biotin-PEG-PLGA) has influenced the surface charge from -0.2 mV to 1.16 mV. The SEM and TEM analysis was carried out for morphological evaluation of LPHNs which was shown in the Figure 5.20. The data revealed that the developed LPHNs were spherical with uniform distribution. The %EE of HPPH in the LPHNs (HPPH-LPHNs) were found to be $67.34 \pm 2.02\%$, whereas Biotin@HPPH-LPHNs was approx. $66.23 \pm 1.17\%$ which indicated better encapsulation of HPPH in both the nanocarrier system that assures substantial cargo potential of the designed systems.

Table 5.26: Physicochemical characterisation of HPPH loaded Fresh LPHNs

Formulation	PS (nm)	PDI	ZP (mV)	EE (%)
HPPH-LPHNs	152.6 \pm 8.1	0.217 \pm 0.1	-0.2 \pm 0.06	67.34 \pm 2.02
Biotin@HPPH-LPHNs	156.3 \pm 13.2	0.208 \pm 0.56	1.16 \pm 0.30	66.23 \pm 1.17

PS: Particle Size; PDI: Poly dispersity index ZP: Zeta Potential; EE: Entrapment Efficiency

5.8.4. Freeze drying of HPPH loaded LPHNs

The freeze drying of HPPH loaded LPHNs were carried out using four different cryoprotectants including sucrose, mannitol, trehalose, and PEG-4000 for three different concentrations i.e. 2.5%, 5% and 10% w/w. Afterward, these lyophilized LPHNs samples were subjected to particle size and PDI analysis and the obtained results were shown in table 5.27.

Table 5. 27: Lyophilization screening for HPPH loaded LPHNs with different cryoprotectant

Formulation	Mean diameter (nm)	PDI
1. Lyophilized LPHNs with 2.5% Mannitol		
HPPH-LPHNs	416.26 \pm 15.20	0.44 \pm 0.02
Biotin@HPPH-LPHNs	357.63 \pm 7.53	0.38 \pm 0.01
2. Lyophilized LPHNs with 5% Mannitol		
HPPH-LPHNs	351.79 \pm 17.03	0.34 \pm 0.02
Biotin@HPPH-LPHNs	342.85 \pm 5.50	0.38 \pm 0.01
3. Lyophilized LPHNs with 10 % Mannitol		
HPPH-LPHNs	352.73 \pm 14.10	0.32 \pm 0.004
Biotin@HPPH-LPHNs	285.63 \pm 24.04	0.35 \pm 0.02
4. Lyophilized LPHNs with 2.5% Sucrose		
HPPH-LPHNs	320.22 \pm 17.25	0.37 \pm 0.02
Biotin@HPPH-LPHNs	301.56 \pm 4.14	0.37 \pm 0.009
5. Lyophilized LPHNs with 5% Sucrose		
HPPH-LPHNs	216.53 \pm 1.63	0.32 \pm 0.01
Biotin@HPPH-LPHNs	269.16 \pm 15.63	0.34 \pm 0.008
6. Lyophilized LPHNs with 10% Sucrose		
HPPH-LPHNs	226.83 \pm 8.45	0.32 \pm 0.01
Biotin@HPPH-LPHNs	244.58 \pm 14.52	0.33 \pm 0.02
7. Lyophilized LPHNs with 2.5 %Trehalose		
HPPH-LPHNs	167.81 \pm 1.82	0.23 \pm 0.002
Biotin@HPPH-LPHNs	166.16 \pm 3.69	0.22 \pm 0.009
8. Lyophilized LPHNs with 5 % Trehalose		
HPPH-LPHNs	150.63 \pm 4.76	0.21 \pm 0.007
Biotin@HPPH-LPHNs	156.79 \pm 2.12	0.21 \pm 0.01
9. Lyophilized LPHNs with 10 % Trehalose		
HPPH-LPHNs	143.16 \pm 4.04	0.20 \pm 0.01
Biotin@HPPH-LPHNs	190.93 \pm 3.91	0.20 \pm 0.005
10. Lyophilized LPHNs with 2.5 %PEG4000		
HPPH-LPHNs	199.37 \pm 8.16	0.33 \pm 0.05
Biotin@HPPH-LPHNs	228.86 \pm 5.87	0.32 \pm 0.02
11. Lyophilized LPHNs with 5 % PEG 4000		
HPPH-LPHNs	196.46 \pm 10.41	0.32 \pm 0.02
Biotin@HPPH-LPHNs	181.22 \pm 11.53	0.31 \pm 0.01
12. Lyophilized LPHNs with 10 % PEG 4000		

HPPH-LPHNs	162.6±8.4	0.22±0.05
Biotin@HPPH-LPHNs	163.5±11.78	0.21±0.60

PS: Particle Size; PDI: Poly dispersity Index

From the obtained data (table 5.27), 10% PEG 4000 w/w showed better physicochemical profile as compared to other groups. Subsequently, the physicochemical parameter (Particle size and PDI) of lyophilized LPHNs (LPHNs with 10% PEG 4000 w/w) were nearly unchanged compared to fresh LPHNs (Table 5.28).

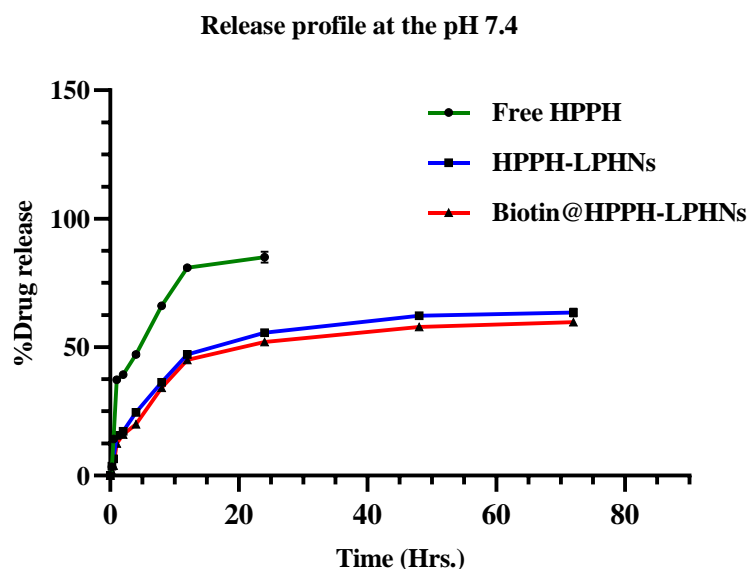
Table 5.28: Physicochemical characterisation of Optimised HPPH loaded LPHNs (Lyophilised)

Formulation	PS (nm)	PDI	ZP (mV)	EE (%)	DL (%)
HPPH-LPHNs	162.6 ±8.4	0.220±0.56	-0.1±0.01	58.52±7.19	8.20 ±0.61
Biotin@HPPH-LPHNs	163.5 ±11.78	0.213±0.60	2.2 ±0.20	58.36±4.31	8.40 ±0.22

PS: Particle Size; PDI: Poly dispersity Index ZP: Zeta Potential; EE: Entrapment Efficiency; DL: Drug Loading

5.8.5. *In vitro* release study

The release profile of HPPH encapsulated LPHNs and pure HPPH was performed using dialysis bag method. As shown in the figure 5.21, the release profile of pure HPPH described 90% of drug released from the dialysis bag within the initial 12 hr. Whereas encapsulated HPPH-LPHNs followed a biphasic release pattern i.e., 20% CDR from both the LPHNs (HPPH-LPHNs and Biotin@HPPH-LPHNs) in first 4 h and remaining ~40% was released till 72 hr.



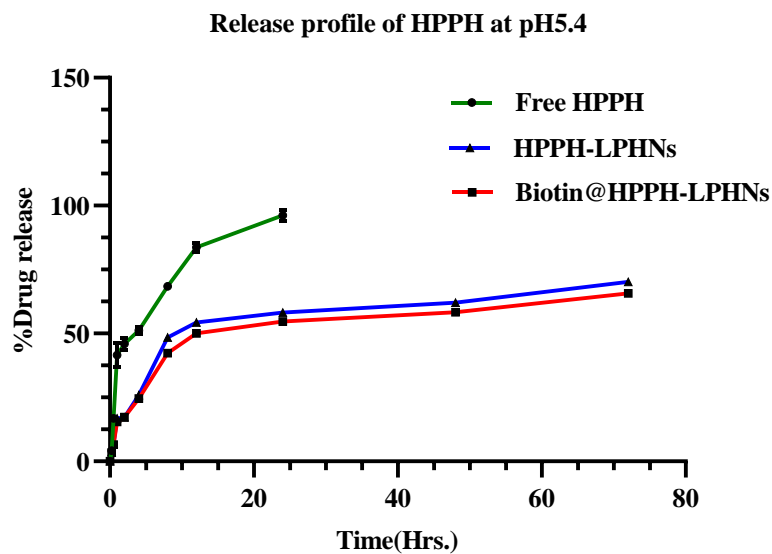


Figure 5.21: In vitro release study of free HPPH, HPPH-LPHNs and Biotin@HPPH-LPHNs in pH 7.4 and pH 5.4

5.8.6. Drug-excipient compatibility study

As depicted in the figure 5.22, the DSC thermogram of free HPPH showed melting peak at 205°C. In case of LPHNs, the melting point peak disappeared at 205°C which indicate encapsulation of HPPH in nanocarrier system.

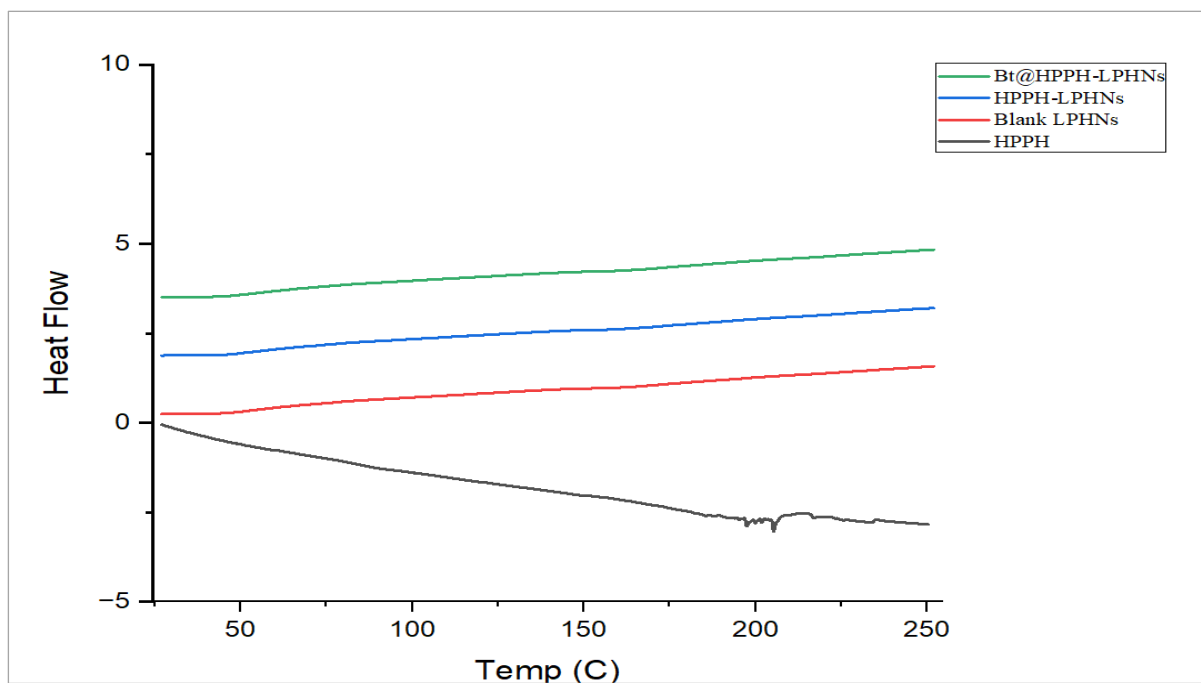


Figure 5.22: DSC thermogram of HPPH and its LPHNs (Blank LPHNs, HPPH-LPHNs and Biotin@HPPH-LPHNs)

5.8.7. Measurement of singlet oxygen

The singlet-oxygen-generating potential of HPPH and its LPHNs was detected using the Singlet Oxygen Sensor Green (SOSG) probe at excitation wavelength of 494 nm. Notably, the SOSG's fluorescence intensity from both LPHNs (HPPH-LPHNs and Biotin@HPPH-LPHNs) and pure HPPH exhibits an exposure time-dependent enhancement, indicating increased $^1\text{O}_2$ generation (figure 5.23). The fluorescence intensity of HPPH was significantly reduced due to encapsulation of HPPH in nanocarrier, the $^1\text{O}_2$ generation ability of both nanocarrier (HPPH-LPHNs and Biotin@HPPH-LPHNs) was ~60 % relative to that of pure HPPH.

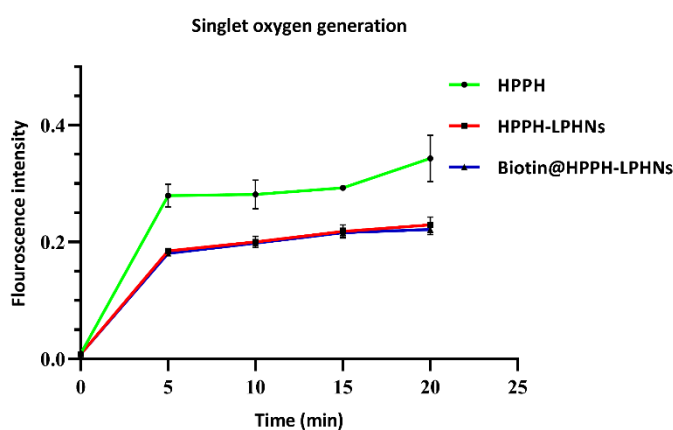


Figure5.23: SOSG analysis of HPPH and its LPHNs

5.8.8. Storage stability Studies

The stability of lyophilized LPHNs were characterized with two different storage conditions i.e., 4 °C/65% RH and 25 °C/60% RH for 90 days. The results depicted that LPHNs were stable at both the conditions as no significant change was observed in avg. particle size and PDI in comparison to fresh nanocarrier (Figure 5.24).

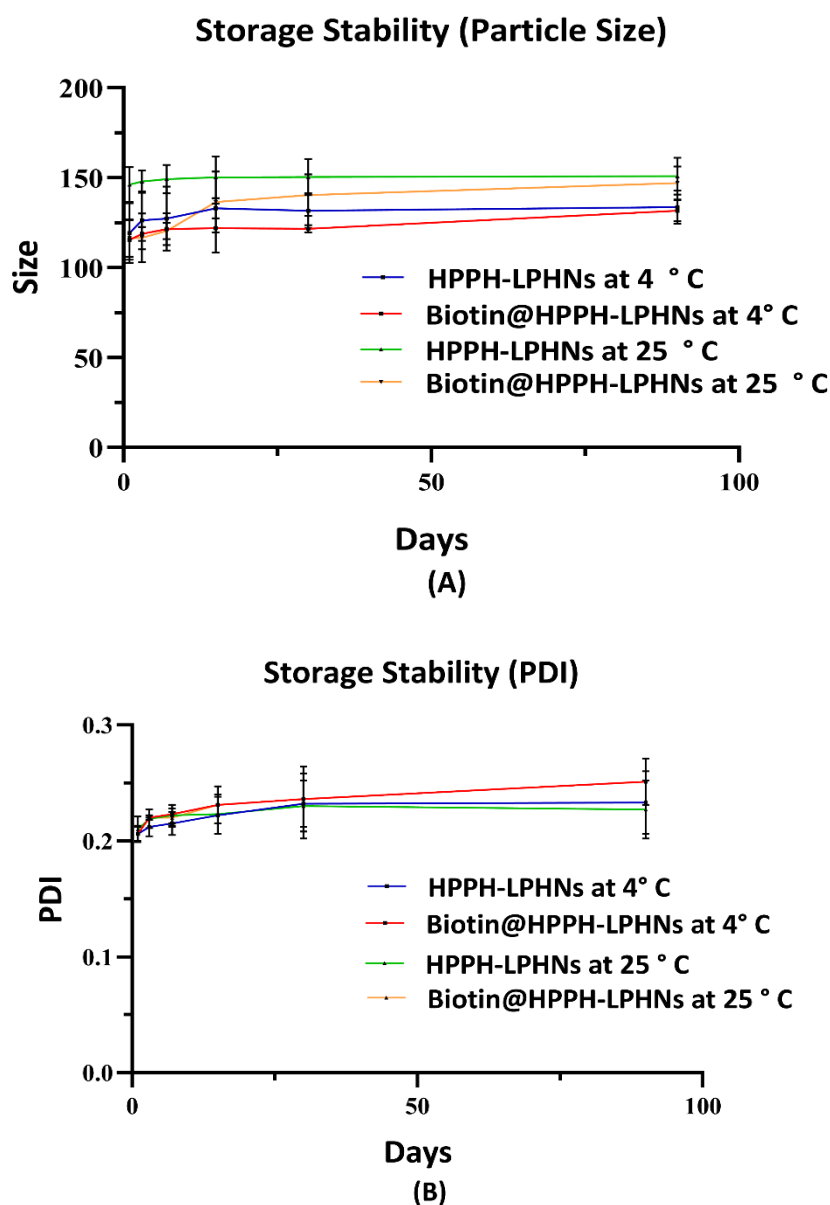


Figure 5.24: Storage stability study of HPPH loaded LPHNs; A) Particle size; B) PDI

5.8.9. Cell culture studies

5.8.9.1. Cytotoxicity

The in vitro cytotoxicity was studied using MTT assay in 4T1 breast cancer cells with following treatment of free HPPH, HPPH-LPHNs, Biotin@HPPH-LPHNs and Blank-LPHNs. As shown in the Figure 5.25, it was found that the survival rate of 4T1 was significantly reduced with LPHNs in comparison to pure HPPH after 48 hr. incubation. Subsequently, IC_{50} values of Biotin@HPPH-LPHNs, HPPH-LPHNs and pure HPPH was $3.90\mu\text{M}$, $8.80\mu\text{M}$ and $10\mu\text{M}$ respectively. Furthermore, the developed blank nanocarrier showed no cytotoxicity.

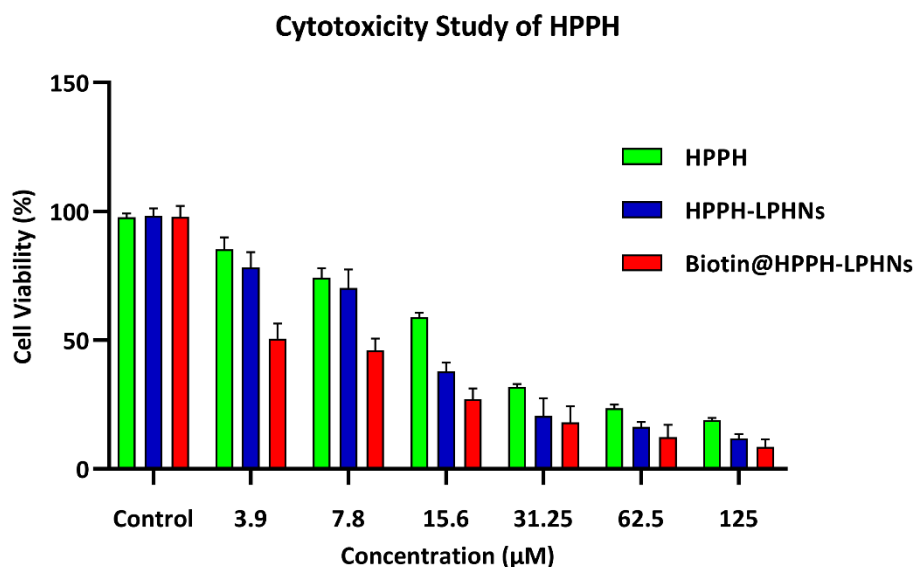


Figure 5.25: invitro cytotoxicity Study of HPPH and its LPHNs (pure HPPH, HPPH-LPHNs, and Biotin@HPPH-LPHNs)

5.8.9.2. Cellular Uptake analysis of HPPH and its LPHNs

In order to understand the internalization capacity of biotin tagged LPHNs, the cellular uptake was performed by using confocal microscopy. The fluorescence intensity was observed for 4hr and 8hr. The Red color indicates presence of LPHNs and on the other hand, blue color specifies cell nucleus. As shown in the Figure 5.26, the fluorescence intensity of Biotin@HPPH-LPHNs was stronger than HPPH-LPHNs at both the time interval.

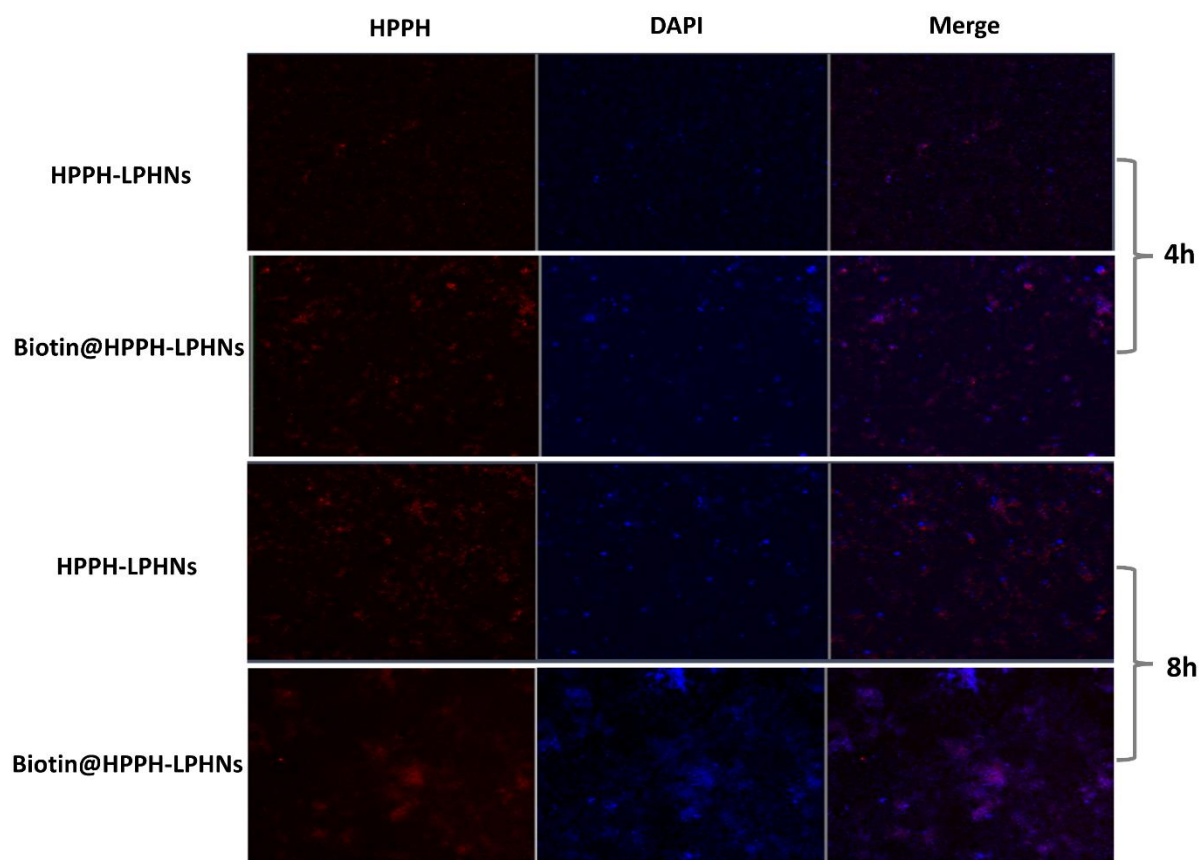


Figure 5.26: In vitro cellular uptake assay of HPPH loaded LPHNs (pure HPPH, HPPH-LPHNs, and Biotin@HPPH-LPHNs)

5.8.9.3. Measurement of ROS generation

The intracellular ROS generation was studied using a fluorescence probe, 2',7'-dichlorofluorescein diacetate (DCFH-DA). After the cells were treated with pure HPPH, HPPH-LPHNs and Biotin@HPPH-LPHNs at the dose of IC_{50} , all the groups were subjected to light irradiation with 650 nm at a light density of 200 mW cm^{-2} for 15min. Then, it was incubated for 24 hr. As shown in Figure 5.27, the intracellular ROS level of Biotin@HPPH-LPHNs was higher than that of HPPH-LPHNs and pure HPPH as it shows higher color intensity of DCFH-DA.

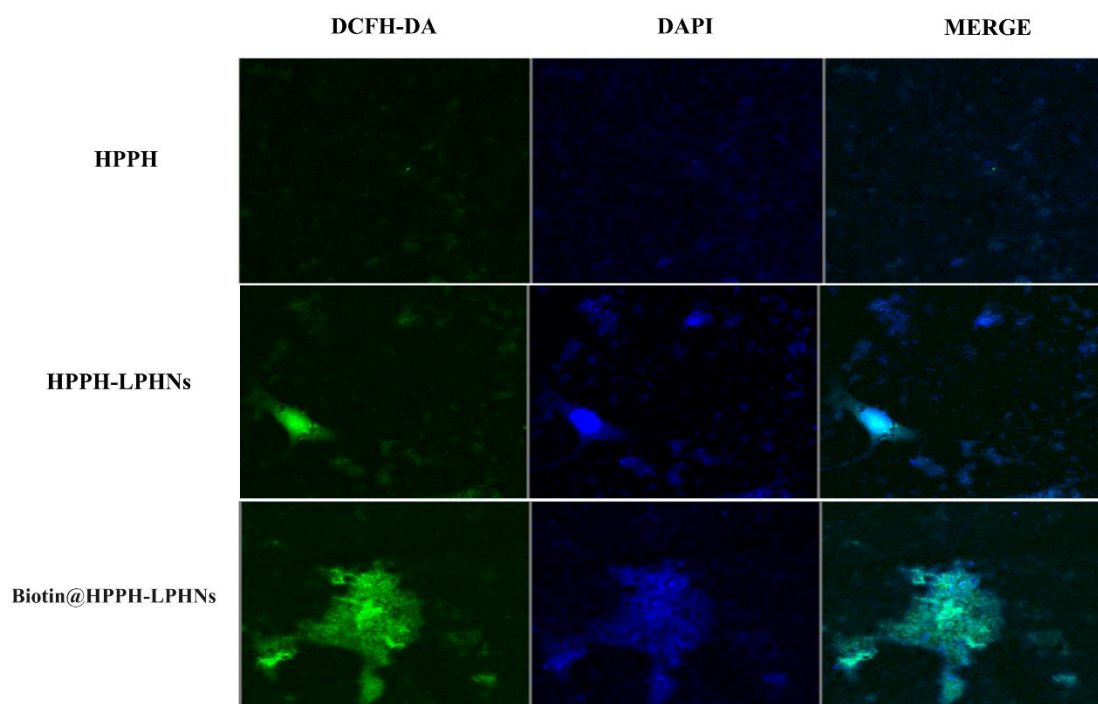


Figure 5.27: In-vitro ROS Study of HPPH and its LPHNs (pure HPPH, HPPH-LPHNs, and Biotin@HPPH-LPHNs)

5.8.9.4. Apoptosis Assay of HPPH and its LPHNs

The cell apoptosis of pure HPPH and its LPHNs was studied using an Annexin V-FITC apoptosis detection kit. Then after, all the treated group were irradiated with 650 nm. As shown in Figure 5.28, the apoptosis of HPPH, HPPH-LPHNs were 4% and 8% respectively, while Biotin@HPPH-LPHNs exhibited 52% apoptosis which is higher than that of other groups.

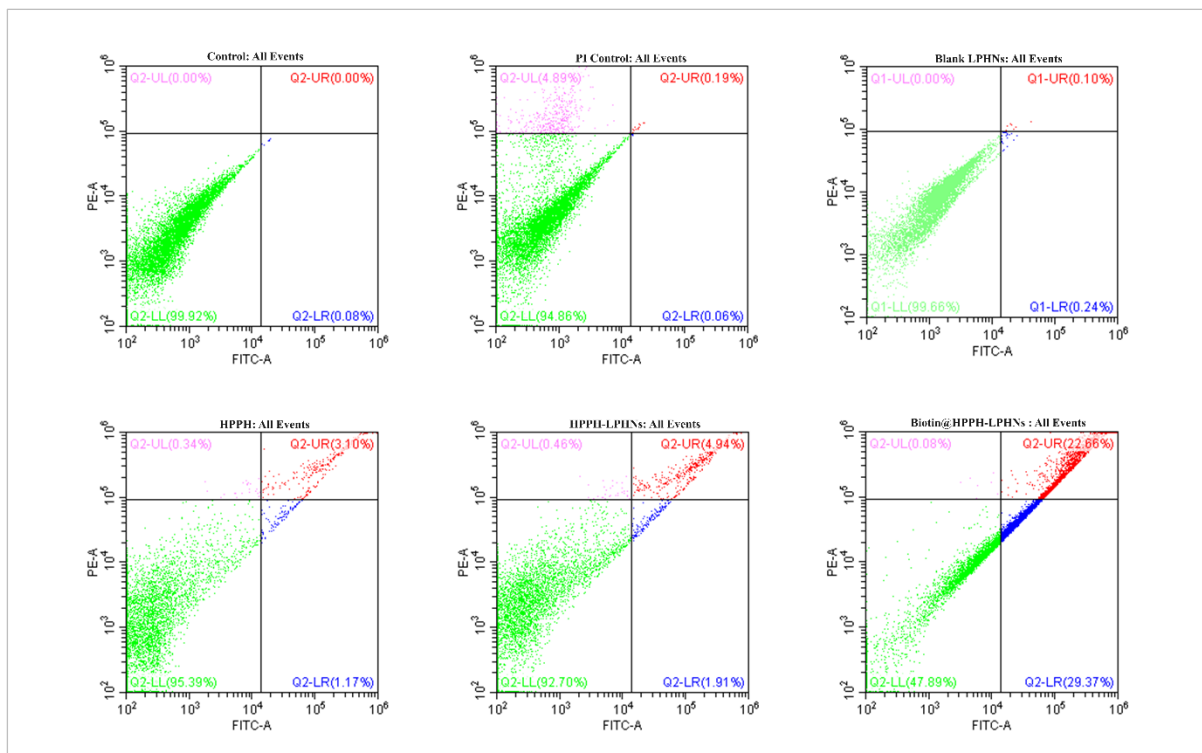


Figure 5.28: Apoptosis analysis of HPPH and its LPHNs

5.8.10. Hemolysis Study of HPPH and its LPHNs

Hemolysis plays a crucial role in order to understand the toxicity and hypersensitivity profile of the nanocarrier. The study was conducted for developed LPHNs using RBCs to estimate the hemolytic potential of the nanoparticles. As shown in the Figure 5.29, the pure HPPH showed hemolytic index of less than 2% while LPHNs (HPPH-LPHNs and Biotin@HPPH-LPHNs) exhibited hemolytic activity less than 1.5%.

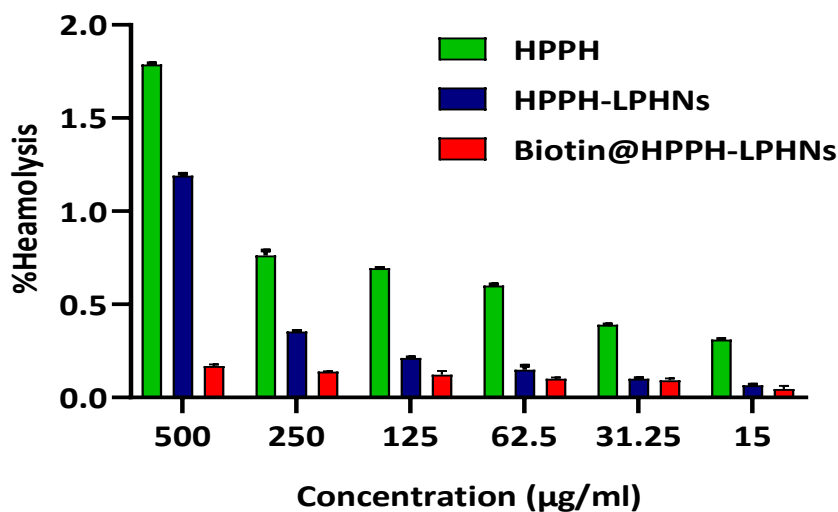


Figure 5.29: Hemolysis study of HPPH and its LPHNs

5.8.11. In vivo pharmacokinetic study

For estimating in-vivo potential of HPPH encapsulated LPHNs, the i.v. pharmacokinetics study was carried out at 5mg/kg.bw in Balb/c mice and the plasma concentration-time profile were shown in Figure 5.30, and further, plasma concentration-plasma profile was subjected to non-compartmental analysis using WinNonlin software 8.3 version (Certara, UK).

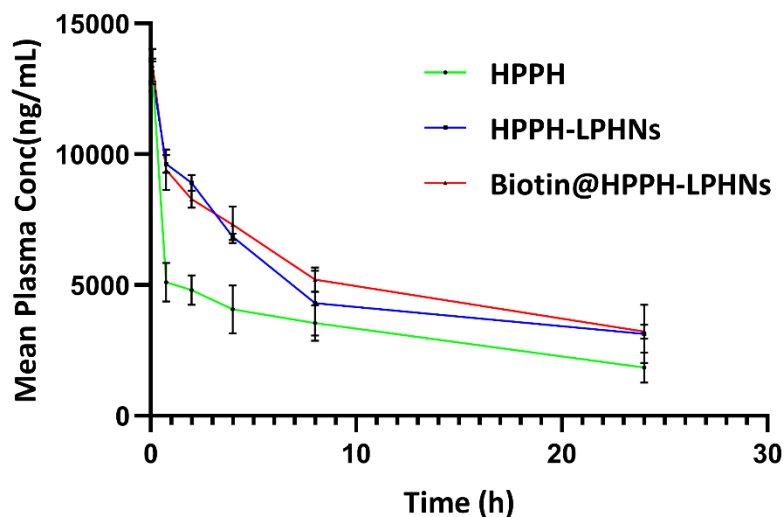


Figure 5.30: In vivo pharmacokinetic study of HPPH and its LPHNs

Further, the comparative result of HPPH and its LPHNs were depicted in table 5.29. The resultant LPHNs showed an improved pharmacokinetics of HPPH in terms of $T_{1/2}$, AUC, Clearance etc. The area under curve (AUC) was found to be 116647.5 ± 22067.11 h*ng/mL and 123354.6 ± 26533.07 h*ng/mL for HPPH-LPHNs and Biotin@HPPH-LPHNs respectively which was higher in comparison to pure HPPH i.e., 72575.11 ± 9169.30 h*ng/mL. In addition, the plasma half-life ($t_{1/2}$) also improved with LPHNs (HPPH-LPHNs and Biotin@HPPH-LPHNs) when compared to pure HPPH. Other pharmacokinetic parameters such as volume of distribution, C_0 , clearance etc. are shown in the Table no. 5.29.

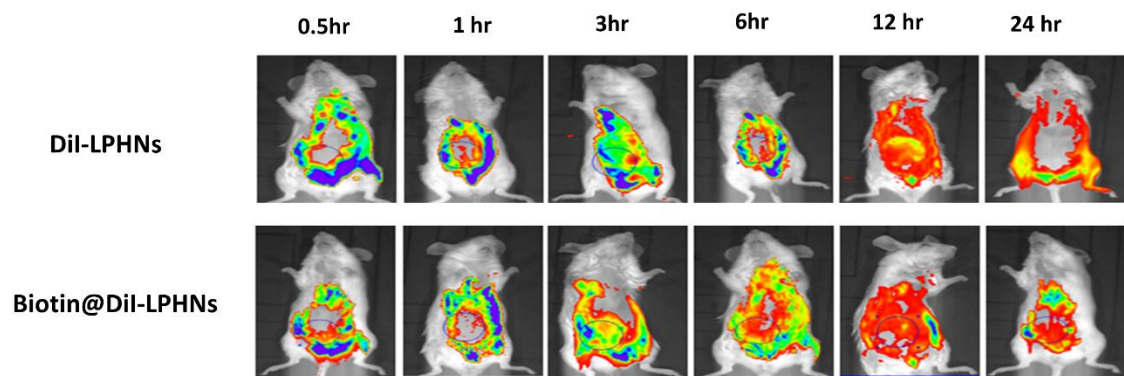
Table 5.29: In-vivo pharmacokinetic profile of HPPH loaded LPHNs (Dose:5mg/kg.bw; Mean \pm SD; n=3)

Parameters	Unit	Free HPPH	Biotin@HPPH-LPHNs	HPPH-LPHNs
C_0	ng/mL	13858.28 \pm 2179.87	13663.33 \pm 753.1788	13448.89 \pm 649.30
T_{max}	h	0.08 \pm 0.00	0.08 \pm 0.00	0.08 \pm 0.00
AUC _{last}	h*ng/mL	72575.11 \pm 9169.30	123354.6 \pm 26533.07	116647.5 \pm 22067.11
AUC _{0-∞}	h*ng/mL	104818.41 \pm 5564.77	287203.8 \pm 108433.6	263302.4 \pm 87136.41
Vd _{obs}	mL/kg	1049.30 \pm 236.37	846.19 \pm 222.49	914.8294 \pm 197.19

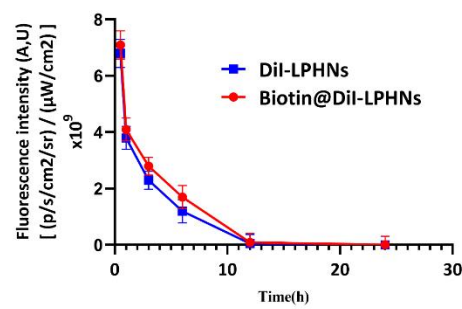
Cl_{obs}	mL/h/kg	47.79±2.61	18.74±7.07	20.2308±5.62
K_e	1/h	0.05±0.01	0.02±0.00	0.021889±0.00
T_{1/2}	h	15.15±2.76	32.01±3.86	31.82289±2.75

5.8.12. In-vivo imaging and biodistribution study

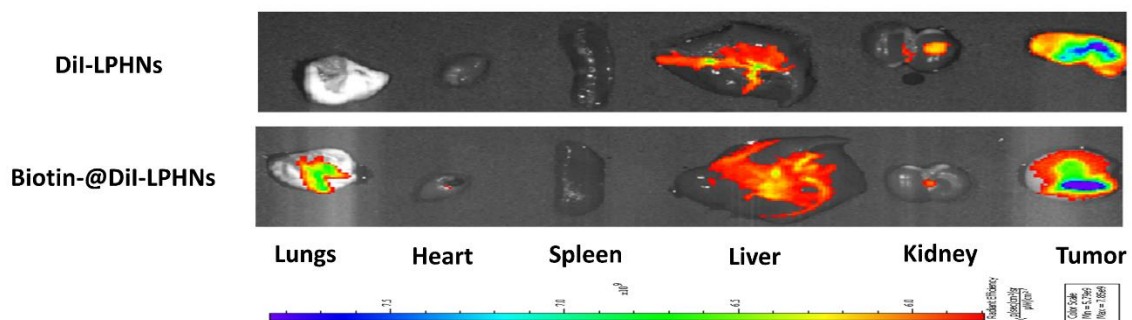
To understand the biodistribution of LPHNs (Biotin tagged and nontagged), DiI dye loaded LPHNs (DiI-LPHNs and Biotin@DiI-LPHNs) was formulated and subjected to both in-vivo and ex-vivo fluorescence imaging study in tumor bearing Balb/c mice. The significant tumor accumulation was shown with Biotin@DiI-LPHNs for a longer period of time against DiI-LPHNs as shown in the figure no. 5.31. The tumor accumulation of both LPHNs was nearly similar till 1 h, but DiI-LPHNs could not be retained for more time. In contrast, Biotin@DiI-LPHNs were retained in tumor area till 24 hr. Further, treated mice were sacrificed and their vital organs were collected, imaged, and shown in Figure 5.31 (C). The fluorescence images (ex vivo) revealed that mice treated with Biotin@DiI-LPHNs have very high tumoral accumulation than DiI-LPHNs i.e., Biotin@DiI-LPHNs showed 1.2-fold time higher than DiI-LPHNs. Additionally, it was also observed that other than tumour area, both the Dye loaded nanocarrier showed higher accumulation in liver as it plays a vital role in metabolism. Further, accumulation of Biotin@DiI-LPHNs was observed lesser in vital organs like spleen, and kidneys compared to DiI-LPHNs as shown by low fluorescence intensity.



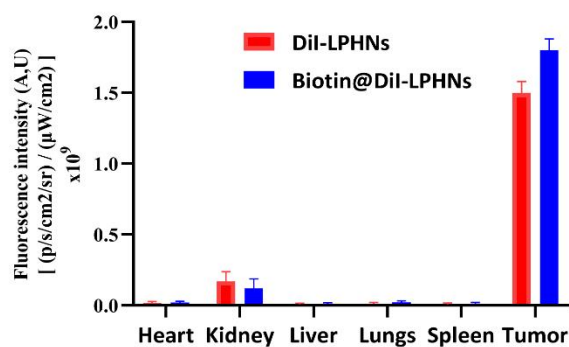
(A)



(B)



(C)



(D)

Figure 5.31: In vivo biodistribution study of HPPH loaded LPHNs (A) Time-dependent fluorescence images of tumor-bearing BALB/c mice after i.v. administration; (B) Graph representing the fluorescence intensity for the region of interest; (C) Ex vivo fluorescence images of major organs and tumor excised at

24 h post-injection; (D) Mean fluorescent intensity of fluorescence probe tagged formulations in tumors and organs.

5.8.13. Safety study of HPPH loaded LPHNs

The sub-acute toxicity study was carried out in the BALB/c mice as per OECD guidelines to evaluate the safety of LPHNs. The study was analyzed as a parameter of behavioral analysis, body weight observation and tissue necrosis of major vital organs of healthy female Balb/C mice upon repeated administration of HPPH and its nanocarrier. All the animal groups showed normal behavior and no significant change in body weight during the study period. As shown in the Figure no. 5.32, all the tissues of vital organs of the treated group i.e., HPPH, HPPH-LPHNs (non-targeted) and Biotin@HPPH-LPHNs (Targeted) showed normal and similar construction as that of the control mice, which indicates that there is no toxicity and ensures that the prepared LPHNs of HPPH were biocompatible to the biological system.

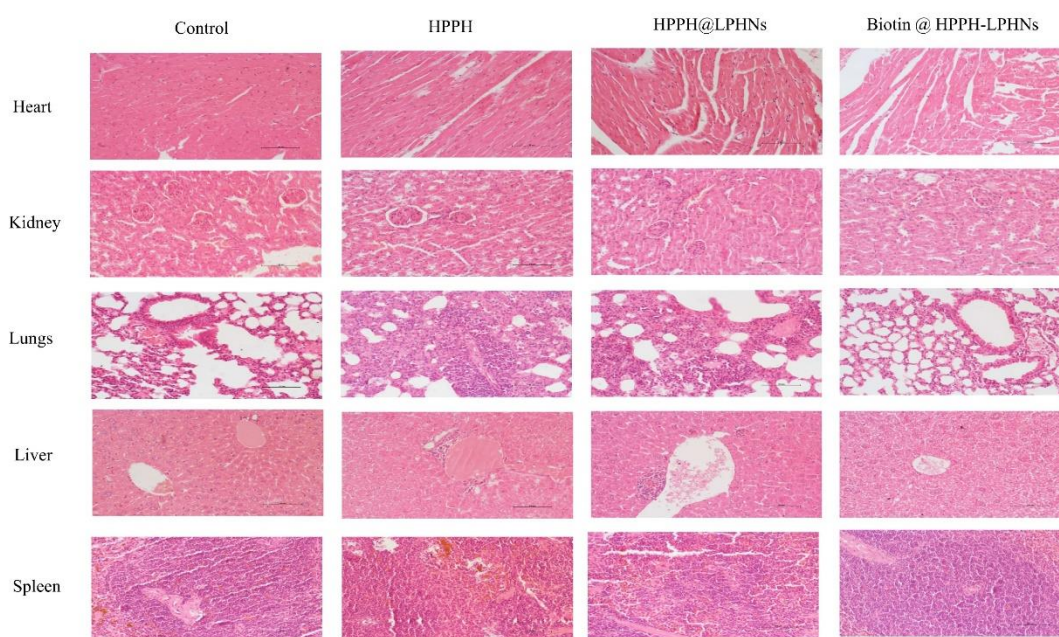


Figure 5.32: Safety evaluation study of HPPH loaded LPHNs

Additionally, biochemical analysis was performed for all the groups i.e., Control (saline), Pure HPPH, HPPH-LPHNs and Biotin@HPPH-LPHNs. The hematological and serological parameters were conducted and it was found that pure HPPH and its LPHNs exhibited normal ranges, which were similar to the saline group, indicating the absence of abnormal side effects (Table 5.30).

Table 5.30: Biochemical analysis of HPPH and its LPHNs

Parameter	Unit	Control	HPPH	HPPH-LPHNs	Biotin@HPPH-LPHNs
Hematology					
Hemoglobin (HB%)	gm%	13.9	13.5	12.2	12.7
TLC	/cumm	3000	3150	2220	3200
Differential Leucocytes Count (DLC)					
Neutrophile	%	30	31	28	26
Lymphocytes	%	65	58	55	56
Eosinophils	%	5	4	4	5
Monocytes	%	0	0	0	0
Basophils	%	0	0	0	0
TRBC	million/cumm	6.9	6.19	5.94	6.21
APC	Lacks/cumm	6.02	6.05	5.96	6.10
PCV	%	39	38	41	37
MCV	fL	51	50	49	52
MCH	Pg	18	16	14	15
MCHC	g/dL	34	30	32	36
TEC	cells/cumm	350	360	300	390
Biochemistry					
Blood Urea	mg%	8	10	10	12
Serum Creatinine	mg%	0.26	0.32	0.34	0.29
Serum Cholesterol	mg%	29	41	39	38
L.F.T					
Triglycerides	mg%	11	12	18	16
AST/SGOT	U/L	45	39	45	35
ALT/SGPT	U/L	36	43	37	41
Serum Bilirubin					
Total	mg%	0.5	0.53	0.60	0.56
Direct	mg%	0.31	0.31	0.35	0.31
Indirect	mg%	0.19	0.21	0.24	0.22
Total Protein	gm%	4.6	4.4	4.5	4.4
Albumin	gm%	2.8	3.0	2.6	2.8
Globulin	gm%	1.8	1.6	2.0	1.8

5.9. Development and characterization of OLA loaded LPHNs

5.9.1. Physicochemical Characterization

The LPHNs (lyophilized and non-lyophilized samples) were characterized with respect to particle size, PDI, zeta potential, % entrapment efficiency, % drug loading and morphological evaluation. The obtained results have been summarized in table 5.31 and depicted in Figure 5.33. Both lyophilized and non-lyophilized samples showed the particles size less than 150 nm with narrow PDI (~ 0.21). The zeta potential for the OLA-LPHNs were found to be ~ 0.4 mV for both lyophilized and non-lyophilized samples, while for the St@OLA-LPHNs and St/Biotin@OLA-LPHNs sample this value were much higher, i.e., ~ 28 mV. The % entrapment efficiency was in the range of 56-67% with % drug loading value of ~9%.

Table 5.31: Physicochemical characterization of the OLA loaded LPHNs (Fresh LPHNs; n=3, Mean± SD)

Formulation	Mean diameter (nm)	PDI	Zeta potential (mV)	Encapsulation efficacy (%)
OLA-LPHNs	121.6 ±10.2	0.0913±0.13	-0.3±0.02	65.32±2.08
St@OLA-LPHNs	138.3 ±12.1	0.201±0.12	27.4±0.30	67.14±4.12
St/Biotin@OLA-LPHNs	138.6 ±10.2	0.203±0.13	25.3±0.10	65.32±2.08

PS: Particle Size; PDI: Poly dispersity index ZP: Zeta Potential; EE: Entrapment Efficiency

Additionally, SEM image showed that OLA loaded nanoparticles were nano-metric in size with spherical shape which matches with result of DLS analysis (Figure 5.33). It could provide less aggregation with enhanced stability.

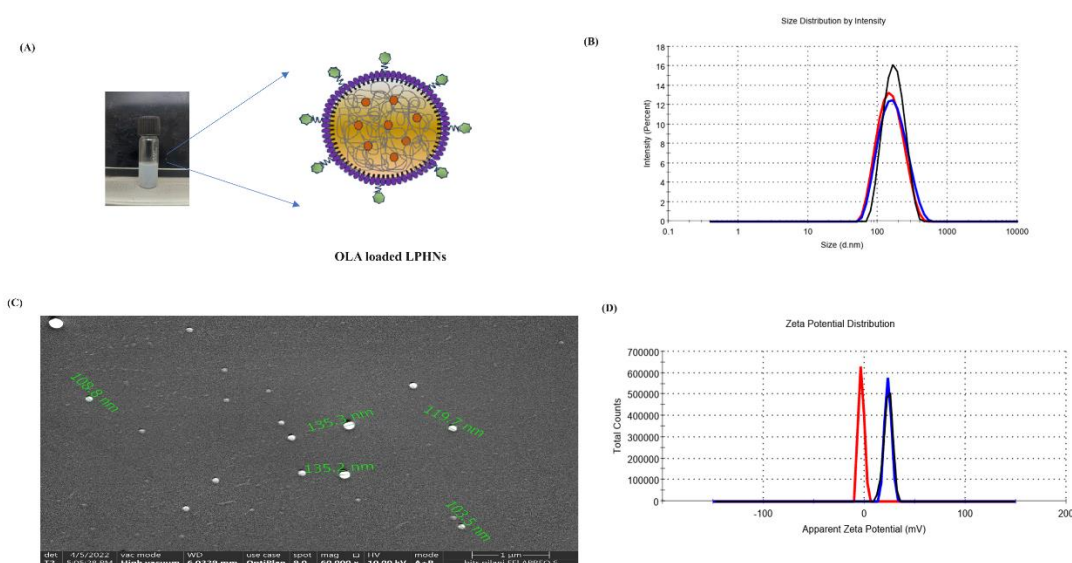


Figure 5.33: Morphological Characterization of OLA loaded LPHNs (A) Sample of St/Biotin@OLA-LPHNs; (B) Particle size of non-lyophilized samples, i.e., OLA-LPHNs (red), St@OLA-LPHNs(black), St/Biotin@OLA-LPHNs St/Biotin@OLA-LPHNs(blue); (C) SEM image of St/Biotin@OLA-LPHNs; (D) Zeta potential of OLA-LPHNs (red), St@OLA-LPHNs (black), St/Biotin@OLA-LPHNs (blue)

5.9.2. Freeze drying of OLA loaded LPHNs

The freeze drying of OLA loaded LPHNs were carried out using four different cryoprotectants including sucrose, mannitol, trehalose, and PEG-4000 for three different concentrations i.e. 2.5%, 5% and 10% w/w. Afterward, these lyophilized LPHNs sample were subjected to physiochemical characterization with respect to PS and PDI analysis and the obtained lyophilization results were shown in table 5.32.

Table 5.32: Lyophilization screening for OLA loaded LPHNs with different cryoprotectant

Formulation	Mean diameter (nm)	PDI
1. Lyophilized LPHNs with 2.5% Mannitol		
OLA-LPHNs	380.63±16.34	0.431±0.02
St@OLA-LPHNs	402.93±6.43	0.42±.01
St/Biotin@OLA-LPHNs	360.97±2.41	0.419±0.01
2. Lyophilized LPHNs with 5% Mannitol		
OLA-LPHNs	363.87±5.16	0.427±0.03
St@OLA-LPHNs	339.80±4.06	0.34±.03
St/Biotin@OLA-LPHNs	346.19±1.94	0.38±0.02
3. Lyophilized LPHNs with 10 % Mannitol		
OLA-LPHNs	347.30±26.55	0.35±0.03
St@OLA-LPHNs	349.40±8.92	0.36±.00
St/Biotin@OLA-LPHNs	305.30±13.95	0.35±0.02
4. Lyophilized LPHNs with 2.5% Sucrose		
OLA-LPHNs	212.50±16.02	0.33±0.04
St@OLA-LPHNs	313.56±5.79	0.37±0.04
St/Biotin@OLA-LPHNs	305.56±4.98	0.38±0.00
5. Lyophilized LPHNs with 5% Sucrose		
OLA-LPHNs	212.50±16.02	0.33±0.04
St@OLA-LPHNs	217.86±2.58	0.33±0.02
St/Biotin@OLA-LPHNs	272.50±2.00	0.35±0.02
6. Lyophilized LPHNs with 10% Sucrose		
OLA-LPHNs	206.83±7.21	0.33±0.04
St@OLA-LPHNs	230.16±2.91	0.33±0.02
St/Biotin@OLA-LPHNs	245.91±16.21	0.34±.04
7. Lyophilized LPHNs with 2.5 %Trehalose		
OLA-LPHNs	180.17±17.97	0.22±0.01
St@OLA-LPHNs	170.82±1.79	0.24±0.01
St/Biotin@OLA-LPHNs	166.17±3.69	0.22±0.01
8. Lyophilized LPHNs with 5 % Trehalose		
OLA-LPHNs	143.50±5.36	0.22±0.21
St@OLA-LPHNs	148.63±1.59	0.21±0.01
St/Biotin@OLA-LPHNs	156.80±2.12	0.22±0.01
9. Lyophilized LPHNs with 10 % Trehalose		
OLA-LPHNs	135.37±1.20	0.21±0.00
St@OLA-LPHNs	142.54±7.40	0.20±0.02
St/Biotin@OLA-LPHNs	143.50±15.28	0.21±0.01
10. Lyophilized LPHNs with 2.5 %PEG4000		
OLA-LPHNs	261.50±17.71	0.29±0.03
St@OLA-LPHNs	272.71±5.05	0.33±.05
St/Biotin@OLA-LPHNs	233.20±1.85	0.34±0.01
11. Lyophilized LPHNs with 5 % PEG 4000		
OLA-LPHNs	258.17±13.38	0.29±0.03
St@OLA-LPHNs	207.80±5.66	0.33±0.02
St/Biotin@OLA-LPHNs	191.23±3.70	0.32±0.01
12. Lyophilized LPHNs with 10 % PEG 4000		
OLA-LPHNs	156.83±17.53	0.29±0.03
St@OLA-LPHNs	159.99±1.96	0.28±0.01
St/Biotin@OLA-LPHNs	175.27±6.28	0.28±0.04

PS: Particle Size; PDI: Poly dispersity Index;

From the obtained data (Table 5.32), 10% w/w trehalose showed better physicochemical profile as compared to other groups. Subsequently, the physicochemical parameter of lyophilized LPHNs with 10% w/w trehalose showed nearly similar result as compared to fresh LPHNs (Table 5.33).

Table 5.33: Physicochemical characterisation of Optimised OLA loaded LPHNs

Formulation	Mean diameter (nm)	PDI	Zeta potential (mV)	Encapsulation efficacy (%)	Drug loading (%)
OLA-LPHNs	135.3 ±12.1	0.211±0.12	-0.4±0.01	56.14±8.12	8.9 ±0.10
St@OLA-LPHNs	142.4 ±10.7	0.203±0.06	25.2±0.20	65.32±6.18	8.30 ±0.56
St/Biotin@OLA-LPHNs	143.5 ±11.27	0.208±0.20	24.8±0.60	63.16±10.01	8.70 ±0.11

PS: Particle Size; PDI: Poly dispersity index ZP: Zeta Potential; EE: Entrapment Efficiency; DL: Drug Loading

5.9.3. *In vitro* release study

The release study was performed using dialysis bag method in two different pH conditions, that is 5.4 and 7.4. From the results, it has been revealed that for all the LPHNs samples, approx. 40% drug release was observed within first 4 hr., while remaining 60% of release was completed in the duration of 48 hr. Whereas, in case of free drug, the complete release was attained within 2 hr. (Figure 5.34).

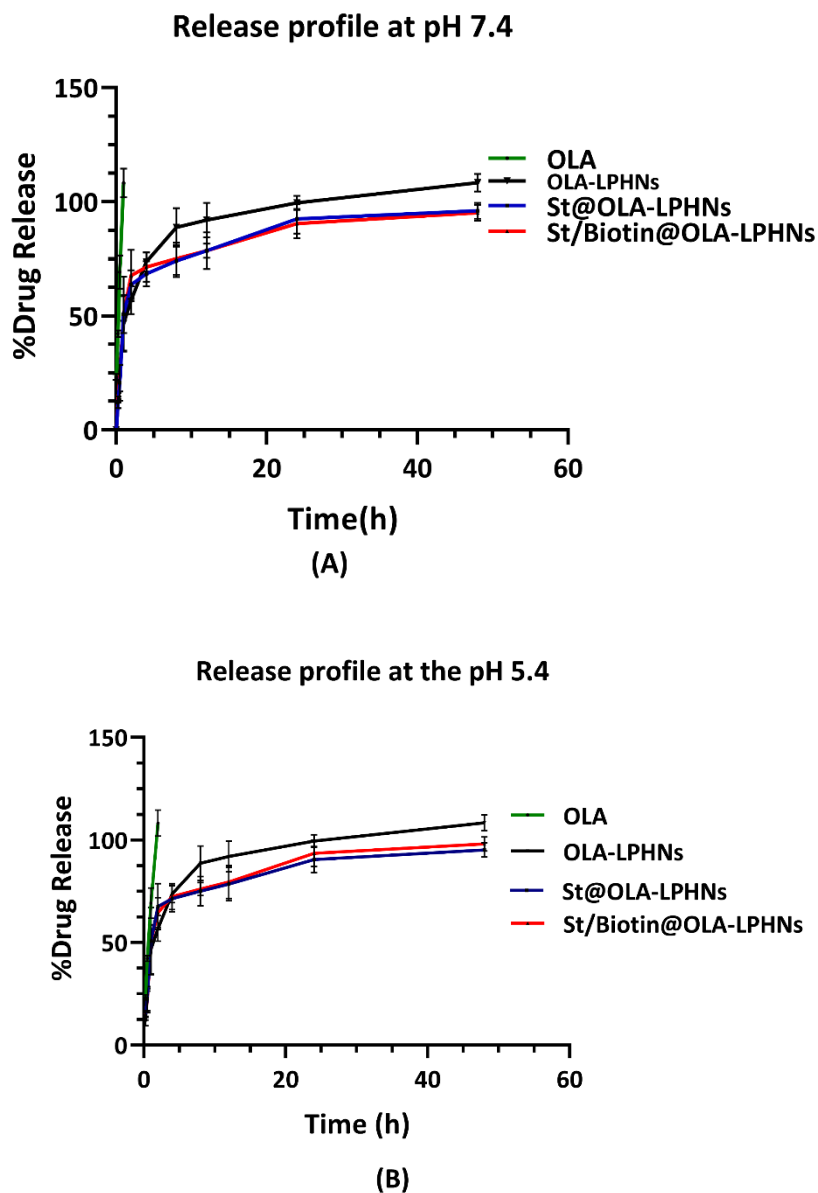
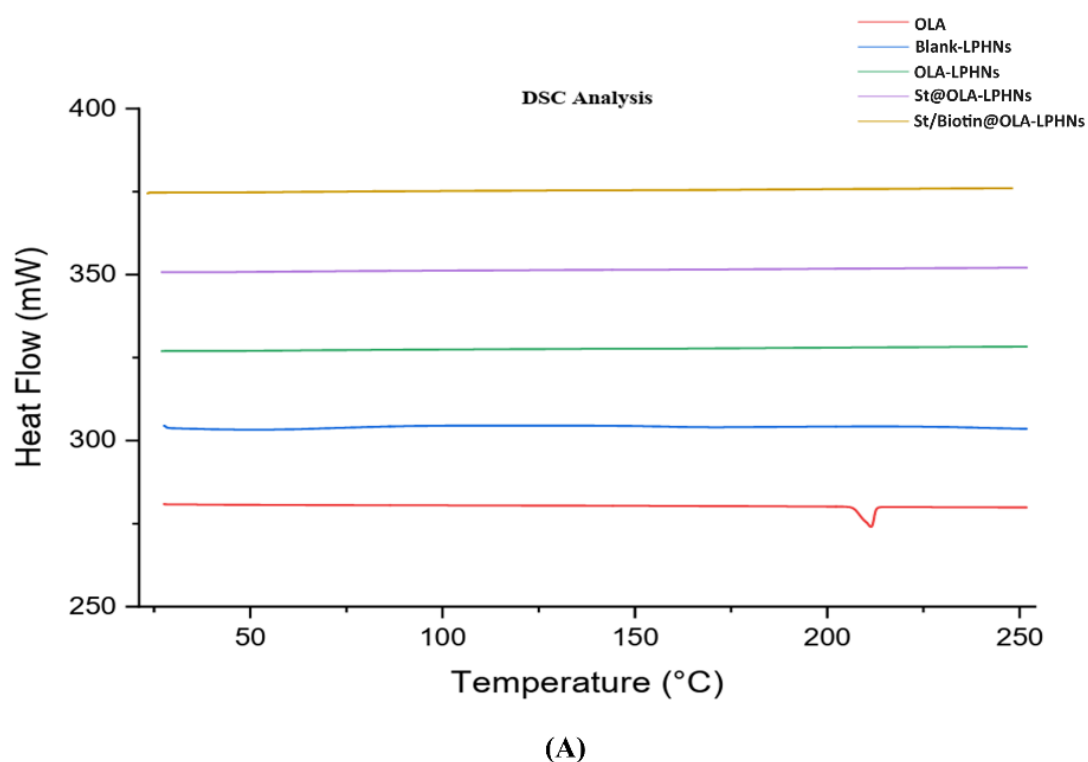


Figure 5.34: *In vitro* release study of free OLA, OLA-LPHNs, St@OLA-LPHNs and Biotin/St@OLA-LPHNs in pH 7.4 and pH 5.4.

5.9.4. Physical state characterization

5.9.4.1. Attenuated total reflection-IR (ATR-IR)

The IR spectra of the pure drug, targeted cationic blank LPHNs (Blank-LPHNs), OLA-LPHNs, St@OLA-LPHNs and St/Biotin@OLA-LPHNs were illustrated in Figure 5.35(B). The major characteristic peak for pure drug was observed at 3186.12 cm^{-1} due to N-H stretching, 1631 cm^{-1} due to -C=O aromatic stretching and 1407 cm^{-1} due to -C-H bending. While in case of nanoparticles, the peak intensity was found to be low compared to the pure drug.



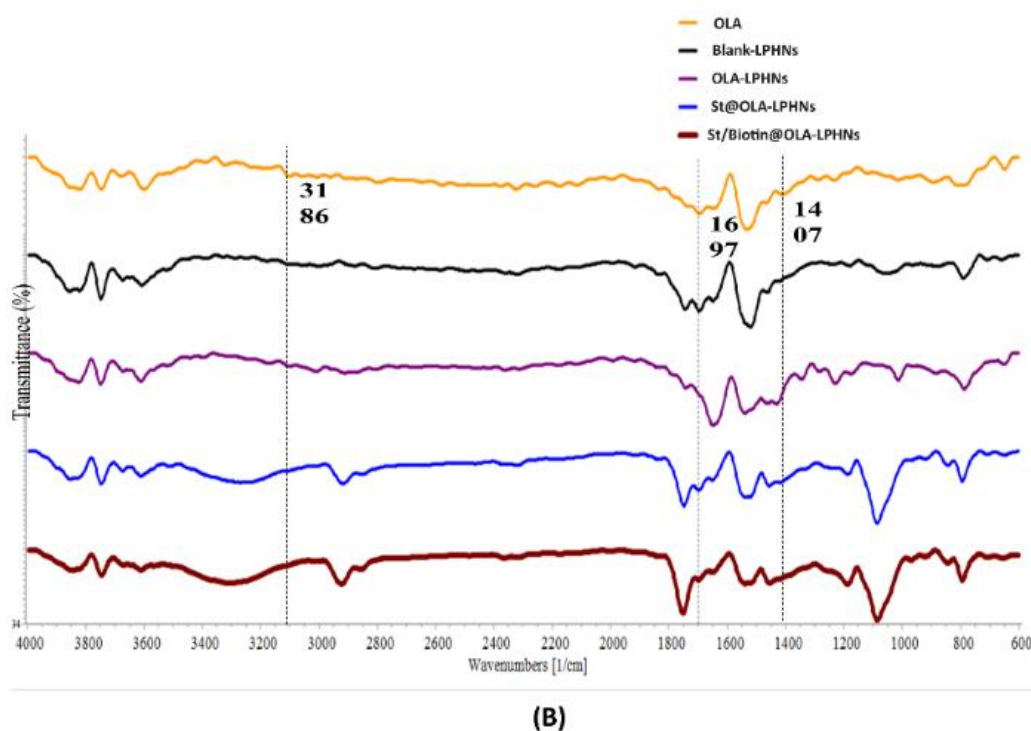


Figure 5.35: Physical state characterization of OLA and its LPHNs; (A) DSC thermogram and (B) IR spectra of pure drug (OLA) and OLA loaded LPHNs (Targeted cationic Blank-LPHNs and OLA loaded LPHNs).

5.9.4.2. Differential scanning calorimetry

The thermogram of the pure drug, targeted cationic blank LPHNs (Blank-LPHNs), OLA-LPHNs, St@OLA-LPHNs and St/Biotin@OLA-LPHNs were illustrated in Figure 5.35(A). The DSC thermogram of OLA unveiled a sharp melting peak at 210.63 °C., whereas the melting point peak of OLA in LPHNs completely disappeared.

5.9.5. Stability studies of LPHNs

The stability of lyophilized samples was characterized for 3 months storage with two different storage conditions i.e., 4 °C/65% RH and 25 °C/60% RH. From their results, it was observed that the stability samples with both storage condition showed no significant changes in PDI and particle size compared to the fresh batch (Figure 5.36).

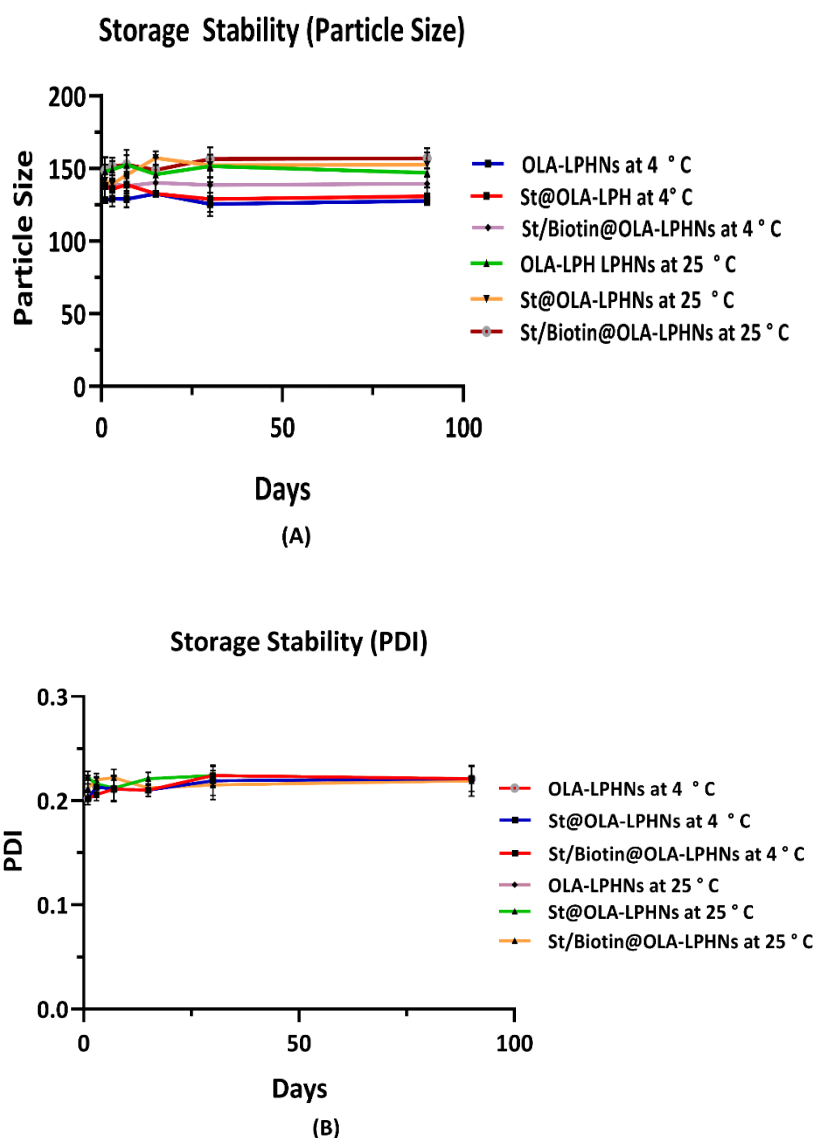


Figure 5.36: Storage stability study of lyophilized OLA loaded LPHNs at two different conditions, i.e., 4 °C/65% RH and 25 °C/60% RH (3 months duration)

5.9.6. Cell culture studies of OLA loaded LPHNs

5.9.6.1. *Invitro cytotoxicity*

The in vitro cytotoxicity was studied using MTT assay in 4T1 breast cancer cells, following treatment of OLA, OLA-LPHNs, St@OLA-LPHNs, St/Biotin@OLA-LPHNs and blank nanoparticle. Based on the % cell viability data obtained after 48 hr. period, IC₅₀ value was calculated and it was 7.3μM, 26.76 μM, 29.63 μM and 60μM for St/Biotin@OLA-LPHNs St@OLA-LPHNs, OLA-LPHNs, and OLA, respectively (Figure 5.37).

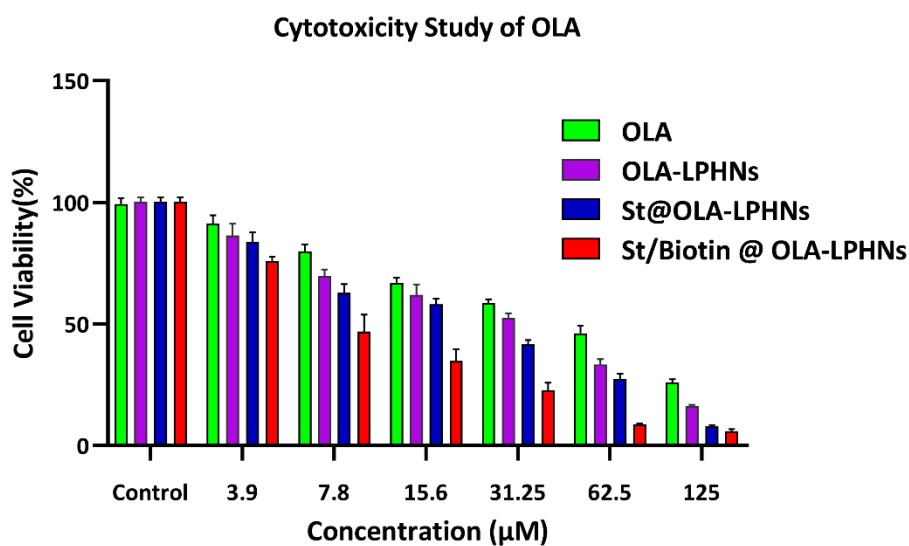


Figure 5.37 *In vitro* cytotoxic effect of different concentration of free drug (OLA), OLA-LPHNs, St@OLA-LPHNs and St/Biotin@OLA-LPHNs; Control represents media control (green color), non-cationic blank LPHNs (violet color), non-targeted cationic blank LPHNs (blue color) and targeted cationic blank LPHNs

5.9.6.2. Cellular uptake study

The cellular uptake of LPHNs was performed in 4T1 cell line using a hydrophobic dye i.e., coumarin-6 which is commonly employed for uptake studies of nanoparticle. The fluorescence intensity of coumarin-6 loaded LPHNs (C6-LPHNs, St@C6-LPHNs and St/Biotin@C6-LPHNs) estimated using confocal microscopy at 525 nm has been shown in the Figure 5.38.

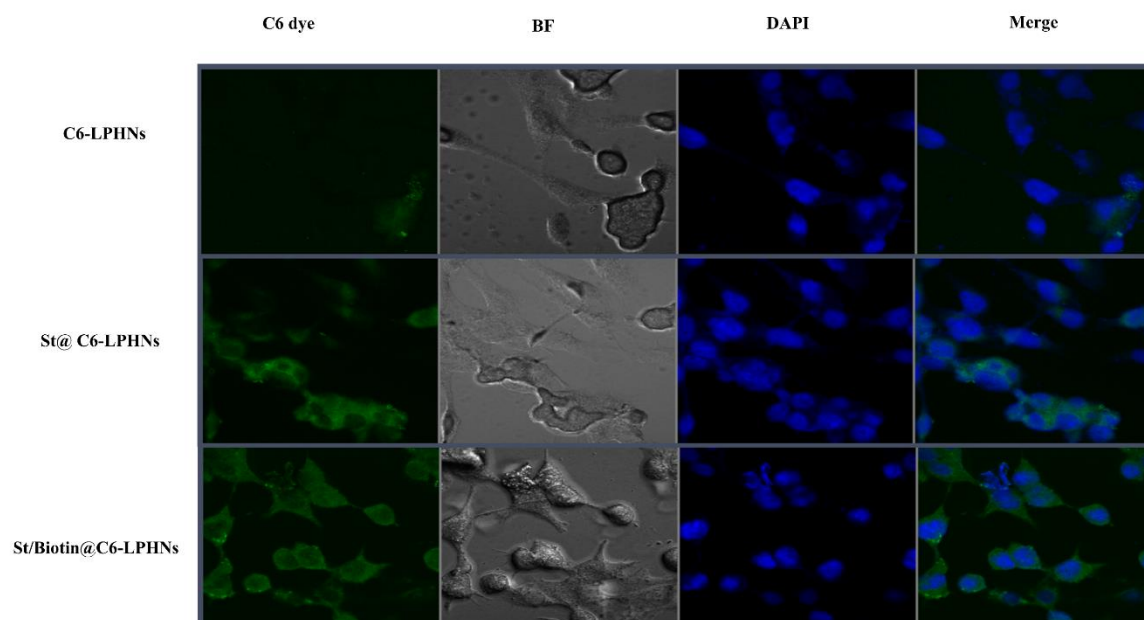


Figure 5.38: *In vitro* cellular uptake of the coumarin-6 loaded LPHNs (C6-LPHNs, St@C6-LPHNs and Biotin/St@C6-LPHNs) estimated using confocal microscopy at 525 nm

5.9.6.3. Apoptosis assay

Apoptosis assay was performed in 4T1 cell line using flow cytometry. For the analysis, the graph was plotted between FITC-A (x-axis) and PI (y-axis); further, four distinct phenotypes were distinguished: viable (lower left quadrant, Q3), early apoptotic cells (lower right quadrant, Q4), late apoptotic and necrotic (upper right quadrant, Q2) and damaged cells (upper left quadrant, Q1) (Figure 5.39). The cell line was treated with OLA and their nanoparticles at the IC₅₀ dose. The apoptotic cell death in OLA solution was 9% whereas resulting nanoparticles i.e., OLA-LPHNs, St@OLA-LPHNs and St/Biotin@OLA-LPHNs unveiled 13.83%, 20.7 % and 72.1% respectively at 48 h.

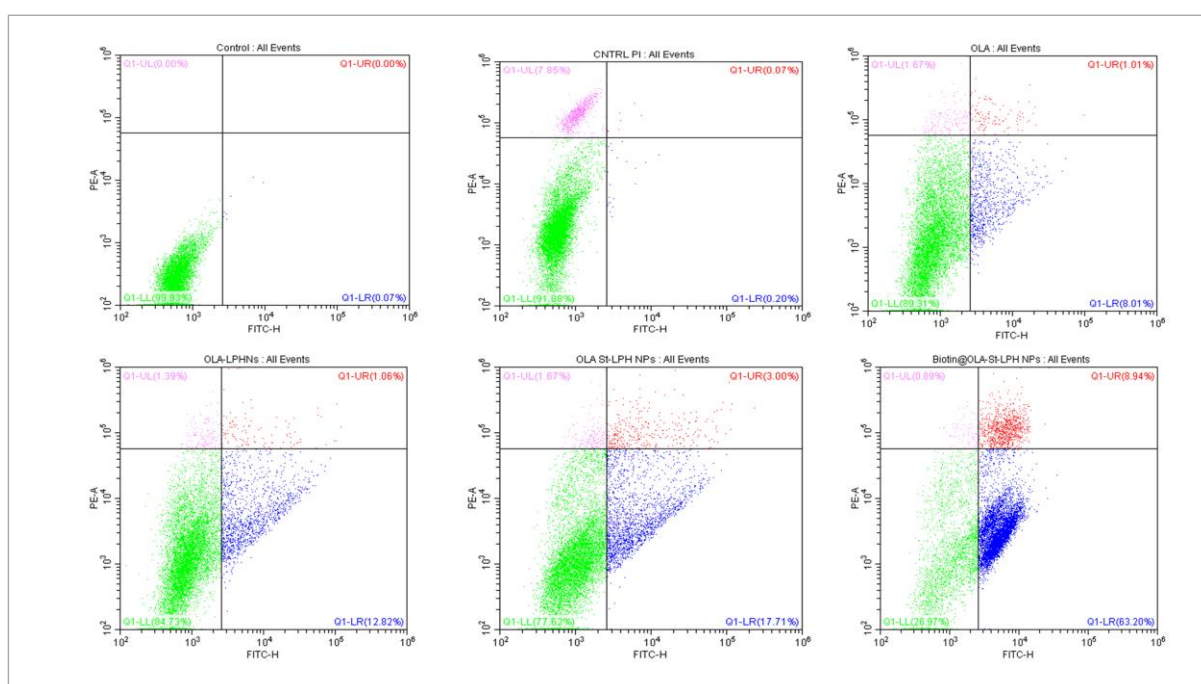


Figure 5.39: Apoptotic assay study in 4T1 cells of OLA, OLA-LPHNs, St@OLA-LPHNs and St/Biotin@OLA-LPHNs

5.9.7. Blood compatibility study (Hemolysis study) of OLA and its LPHNs

Hemolysis of nanoparticle was performed using RBCs of mice. The pure OLA showed hemolytic index of approx. 1.5% whereas, the LPHNs (OLA-LPHNs, St@OLA-LPHNs and Biotin@OLA-LPHNs) exhibited hemolytic index below 1.5% as depicted in Figure 5.40.

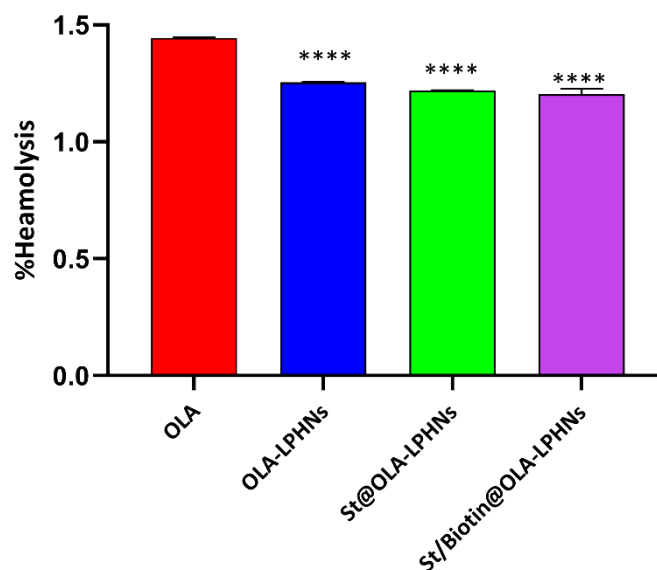


Figure 5.40: Blood compatibility study of pure OLA, OLA-LPHNs, St@OLA-LPHNs and St/Biotin@OLA-LPHNs using RBCs cells

5.9.8. *In vivo* pharmacokinetic study

The pharmacokinetics study was carried out in Balb/C mice. The pharmacokinetic samples were processed and analyzed using LC-MS/MS (Waters Corps., USA). The plasma concentration-time profile is shown in Figure 5.41. All the pharmacokinetic parameters were computed via WinNonlin software 8.3 version (Certara, UK) which was depicted in table 5.34.

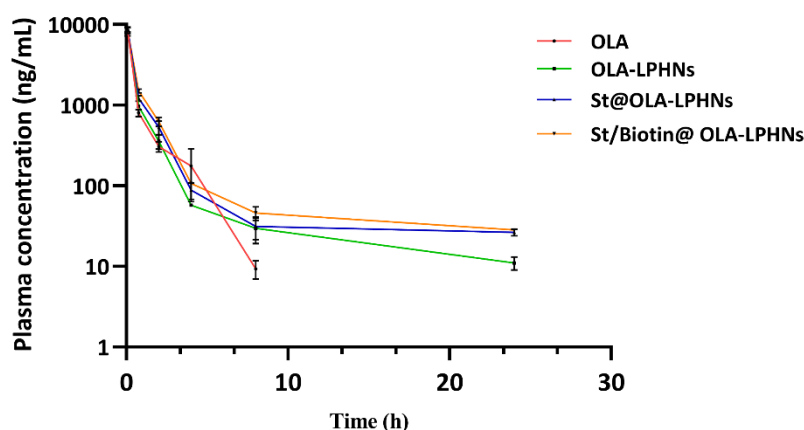


Figure 5.41: *In vivo* pharmacokinetic study of pure OLA, OLA-LPHNs, St@OLA-LPHNs and St/Biotin@OLA-LPHNs

The $AUC_{0-\infty}$ was found to be greater in St/Biotin@OLA-LPHNs (i.e., 14824.27 ± 2094.51 ng.h/ml) in comparison of free drug (5149.59 ± 1050.38 ng.h/ml). The Elimination rate constant

(K_e) ($0.03 \pm 0.007 \text{ h}^{-1}$) of nanoparticles (St/Biotin@OLA-LPHNs) was significantly lower than that of free OLA ($0.18 \pm 0.16 \text{ h}^{-1}$). The biological half-life for the free drug was found to be $5.74 \pm 3.35 \text{ h}$, whereas, for OLA-LPHNs, St@OLA-LPHNs and St/Biotin@OLA-LPHNs, these values were 12.85 ± 4.08 , 15.46 ± 0.12 , $17.50 \pm 1.42 \text{ h}$ respectively. All other pharmacokinetic parameters have been shown in the table 5.34.

Table 5.34: In-vivo pharmacokinetic study data of OLA (Dose: 30mg/kg.bw; n=5; Mean \pm SD)

Parameter	Unit	OLA	OLA-LPHNs	St@OLA-LPHNs	St/Biotin@OLA-LPHNs
C_0	ng/mL	9350.89 \pm 1675.39	9622.18 \pm 569.10	9692.22 \pm 503.15	9890.05 \pm 295.20
T_{max}	h	0.08 \pm 0.00	0.08 \pm 0	0.08 \pm 0	0.08 \pm 0
AUC_{last}	h*ng/mL	5149.59 \pm 1050.38	13807.67 \pm 1165.80	13896.29 \pm 3652.49	14824.27 \pm 2094.51
Vd_{obs}	mL/kg	50778.67 \pm 33690.97	39902.54 \pm 8581.44	33714.56 \pm 33951.40	32691.13 \pm 2953.98
Cl_{obs}	mL/h/kg	5781.59 \pm 1086.37	1754.72 \pm 236.09	1583.19 \pm 1511.485	1531.71 \pm 173.71
K_e	1/h	0.18 \pm 0.16	0.05 \pm 0.02	0.04 \pm 0.00	0.03 \pm 0.00
$T_{1/2}$	h	5.74 \pm 3.35	12.85 \pm 4.08	15.46 \pm 0.12	17.50 \pm 1.42

5.9.9. In-vivo imaging and biodistribution study

The developed dye loaded LPHNs (DiI-LPHNs, St@DiI-LPHNs and St/Biotin@DiI-LPHNs) was subjected to both in-vivo and ex-vivo fluorescence imaging study in tumor bearing Balb/c mice. The significant tumor accumulation was shown with St/Biotin@DiI-LPHNs for a longer period of time against DiI-LPHNs as shown in the Figure 5.42. The tumor accumulation of both LPHNs were nearly similar at 1 h, but DiI-LPHNs and St@ DiI-LPHNs could not be retained for more time. In contrast, St/Biotin@DiI-LPHNs were retained in tumor area and the distribution was highest at 36 hr. Further, treated mice were sacrificed and their vital organs were collected, imaged, and shown in Figure 5.42. The images revealed that mice treated with St/Biotin@DiI-LPHNs have very high tumoral accumulation than DiI-LPHNs. Further, accumulation of St/Biotin@DiI-LPHNs was observed lesser in vital, organs like spleen, and kidneys compared to DiI-LPHNs as shown by low fluorescence intensity.

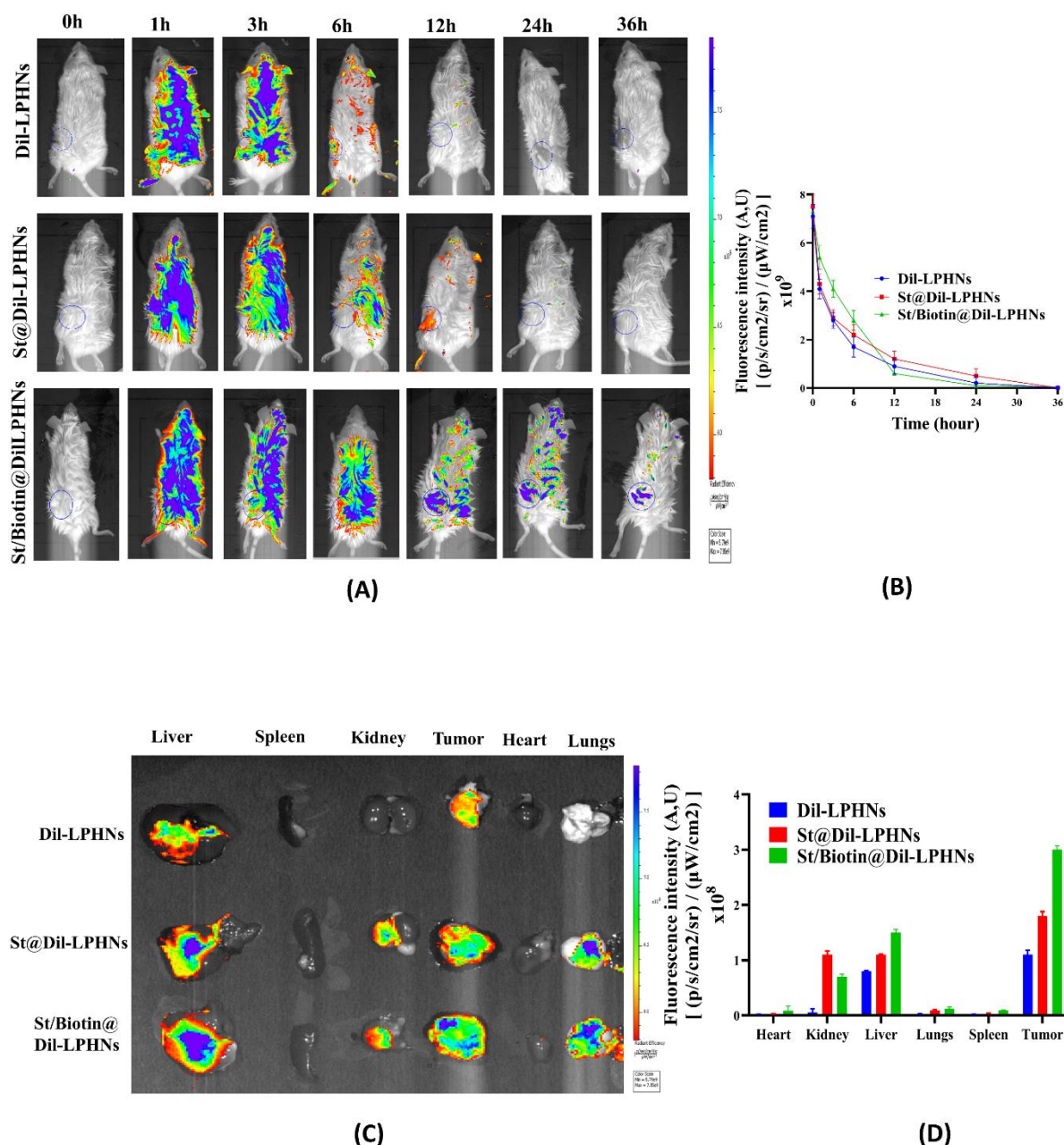


Figure 5.42: In vivo biodistribution study of HPPH and OLA co-loaded LPHNs (A) Time-dependent fluorescence images of tumor-bearing BALB/c mice after i.v. administration; (B) Graph representing the fluorescence intensity for the region of interest; (C) Ex vivo fluorescence images of major organs and tumor excised at 36 h post-injection; (D) Mean fluorescent intensity of fluorescence probe tagged formulations in tumors and organs

5.9.10. Safety study for OLA loaded LPHNs

The evaluation of safety for the developed LPHNs were carried out by performing toxicological study in the Balb/c mice. Briefly, pure drug and LPHNs equivalent to the dose of 30 mg/kg body weight were administered intravenously as single dose to the mice at a frequency of 48 hr. for the total duration of 21 days. The body weight of the treated mice was assessed for all the group (pure drug, OLA-LPHNs, St@ OLA-LPHNs and St/Biotin@ OLA-LPHNs) at initial

dosing and after completions of study and it was found that no change in body weight. Further, on completion of study, the animals were sacrificed and various organs collected and subjected for the histopathological studies (Figure 5.43). The H&E staining based histological data showed a similar type of profile for nanocarrier in comparison to saline control group.

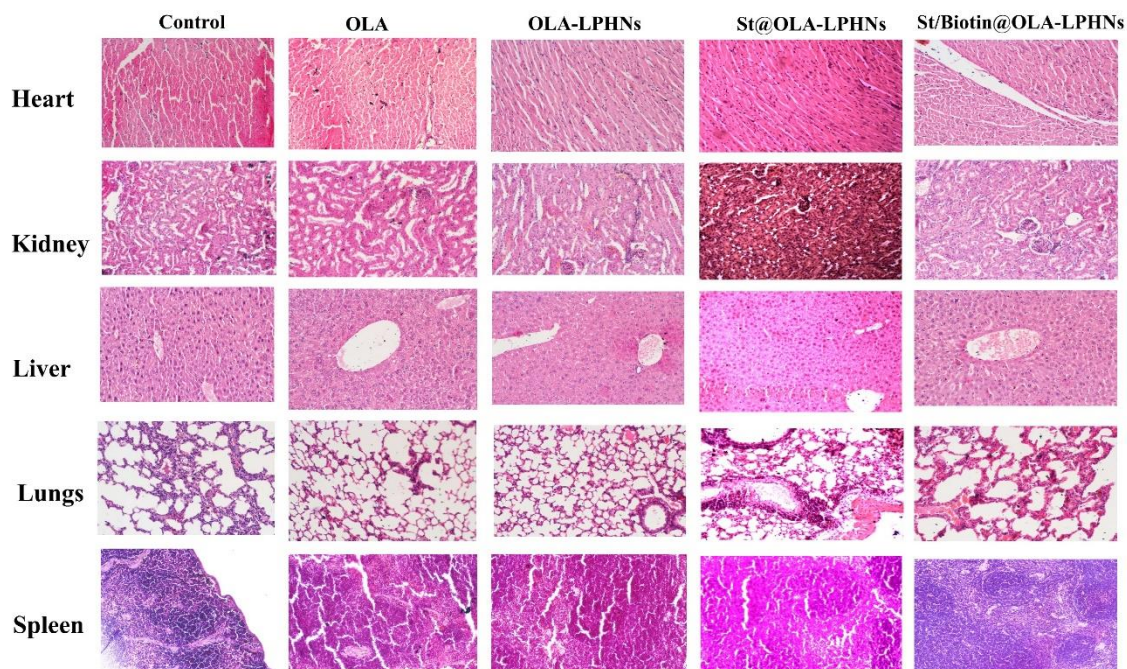


Figure 5.43: Safety evaluation studies of various organs (i.e., heart, kidney, liver, lungs, spleen) using H&E staining

5.10. Fabrication and characterization of HPPH and OLA co-loaded LPHNs

5.10.1 Preparation of HPPH and OLA co-loaded LPHNs

In the recent past, nano-based drug delivery system for cancer management were extensively studied in order to enhance the site-specific accumulation of drug with reduced systemic toxicity. Furthermore, to improve the tumor uptake and increase the residence time of drug, LPHNs based nano carrier systems were majorly focused by the scientists. In this present study, we have developed a surface engineered LPHNs using biotin decorated PEG-PLGA and TPP tagged linoleic acid (Linoleic acid-ss-TPP). The LPHNs systems was fabricated using single emulsification method followed by solvent evaporation and further subjected to various characterization such as physicochemical evaluation, in vitro release, in vitro cell culture and in vivo studies.

5.10.2 Physio-chemical characterization of HPPH and OLA co-loaded LPHNs

The physicochemical characterization of LPHNs were evaluated by particle size, PDI, ZP and %EE and morphological parameter. PS is the intrinsic property of nanoparticle that

influence the drug release pattern, stability and in vivo study of a nanocarrier. For target specific delivery, the particle size range 100-200nm is suitable particularly for delivery to tumor. As shown on the table 5.35., both the LPHNs (Biotin-ss-TPP@HPPH/OLA-LPHNs and Biotin@ HPPH/OLA-LPHNs) didn't show any significant changes in particle size and PDI.

Table 5.35: Physicochemical characterization of HPPH and OLA co-loaded LPHNs (Fresh LPHNs n=3; Mean \pm SD)

Optimized Nanoparticles	PS (nm)	PDI	ZP (mV)	%EE
Biotin@HPPH/OLA-LPHNs	140.1 \pm 3.2	0.201 \pm 0.5	27.1 \pm 0.2	35.1 \pm 5.1 % (HPPH) 78.6 \pm 6.8 % (OLA)
Biotin-ss-TPP@HPPH/OLA-LPHNs	141.3 \pm 5.1	0.203 \pm 0.1	26.3 \pm 0.3	34.1 \pm 6.8 % (HPPH) 75.4 \pm 10.1 % (OLA)

The mean particle size of Biotin-ss-TPP@HPPH/OLA and Biotin@ HPPH/OLA-LPHNs was 140.1 \pm 3.1nm and 141.3 \pm 5.1nm respectively. PDI and Zeta potential of nanoparticles displayed a narrow range and with good stability values that is, 0.201 \pm 0.5 and 27.1 \pm 0.2 mV for Biotin@HPPH/OLA LPHNs and 0.203 \pm 0.1 and 26.3 \pm 0.2 mV for Biotin-ss-TPP@HPPH/OLA LPHNs respectively. FEI-SEM analysis was performed and shape was depicted as spherical with particle size in between 100 and 150 nm.

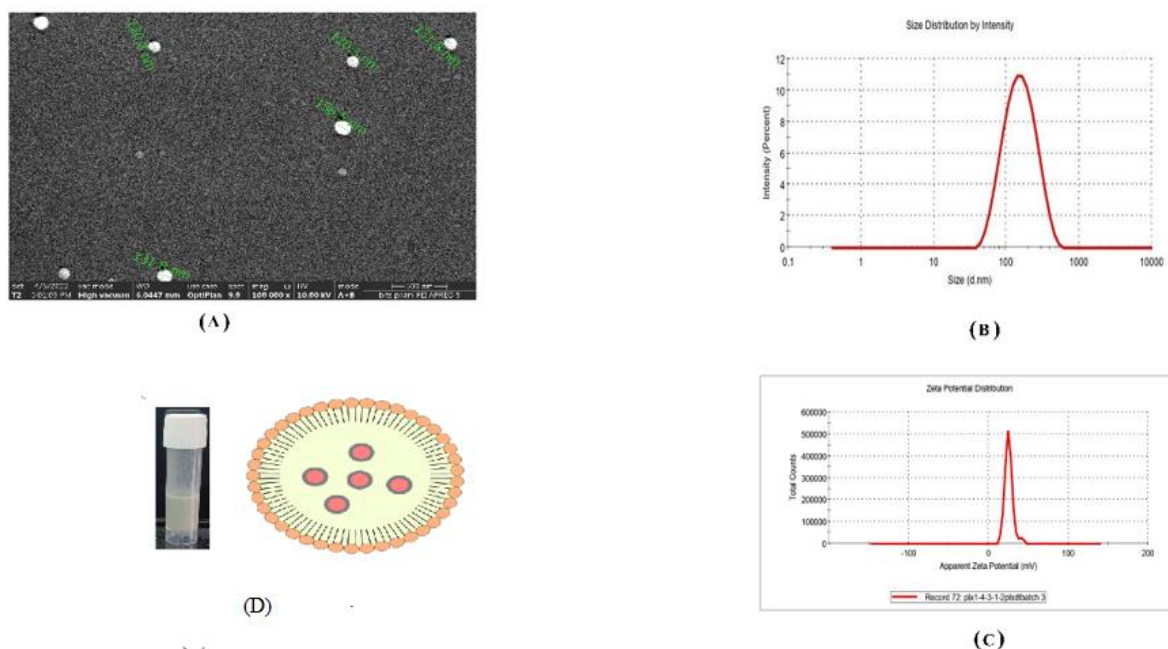


Figure 5.44: Morphological characterization of HPPH and OLA co-loaded LPHNs (A) SEM of Biotin-ss-TPP@HPPH/OLA-LPHNs (B) Particle size of Biotin-ss-TPP@HPPH/OLA-LPHNs (C) Zeta Potential of Biotin-ss-TPP@HPPH/OLA-LPHNs (D) Sample of Biotin-ss-TPP@HPPH/OLA-LPHNs

The entrapment efficiency of HPPH and OLA in the LPHNs was determined with a LC-MS/MS. The %EE was found to be in the range of 32-36% for HPPH and 73-79% for OLA as depicted in table 5.35.

5.10.3 Freeze drying of HPPH and OLA co-loaded LPHNs

The freeze drying of HPPH loaded LPHNs were carried out using four different cryoprotectants including sucrose, mannitol, trehalose, and PEG-4000 for three different concentrations i.e. 2.5%, 5% and 10% w/w. Further, these lyophilized LPHNs were subjected to physiochemical characterization with respect to PS and PDI analysis. The obtained freeze drying results were shown in table 5.36.

Table 5.36: Lyophilization screening for HPPH and OLA co-loaded LPHNs with different cryoprotectant

Formulation	Mean diameter (nm)	PDI
1. Lyophilized LPHNs with 2.5% Mannitol		
Biotin@HPPH/OLA-LPHNs	408.63±13.34	0.461±0.06
Biotin-ss-TPP@HPPH/OLA-LPHNs	406.93±6.43	0.41±0.05
2. Lyophilized LPHNs with 5% Mannitol		
Biotin@HPPH/OLA-LPHNs	383.7±5.1	0.429±0.03
Biotin-ss-TPP@HPPH/OLA-LPHNs	379.80±7.6	0.36±0.03
3. Lyophilized LPHNs with 10 % Mannitol		
Biotin@HPPH/OLA-LPHNs	338.30±17.25	0.39±0.02
Biotin-ss-TPP@HPPH/OLA-LPHNs	349.40±8.92	0.37±0.06
4. Lyophilized LPHNs with 2.5% Sucrose		
Biotin@HPPH/OLA-LPHNs	262.50±11.02	0.32±0.04
Biotin-ss-TPP@HPPH/OLA-LPHNs	253.56±5.9	0.37±0.04
5. Lyophilized LPHNs with 5% Sucrose		
Biotin@HPPH/OLA-LPHNs	232.50±8.02	0.33±0.09
Biotin-ss-TPP@HPPH/OLA-LPHNs	239.86±7.78	0.32±0.02
6. Lyophilized LPHNs with 10% Sucrose		
Biotin@HPPH/OLA-LPHNs	203.3±7.18	0.32±0.08
Biotin-ss-TPP@HPPH/OLA-LPHNs	210.36±8.92	0.31±0.09
7. Lyophilized LPHNs with 2.5 %Trehalose		
Biotin@HPPH/OLA-LPHNs	189.32±12.97	0.25±0.07
Biotin-ss-TPP@HPPH/OLA-LPHNs	195.82±1.92	0.27±0.03
8. Lyophilized LPHNs with 5 % Trehalose		
Biotin@HPPH/OLA-LPHNs	155.50±5.32	0.23±0.21
Biotin-ss-TPP@HPPH/OLA-LPHNs	159.63±7.5	0.21±0.09
9. Lyophilized LPHNs with 10 % Trehalose		
Biotin@HPPH/OLA-LPHNs	145.3±13.20	0.208±0.50
Biotin-ss-TPP@HPPH/OLA-LPHNs	143.6±8.1	0.218±0.01
10. Lyophilized LPHNs with 2.5 %PEG4000		
Biotin@HPPH/OLA-LPHNs	264.50±7.81	0.31±0.03
Biotin-ss-TPP@HPPH/OLA-LPHNs	272.71±5.05	0.32±0.04
11. Lyophilized LPHNs with 5 % PEG 4000		
Biotin@HPPH/OLA-LPHNs	244.17±13.38	0.28±0.03
Biotin-ss-TPP@HPPH/OLA-LPHNs	217.80±5.3	0.30±0.02
12. Lyophilized LPHNs with 10 % PEG 4000		
Biotin@HPPH/OLA-LPHNs	154.83±18.53	0.318±0.06
Biotin-ss-TPP@HPPH/OLA-LPHNs	161.99±4.38	0.32±0.04

PS: Particle Size; PDI: Polydispersity Index

From the obtained data (Table 5.36), 10% w/w trehalose showed better particle size and PDI as compared to other groups. Subsequently, the lyophilized LPHNs with trehalose 10% showed the similar results with the fresh LPHNs. The values were depicted in the Table 5.37.

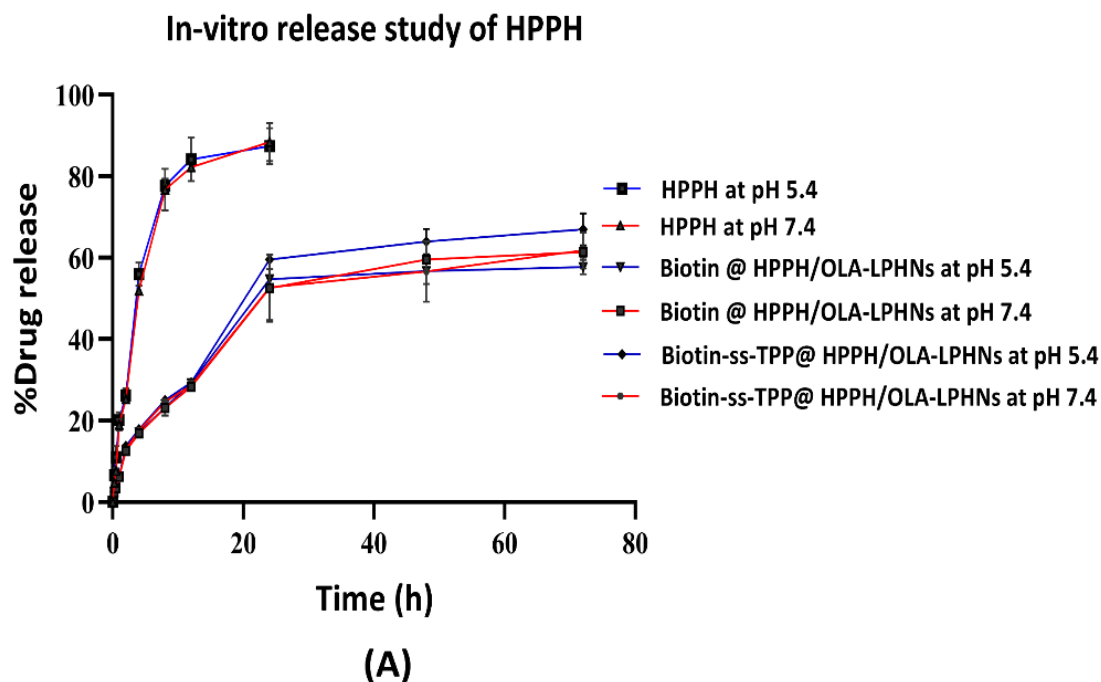
Table 5.37: Physicochemical characterisation of HPPH and OLA coloaded LPHNs (Lyophilised)

Optimized Nanoparticles	PS (nm)	PDI	ZP (mV)	%EE
Biotin@HPPH/OLA-LPHNs	145.3 ±13.2	0.208±0.56	25.4±0.2	34.9 ±5.4 % (HPPH)
				77.8±6.2 % (OLA)
Biotin-ss-TPP@HPPH/OLA-LPHNs	143.6 ±8.1	0.218±0.1	25.8±0.2	32.9±8.8 % (HPPH)
				73.4±10.1 % (OLA)

PS: Particle Size; ZP: Zeta Potential; EE: Entrapment Efficiency; DL: Drug Loading

5.10.4 In vitro release study of HPPH and OLA co-loaded LPHNs

The release profile of the free drug and the two LPHNs was performed using dialysis bag method. It has been revealed that both types of nanoparticles showed a biphasic release profile as shown in Figure 5.45. This shows that the nanoparticle exhibited a burst release pattern followed by a controlled release pattern.



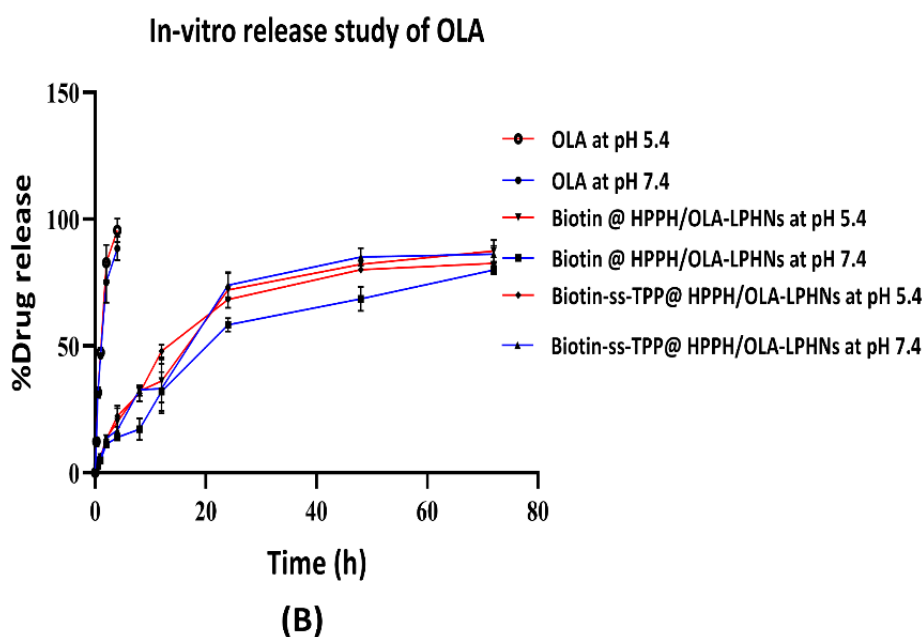


Figure 5.45: In vitro release HPPH and OLA co-loaded LPHNs at pH 7.4 and pH 5.4

5.10.5 Singlet Oxygen Sensor Green (SOSG) measurement of LPHNs

The detection of singlet oxygen for nanoparticle was performed using SOSG fluorescence probe. The different entities such as HPPH, OLA, Biotin@HPPH/OLA LPHNs and Biotin-TPP@HPPH/OLA LPHNs were subjected the SOSG analysis at the concentration of $1\mu\text{g/mL}$ concentration of HPPH and OLA. The sample's singlet oxygen level was evaluated by the SOSG fluorescence enhancement compared with the background or control samples. The results, as seen in Figure 5.46, suggested that Biotin-ss-TPP@HPPH/OLA LPHNs and free HPPH showed a greater fluorescence intensity compared to above mentioned entities.

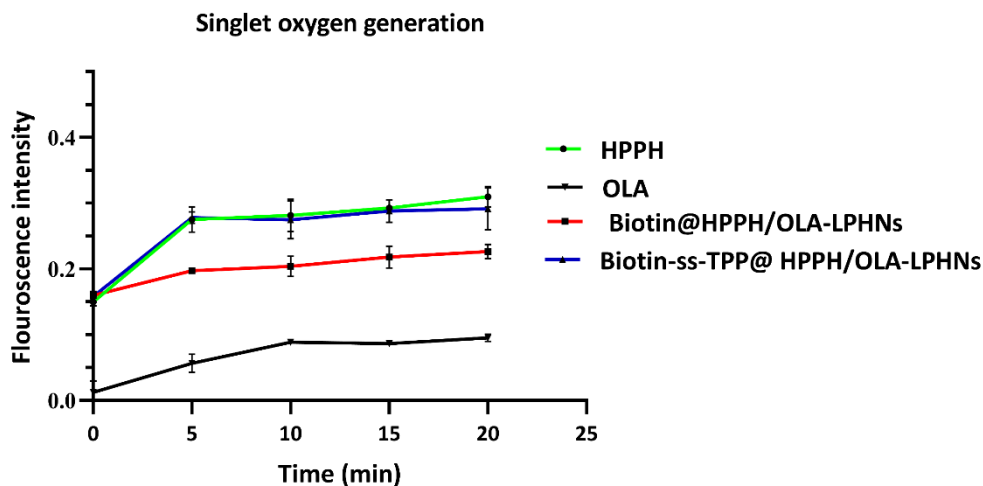
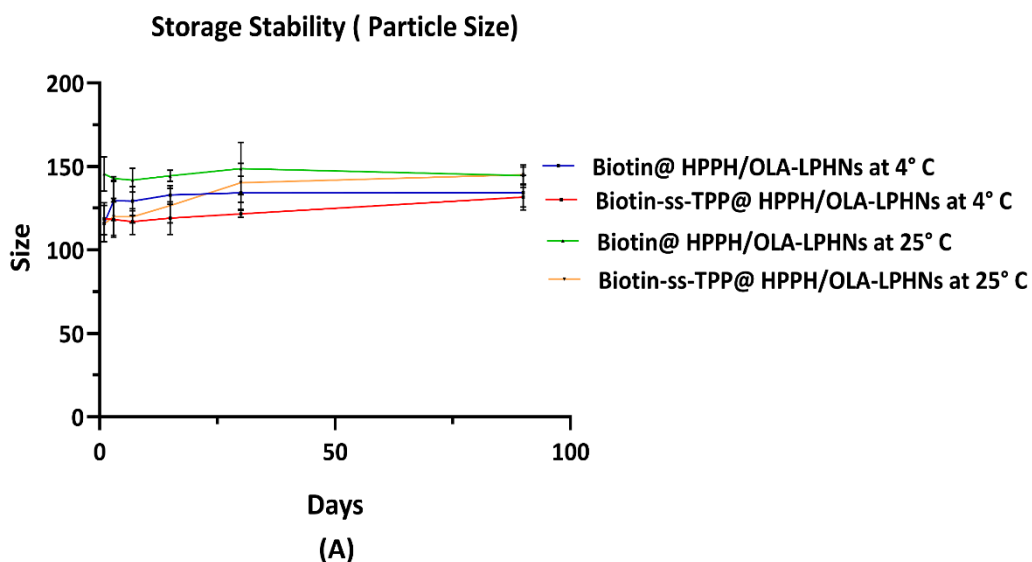


Figure 5.46: In vitro SOSG measurement of HPPH and OLA co-loaded LPHNs

5.10.6 Storage stability study of HPPH and OLA co-loaded LPHNs

In order to understand the physical storage of LPHNs, the lyophilized sample was subjected to colloidal stability study at two different condition (4 and 25) for 90 days. The data showed no significant change in mean particle size and PDI. The value was found to be in the range of 150 nm for size and 0.300 for PDI respectively (Figure 5.47).



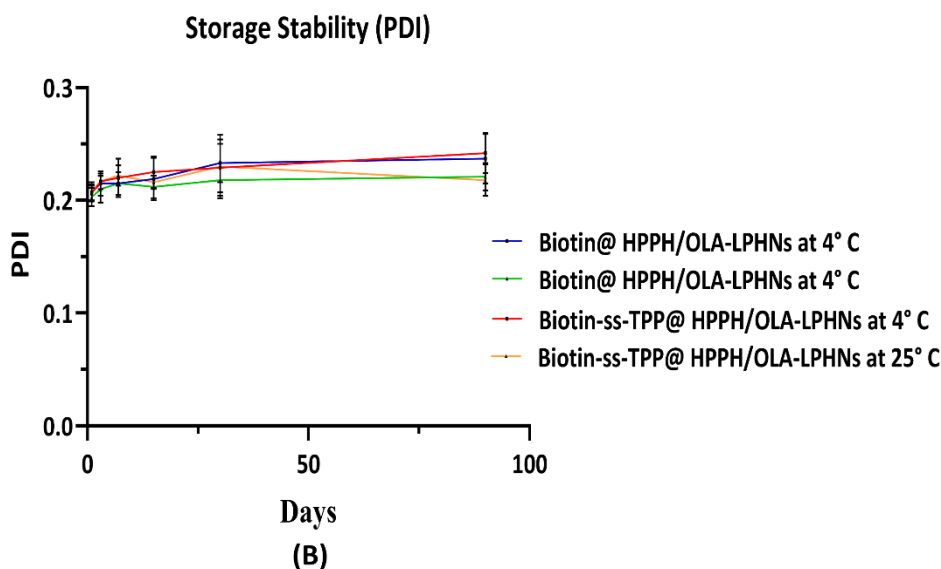


Figure 5.47: Storage stability study of HPPH and OLA co-loaded LPHNs

5.10.7 *Invitro Cell Culture Study of HPPH-OLA (Free drug) and its co-loaded LPHNs*

5.10.7.1 *Evaluation of HPPH and OLA synergy and cytotoxicity study*

The synergistic effect of combining HPPH and OLA was studied in 4T1 cell line. The combination of these two drugs showed a greater cytotoxicity against either single drug alone. The combination index of HPPH and OLA is less than 0.9 which indicated a strong synergy between HPPH and OLA in 4T1 cell line at the molar ratio of 1:6. Further, it was found that Biotin-ss-TPP@HPPH-OLA-LPHNS showed an improved cytotoxicity compared to Biotin@HPPH-OLA-LPHNS and the free drugs. Figure 5.48 shows the results of a dose-response effect and cytotoxicity study where (A) shows cytotoxicity of HPPH and OLA; (B) shows Combination index for HPPH and OLA solution; (C) shows Combination index for Biotin@HPPH/OLA LPHNS; and (D) shows Combination index for Biotin-ss-TPP@HPPH/OLA LPHNS. The cell viability of Biotin-ss-TPP@HPPH-OLA-LPHNS was found to be 14.47%, wherein Biotin @HPPH-OLA-LPHNS and free HPPH and OLA showed 28.80% and 46.27% cell viability at the HPPH/OLA combination of 4 μ M /24 μ M respectively as shown in figure 5.48. Furthermore, Blank LPHNs did not show any significant change in the cell viability.

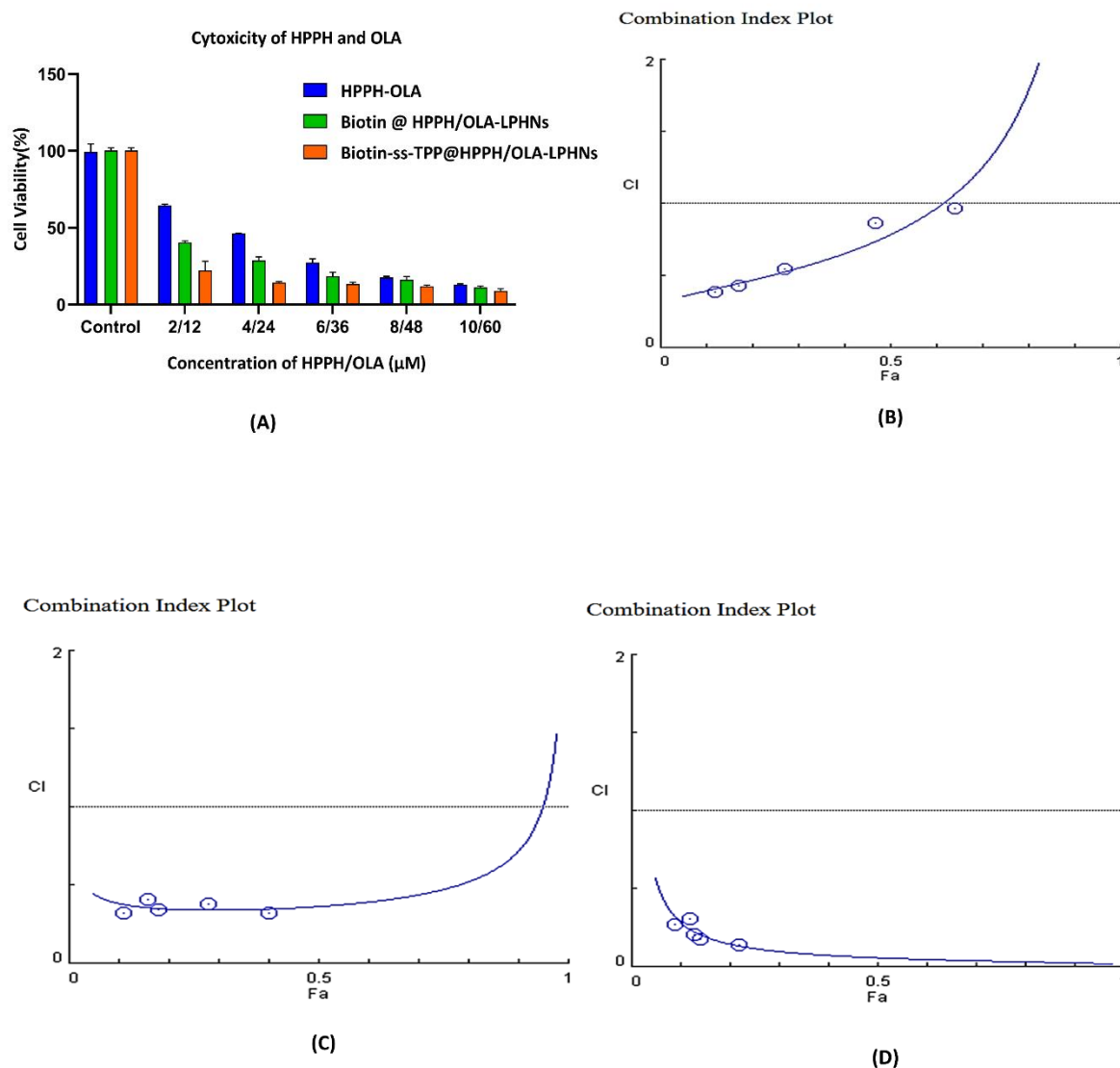


Figure 5.48: Dose-response effect and cytotoxicity study of HPPH and OLA co-loaded LPHNs;(A) cytotoxicity of HPPH and OLA (B)Combination index for HPPH and OLA solution (C) Combination index for Biotin@HPPH/OLA-LPHNs(D) Combination index for Biotin-ss-TPP@ HPPH/OLA-LPHNs

5.10.7.2 Cellular and mitochondrial uptake analysis

The uptake of LPHNs was studied using a hydrophobic dye i.e., coumarin-6 which is commonly employed for uptake studies of nanoparticles. Further, mitochondrial penetration of nanocarrier was also studied using Mito-Traker (Invitrogen). Remarkably, it was found that the intensity of fluorescence of the Biotin-ss-TPP@HPPH/OLA LPHNs were stronger than Biotin@HPPH-OLA LPHNs as shown in Figure 5.49. Likewise, Mito tracker fluorescence intensity was higher in Biotin-ss-TPP@HPPH/OLA LPHNs and this observation indicates

greater mitochondrial transfection of targeted formulation i.e., Biotin-ss-TPP@HPPH-OLA-LPHNs compared to Biotin@HPPH/OLA-LPHNs.

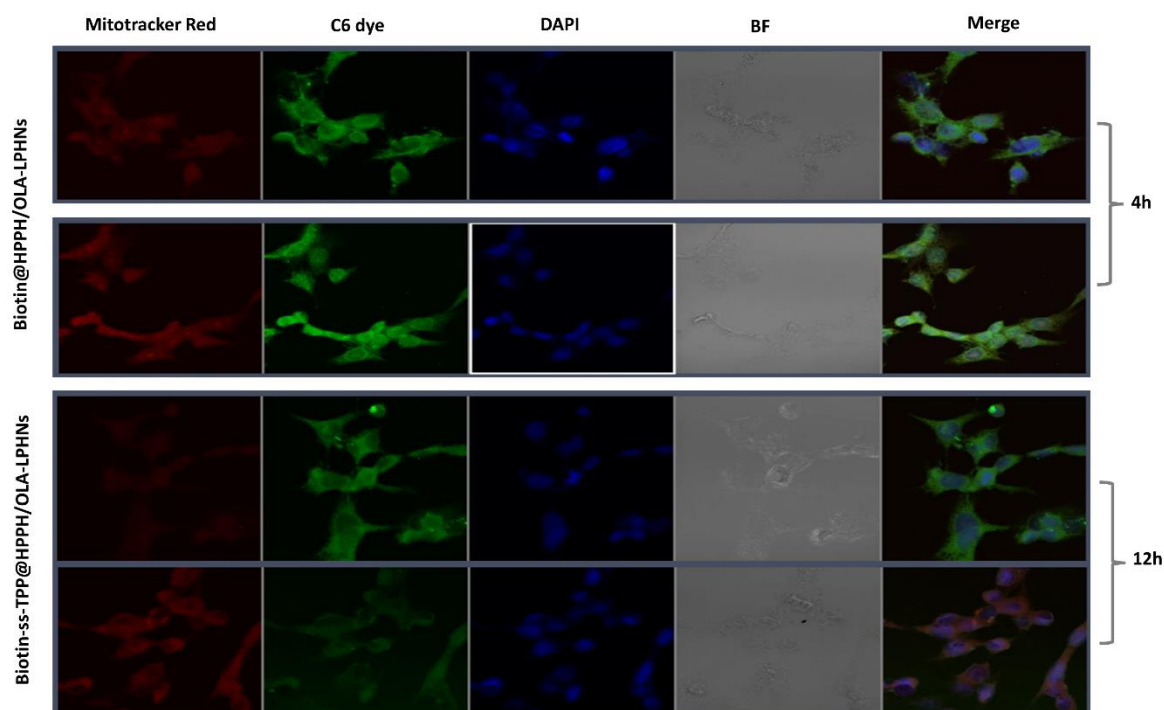


Figure 5.49: In vitro cellular and mitochondrial uptake analysis of HPPH and OLA co-loaded LPHNs (HPPH, OLA, HPPH-OLA, Biotin@HPPH/OLA-LPHNs and Biotin-ss-TPP@HPPH/OLA-LPHNs)

5.10.7.3. Apoptosis Analysis

Apoptosis assay was performed in 4T1 cell line using flow cytometry. The cell line was treated with combination of pure HPPH and OLA and their nano formulation at the IC_{50} dose. The pure solution of HPPH and OLA showed that the apoptotic cells were 16.15%. while cells treated with Biotin@HPPH/OLA-LPHNs and Biotin-ss-TPP@HPPH/OLA-LPHNs unveiled to be 19% and 37.74% respectively at 48 hr. (Figure 5.50) which indicates Biotin-ss-TPP@HPPH/OLA-LPHNs has greater apoptosis response as compared to another group.

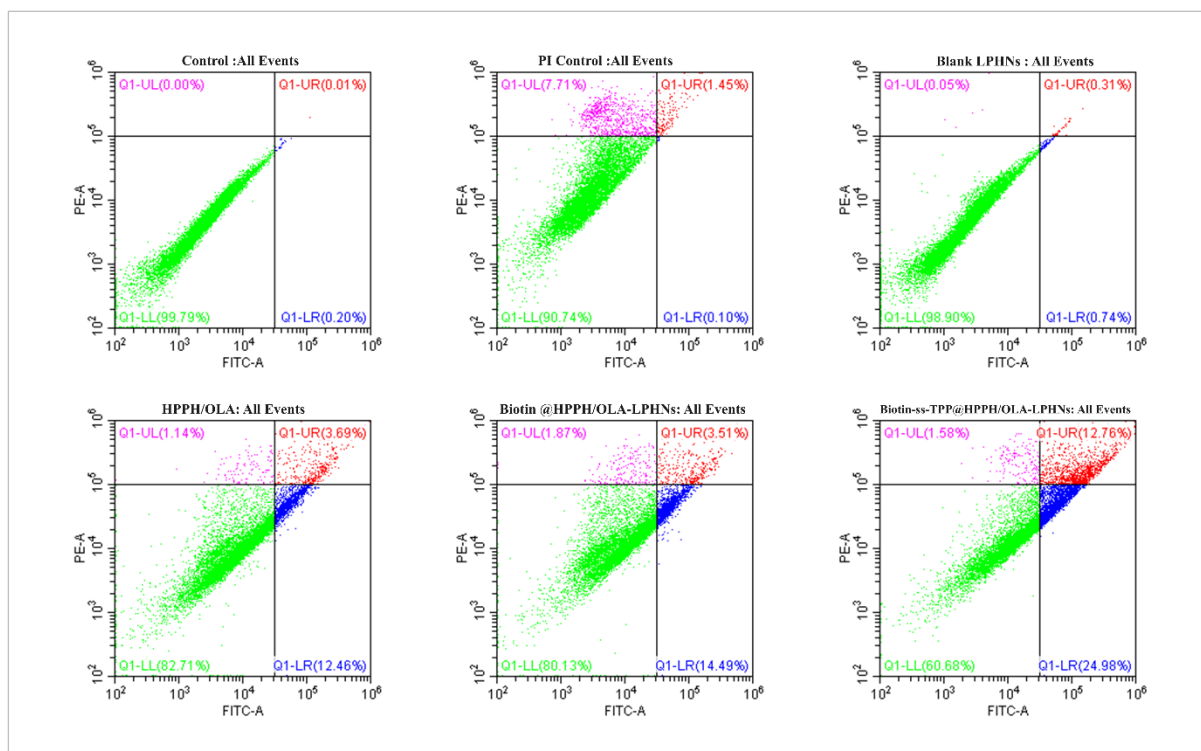


Figure 5.50: Apoptosis Analysis of HPPH and OLA co-loaded LPHNs Apoptosis Analysis of HPPH and OLA co-loaded LPHNs (HPPH-OLA, Biotin@HPPH/OLA-LPHNs and Biotin-ss-TPP@HPPH/OLA-LPHNs)

5.10.7.4 Measurement of ROS generation

The intracellular ROS generation was studied using a fluorescence probe, 2',7'-dichlorofluorescein diacetate (DCFH-DA). After the cells were treated with pure HPPH-OLA, Biotin@HPPH/OLA-LPHNs and Biotin-ss-TPP@HPPH/OLA-LPHNs at the dose of IC₅₀, all the groups were subjected to light irradiation with 650 nm at a light density of 200 mW cm⁻² for 15min. Then, it was incubated for 24 hr. As shown in Figure 5.51, the intracellular ROS level of Biotin-ss-TPP@HPPH/OLA-LPHNs was higher than that of pure HPPH-OLA, Biotin@HPPH/OLA-LPHNs as it showed higher color intensity of DCFH-DA.

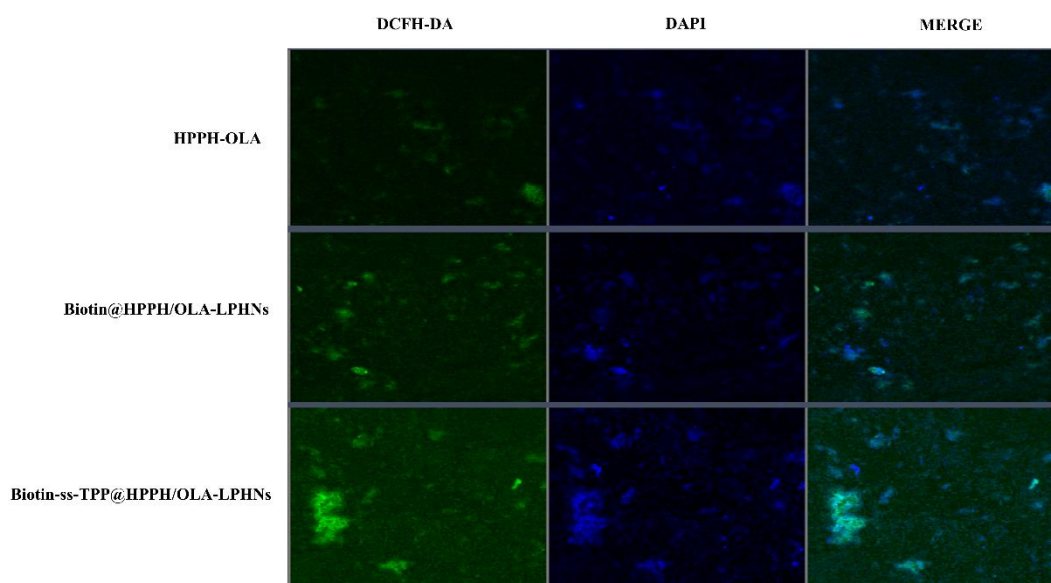


Figure 5.51: In-vitro ROS study of HPPH and OLA co-loaded LPHNs (HPPH-OLA, Biotin@HPPH/OLA-LPHNs and Biotin-ss-TPP@HPPH/OLA-LPHNs)

5.10.8 Hemolysis study of HPPH-OLA (free) and its co-loaded LPHNs

Hemolysis of nanoparticle was performed using RBCs of mice. All the group i.e., pure HPPH-OLA and LPHNs (Biotin@HPPH/OLA-LPHNs and Biotin-ss-TPP@HPPH/OLA-LPHNs) exhibited hemolytic index below 2.0% as depicted in Figure 5.52.

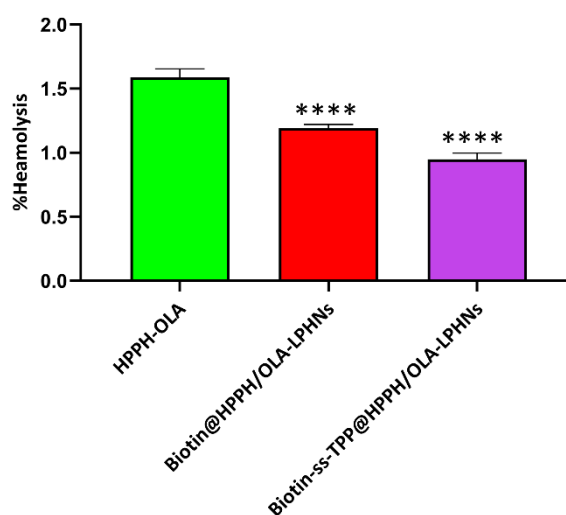


Figure 5.52: Hemolysis study of HPPH and OLA co-loaded LPHNs; Data represent mean \pm SD. ** p value < 0.0001 and *** p value < 0.001 compared with the control group**

5.10.9 In-vivo Pharmacokinetic study of HPPH-OLA(Free) and its co-loaded LPHNs

The pharmacokinetic studies for combination of HPPH and OLA were performed in Balb/C mice at the dose of 5 mg/kg.bw and 30mg/kg.bw for HPPH and OLA respectively through i.v. route. The LC-MS/MS based analysis was done for pharmacokinetic sample to determine the plasma concentration and a graph between plasma concentration versus time profile was plotted as depicted in Fig.5.53.

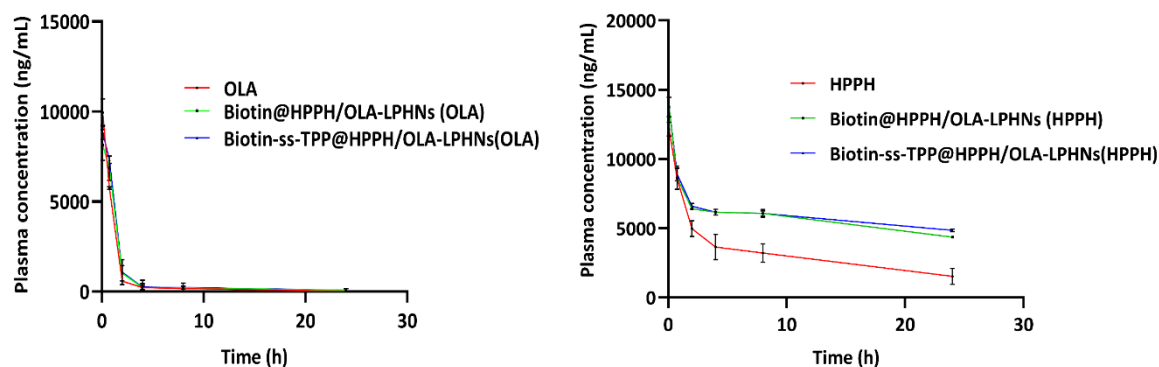


Figure 5.53: In vivo pharmacokinetic study of HPPH and OLA co-loaded LPHNs (HPPH-OLA, Biotin@HPPH/OLA-LPHNs and Biotin-ss-TPP@HPPH/OLA-LPHNs)

The AUC of pure OLA, Biotin@HPPH/OLA-LPHNs (OLA) and Biotin-ss-TPP@HPPH/OLA-LPHNs (OLA) were 5698.76 ± 213.20 h*ng/mL, 12334.88 ± 3776.79 h*ng/mL and 14788.79 ± 2094.51 h*ng/mL respectively. It was observed that both Biotin@HPPH/OLA-LPHNs and Biotin-ss-TPP@HPPH/OLA-LPHNs exhibited similar type of AUC value respectively which was 2-fold time higher than pure OLA when compared to in physical mixture solution of HPPH and OLA. Further, both LPHNs for OLA showed approx.2-fold times better $t_{1/2}$ profile compared to pure physical mixture (HPPH-OLA) indicating longer circulation time in biological system. The clearance (Cl) of LPHNs indicates ~6 fold-time decrease to pure drug solution. In the same way, at the dose 5mg/kg.bw of HPPH, the AUC of pure HPPH, Biotin@HPPH/OLA-LPHNs (HPPH) and Biotin-ss-TPP@HPPH/OLA-LPHNs (HPPH) were 72575.11 ± 9169.30 h*ng/mL, 111783.4 ± 10168.83 h*ng/mL and 116194.31 ± 22449.12 h*ng/mL respectively. All other pharmacokinetic parameter is shown in the table 5.38.

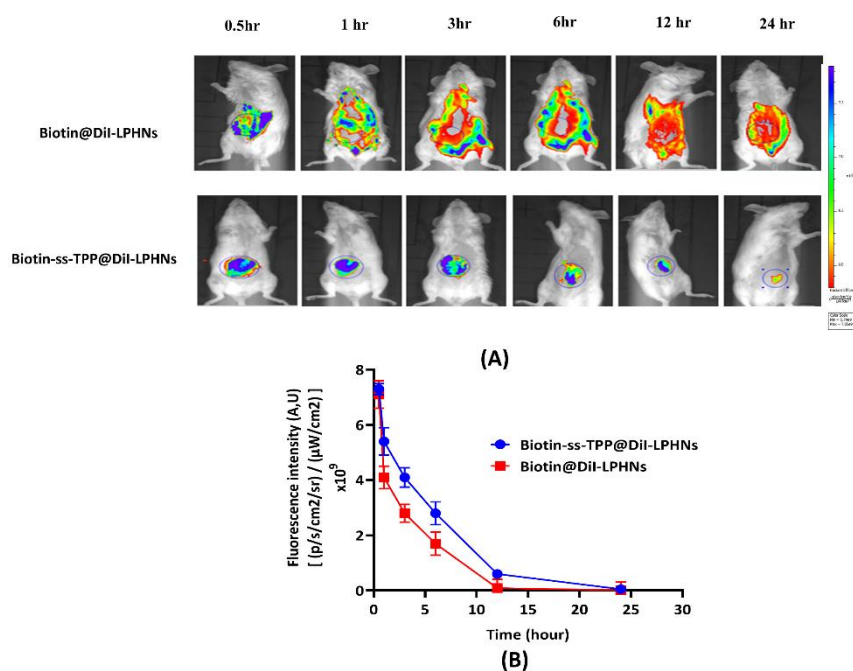
Table 5.38: In vivo pharmacokinetics studies of HPPH and OLA co-loaded LPHNs (HPPH-OLA, Biotin@HPPH/OLA-LPHNs and Biotin-ss-TPP@HPPH/OLA-LPHNs)

Parameters	Unit	HPPH			OLA		
		Free HPPH	Non-Targeted	Targeted	Free OLA	Targeted	Non-Targeted
C ₀	ng/mL	13858.28±2179.87	13340.76±296.98	13411.97±678.91	8806.09±323.51	9574.10±295.20	9735.30±703.69
T _{max}	h	0.08±0.00	0.08±0.00	0.08±0.00	0.08±0	0.08±0.00	0.08±0.00
AUC _{last}	h*ng/mL	72575.11±9169.30	111783.4±10168.83	116194.31±22449.12	5698.76±213.20	14788.79±2094.51	12334.88±3776.79
CL _{obs}	mL/kg	47.79±2.61	23.15±0.847	20.04±5.462	4847.79±133.72	645.44±173.71	743.36±1051.27
K _e	1/h	0.05±0.01	0.026±0.00	0.021±0.0012	0.12±0.00	0.043±0.003	0.044±0.00
T _{1/2}	h	15.15±2.76	26.36±4.129	32.53±1.915	5.34±0.04	15.87±1.42	15.41±0.12

Non-targeted: Biotin@HPPH/OLA-LPHNs; Targeted: Biotin-ss-TPP@HPPH/OLA-LPHNs

5.10.10 In-vivo imaging and biodistribution study of HPPH and OLA co-loaded LPHNs

The developed dye loaded LPHNs (Biotin@DiI-LPHNs and Biotin-ss-TPP@DiI-LPHNs) were subjected to both in-vivo and ex-vivo fluorescence imaging study in tumor bearing Balb/c mice. The significant tumor accumulation was shown with Biotin-ss-TPP@DiI-LPHNs for a longer period of time against Biotin@DiI-LPHNs as shown in the Figure 5.54. It was observed that Biotin-ss-TPP@DiI-LPHNs showed 1.8-fold times higher accumulation in tumour site. Further, treated mice were sacrificed and their vital organs were collected and imaged. The images revealed that mice treated with Biotin-ss-TPP@DiI-LPHNs have very high tumoral accumulation than Biotin@DiI-LPHNs. Further, accumulation of Biotin-ss-TPP@DiI-LPHNs was observed lesser in vital organs like spleen, and kidneys compared to Biotin@DiI-LPHNs as shown by low fluorescence intensity.



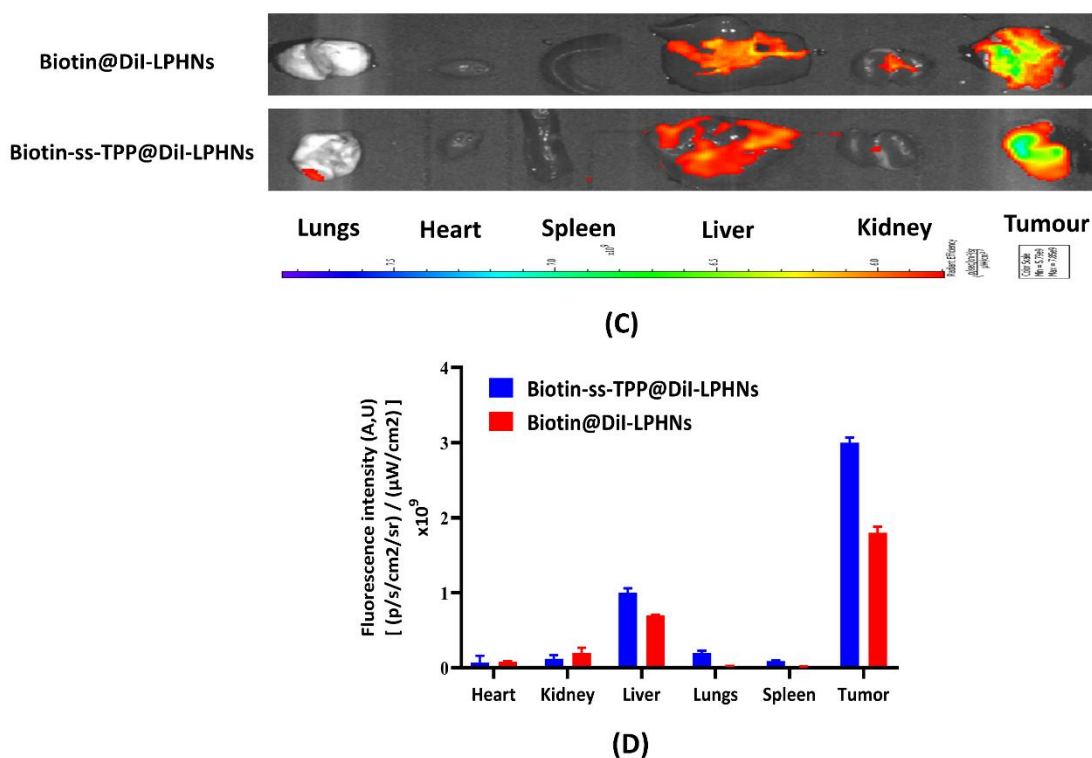
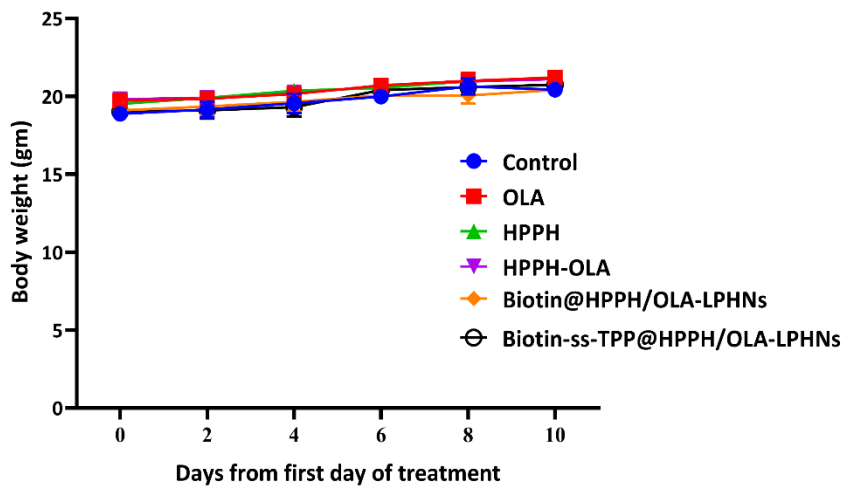


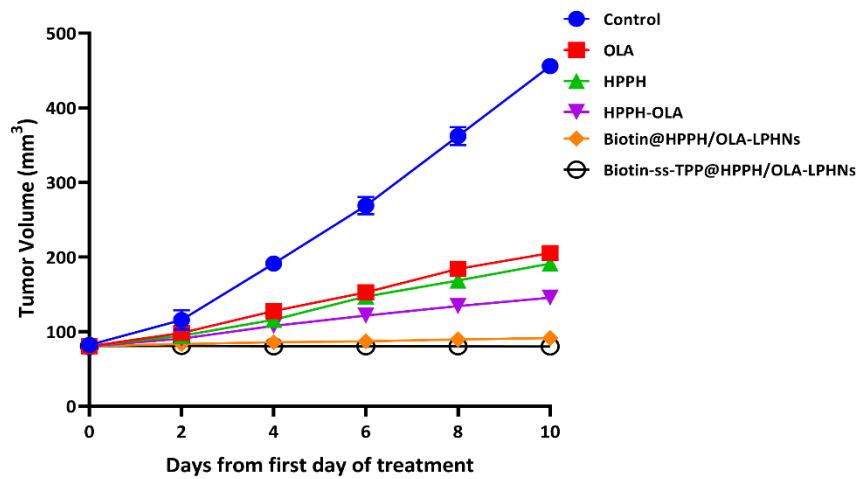
Figure 5.54: Biodistribution study of HPPH and OLA co-loaded LPHNs; (A) Time-dependent fluorescence images of tumor-bearing BALB/c mice after i.v. administration; (B) Graph representing the fluorescence intensity for the region of interest; (C) Ex vivo fluorescence images of major organs and tumor excised at 24 h post-injection; (D) Mean fluorescent intensity of fluorescence probe tagged formulations in tumors and organs.

5.10.11 In vivo efficacy study of HPPH and OLA co-loaded LPHNs

The in vivo efficacy was assessed in Luciferin tagged 4T1 tumor bearing animal using an in vivo imaging technique with the IVIS® Lumina III, PerkinElmer, USA. On days 3, 6, and 10 of the treatment periods, all the animals in each group i.e., HPPH, OLA, Physical mixture of HPPH and OLA(HPPH/OLA), Biotin@HPPH/OLA-LPHNs and Biotin-ss-TPP@HPPH/OLA-LPHNs, were examined for tumor growth, and images were shown in Figure 5.55 and Figure 5.56 corresponding to body weight, tumor volume, tunnel positive cell, luminescence and in vivo efficacy from Day 0 to Day 10. The body weight was checked at every alternative day and no significant changes were found. The Biotin-ss-TPP@HPPH/OLA-LPHNs depicted greater tumor inhibition potential (Figure 5.55 (B)) when compared to other treated grouped. The animal treated with Biotin-ss-TPP@HPPH/OLA-LPHNs and Biotin@HPPH/OLA-LPHNs showed diminished tumour growth, while other groups showed the tumor growth until the end of the study (Figure 5.56).



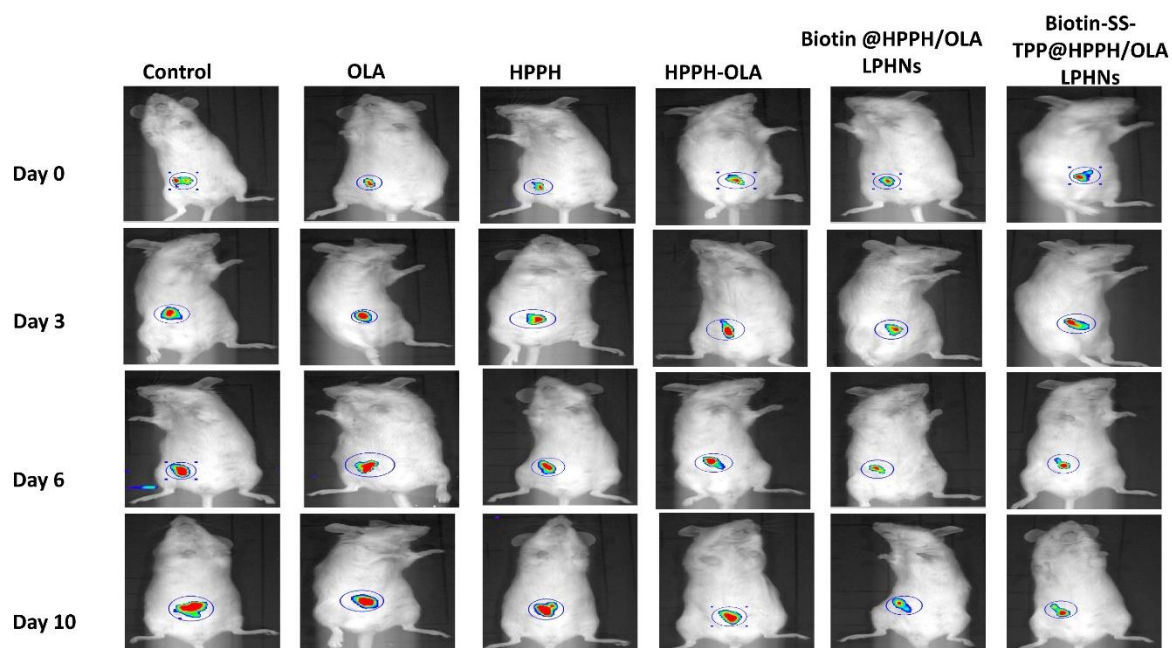
(A)



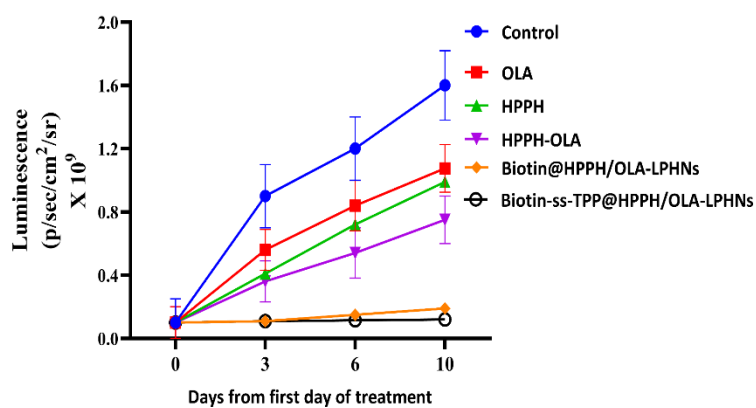
(B)

Figure 5.55: In-vivo efficacy study of HPPH and OLA co-loaded LPHNs

On the 10th day, all the animal were sacrificed. The vital organs of all the group are collected and subjected to sectioning for further analysis i.e., H&E analysis, ROS and Tunnel assay.



(A)



(B)

Figure 5.56: Luminescence intensity of HPPH, OLA, HPPH-OLA, Biotin@HPPH/OLA-LPHNs and Biotin-ss-TPP@HPPH/OLA-LPHNs

Further, in-vivo ROS was also studied using DCFH-DA fluorescence probe. As shown in Figure 5.57, It was found that Biotin-ss-TPP@HPPH-OLA-LPHNs nanoparticle showed greater intensity when compared to the other groups. This could be due to the penetration of nanoparticles into the mitochondria of tumour site.

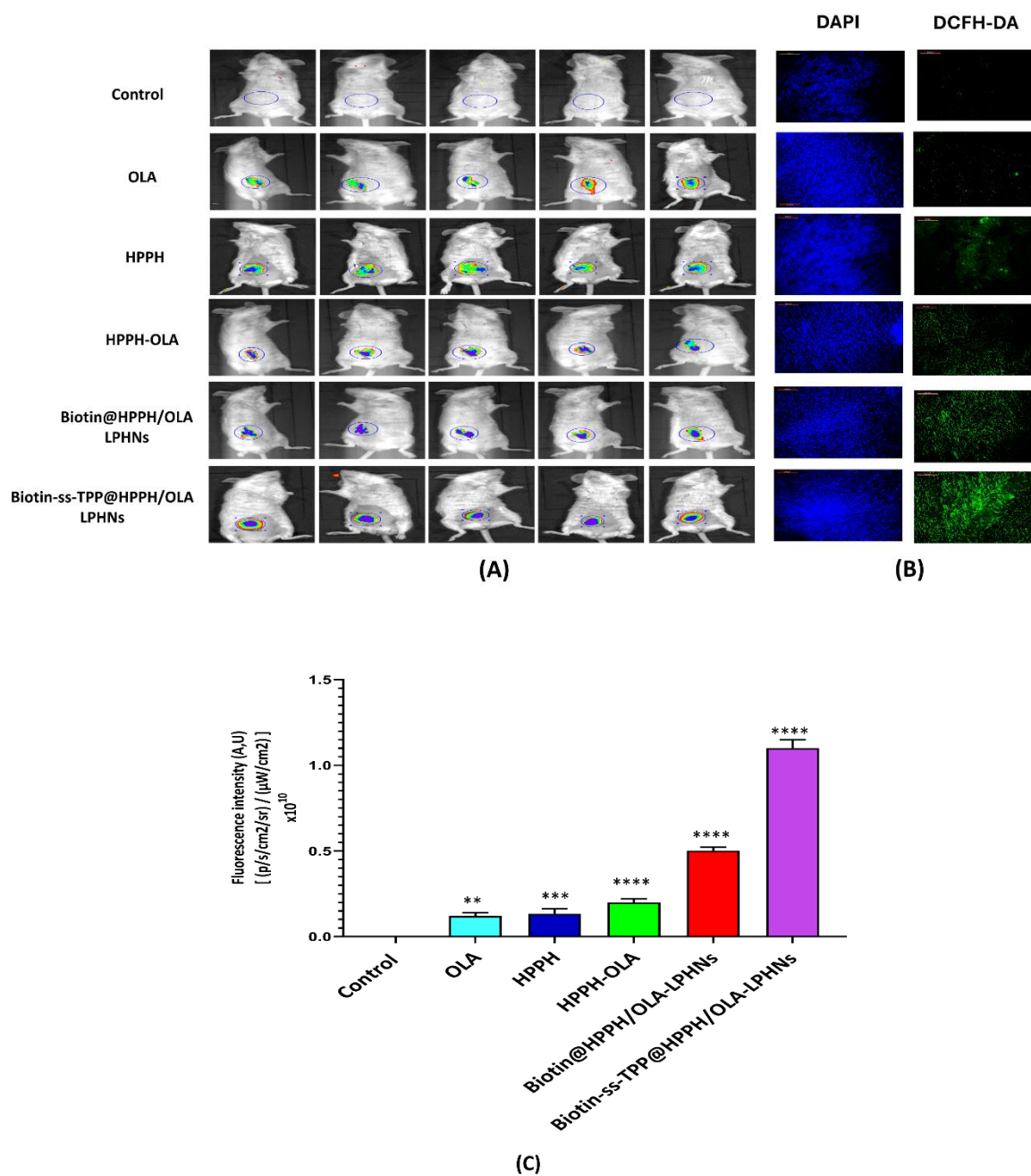
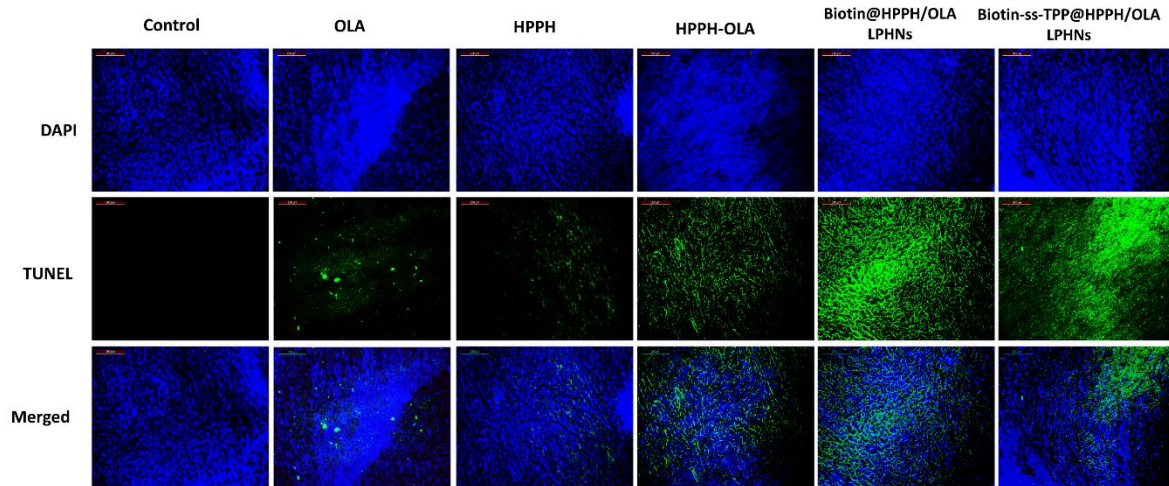
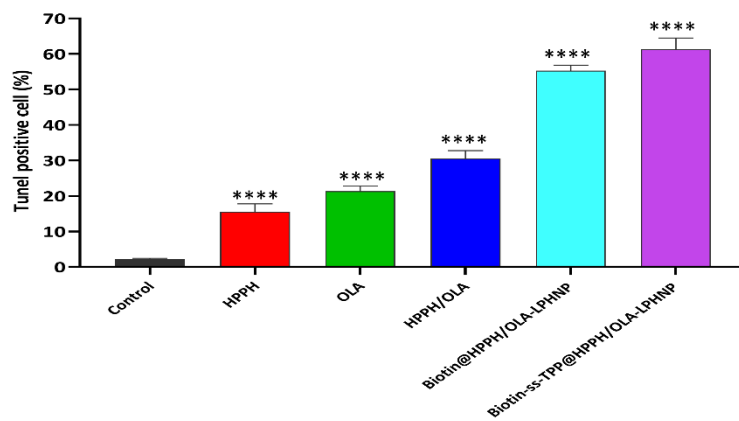


Figure 5.57: In vivo ROS of HPPH and OLA co-loaded LPHNs; Data represent mean \pm SD. ** p value < 0.0001 and *** p value < 0.001 compared with the control group and ** p value < 0.05 compared with the control group**

Further, tumor and organ tissue sections were used for immunohistochemical analysis and tunnel assay. The tunnel assay as shown in Figure 5.58 suggested higher apoptotic response of Biotin-ss-TPP@HPPH/OLA-LPH nanoparticle as compared to other treated group which could possibly be contributing to its effectiveness against cancer cells.



(A)



(B)

Figure 5.58: Tunnell assay of HPPH and OLA co-loaded LPHNs; Data represent mean \pm SD. ** p value < 0.0001 compared with the control group**

Also, histochemical analysis, as shown in Figure 5.59, performed for all the groups/entities using hematoxylin and eosin (H&E) dye, revealed no significant toxicity due to nanocarrier in vital organs of all the animal.

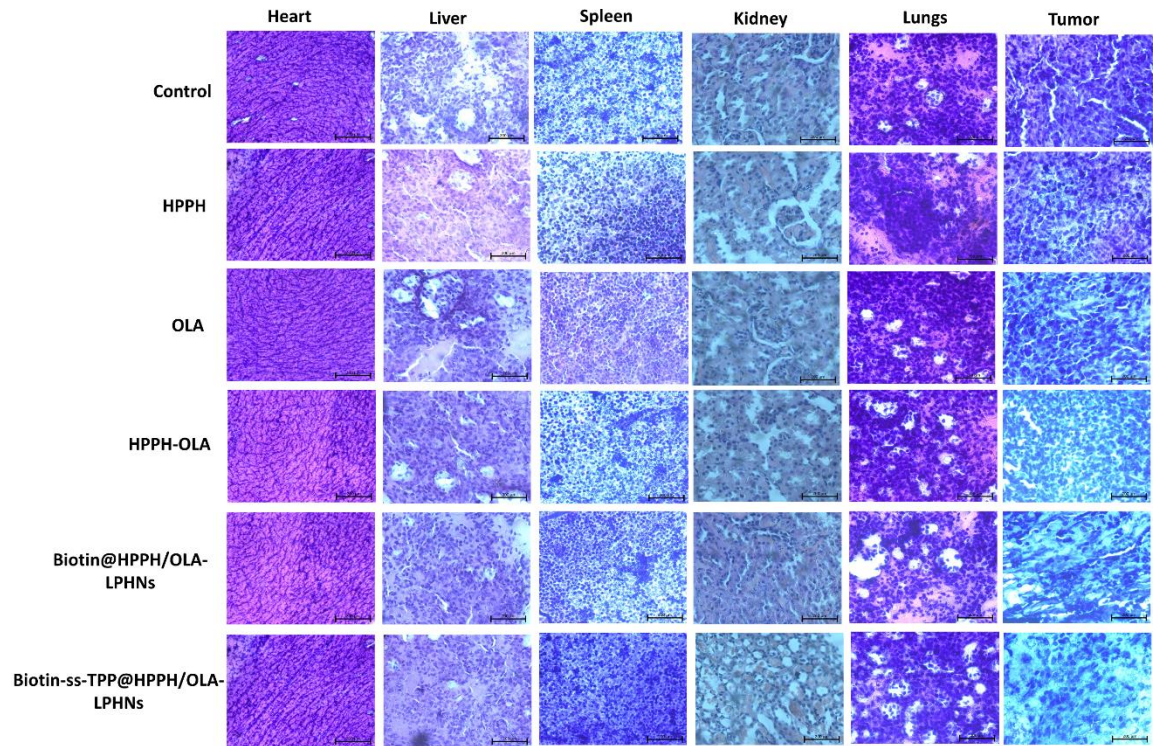


Figure 5.59: Histochemical analysis of HPPH and OLA co-loaded LPHNs (HPPH, OLA, HPPH-OLA, Biotin@HPPH/OLA-LPHNs and Biotin-ss-TPP@HPPH/OLA-LPHNs) using HE staining



DISCUSSION



6. Discussion

TNBC is considered as a highly aggressive sub-type of breast cancer. Due to the lack of surface receptors such as ER, PR and HER2 protein, till date, the management of this disease is under clinical investigation [248]. Scientists' interest in creating novel targets and therapeutic approaches for the treatment of TNBC has increased recently since the efficacy of traditional medication has been hampered by drug resistance, poor targeting, and poor prognosis as well. [6,7]. Xie et. al., and Maksimenko et. al., reported that a mutation in BRCA gene eventually leads to TNBC due to a deficiency in homologous recombination (HR)-mediated DNA double-strand breaks (DSBs) repair [249,250]. Besides, the PARP enzyme over activity is also associated with TNBC progression, as reported by Ossovskaya et. al.,[251] and Rose et. al.[252]. Thus, inhibition of PARP enzyme can lead to accumulation of single-strand breaks, which progresses to double-strand breaks on DNA replication and subsequently on accumulation can lead to genomic instability and tumor cell death. In addition to PARP inhibition, PDT is one of the novel strategy which also showed a promising effectiveness against various solid tumor including breast cancer that can eradicate the tumor cell via ROS induced apoptosis cell death pathway as reported by Kong et al.,[253]. As PARP inhibitors lead to accumulation of unrepaired DSBs, combining this with DNA damage induce by PDT could lead to synergistic effect and might have a synergistic impact that overwhelms the ability of the cancer cell to repair and live. This strategy becomes more important in TNBC because of the frequent presence of defects in DNA repair mechanisms. Furthermore, using PDT in conjunction with PARP inhibitors may provide a way to overcome resistance to either monotherapy.

Therefore, in this research work, we have used HPPH as Photosensitizer for PDT therapy to eradicate the tumor cell via ROS mediated pathway along with OLA, a selective PARP inhibitor which regulate the activity of PARP enzyme against the management of TNBC. We have also evaluated the possibility of therapeutic synergistic effect or additive effect of these two drugs in combination for TNBC treatment as PARPi (OLA) works to resolve the problem associated with PDT resistance. In spite of the advantage of HPPH and OLA, these two molecules have serious limitations including low solubility, poor pharmacokinetics, limited cellular uptake into the target cells, and clinical side effects including DNA damage to the normal cell. Hence, to overcome the pharmacokinetic and pharmacodynamic issues along with adverse events associated with these different therapeutic approaches i.e., PDT and PARPi; a

tumor targeted nanocarrier system development will be a possible approach to enhance its efficacy and minimize its toxic effects., we have developed a lipid-polymer hybrid system which have been surface factionalized with biotin to impart better efficacy via increasing the site-specific accumulation of HPPH and OLA. Additionally, we have also developed HPPH and OLA co-loaded LPHNs which is decorated with 2-different class of chemical ligand (i.e., ROS inducing mitochondrial targeting ligand and Biotin receptor targeting) as multifunctional tumor targeted nanocarrier to improve the therapeutic efficacy along with minimizing toxicity if any exists in comparison with the pure drug in TNBC.

6.1. Analytical and bioanalytical Method development and Validation of HPPH and OLA

6.1.1. Analytical Method development and validation for HPPH and OLA

The LC-MS/MS and RP-HPLC based analytical method were developed and validated for both HPPH and OLA. The calibration curve showed goodness of fit over the concentration range from 50-2000 ng/mL for HPPH and OLA. The run time of the RP-HPLC based validated method for both HPPH and OLA was 8 min which allows the method to be applied for analysis of large number of samples within minimal time and resource utilization. On the other hand, LC-MS/MS based simultaneous analytical method was found linear over concentration range of 1 to 200 ng/mL with the R² value 0.998 and 0.993 for HPPH and OLA respectively. The validation parameter such as selectivity, precision, accuracy robustness and stability met the acceptance criteria as per the regulatory guidelines. All the validated method was selected to analyze the molecule without any excipient interference in the formulation and effectively be utilized for other applications including for analysis of drug entrapment efficiency, drug loading and drug release in nanocarriers based drug delivery system. Furthermore, developed LC-MS/MS based method was also utilized for bioanalysis of HPPH and OLA.

6.1.2. Bioanalytical method development and validation for HPPH and OLA

In the same way, simultaneous bioanalysis method for HPPH and OLA was developed and validated in pooled mice plasma using LC-MS/MS. The method was developed using acetonitrile-methanol-0.1% formic acid containing 5mM ammonium acetate with ratio of 87:10:3 %v/v at flow rate of 0.35mL/min in isocratic mode as it provides symmetric peak shape and good intensity with a shorter run time of 6 min. Moreover, to achieve better recovery of drug from plasma, various sample extraction trial such as PPE, LLE and SPE were employed for HPPH and OLA. LLE with diethyl ether was selected for sample processing as it showed better recovery, symmetric peak, and no interference of biomatrix (matrix effect). The developed method displayed high sensitivity and reliability over a linearity range of 1-

320ng/mL Furthermore, stability study result met acceptance limit as per the ICH M10 guidelines which indicates method was highly suitable for long term routine analysis. Therefore, this validated method could be utilized for in vivo pharmacokinetic study of HPPH and OLA (alone) and combination of HPPH and OLA in Balb/c mice.

6.2. In-vitro and in-vivo efficacy of HPPH and OLA

In the current in vitro study, we found both HPPH and OLA exhibited antitumor activity against 4T1 cell line with IC_{50} value of ~ 10 and $\sim 60 \mu M$ respectively. In addition, their combination (HPPH-OLA) presented the potent synergistic effect on viabilities with CI value of 0.9, 0.86, 0.54, 0.43 and 0.38 at $IC_{10}(2/12 \mu M)$, $IC_{20}(4/24 \mu M)$, $IC_{30}(6/36 \mu M)$, $IC_{40}(6/48 \mu M)$ and $IC_{50}(10/60 \mu M)$ respectively which was shown in figure 5.9. Moreover, the HPPH-OLA exhibited 46.27% of cell viability at the combination dose of $4 \mu M/24 \mu M$.

On the basis of promising in-vitro results, we have explored the anti-tumor therapeutic potential of HPPH and OLA (alone) and its combination (HPPH-OLA) on 4T1 bearing tumor animal model. There are numerous animal models of TNBC developed by injecting MD-MB-231, MDA-MB-468 and 4T1 cell lines. However, to reproduce a pathological and genetically similar TNBC model to humans, 4T1 bearing animal model was chosen as this is an ideal metastasis model with the advantage of being able to be transplanted into immune competent recipients as reported by Kaur et al. [254]. Therefore, we have developed a syngeneic mice model of TNBC using orthotopically injection of 2×10^6 4T1-luc cell lines on Balb/c mice. After treatment with HPPH and OLA, an increased in survival rate of animal was observed when compared with disease group. Furthermore, the tumor volume and body weight of all the treated animal were examined on every alternative day. It was observed that there were no significant changes in body weight, as shown in Figure 5.10. Furthermore, all the treated animals were sacrificed on the 10th day for H&E analysis, ROS analysis and Tunnel assay. H&E analysis revealed that vital organs (heart, liver, spleen, lung, kidney) of the treated animal mice showed no severe histological damage (Fig 5.14). As shown in the figure 5.10, OLA treated group showed rapid tumor growth as compared to other treatment group. Similar to our study, Hu et al. also found that OLA showed less anti-tumor effects when used alone and demonstrated that this was observed due to less significant cytotoxicity and inability to generate a strong immune response via ROS pathway [255]. However, HPPH treated group produced ROS to damage tumor cells but it was not a significant response as accumulation of HPPH in tumor cell was less. In addition to our findings, Ren-Jiang Kong et al. reported similar result with same class of photosensitizer (chlorin e6). This may be due to the repair mechanism

of tumor cells, the efficacy of PDT alone is limited[253]. After treatment with combination of HPPH with OLA, the tumor suppression rate was significantly increased when compared to the HPPH group. In addition to tumor suppression data, in-vivo ROS study and Tunnel assay showed that apoptosis was increased with combination of HPPH and OLA significantly as compared with disease control group and treatment with HPPH and OLA-alone. This observation stated that combination of HPPH and OLA offers a promising synergistic efficacy against TNBC by reducing DNA damage repair via downregulation of PARP enzyme action which could enhance the efficiency of PDT against the TNBC.

6.3.In-vivo pharmacokinetics study of free HPPH and OLA

The pharmacokinetic studies for HPPH and OLA and its combination (HPPH-OLA) were carried out in Balb/c mice and a plasma concentration versus time profile was plotted as represented in Fig.5.15. The result showed a shorter biological half-life of OLA i.e., 5.7 hr. and also indicates high rate of elimination, while half-life of HPPH was found to be 15hr. Furthermore, it was evident that OLA has a very less AUC as shown in Table.5.15. Thus, there is a need of improvement in pharmacokinetic profile for betterment of TNBC treatment. Moreover, the pharmacokinetic data of HPPH-OLA suggested the combination (HPPH and OLA) did not find any significant pharmacokinetic interaction after administration in animals which could be in the favor of development of combination delivery for the treatment of TNBC. Based on the in-vitro and in-vivo results, we further planned to circumvent the observed problems i.e., poor pharmacokinetic, poor pharmacodynamic and lack of tumor targeting specificity of HPPH and OLA using surface engineered targeted nano drug delivery systems that were developed and biologically evaluated.

6.4.Development and characterization of HPPH loaded LPHNs

HPPH is a second generation chlorin based photosensitizer which have limitations of poor aqueous solubility, poor stability, photo bleaching etc. A report by Yang et al. stated that surface decoration with biotin can improve the tumor targetability of a nanoparticle[256]. In addition to this, Taymouri et al. developed biotin decorated sunitinib NLC for the management of lung cancer. They found that biotin-NLC (targeted) showed efficient cytotoxicity as compared to sunitinib loaded NLC (non-targeted)[257]. Therefore, we used biotin for surface functionalization of LPHNs to reduce the limitations associated with HPPH by improving the site specific targetability capacity against TNBC.

For the fabrication of LPHNs, a single step emulsification method followed by evaporation was adopted. The preliminary trials of LPHNs showed no major changes with respect to

physiochemical parameter such as PS, PDI, ZP and %EE while using Biotin-PEG-PLGA, instead of polymer (PEG-PLGA). Therefore, amount of HPPH and Polymer (PEG-PLGA/Biotin-PEG-PLGA) were kept constant during the optimization of the formulation. On the other hand, PVA concentration and amount of phospholipid (DC₈₉PC) were screened for the LPHNs. The optimization was performed by CCD method using DOE software (version 7.3, USA). Furthermore, the obtained model was validated at 2 independent variable combination and further, %RSE was within the ± 5.00 which described the acceptability of the model.

The optimized LPHNs i.e., HPPH-LPHNs and Biotin@HPPH-LPHNs showed the particle size in a range of 150-157 nm. As shown in the table no. 5.26 & 5.28, the %EE was found to be in a range of 60-65% for LPHNs. It was observed that particle size of Biotin@HPPH-LPHNs was slightly higher than HPPH-LPHNs that was not statistically significant. Similar findings were also reported by Mehdizadeh et al., they demonstrated that it might be due to the presence of biotin in PEG-PLGA in surface of nanocarriers[239]. Further, it could not hamper the crucial properties of the nanocarrier as it is within the 200nm. This evidence can promote passive targeting of drug at tumour site via EPR effect [258]. The results also depicted that Biotin@HPPH-LPHNs has greater DL% capacity in comparison with HPPH-LPHNs (Table-5.26). Notably, the Biotin@HPPH-LPHNs showed $1.16\pm 0.3\text{mV}$ as surface charge which is higher in comparison to HPPH-LPHNs that may attribute enhanced stability and cellular uptake (Table 5.26). This result is in line with previous findings indicated by Hanurry et al and Mehdizadeh et al. They reported that the nanoparticle offers improved stability and cellular uptake due to enhancement of surface charge as it can deliver sufficient charge for electrostatic repulsion among nanoparticles and avoid the agglomeration of particles which promotes reduction in particle size and uniform narrow size distribution[239,259]. Thus, our Biotin@HPPH-LPHNs may eventually provide better stability and enhanced cellular uptake. The morphological evaluation of LPHNs was performed using SEM and TEM. The result displayed the spherical geometry with no significant aggregation of particle for both the LPHNs. To improve the storage stability, further a lyophilization screening was studied. Different cryoprotectant such as mannitol, trehalose, sucrose, and PEG 4000 at three concentrations i.e., 2.5, 5, and 10 %w/w was examined for both the LPHNs. After freeze drying, the powder LPHNs were redispersed in deionized water, and the physiochemical parameters viz. size, PDI, and surface charge, entrapment and %DL values were measured. The result suggested 10% PEG4000 offers suitable cryoprotection as these values remained

most unaffected when compared to fresh LPHNs. However, other cryoprotectant treated LPHNs sample showed increase in the size and PDI in comparison to fresh LPHNs (Table 5.26, 5.27, and 5.28). Thus, 10 % w/w PEG4000 was selected for the further evaluation.

The release behavior of HPPH encapsulated LPHNs (Biotin@HPPH-LPHNs and HPPH-LPHNs) depicted biphasic release pattern i.e., initially, it showed burst release for 4hr followed by sustained release till 72hr. The result are in line with previous research conducted by Salatin et al. According to them, initial burst release of drug from nanoparticle might be due to absorption of drug on the surface of the nanoparticles and followed by a sustain release resulting from the encapsulation of the drug in the core of the nanoparticles[260]. In addition, the release rate of HPPH from both LPHNs in pH7.4 was observed to be lower than pH5.4. Similar to our study, Zolnik et al. also found the same release pattern in their study and they demonstrated that PLGA degrades quickly in acidic pH when compared to physiological pH due to breakdown of PLGA by ester hydrolysis [261].

Furthermore, in order to understand the physical state behavior, DSC thermograph was used for the developed LPHNs and pure HPPH. The DSC thermogram of HPPH showed a melting peak at 205.63 °C while no melting point peak was observed in case of lyophilized LPHNs; therefore, the result suggested that HPPH is completely encapsulated in the nanocarrier system. Moreover, a storage stability of lyophilized LPHNs was also performed for 90 days. The results revealed no significant changes in physicochemical parameter and the drug content of stability sample did not show any degradation during storage condition i.e., the value of drug content is similar to the fresh LPHNs. So, developed LPHNs could be utilized for various pre-clinical and clinical evaluation. The SOSG study was also carried out for pure HPPH and its LPHNs to predict the ROS generation capacity. The result showed that the pure HPPH has higher fluorescence intensity compared to its LPHNs. Rong et al conducted a similar study and found that free drug showed more singlet oxygen(1O_2) generation capacity, which is one of the crucial properties to facilitate PDT activity, as compared to its nanoparticle. They suggested although free HPPH showed high 1O_2 but PDT activity also depends on intratumoral delivery and cellular uptake a [262]. Thus, the decrease in fluorescence intensity and 1O_2 generation in LPHNs could be remunerated. The in-vitro hemolysis study shows the safe nature of Biotin@HPPH-LPHNs on RBCs as they have low hemolytic index i.e., below 1.5 % over all the concentrations in comparison to the HPPH-LPHNs and pure HPPH (fig. 5.29). Similar to our study , Wang et al., reported that hemolytic activity below 2% does not produce any

significant side effect to RBCs[263]. This evidence indicates that our developed LPHNs could be biocompatible and safe for further use in animal model.

Furthermore, cytotoxicity results depicted that Biotin@HPPH-LPHNs showed a significant cellular death than HPPH-LPHNs and pure HPPH i.e., the value was approx. 1.2-fold times higher than from HPPH-LPHNs and 3-fold times higher than pure HPPH respectively. This extensive improvement in cytotoxicity effect can be explained because of the presence of biotin. Abolmaali et al. developed a biotin-PEG conjugated nanogels of carboxymethyl polyethyleneimine for active delivery of anticancer drug against TNBC. Their result showed increased therapeutic efficacy due to active targeting of biotin receptors overexpressed in triple negative 4 T1 breast tumors[264]. Therefore, the evidence suggests that presence of biotin shows improved cytotoxicity of HPPH in the cells treated with Biotin@HPPH-LPHNs. Further, internalization of Biotin@HPPH-LPHNs by 4T1 cells was higher in comparison to HPPH-LPHNs and pure HPPH as it shows the enhanced fluorescence intensity which confirmed the improved distribution of Biotin@HPPH-LPHNs in cytoplasm of cells. Consequently, Blank-LPHNs exhibited no cytotoxicity which indicate that the nanocarrier is safe to encapsulate the HPPH. The in-vitro ROS generation study suggested enhanced fluorescence intensity of Biotin@HPPH-LPHNs compared to HPPH-LPHNs and pure HPPH. However, singlet oxygen generation was found to be more in case of pure HPPH. But, the possible reason could be higher cellular uptake due to presence of PEG-Biotin, disulfide bond and linoleic acid in nanocarrier system promotes the production of ROS as a similar observation was demonstrated previously by Wang et al. and Hatanaka et al. respectively [265,266]. The apoptotic ratio of Biotin@HPPH-LPHNs was also found to be 13-folds greater compared to pure HPPH. This suggested that the Biotin@HPPH-LPHNs could remarkably enhance the antitumor effects of the nanoparticles. Thus, combining all the cell culture result, Biotin@HPPH-LPHNs could effectively increase the invitro antitumor activity against the management of TNBC. Moreover, the in-vivo pharmacokinetics study was carried out in Balb/c at dose of 5mg/kg.bw via i.v. route of administration. The AUC of Biotin@HPPH-LPHNs for 24 hr. was 123354.6 ± 26533.07 hr*ng/mL which is 1.1-fold times higher than HPPH-LPHNs and 2-fold times greater than pure HPPH. It clearly indicates that the area of exposure of HPPH improved significantly with Biotin@HPPH-LPHNs. The plasma half-life of Biotin@HPPH-LPHNs was observed to be increased 2 times as compared to pure HPPH. The volume of distribution for Biotin@HPPH-LPHNs was showing narrow distribution which is significantly 1.2 times higher than pure HPPH and HPPH-LPHNs, demonstrating the

Biotin@HPPH-LPHNs may show higher exposure of HPPH at tumor tissue. The clearance of Biotin@HPPH-LPHNs was reduced to 2.6 times in comparison with pure HPPH that indicates longer circulation time in biological system. The in-vivo-biodistribution result showed Biotin@DiI-LPHNs has a 1.1-folds higher DiI-LPHNs accumulation in comparison with HPPH-LPHNs (Fig.5.31). This evidence related to improve in accumulation of nanocarrier (Biotin@DiI-LPHNs) is also lining to our pharmacokinetic study (narrow volume of distribution). HE staining data of LPHNs showed no toxicity when compared to control group. The above results demonstrate the magnificent tumor targeting capability of Biotin@HPPH-LPHNs against TNBC. Our finding suggests the administration of HPPH in LPHNs with biotin surface modification could be a promising strategy in the treatment of TNBC.

6.5. Fabrication and evaluation of OLA loaded LPHNs

Designing of effective therapeutics for the treatment of TNBC has always been challenging due to the lack of expression of the molecular markers(ER,PR and Her 2) [267]. Recent studies suggested that OLA, a selective PARPi, is a promising drug in improving the therapeutic outcomes in TNBC patients. However, OLA has also associated with few limitations including poor pharmacokinetic, poor pharmacodynamic and undesired toxicity hinder its therapeutic effectiveness [268,269]. Thus, a well-designed delivery system is required for OLA to address the above-mentioned issues which can provide better management of TNBC. In the recent past, hybrid lipopolymeric nano delivery systems have attracted the attention towards the targeted delivery of anticancer drugs for the management of TNBC as it provides various distinct advantages and scope of customization in nanocarrier systems [270]. Therefore, in this work, we have fabricated lipo-polymeric hybrid nano-based delivery system for the OLA against TNBC. Furthermore, the report by Yang et al. stated that surface modification with biotin can improve the site specific accumulation of drug in tumor cell[256]. In addition to this, Taymouri et al. developed biotin decorated sunitinib NLC for the management of lung cancer. They found that biotin-NLC (targeted) showed efficient cytotoxicity as compared to sunitinib loaded NLC (non-targeted)[257]. Further, Talat et al. reported a lipidic nanocarrier system for fisetin for breast cancer management using stearylamine. They found that presence of stearylamine in lipidic nanoparticle has enhanced the cellular uptake of drug in breast cancer tissue[271]. Therefore, to provide active targeting and achieving better cellular uptake and apoptosis, we have accomplished surface functionalization to our developed LPHNs with biotin and stearylamine to reduce the

limitations associated with OLA by improving the pharmacokinetics and reducing the off-target side effect for the better management of TNBC.

Firstly, the LPHNs based nanocarrier for OLA was prepared using single emulsification method followed by solvent evaporation. The developed LPHNs were subjected to physiochemical characterization for PS, PDI, ZP, %EE and %DL. Further, freeze drying of LPHNs was carried out with different cryoprotectants (mannitol, sucrose, PEG4000 and trehalose). The result showed 10% (w/w) Trehalose has better profile as compared to other groups (Table 5.32) and was subsequently used to improve the storage stability of LPHNs. Both lyophilized and non-lyophilized LPHNs samples showed the particles size less than 150 nm with narrow PDI (~ 0.21) that were mentioned in Table 5.31, and 5.33. Further, the SEM analysis, indicates the spherical shape of the nanoparticles. Dolai et. al reported that particles size less than 150 nm with spherical shape provides excellent candidate for the enhanced permeability and retention effect [272]. Similarly, Donahue et. al also reported that optimum particle size facilitates the enhanced cellular uptake [272,273]. Besides, narrow range PDI with positive zeta potential can provide an improved uptake and stability in biological environment to the nanocarrier, as reported by Jeon and Foroozandeh et. al [274,275]. Moreover, the spherical shape provides the advantage of less aggregation with enhanced stability [276]. Thus, our resultant LPHNs(OLA-LPHNs, St@OLA-LPHNs and St/Biotin@OLA-LPHNs) may deliver better stability and enhanced cellular uptake. Furthermore, the entrapment efficiency and drug loading for nanoparticles (OLA-LPHNs, St@OLA-LPHNs and St/Biotin@OLA-LPHNs) was estimated using RP-HPLC. It was found that %EE and %DL of all the LPHNs (OLA-LPHNs, St@OLA-LPHNs and St/Biotin@OLA-LPHNs) were in the range of 56-68 % and below 9.2 % respectively (Table 5.31 & Table 5.33). In order to study the physical state of the OLA in LPHNs studies such as DSC were performed. We found a characteristic melting point peak at 210 °C in case of free OLA, whereas developed LPHNs don't show any melting point peak at 210 °C. According to report by Herdiana et. al, the crystallinity of drug incorporated in the NPs can affect the in vitro and in vivo release patterns and solubility of drug as well [277]. Also, in a study conducted by Amjadi et. al. the DSC result suggested that the absence of melting point peak of drug in nanoparticle is because of alteration in the drug crystallinity either in form of amorphous or disordered crystalline phase [278]. Thus, the evidence suggest that OLA is completely encapsulated in LPHNs system. The storage stability for OLA loaded LPHNs was studied and result showed the developed nanocarriers could provide stable environment to the drug and do not show any leaching effect till 90 days

(Figure.5.36). The release study of OLA loaded LPHNs was conducted to understand the integrity and stability of nanocarrier in normal physiological condition (pH7.4) and in tumor microenvironment as well. It was shown that all the LPHNs (OLA-LPHNs, St@OLA-LPHNs and St/Biotin@OLA-LPHNs) followed the biphasic release profile; i.e. approx. 40% drug release from all the LPHNs within 4 h and remaining 60% was completely released in the duration of 48 h whereas in the case of pure OLA, the complete release was observed within 2 hr. (Figure 5.34). The fraction of initial burst release of OLA from nanocarrier may probably be related to the presence of a lipidic environment, stearylamine and phospholipid (SPC 100) in the nanocarrier system. This burst release can act as a loading dose which is supportive for inhibition of tumor growth within the first hours of administration. Further, it followed a controlled type release pattern which might be due to the high hydrophobicity nature of OLA and PLGA that prevented the diffusion of OLA from the nanocarrier into the aqueous medium. Similar findings as reported by Mandal et. al., are in line with our result [279]. Further, the release study of OLA loaded LPHNs showed faster release of drug in acidic pH in comparison to physiological pH which can be an advantageous feature for better penetration of OLA in the tumor acidic environment. On the other hand, the slow release of OLA at physiological pH compared to the acidic condition ensures the NP stability in blood during its way to the tumor sites. Thus, it can be that the prepared LPHNs (OLA-LPHNs, St@OLA-LPHNs and St/Biotin@OLA-LPHNs) are capable of acting as a sustained type delivery approach at the tumor site.

Furthermore, *in-vitro* cytotoxicity results suggested that the survival rate of 4T1 cells was significantly reduced in the case of St/Biotin@OLA-LPHNs compared to pure OLA and non-targeted nanocarrier (St@OLA-LPHNs and OLA-LPHNs) after 48 h incubation. On the other hand, the developed blank LPHNs (without drug) showed no cytotoxicity and it could be assumed that the excipients used for the nanoparticle are safe and non-toxic. Further, in order to understand the internalization of OLA loaded LPHNs, coumarin 6 (C6) loaded LPHNs were prepared which demonstrated the distribution of LPHNs in the cytoplasm of cells. It was observed that St/Biotin@OLA-LPHNs showed high color intensity when compared to all other OLA loaded LPHNs (OLA-LPHNs and St@OLA-LPHNs). Our results are in line with the study reported by Vassoudevane et. al. They stated that stearylamine confers the positive charge to the nanoparticles, which facilitates the enhanced cellular uptake as the cell membrane is negatively charged which has a tendency to interact with the positively charged moiety. [280]. Similar results for enhanced cytotoxicity and improved cellular uptake in cancer cells due to surface modification of anti-cancer drug (Hydroxycamptothecin) loaded nanoparticle with biotin was

also demonstrated by He et. al[281]. Additionally, the apoptosis study showed St/Biotin@OLA-LPHNs has 8-fold time higher apoptotic ratio as compared to free OLA. On considering all the cell-based assay result, our developed nanoformulation (St/Biotin@OLA-LPHNs) indicates a promising in-vitro antitumor activity against TNBC cell.

The pharmacokinetic study was conducted in Balb/c mice at the dose of 30mg/kg.bw. According to Din et. al, the ideal nanocarrier system should exhibit the desired pharmacokinetic profile, which is required for the improved efficacy and reduced side effects[282]. Our pharmacokinetic results revealed that OLA loaded LPHNs displayed a significantly higher plasma level of OLA in comparison to pure OLA with subsequent increase in AUC of OLA. The $AUC_{0-\infty}$ of St/Biotin@OLA-LPHNs was found 3-folds higher in comparison to OLA solution, which indicates St/Biotin@OLA-LPHNs has longer exposure ability in systemic circulation. Furthermore, St/Biotin@OLA-LPHNs showed less clearance as compared to OLA which indicates long circulation time of drug in biological system. Therefore, it can be suggested that encapsulation of OLA into the LPHNs not only reduced the rate of elimination of OLA from the bloodstream but it also provides a long circulation time in biological system thereby reducing the requirement of frequent dosing. Additionally, the in vivo biodistribution result showed high accumulation of St/Biotin@OLA-LPHNs at tumor site as compared to other OLA loaded LPHNs (OLA-LPHNs and St@OLA-LPHNs) which was shown in the figure 5.42. Similar to our study, other research studies also found that presence of biotin in nanocarrier can enhance the accumulation of drug in tumor tissue[283,284]. Thus, our developed formulation possibly enhances the site-specific accumulation of OLA in tumor cells due to surface decoration with biotin which is having high affinity with tumour cells. The resultant OLA loaded LPHNs showed no toxicity in animal that indicates the nanocarrier is safe to use for further biological evaluation. Taken all together, developed St/Biotin@OLA-LPHNs is beneficial for further applications and commercialization in future.

6.6. Development and evaluation of HPPH and OLA co-loaded LPHNs

Now a days, application of PDT has become promising therapeutics in cancer management due to its unique advantages of wide applicability, better selectivity, and slight side effects. 2-[1-hexyloxyethyl]-2- HPPH is a second-generation, lipophilic, chlorin-based small molecule photosensitizer for PDT, which is capable of inducing cell apoptosis by utilizing strong oxidation abilities of ROS against nucleic acids, enzymes, and cellular membranes. However, HPPH can directly damage tumor cell DNA and induce immunogenic cell death in tumor cell to achieve immune function, its practical application is not satisfactory for tumor

prognosis[255,285]. The primary reason for reduced PDT action is due to impediment by the action of the nuclear enzyme poly (ADP-ribose) polymerase (PARP) which is involved in the repair of DNA by binding to the specific location of single-strand damage on the DNA molecule, and in turn, facilitating the repair process[255,285]. Hence, the inhibition of PARP has the capacity to enhance the effectiveness of PDT. Therefore, combination with PARP inhibitor can be a one of the best approaches to overcome disadvantages of PDT as the PARP inhibitor induces mutagenic homologous recombination that disturb other DNA repair pathways. Along with the advantage, there are few limitations also associated with HPPH and OLA which hinder the clinical effectiveness to treat the TNBC [286]. For this purpose, a LPHNs system will be a better approach for the management of TNBC as it possess unique feature such as high encapsulation efficiency, narrow range of particle size, sustained release, high biocompatibility, biodegradability, better pharmacokinetic and pharmacodynamics [287]. In addition to this, Dave et. al also reported that surface modification of LPHNs by chemical ligands like biotin, folic acid, TPP, azobenzene etc., show enhanced intracellular uptake, high tumor site accumulation of drug[287].

In accordance with all the aspects, in this work, we have developed a Biotin and TPP decorated HPPH and OLA co-encapsulated LPHNs using single step emulsification method followed by solvent evaporation. Further, we have characterized the physicochemical parameters including their particle size, zeta potential, morphology, stability, in-vitro release and evaluated the drug loading capacity of fresh LPHNs. Further, freeze drying of LPHNs was carried out with different cryoprotectants (mannitol, sucrose, PEG4000 and trehalose). The result showed 10% (w/w) Trehalose has better profile as compared to other groups (Table 5.36) and was subsequently used to improve the storage stability of LPHNs. The resultant nanoparticle showed optimal physicochemical properties high drug loading capacity and better release profile which facilitate for the in vitro and in vivo evaluation for LPHNs (HPPH-OLA). Moreover, the SOSG study was carried out to understand the singlet oxygen capacity which is a critical factor for ROS induced PDT activity. The result indicates Biotin-ss-TPP@HPPH/OLA-LPHNs showed slightly less fluorescence intensity i.e., ~3% less fluorescence intensity when compared to pure HPPH. The results lie in concordance with the study conducted by Rong et. al, as per their findings the ROS production that only depends upon singlet oxygen generation capacity but also depends upon cellular uptake and intratumoral delivery. [262]. Thus, low intensity observed in our formulation (Biotin-ss-TPP@HPPH/OLA-LPHNs) can be compensated.

In order to understand the in-vitro anti-tumor effect against TNBC, we performed cellular studies like cytotoxicity, cellular uptake, in vitro ROS, and apoptosis. Both the LPHNs (Biotin-ss-TPP@HPPH/OLA-LPHNs and Biotin@HPPH/OLA-LPHNs) were assessed for their cytotoxicity in the 4T1 breast cancer cells. As shown in Fig.5.48, the Biotin-ss-TPP@HPPH/OLA-LPHNs displayed more cytotoxicity in comparison to Biotin@HPPH/OLA-LPHNs. Moreover, the synergistic potential of HPPH and OLA was also evaluated. The result showed that nanoparticles (Biotin-ss-TPP@HPPH/OLA-LPHNs) showed a better synergistic cytotoxicity effect with CI values below 0.5 as compared with Biotin@HPPH/OLA-LPHNs and pure solution of HPPH-OLA. Therefore, the enhanced synergistic effect of Biotin-ss-TPP@HPPH/OLA-LPHNs as compared to Biotin@HPPH/OLA-LPHNs (non-targeted) and free HPPH may eventually be due to the high cellular uptake of nanoparticles due to mitochondrial mediated endocytosis resulting in higher accumulation of drug within the cells and could also synergize due to presence of disulfide bond in lipid backbone. The similar result is also reported by Li et al. and Nam et al. [288,289]. Further, the above-mentioned synergistic effect can also be confirmed by our cellular and mitochondrial uptake study as the Biotin-ss-TPP@HPPH/OLA-LPHNs showed efficient mitochondrial uptake when compared to Biotin@HPPH/OLA-LPHNs (Figure 5.49). Subsequently, Blank-LPHNs showed no toxicity to 4T1, this phenomenon ensures that the LPHNs is safe and biocompatible to encapsulate HPPH and OLA against TNBC. Besides, we also observed high apoptosis in case of Biotin@HPPH/OLA-LPHNs. The apoptotic potential of Biotin-ss-TPP@HPPH/OLA-LPHNs was found to be 2-fold times higher than free HPPH-OLA solution (figure 5.50) which can be correlated with enhanced mitochondrial uptake. This result is in line with previous finding of Lin Ye et al. They developed a 7-hydroxyl coumarin loaded TPP-PLA nanoparticle for glioblastoma management. The TPP-PLLA NPs were mostly co-localized with mitochondria (red) while PLLA NPs(non-targeted) were disorderly distributed in the cells after 10 h of cell uptake indicating that TPP-PLLA NPs had significant mitochondria targeting properties and effectively delivered drugs to the mitochondria [290]. Taken together, increased mitochondrial delivery of Biotin@HPPH/OLA-LPHNs was due to presence of disulfide bond and TPP, thereby improving the cellular uptake and enhanced apoptosis induced cell death which support the antitumor activity against TNBC.

Further, hemolysis study was conducted to ensure the biocompatibility of LPHNs. It was found that LPHNs (Biotin-ss-TPP@HPPH/OLA-LPHNs and Biotin@HPPH/OLA-LPHNs) exhibited hemolytic index below 2% which indicates the LPHNs is safe to use in animal study.

Similar to our study, several research studies also found that hemolytic index below 2% did not show any hypersensitive reaction and toxicity to biological system[291].

The pharmacokinetic profile represented the overall significant enhancement in pharmacokinetic parameters with Biotin-ss-TPP@HPPH/OLA-LPHNs as compared to free HPPH-OLA solution (figure 5.53). Moreover, the DiI loaded LPHNs was prepared for biodistribution evaluation of LPHNs (Biotin@HPPH/OLA-LPHNs and Biotin-ss-TPP@HPPH/OLA-LPHNs). It was observed that Biotin-ss-TPP@DiI-LPHNs showed greater accumulation of DiI in the tumour site which was 2-fold times higher than the Biotin@DiI-LPHNs (figure 5.54). Further, to investigate the antitumor activity, Lucifer-tagged 4T1 bearing Balb/c model was developed and different treatment with respect dose 30mg/kg.bw for OLA and 5mg/kg.bw for HPPH were administered to the 4T1 tumor bearing animal. Afterward, the tumor volume and body weight of all the treated mice were examined on every alternative day. It has been shown that there were no significant changes in body weight, as shown in Fig. 5.55. Further, all the treated group were sacrificed on the 10th day for analysis. H&E analysis revealed that vital organs (heart, liver, spleen, lung, kidney) of the treated animal mice showed no severe histological damage (Fig 5.59). As shown in the figure 5.55 and Fig. 5.56, Biotin@HPPH/OLA-LPHNs treated group showed rapid inhibition in tumor suppression as compared to other group (HPPH, OLA, HPPH-OLA and @HPPH/OLA-LPHNs). Further, this reduction in tumor growth was confirmed by in-vivo ROS data and tunnel apoptosis data which was shown in figure 5.57 and figure 5.58. Similar result related to reduction in tumor growth was also previously reported by Ye et al. They demonstrated inhibition of tumor growth is probably due to presence of TPP in nanocarrier that can facilitate ROS induced apoptosis. This might be attributed due to presence of TPP that facilitates its passage across the cell membrane due to the presence of three phenyl groups in its functional backbone. Furthermore, high accumulation of TPP in mitochondria can collapse the mitochondria membrane potential and finally facilitate apoptosis via mitochondrial-mediated pathway [290]. In another study, Zhou et al. reported that TPP-conjugated TPGS1000 nanoparticle facilitated the mitochondrial targeting and uptake of paclitaxel which induce the apoptosis in drug-resistant cancer by releasing cytochrome C, and initiating a cascade of caspase 9 and caspase 3 reactions[292]. In addition to mitochondrial targeting, inhibition of tumor growth can also be facilitated due to several possible reasons a) improved residence time due to presence of PEG in nanocarrier backbone that enhance circulation time by avoiding RES uptake b) enhanced biodistribution profile at the tumor site and passive targeting to tumor through EPR effect c) active targeting

ability of the Biotin-ss-TPP@HPPH/OLA-LPHNs enabled the drug to accumulate in the biotin receptor-expressing tumor tissue[293].

Thus, the above-mentioned results support and establish the magnificent tumor targeting capability of Biotin-ss-TPP@HPPH/OLA-LPHNs against TNBC. In nutshell, it can be said that the treatment with combination of HPPH and OLA in LPHNs system decorated with biotin and TPP can be an effective strategy in the management of TNBC. Further, it could be translated for clinical application.



CONCLUSION, SUMMARY AND FUTURE SCOPE



7. Conclusion and Summary

- This research work is focused to evaluate the photodynamic therapy (HPPH) and PARP inhibitor (OLA) for their therapeutic potential against TNBC.
- The anti-cancer potential of PDT (HPPH) and OLA in TNBC was estimated by the in-vitro and in-vivo studies using 4T1 cell line (cytotoxicity) and the syngeneic TNBC animal model (4T1 bearing tumor mice model). We have observed that the HPPH and OLA significantly reduce the survival rate in 4T1 cells, representing the antitumoral potential of HPPH and OLA and no significant morphological changes were observed in the 4T1 cell line. Moreover, combination HPPH and OLA showed the combination index value below 0.8, indicating the possible synergistic effect. Based on the cytotoxicity result, we have proceeded to in vivo experiments. The Balb/c mice were injected with TNBC cell line (luc-4T1 cell line) with a cell count of 2×10^6 in PBS exactly at mammary pad through a disposable syringe. The developed TNBC orthotopic murine models was confirmed by bioimaging system (IVIS® Lumina III, PerkinElmer, USA). Afterward, HPPH (Dose 5mg/kg.bw), OLA (Dose 30mg/kg.bw) and in combination of HPPH with OLA were administered in TNBC bearing Balb/c mice. A substantial enhancement ($p < 0.001$) in the tumor suppression and enhanced apoptosis cell death pathway was observed when compared to diseased animal. Moreover, to check the pharmacokinetic profile and interaction between HPPH and OLA, pharmacokinetic studies of HPPH, OLA and in combination of HPPH and OLA was performed in Balb/C mice. The results confirmed various pharmacokinetic problem of OLA i.e., short plasma half-life ($t_{1/2}$) i.e., 5.74 ± 3.35 hr., a high-rate of elimination and low volume of distribution in case of OLA. Further, to check the compatibility of HPPH and OLA, the pharmacokinetic data suggested the combination of HPPH and OLA did not find any significant pharmacokinetic interaction after administration in animal.
- Therefore, to circumvent the problems associated with poor pharmacokinetic and pharmacodynamic of HPPH and OLA, we have fabricated three different LPHNs system for HPPH and OLA (alone) and nano carrier-based co-delivery of HPPH and OLA (HPPH-OLA). The developed nano-formulation were biologically characterized using Balb/c mice model. Firstly, we have synthesized amphilic targeted co-polymer (Biotin-PEG-PLGA) and a novel lipid molecule (Linoleic acid-ss-TPP) that characterized using NMR and LC-

MS/MS. which were further utilized in our nano delivery system for site-specific tumor targeting to treat the TNBC.

- HPPH loaded lipid polymer hybrid nanoparticles (LPHNs) were formulated using a single emulsification method followed by evaporation. Further, to optimize the LPHNs, the effect of independent parameters (i.e., concentration of PVA solution and amount of DC89PC) on response parameters (i.e., Particle Size and % Entrapment efficiency) were studied using the CCD based response surface methodology via DOE approach. The comparative analysis of physiochemical properties such as average Particle size (PS), Polydispersity index (PDI) and zeta potential of the optimized LPHNs with fresh and after freeze drying were studied. The morphological evaluation of LPHNs was carried out using SEM analysis. The data revealed that the developed LPHNs were spherical with uniform distribution. The release profile of pure HPPH described complete drug release from the dialysis bag within 12 h. Whereas HPPH encapsulated LPHNs followed a biphasic release pattern i.e., a biphasic release profile. The stability of lyophilized LPHNs was characterized with two different storage condition i.e., 4 °C/65% RH and 25 °C/60% RH for 90 days to understand the shelf life of the LPHNs. The singlet-oxygen-generating potential of HPPH and its LPHNs was detected by the Singlet Oxygen Sensor Green (SOSG) assay at the excitation wavelength 494 nm. Notably, the fluorescence intensity of HPPH was significantly reduced due to encapsulation of HPPH in nanocarrier, the ¹O₂ generation ability of both nanocarrier (HPPH-LPHNs and Biotin@HPPH-LPHNs) was reduced by ~60 % relative to that of pure HPPH. Although, singlet oxygen generation is the key for ROS production in cancer cell. In spite of that, production of ROS also depends upon cellular uptake of the HPPH. Therefore, it can be compensated. Furthermore, in vitro cellular studies confirmed that HPPH loaded LPHNs significantly improved the cell viability, cellular uptake, ROS generation and apoptosis induced cell death when compared to free HPPH. The in vivo pharmacokinetics and biodistribution studies have shown that Biotin@HPPH-LPHNs significantly enhanced the pharmacokinetic parameter and improved tumor accumulation capacity as compared to HPPH-LPHNs(non-targeted) and free HPPH. Moreover, no toxicity was observed in pure HPPH and HPPH loaded LPHNs, indicating that fabricated LPHNs for HPPH is biocompatible.
- In the same way, the LPHNs for OLA (i.e., OLA-LPHNs, St@OLA-LPHNs and St/Biotin@OLA-LPHNs) was fabricated using emulsification followed by solvent evaporation method. The OLA loaded LPHNs (both lyophilized and non-lyophilized

LPHNs) were characterized with respect to PS, PDI, zeta potential, shape, %EE and % DL. Additionally, SEM image showed that OLA loaded nanoparticles were nano-metric in size with spherical shape which matches with result of DLS analysis. It has also been observed that LPHNs were less aggregated with enhanced stability. Both DSC and IR results confirmed that OLA is completely encapsulated in the LPHNs. The stability of lyophilized nanocarrier was evaluated for 3 months with two different storage conditions i.e., 4 °C/65% RH and 25 °C/60% RH. It was observed that the stability samples with both storage condition showed no significant changes in PDI and PS compared to the fresh batch. Hemolysis of nanoparticle was performed using RBCs of mice. The pure OLA and its LPHNs (OLA-LPHNs, St@OLA-LPHNs and St/Biotin@OLA-LPHNs) showed hemolytic index of approx. 1.5%. Furthermore, in vitro cellular studies confirmed that OLA loaded LPHNs significantly improved the cell viability, cellular uptake and apoptosis as compared to free OLA. The in vivo pharmacokinetics confirmed that Biotin@HPPH-LPHNs significantly enhanced the pharmacokinetic parameter with respect to biological half-life, AUC, Clearance and rate of elimination. Further, Biodistribution study was performed using DiI dye for all the nanocarrier and found that improved tumor accumulation capacity of St/Biotin@OLA-LPHNs when compared to other non-targeted nanocarrier. No toxicity was observed in the treated group when compared to control group, indicating OLA loaded LPHNs to be biocompatible and safe.

- In addition, co-encapsulated HPPH and OLA in LPHNs were also formulated by single emulsification method using the stearylamine, Biotin-PEG-PLGA, linoleic acid-ss-TPP and PVA. Further, the designed nanocarrier was subjected to physiochemical characterization. It was observed that the PS was found in between the range of 100-200 nm which is in line with SEM analysis and further, the FEI-SEM data representing the spherical morphology of the particle with uniform size distribution across nanocarrier systems. The release profile of the free drug and LPHNs was performed using dialysis bag method. The drug loaded nanoparticle exhibited a burst release followed by controlled release pattern which could provide a better residence time of drug in biological system. The cytotoxicity of HPPH and Olaparib co-encapsulated LPHNs were studied in 4T1 cell line. The result suggested that Biotin-ss-TPP@HPPH/OLA-LPHNs showed 14.47% cell death at combination dose of 4 μ M and 24 μ M for HPPH and OLA respectively, while Biotin @HPPH-OLA-LPHNs and pure combination of HPPH and Olaparib showed 28.80 % and 46.27% cell death respectively. Blank LPHNs did not show any significant change in the cell viability. The

cellular uptake of LPHNs was performed by using a hydrophobic dye i.e., coumarin-6. Further, to evaluate mitochondrial penetration of nanocarrier, Mito-tracker (Red) was also used. The fluorescence intensity of Biotin-ss-TPP@HPPH/OLA LPHNs was stronger than Biotin@HPPH/OLA-LPHNs. The Mito tracker fluorescence intensity of Biotin-ss-TPP@HPPH/OLA-LPHNs was stronger when compared to Biotin@HPPH/OLA-LPHNs. The apoptosis study suggested that Biotin-ss-TPP@HPPH/OLA-LPHNs exhibited 37.74% of apoptotic ratio which is 2.32-fold time and 1.9-fold time higher from pure HPPH-OLA and Biotin@HPPH/OLA-LPHNs respectively. Moreover, the resultant HPPH and OLA co-encapsulated LPHNs showed improved pharmacokinetics as compared to free drug. Moreover, the biodistribution of Biotin@DiI-LPHNs and Biotin-ss-TPP@DiI-LPHNs was carried out and the results showed a greater tumor accumulation with Biotin-ss-TPP@DiI-LPHNs in comparison to Biotin@DiI-LPHNs which is 1.6-fold times higher. The in-vivo efficacy was assessed in Luciferin tagged 4T1 tumor bearing animal. Notably, the result suggested Biotin-ss-TPP@HPPH/OLA-LPHNs treated animal showed significant tumor suppression when compared to combination of HPPH and OLA and Biotin@HPPH/OLA-LPHNs. Further, Biotin-ss-TPP@HPPH-OLA LPHNs treated animal group showed a higher intensity of in vivo ROS generation compared to other group i.e., HPPH, OLA, physical mixture HPPH and OLA and Biotin@HPPH/OLA-LPHNs. It could be due to better penetration of drug loaded nanoparticle in mitochondrial site of tumour tissue. The tunnel assay also suggested higher apoptotic response of Biotin-ss-TPP@ HPPH/OLA-LPHNs (exhibits 2.1-fold time apoptotic ratio) in comparison to combination of pure HPPH and OLA. Also, histochemical analysis was performed for all group using H&E staining. No toxicity was observed in vital organ, which may be due to effective drug encapsulation into the nanocarriers system.

- Therefore, succinctly, our work demonstrated that this surface modified LPHNs based therapeutic strategies could be utilized HPPH and Olaparib with improved target specific biodistribution leading to enhanced anti-tumor efficacy against TNBC along with reduced toxicity.

8. Salient findings from the present research work

- Our research work confirmed that both HPPH and OLA are effective against TNBC. Moreover, their combination has also confirmed synergistic response against TNBC. Therefore, it could pave the way for facilitating further clinical translation avenue.
- The di-block amphiphilic co-polymer (Biotin-PEG-PLGA) and lipid (DC89PC, Linoleic acid and Linoleic acid-ss-TPP) were synthesized and characterized using NMR and LC-MS/MS.
- The LPHNs system were fabricated and evaluated for HPPH and OLA (alone) and their combination (HPPH-OLA) to treat TNBC.
- Also, developed nanocarrier system for HPPH and OLA-alone and co-delivery system, significantly circumvented the pharmacokinetic problem including short half-life, high elimination rate, and biological instability.
- In addition, the bio-distribution studies of surface modified LPHNs encapsulated HPPH and OLA) (alone) and co-encapsulated HPPH and Olaparib has been carried out in 4T1 mouse model which showed enhanced drug accumulation in tumour site. Thus, it is evident that developed LPHNs delivered both HPPH and OLA selectively to TNBC tissue that could minimize the toxicity.
- Moreover, surface engineered co encapsulated (HPPH and OLA) LPHNs (Biotin@HPPH/OLA-LPHNs and Biotin-ss-TPP@HPPH/OLA-LPHNs) showed significant tumour suppression activity when compared with free drug. There was no toxicity observed with these two drugs loaded LPHNs.
- Therefore, our work demonstrated that this surface modified LPHNs based therapeutic strategies could be utilized for HPPH and Olaparib with improved target specific delivery as confirmed by biodistribution that may lead to enhanced anti-tumour efficacy against TNBC along with reduced toxicity.

9. Future scope of this work

The present research work established that both HPPH and OLA has a therapeutic potential against the TNBC. Furthermore, evidenced that combination of HPPH and OLA provides an effective synergetic therapeutic potential for the management of TNBC. Based on these findings, utilizing the obtained evidence future research can be performed as:

- Exploring the advantage of third generation and other second generation chlorin based PDT molecules may further open novel paths for therapeutic management of Breast cancer including TNBC.
- Co-delivery of PDT with different classes of drugs such EGRF inhibitor, PD-1 inhibitor and gene therapy may be studied for exploring the synergistic potential in TNBC conditions
- The synthesized di-block co-polymer and novel lipid molecules can be further modified for site specific delivery to the TNBC tissue for its better management.
- The pharmaceutical dosage form can be modified using different alternative approaches such as development of other type of nanocarrier system, alternative method of preparation, and exploring other excipients to improve the drug loading and targetability that may eventually minimize the side effect and cost of product.
- The method of preparation and process control parameters could be further modified for the scale-up and manufacturing of the nanocarrier for the industrial application.
- The developed nanocarrier may be further modified for dosage form design for patient compliance.
- The safety investigations can be performed for long-term usage of the product.



BIBLIOGRAPHY



10. Bibliography

- [1] B. Smolarz, A.Z. Nowak, H. Romanowicz, Breast Cancer-Epidemiology, Classification, Pathogenesis and Treatment (Review of Literature)., *Cancers (Basel)*. 14 (2022). <https://doi.org/10.3390/cancers14102569>.
- [2] W.J. Irvin, L.A. Carey, What is triple-negative breast cancer?, *Eur. J. Cancer*. 44 (2008) 2799–2805. <https://doi.org/10.1016/J.EJCA.2008.09.034>.
- [3] P. Neven, Brouckaert, Wildiers, Floris, Update on triple-negative breast cancer: prognosis and management strategies, *Int. J. Womens. Health*. (2012) 511. <https://doi.org/10.2147/ijwh.s18541>.
- [4] N.M. Almansour, Triple-Negative Breast Cancer: A Brief Review About Epidemiology, Risk Factors, Signaling Pathways, Treatment and Role of Artificial Intelligence, *Front. Mol. Biosci*. 9 (2022) 1–15. <https://doi.org/10.3389/fmolb.2022.836417>.
- [5] Z. Momenimovahed, H. Salehiniya, Epidemiological characteristics of and risk factors for breast cancer in the world., *Breast Cancer (Dove Med. Press)*. 11 (2019) 151–164. <https://doi.org/10.2147/BCTT.S176070>.
- [6] M.D. Burstein, A. Tsimelzon, G.M. Poage, K.R. Covington, A. Contreras, S.A.W. Fuqua, M.I. Savage, C.K. Osborne, S.G. Hilsenbeck, J.C. Chang, G.B. Mills, C.C. Lau, P.H. Brown, Comprehensive genomic analysis identifies novel subtypes and targets of triple-negative breast cancer, *Clin. Cancer Res*. 21 (2015) 1688–1698. <https://doi.org/10.1158/1078-0432.CCR-14-0432/270898/AM/COMPREHENSIVE-GENOMIC-ANALYSIS-IDENTIFIES-NOVEL>.
- [7] R. Bissanum, S. Chaichulee, R. Kamolphiwong, R. Navakanitworakul, K. Kanokwiroon, Molecular classification models for triple negative breast cancer subtype using machine learning, *J. Pers. Med*. 11 (2021) 881. <https://doi.org/10.3390/JPM11090881/S1>.
- [8] S.G. Ahn, S.J. Kim, C. Kim, J. Jeong, Molecular Classification of Triple-Negative Breast Cancer, *J. Breast Cancer*. 19 (2016) 223. <https://doi.org/10.4048/JBC.2016.19.3.223>.
- [9] B.D. Lehmann, J.A. Pietenpol, A.R. Tan, Triple-Negative Breast Cancer: Molecular Subtypes and New Targets for Therapy, *Am. Soc. Clin. Oncol. Educ. B*. (2015) e31–e39. https://doi.org/10.14694/edbook_am.2015.35.e31.
- [10] G.K. Gupta, A.L. Collier, D. Lee, R.A. Hoefler, V. Zheleva, L.L.S. van Reesema, A.M. Tang-Tan, M.L. Guye, D.Z. Chang, J.S. Winston, B. Samli, R.J. Jansen, E.F. Petricoin,

- M.P. Goetz, H.D. Bear, A.H. Tang, Perspectives on Triple-Negative Breast Cancer: Current Treatment Strategies, Unmet Needs, and Potential Targets for Future Therapies, *Cancers (Basel)*. 12 (2020) 1–33. <https://doi.org/10.3390/CANCERS12092392>.
- [11] O. Obidiro, G. Battogtokh, E.O. Akala, Triple Negative Breast Cancer Treatment Options and Limitations: Future Outlook, *Pharmaceutics*. 15 (2023). <https://doi.org/10.3390/PHARMACEUTICS15071796>.
- [12] H.A. Wahba, H.A. El-Hadaad, Current approaches in treatment of triple-negative breast cancer, *Cancer Biol. Med.* 12 (2015) 106. <https://doi.org/10.7497/J.ISSN.2095-3941.2015.0030>.
- [13] E. Andreopoulou, J.A. Sparano, Chemotherapy in Patients with Anthracycline- and Taxane-Pretreated Metastatic Breast Cancer: An Overview., *Curr. Breast Cancer Rep.* 5 (2013) 42–50. <https://doi.org/10.1007/s12609-012-0097-1>.
- [14] K.O. Alfarouk, C.-M. Stock, S. Taylor, M. Walsh, A.K. Muddathir, D. Verduzco, A.H.H. Bashir, O.Y. Mohammed, G.O. Elhassan, S. Harguindey, S.J. Reshkin, M.E. Ibrahim, C. Rauch, Resistance to cancer chemotherapy: failure in drug response from ADME to P-gp., *Cancer Cell Int.* 15 (2015) 71. <https://doi.org/10.1186/s12935-015-0221-1>.
- [15] F. Borri, A. Granaglia, Pathology of triple negative breast cancer, *Semin. Cancer Biol.* 72 (2021) 136–145. <https://doi.org/10.1016/j.semcancer.2020.06.005>.
- [16] B.S. Yadav, P. Chanana, S. Jhamb, Biomarkers in triple negative breast cancer: A review., *World J. Clin. Oncol.* 6 (2015) 252–263. <https://doi.org/10.5306/wjco.v6.i6.252>.
- [17] B. Na, X. Yu, T. Withers, J. Gilleran, M. Yao, T.K. Foo, C. Chen, D. Moore, Y. Lin, S.D. Kimball, B. Xia, S. Ganesan, D.R. Carpizo, Therapeutic targeting of BRCA1 and TP53 mutant breast cancer through mutant p53 reactivation, *Npj Breast Cancer*. 5 (2019) 14. <https://doi.org/10.1038/s41523-019-0110-1>.
- [18] H. Masuda, D. Zhang, C. Bartholomeusz, H. Doihara, G.N. Hortobagyi, N.T. Ueno, Role of epidermal growth factor receptor in breast cancer, *Breast Cancer Res. Treat.* 136 (2012) 331–345. <https://doi.org/10.1007/S10549-012-2289-9>.
- [19] R. Pradhan, A. Dey, R. Taliyan, A. Puri, S. Kharavtekar, S.K. Dubey, Recent Advances in Targeted Nanocarriers for the Management of Triple Negative Breast Cancer, *Pharmaceutics*. 15 (2023). <https://doi.org/10.3390/pharmaceutics15010246>.
- [20] M. Oshi, S. Gandhi, Y. Tokumaru, L. Yan, A. Yamada, R. Matsuyama, T. Ishikawa, I.

- Endo, K. Takabe, Conflicting roles of EGFR expression by subtypes in breast cancer., *Am. J. Cancer Res.* 11 (2021) 5094–5110.
- [21] L. Yin, J.J. Duan, X.W. Bian, S.C. Yu, Triple-negative breast cancer molecular subtyping and treatment progress, *Breast Cancer Res.* 22 (2020). <https://doi.org/10.1186/S13058-020-01296-5>.
- [22] A. Arcaro, A.S. Guerreiro, The phosphoinositide 3-kinase pathway in human cancer: genetic alterations and therapeutic implications., *Curr. Genomics.* 8 (2007) 271–306. <https://doi.org/10.2174/138920207782446160>.
- [23] D.A. Tumbarello, C.E. Turner, Hic-5 Contributes to Transformation Through a RhoA / ROCK-dependent Pathway, *J. Cell. Physiol.* 211(3) (2006) 736–747. <https://doi.org/10.1002/JCP>.
- [24] R. Giordo, Z. Wehbe, P. Paliogiannis, A.H. Eid, A.A. Mangoni, G. Pintus, Nano-targeting vascular remodeling in cancer: Recent developments and future directions, *Semin. Cancer Biol.* 86 (2022) 784–804. <https://doi.org/https://doi.org/10.1016/j.semcancer.2022.03.001>.
- [25] W. Wang, U. Kansakar, V. Markovic, K. Sossey-Alaoui, Role of Kindlin-2 in cancer progression and metastasis, *Ann. Transl. Med.* 8 (2020) 901–901. <https://doi.org/10.21037/atm.2020.03.64>.
- [26] Z. Elgundi, M. Papanicolaou, G. Major, T.R. Cox, J. Melrose, J.M. Whitelock, B.L. Farrugia, Cancer Metastasis: The Role of the Extracellular Matrix and the Heparan Sulfate Proteoglycan Perlecan, *Front. Oncol.* 9 (2020). <https://doi.org/10.3389/fonc.2019.01482>.
- [27] S.-O. Lim, C.-W. Li, W. Xia, H.-H. Lee, S.-S. Chang, J. Shen, J.L. Hsu, D. Raftery, D. Djukovic, H. Gu, W.-C. Chang, H.-L. Wang, M.-L. Chen, L. Huo, C.-H. Chen, Y. Wu, A. Sahin, S.M. Hanash, G.N. Hortobagyi, M.-C. Hung, EGFR Signaling Enhances Aerobic Glycolysis in Triple-Negative Breast Cancer Cells to Promote Tumor Growth and Immune Escape., *Cancer Res.* 76 (2016) 1284–1296. <https://doi.org/10.1158/0008-5472.CAN-15-2478>.
- [28] E.J. Koen, A.B. Collier, Particle-in-cell simulations of a beam driven plasma, *Phys. Plasmas.* To be subm (2010) 1420–1428. <https://doi.org/10.1172/JCI39104.1420>.
- [29] A.J. Gooding, W.P. Schiemann, Epithelial-mesenchymal transition programs and cancer stem cell phenotypes: Mediators of breast cancer therapy resistance, *Mol. Cancer Res.* 18 (2020) 1257–1270. <https://doi.org/10.1158/1541-7786.MCR-20-0067>.

- [30] A. Glaviano, A.S.C. Foo, H.Y. Lam, K.C.H. Yap, W. Jacot, R.H. Jones, H. Eng, M.G. Nair, P. Makvandi, B. Georger, M.H. Kulke, R.D. Baird, J.S. Prabhu, D. Carbone, C. Pecoraro, D.B.L. Teh, G. Sethi, V. Cavalieri, K.H. Lin, N.R. Javidi-Sharifi, E. Toska, M.S. Davids, J.R. Brown, P. Diana, J. Stebbing, D.A. Fruman, A.P. Kumar, PI3K/AKT/mTOR signaling transduction pathway and targeted therapies in cancer., *Mol. Cancer.* 22 (2023) NA-NA. <https://go.gale.com/ps/i.do?p=HRCA&sw=w&issn=14764598&v=2.1&it=r&id=GAL E%7CA761456341&sid=googleScholar&linkaccess=fulltext>.
- [31] N. Dey, P. De, B. Leyland-Jones, PI3K-AKT-mTOR inhibitors in breast cancers: From tumor cell signaling to clinical trials, *Pharmacol. Ther.* 175 (2017) 91–106. <https://doi.org/10.1016/J.PHARMTHERA.2017.02.037>.
- [32] M. Gasparyan, M.-C. Lo, H. Jiang, C.-C. Lin, D. Sun, Combined p53- and PTEN-deficiency activates expression of mesenchyme homeobox 1 (MEOX1) required for growth of triple-negative breast cancer., *J. Biol. Chem.* 295 (2020) 12188–12202. <https://doi.org/10.1074/jbc.RA119.010710>.
- [33] R.L.B. Costa, H.S. Han, W.J. Gradishar, Targeting the PI3K/AKT/mTOR pathway in triple-negative breast cancer: a review, *Breast Cancer Res. Treat.* 169 (2018) 397–406. <https://doi.org/10.1007/s10549-018-4697-y>.
- [34] T. Tian, X. Li, J. Zhang, mTOR signaling in cancer and mtor inhibitors in solid tumor targeting therapy, *Int. J. Mol. Sci.* 20 (2019) 1–34. <https://doi.org/10.3390/ijms20030755>.
- [35] P. Fojtík, D. Beckerová, K. Holomková, M. Šenfluk, V. Rotrekl, Both Hypoxia-Inducible Factor 1 and MAPK Signaling Pathway Attenuate PI3K/AKT via Suppression of Reactive Oxygen Species in Human Pluripotent Stem Cells, *Front. Cell Dev. Biol.* 8 (2021) 1–18. <https://doi.org/10.3389/fcell.2020.607444>.
- [36] B. Muz, P. de la Puente, F. Azab, A.K. Azab, The role of hypoxia in cancer progression, angiogenesis, metastasis, and resistance to therapy., *Hypoxia (Auckland, N.Z.)*. 3 (2015) 83–92. <https://doi.org/10.2147/HP.S93413>.
- [37] K. Yoshida, Y. Miki, Role of BRCA1 and BRCA2 as regulators of DNA repair, transcription, and cell cycle in response to DNA damage, *Cancer Sci.* 95 (2004) 866–871. <https://doi.org/10.1111/J.1349-7006.2004.TB02195.X>.
- [38] C.S. Walsh, Two decades beyond BRCA1/2: Homologous recombination, hereditary cancer risk and a target for ovarian cancer therapy, *Gynecol. Oncol.* 137 (2015) 343–

350. <https://doi.org/10.1016/J.YGYNO.2015.02.017>.
- [39] R. Roy, J. Chun, S.N. Powell, BRCA1 and BRCA2: different roles in a common pathway of genome protection., *Nat. Rev. Cancer.* 12 (2011) 68–78. <https://doi.org/10.1038/nrc3181>.
- [40] A. Bosch, P. Eroles, R. Zaragoza, J.R. Viña, A. Lluch, Triple-negative breast cancer : Molecular features , pathogenesis , treatment and current lines of research, *Cancer Treat. Rev.* 36 (2010) 206–215. <https://doi.org/10.1016/j.ctrv.2009.12.002>.
- [41] H. Chen, J. Wu, Z. Zhang, Y. Tang, X. Li, S. Liu, S. Cao, X. Li, Association Between BRCA Status and Triple-Negative Breast Cancer: A Meta-Analysis, *Front. Pharmacol.* 9 (2018). <https://doi.org/10.3389/FPHAR.2018.00909>.
- [42] E.R. Copson, T.C. Maishman, W.J. Tapper, R.I. Cutress, S. Greville-Heygate, D.G. Altman, B. Eccles, S. Gerty, L.T. Durcan, L. Jones, D.G. Evans, A.M. Thompson, P. Pharoah, D.F. Easton, A.M. Dunning, A. Hanby, S. Lakhani, R. Eeles, F.J. Gilbert, H. Hamed, S. Hodgson, P. Simmonds, L. Stanton, D.M. Eccles, Germline BRCA mutation and outcome in young-onset breast cancer (POSH): a prospective cohort study, *Lancet Oncol.* 19 (2018) 169–180. [https://doi.org/10.1016/S1470-2045\(17\)30891-4](https://doi.org/10.1016/S1470-2045(17)30891-4).
- [43] E. Choi, G. im Mun, J. Lee, H. Lee, J. Cho, Y.S. Lee, BRCA1 deficiency in triple-negative breast cancer: Protein stability as a basis for therapy, *Biomed. Pharmacother.* 158 (2023) 114090. <https://doi.org/10.1016/j.biopha.2022.114090>.
- [44] M. Lee, I.A. Park, S.H. Heo, Y.A. Kim, G. Gong, H.J. Lee, Association between p53 expression and amount of tumor-infiltrating lymphocytes in triple-negative breast cancer, *J. Pathol. Transl. Med.* 53 (2019) 180–187. <https://doi.org/10.4132/jptm.2019.02.08>.
- [45] H. Wang, M. Guo, H. Wei, Y. Chen, Targeting p53 pathways: mechanisms, structures, and advances in therapy, *Signal Transduct. Target. Ther.* 2023 81. 8 (2023) 1–35. <https://doi.org/10.1038/s41392-023-01347-1>.
- [46] N.C. Synnott, A. Murray, P.M. McGowan, M. Kiely, P.A. Kiely, N. O’Donovan, D.P. O’Connor, W.M. Gallagher, J. Crown, M.J. Duffy, Mutant p53: a novel target for the treatment of patients with triple-negative breast cancer?, *Int. J. Cancer.* 140 (2017) 234–246. <https://doi.org/10.1002/IJC.30425>.
- [47] J.L. da Silva, N.C. Cardoso Nunes, P. Izetti, G.G. de Mesquita, A.C. de Melo, Triple negative breast cancer: A thorough review of biomarkers, *Crit. Rev. Oncol. Hematol.* 145 (2020) 102855. <https://doi.org/10.1016/j.critrevonc.2019.102855>.

- [48] C. Zhang, J. Liu, D. Xu, T. Zhang, W. Hu, Z. Feng, Gain-of-function mutant p 53 in cancer progression and therapy, 12 (2020) 674–687.
- [49] S.C. Linn, A.H. Honkoop, K. Hoekman, P. van der Valk, H.M. Pinedo, G. Giaccone, p53 and P-glycoprotein are often co-expressed and are associated with poor prognosis in breast cancer, *Br. J. Cancer*. 74 (1996) 63–68. <https://doi.org/10.1038/bjc.1996.316>.
- [50] C.E. Helt, W.A. Cliby, P.C. Keng, R.A. Bambara, M.A. O'Reilly, Ataxia telangiectasia mutated (ATM) and ATM and Rad3-related protein exhibit selective target specificities in response to different forms of DNA damage, *J. Biol. Chem.* 280 (2005) 1186–1192. <https://doi.org/10.1074/jbc.M410873200>.
- [51] R.S. Tibbetts, K.M. Brumbaugh, J.M. Williams, J.N. Sarkaria, W.A. Cliby, S.Y. Shieh, Y. Taya, C. Prives, R.T. Abraham, A role for ATR in the DNA damage-induced phosphorylation of p53, *Genes Dev.* 13 (1999) 152–157. <https://doi.org/10.1101/gad.13.2.152>.
- [52] J. Chen, The cell-cycle arrest and apoptotic and progression, *Cold Spring Harb. Perspect. Med.* 6 (2016) 1–16.
- [53] A.J. Eustace, M.J. Lee, G. Colley, J. Roban, T. Downing, P.J. Buchanan, Aberrant calcium signalling downstream of mutations in TP53 and the PI3K/AKT pathway genes promotes disease progression and therapy resistance in triple negative breast cancer., *Cancer Drug Resist. (Alhambra, Calif.)*. 5 (2022) 560–576. <https://doi.org/10.20517/cdr.2022.41>.
- [54] R. Vélez-Cruz, D.G. Johnson, The retinoblastoma (RB) tumor suppressor: Pushing back against genome instability on multiple fronts, *Int. J. Mol. Sci.* 18 (2017). <https://doi.org/10.3390/ijms18081776>.
- [55] K. Engeland, Cell cycle regulation: p53-p21-RB signaling, *Cell Death Differ.* 29 (2022) 946–960. <https://doi.org/10.1038/s41418-022-00988-z>.
- [56] P. Indovina, F. Pentimalli, N. Casini, I. Vocca, A. Giordano, RB1 dual role in proliferation and apoptosis: Cell fate control and implications for cancer therapy, *Oncotarget*. 6 (2015) 17873–17890. <https://doi.org/10.18632/oncotarget.4286>.
- [57] C. Bertoli, J.M. Skotheim, R.A.M. de Bruin, Control of cell cycle transcription during G1 and S phases, *Nat. Rev. Mol. Cell Biol.* 14 (2013) 518–528. <https://doi.org/10.1038/nrm3629>.
- [58] M. Peyressatre, C. Prével, M. Pellerano, M.C. Morris, Targeting cyclin-dependent kinases in human cancers: From small molecules to peptide inhibitors, *Cancers (Basel)*.

- 7 (2015) 179–237. <https://doi.org/10.3390/cancers7010179>.
- [59] L. Ding, J. Cao, W. Lin, H. Chen, X. Xiong, H. Ao, M. Yu, J. Lin, Q. Cui, The roles of cyclin-dependent kinases in cell-cycle progression and therapeutic strategies in human breast cancer, *Int. J. Mol. Sci.* 21 (2020) 1–28. <https://doi.org/10.3390/ijms21061960>.
- [60] A. Takahashi, N. Ohtani, E. Hara, Irreversibility of cellular senescence: Dual roles of p16INK4a/Rb-pathway in cell cycle control, *Cell Div.* 2 (2007) 1–5. <https://doi.org/10.1186/1747-1028-2-10>.
- [61] R.A. Jones, T.J. Robinson, J.C. Liu, M. Shrestha, V. Voisin, Y. Ju, P.E.D. Chung, G. Pellecchia, V.L. Fell, S. Bae, L. Muthuswamy, A. Datti, S.E. Egan, Z. Jiang, G. Leone, G.D. Bader, A. Schimmer, E. Zacksenhaus, RB1 deficiency in triple-negative breast cancer induces mitochondrial protein translation, *J. Clin. Invest.* 126 (2016) 3739–3757. <https://doi.org/10.1172/JCI81568>.
- [62] M. Longacre, N.A. Snyder, G. Housman, M. Leary, K. Lapinska, S. Heerboth, A. Willbanks, S. Sarkar, A comparative analysis of genetic and epigenetic events of breast and ovarian cancer related to tumorigenesis, *Int. J. Mol. Sci.* 17 (2016). <https://doi.org/10.3390/ijms17050759>.
- [63] A.E. Marshall, M. V Roes, D.T. Passos, M.C. DeWeerd, A.C. Chaikovsky, J. Sage, C.J. Howlett, F.A. Dick, RB1 Deletion in Retinoblastoma Protein Pathway-Disrupted Cells Results in DNA Damage and Cancer Progression, *Mol. Cell. Biol.* 39 (2019) e00105-19. <https://doi.org/10.1128/MCB.00105-19>.
- [64] A.M. Raizis, H.M. Racher, A. Foucal, H. Dimaras, B.L. Gallie, P.M. George, DNA hypermethylation/boundary control loss identified in retinoblastomas associated with genetic and epigenetic inactivation of the RB1 gene promoter, *Epigenetics.* 16 (2021) 940–954. <https://doi.org/10.1080/15592294.2020.1834911>.
- [65] S. Hejmady, R. Pradhan, A. Alexander, M. Agrawal, G. Singhvi, B. Gorain, S. Tiwari, P. Kesharwani, S.K. Dubey, Recent advances in targeted nanomedicine as promising antitumor therapeutics, *Drug Discov. Today.* 25 (2020) 2227–2244. <https://doi.org/10.1016/J.DRUDIS.2020.09.031>.
- [66] B.D. Lehmann, B. Jovanović, X. Chen, M. V. Estrada, K.N. Johnson, Y. Shyr, H.L. Moses, M.E. Sanders, J.A. Pietenpol, Refinement of triple-negative breast cancer molecular subtypes: Implications for neoadjuvant chemotherapy selection, *PLoS One.* 11 (2016) 1–22. <https://doi.org/10.1371/journal.pone.0157368>.
- [67] M. Nedeljković, A. Damjanović, Mechanisms of Chemotherapy Resistance in Triple-

- Negative Breast Cancer-How We Can Rise to the Challenge, *Cells*. 8 (2019). <https://doi.org/10.3390/CELLS8090957>.
- [68] J.J.G. Marin, M.R. Romero, A.G. Blazquez, E. Herraez, E. Keck, O. Briz, Importance and limitations of chemotherapy among the available treatments for gastrointestinal tumours., *Anticancer. Agents Med. Chem.* 9 (2009) 162–184. <https://doi.org/10.2174/187152009787313828>.
- [69] S. Zimmermann, R. Dziadziuszko, S. Peters, Indications and limitations of chemotherapy and targeted agents in non-small cell lung cancer brain metastases, *Cancer Treat. Rev.* 40 (2014) 716–722. <https://doi.org/10.1016/j.ctrv.2014.03.005>.
- [70] L.A. Korde, M.R. Somerfield, L.A. Carey, J.R. Crews, N. Denduluri, E.S. Hwang, S.A. Khan, S. Loibl, E.A. Morris, A. Perez, M.M. Regan, P.A. Spears, P.K. Sudheendra, W.F. Symmans, R.L. Yung, B.E. Harvey, D.L. Hershman, Neoadjuvant Chemotherapy, Endocrine Therapy, and Targeted Therapy for Breast Cancer: ASCO Guideline., *J. Clin. Oncol. Off. J. Am. Soc. Clin. Oncol.* 39 (2021) 1485–1505. <https://doi.org/10.1200/JCO.20.03399>.
- [71] A. Baranova, M. Krasnoselskyi, V. Starikov, S. Kartashov, I. Zhulkevych, V. Vlasenko, K. Oleshko, O. Bilodid, M. Sadchikova, Y. Vinnyk, Triple-negative breast cancer: current treatment strategies and factors of negative prognosis., *J. Med. Life.* 15 (2022) 153–161. <https://doi.org/10.25122/jml-2021-0108>.
- [72] H. Zhang, Z. Wang, W. Liu, P. Wang, X. Zhang, Breast-Conserving Surgery in Triple-Negative Breast Cancer: A Retrospective Cohort Study, Evidence-Based Complement. Altern. Med. 2023 (2023) 5431563. <https://doi.org/10.1155/2023/5431563>.
- [73] S. Hejmady, R. Pradhan, A. Alexander, M. Agrawal, G. Singhvi, B. Gorain, S. Tiwari, P. Kesharwani, S.K. Dubey, Recent advances in targeted nanomedicine as promising antitumor therapeutics, *Drug Discov. Today.* 25 (2020) 2227–2244. <https://doi.org/10.1016/j.drudis.2020.09.031>.
- [74] Y. Nitheesh, R. Pradhan, S. Hejmady, R. Taliyan, G. Singhvi, A. Alexander, P. Kesharwani, S.K. Dubey, Surface engineered nanocarriers for the management of breast cancer, *Mater. Sci. Eng. C.* 130 (2021) 112441. <https://doi.org/10.1016/j.msec.2021.112441>.
- [75] S. Hejmady, R. Pradhan, A. Alexander, M. Agrawal, G. Singhvi, B. Gorain, S. Tiwari, P. Kesharwani, S.K. Dubey, Recent advances in targeted nanomedicine as promising antitumor therapeutics., *Drug Discov. Today.* 25 (2020) 2227–2244.

- <https://doi.org/10.1016/j.drudis.2020.09.031>.
- [76] H.L. McArthur, Innovations and Challenges in the Treatment of Metastatic Triple-Negative Breast Cancer, *J. Oncol. Pract.* 14 (2018) 290–291. <https://doi.org/10.1200/JOP.18.00224>.
- [77] R. Mahmoud, P. Ordóñez-Morán, C. Allegrucci, Challenges for Triple Negative Breast Cancer Treatment: Defeating Heterogeneity and Cancer Stemness., *Cancers (Basel)*. 14 (2022). <https://doi.org/10.3390/cancers14174280>.
- [78] M.A. Khan, V.K. Jain, M. Rizwanullah, J. Ahmad, K. Jain, PI3K/AKT/mTOR pathway inhibitors in triple-negative breast cancer: a review on drug discovery and future challenges, *Drug Discov. Today*. 24 (2019) 2181–2191. <https://doi.org/10.1016/j.drudis.2019.09.001>.
- [79] R. Johnson, N. Sabnis, W.J. McConathy, A.G. Lacko, The potential role of nanotechnology in therapeutic approaches for triple negative breast cancer, *Pharmaceutics*. 5 (2013) 353–370. <https://doi.org/10.3390/pharmaceutics5020353>.
- [80] K.G.K. Deepak, R. Vempati, G.P. Nagaraju, V.R. Dasari, S. Nagini, D.N. Rao, R.R. Malla, Tumor microenvironment: Challenges and opportunities in targeting metastasis of triple negative breast cancer, *Pharmacol. Res.* 153 (2020) 104683. <https://doi.org/10.1016/j.phrs.2020.104683>.
- [81] J. Collignon, L. Lousberg, H. Schroeder, G. Jerusalem, Triple-negative breast cancer: Treatment challenges and solutions, *Breast Cancer Targets Ther.* 8 (2016) 93–107. <https://doi.org/10.2147/BCTT.S69488>.
- [82] C.A. Robertson, D.H. Evans, H. Abrahamse, Photodynamic therapy (PDT): A short review on cellular mechanisms and cancer research applications for PDT, *J. Photochem. Photobiol. B Biol.* 96 (2009) 1–8. <https://doi.org/10.1016/j.jphotobiol.2009.04.001>.
- [83] M.J. Lamberti, N.B.R. Vittar, V.A. Rivarola, Breast cancer as photodynamic therapy target: Enhanced therapeutic efficiency by overview of tumor complexity., *World J. Clin. Oncol.* 5 (2014) 901–907. <https://doi.org/10.5306/wjco.v5.i5.901>.
- [84] K.V. Krishna, N. Saha, A. Puri, Pre-clinical compartmental pharmacokinetic modeling of 2-[1-hexyloxyethyl]-2-devinyl pyropheophorbide-a (HPPH) as a photosensitizer in rat plasma by validated HPLC method, (2019). <https://doi.org/10.1039/c8pp00339d>.
- [85] E.C. Aniogo, B. Plackal Adimuriyil George, H. Abrahamse, The role of photodynamic therapy on multidrug resistant breast cancer, *Cancer Cell Int.* 19 (2019) 1–14. <https://doi.org/10.1186/s12935-019-0815-0>.

- [86] M. Czarnecka-Czapczyńska, D. Aebisher, P. Oleś, B. Sosna, M. Krupka-Olek, K. Dynarowicz, W. Latos, G. Cieślar, A. Kawczyk-Krupka, The role of photodynamic therapy in breast cancer – A review of in vitro research, *Biomed. Pharmacother.* 144 (2021). <https://doi.org/10.1016/j.biopha.2021.112342>.
- [87] N. Tung, J.E. Garber, PARP inhibition in breast cancer: progress made and future hopes, *Npj Breast Cancer.* 8 (2022) 1–5. <https://doi.org/10.1038/s41523-022-00411-3>.
- [88] L. Cortesi, H.S. Rugo, C. Jackisch, An Overview of PARP Inhibitors for the Treatment of Breast Cancer., *Target. Oncol.* 16 (2021) 255–282. <https://doi.org/10.1007/s11523-021-00796-4>.
- [89] G. Guney Eskiler, G. Cecener, U. Egeli, B. Tunca, Talazoparib nanoparticles for overcoming multidrug resistance in triple-negative breast cancer, *J. Cell. Physiol.* 235 (2020) 6230–6245. <https://doi.org/10.1002/jcp.29552>.
- [90] N.R. Vysyaraju, M. Paul, S. Ch, B. Ghosh, S. Biswas, Olaparib@human serum albumin nanoparticles as sustained drug-releasing tumour-targeting nanomedicine to inhibit growth and metastasis in the mouse model of triple-negative breast cancer, *J. Drug Target.* (2022). <https://doi.org/10.1080/1061186X.2022.2092623>.
- [91] D. Lee, S. Kwon, S. young Jang, E. Park, Y. Lee, H. Koo, Overcoming the obstacles of current photodynamic therapy in tumors using nanoparticles, *Bioact. Mater.* 8 (2022) 20–34. <https://doi.org/10.1016/j.bioactmat.2021.06.019>.
- [92] Z.-J. Zhang, K.-P. Wang, J.-G. Mo, L. Xiong, Y. Wen, Photodynamic therapy regulates fate of cancer stem cells through reactive oxygen species., *World J. Stem Cells.* 12 (2020) 562–584. <https://doi.org/10.4252/wjsc.v12.i7.562>.
- [93] J.A. Magalhães, D.C. Arruda, M.S. Baptista, D.B. Tada, Co-Encapsulation of Methylene Blue and PARP-Inhibitor into Poly(Lactic-Co-Glycolic Acid) Nanoparticles for Enhanced PDT of Cancer., *Nanomater.* (Basel, Switzerland). 11 (2021). <https://doi.org/10.3390/nano11061514>.
- [94] S. Lei, F. Ge, M. Lin, X. Wang, J. Shen, Y. Yang, J. Deng, Z. Wang, J. Wang, K. Li, PARP inhibitors diminish DNA damage repair for the enhancement of tumor photodynamic therapy, *Photodiagnosis Photodyn. Ther.* 40 (2022) 103058. <https://doi.org/10.1016/j.pdpdt.2022.103058>.
- [95] N. Jin, Y. Xia, Q. Gao, Combined PARP inhibitors and small molecular inhibitors in solid tumor treatment (Review), *Int. J. Oncol.* 62 (2023) 1–16. <https://doi.org/10.3892/ijo.2023.5476>.

- [96] X. Kong, Y. Qi, X. Wang, R. Jiang, J. Wang, Y. Fang, J. Gao, K. Chu Hwang, Nanoparticle drug delivery systems and their applications as targeted therapies for triple negative breast cancer, *Prog. Mater. Sci.* 134 (2023) 101070. <https://doi.org/10.1016/j.pmatsci.2023.101070>.
- [97] S. Liu, J. Li, L. Gu, K. Wu, H. Xing, Nanoparticles for Chemoimmunotherapy Against Triple-Negative Breast Cancer., *Int. J. Nanomedicine.* 17 (2022) 5209–5227. <https://doi.org/10.2147/IJN.S388075>.
- [98] V. Thakur, R.V. Kutty, Recent advances in nanotheranostics for triple negative breast cancer treatment, *J. Exp. Clin. Cancer Res.* 38 (2019) 1–22. <https://doi.org/10.1186/s13046-019-1443-1>.
- [99] M.J. Mitchell, M.M. Billingsley, R.M. Haley, M.E. Wechsler, N.A. Peppas, R. Langer, Engineering precision nanoparticles for drug delivery, *Nat. Rev. Drug Discov.* 20 (2021) 101–124. <https://doi.org/10.1038/s41573-020-0090-8>.
- [100] J.K. Patra, G. Das, L.F. Fraceto, E. Vangelie, R. Campos, P. Rodriguez, L. Susana, A. Torres, L. Armando, D. Torres, R. Grillo, Nano based drug delivery systems : recent developments and future prospects, *J. Nanobiotechnology.* (2018) 1–33. <https://doi.org/10.1186/s12951-018-0392-8>.
- [101] R. Jadia, J. Kydd, P. Rai, Remotely Phototriggered, Transferrin-Targeted Polymeric Nanoparticles for the Treatment of Breast Cancer, 2018. <https://doi.org/10.1111/php.12903>.
- [102] A. De, P. Roychowdhury, N.R. Bhuyan, Y.T. Ko, S.K. Singh, Folic Acid Functionalized Diallyl Trisulfide – Solid Lipid, (2023) 1–17.
- [103] N.M. Binu, D. Prema, J. Prakash, K. Balagangadharan, P. Balashanmugam, N. Selvamurugan, G.D. Venkatasubbu, Folic acid decorated pH sensitive polydopamine coated honeycomb structured nickel oxide nanoparticles for targeted delivery of quercetin to triple negative breast cancer cells, *Colloids Surfaces A Physicochem. Eng. Asp.* 630 (2021) 127609. <https://doi.org/10.1016/j.colsurfa.2021.127609>.
- [104] G. Vivo-Llorca, V. Candela-Noguera, M. Alfonso, A. García-Fernández, M. Orzáez, F. Sancenón, R. Martínez-Máñez, MUC1 Aptamer-Capped Mesoporous Silica Nanoparticles for Navitoclax Resistance Overcoming in Triple-Negative Breast Cancer, *Chem. - A Eur. J.* 26 (2020) 16318–16327. <https://doi.org/10.1002/chem.202001579>.
- [105] S. Sadat Abolmaali, S. Zarenejad, Y. Mohebi, H. Najafi, S. Javanmardi, M. Abedi, A. Mohammad Tamaddon, Biotin receptor-targeting nanogels loaded with methotrexate for

- enhanced antitumor efficacy in triple-negative breast cancer in vitro and in vivo models., *Int. J. Pharm.* 624 (2022) 122049. <https://doi.org/10.1016/j.ijpharm.2022.122049>.
- [106] X. Hong, X. Xu, Z. Liu, S. Liu, J. Yu, M. Wu, Y. Ma, Q. Shuai, Hyaluronan-fullerene/AIEgen nanogel as CD44-targeted delivery of tirapazamine for synergistic photodynamic-hypoxia activated therapy., *Nanotechnology.* 32 (2021). <https://doi.org/10.1088/1361-6528/ac18da>.
- [107] J. Shi, Y. Ren, J. Ma, X. Luo, J. Li, Y. Wu, H. Gu, C. Fu, Z. Cao, J. Zhang, Novel CD44-targeting and pH/redox-dual-stimuli-responsive core-shell nanoparticles loading triptolide combats breast cancer growth and lung metastasis, *J. Nanobiotechnology.* 19 (2021) 1–22. <https://doi.org/10.1186/s12951-021-00934-0>.
- [108] A.S. Burande, M.K. Viswanadh, A. Jha, A.K. Mehata, A. Shaik, N. Agrawal, S. Poddar, S.K. Mahto, M.S. Muthu, EGFR Targeted Paclitaxel and Piperine Co-loaded Liposomes for the Treatment of Triple Negative Breast Cancer, *AAPS PharmSciTech.* 21 (2020) 1–12. <https://doi.org/10.1208/s12249-020-01671-7>.
- [109] K.H. Jung, J.H. Lee, J.W. Park, D.H. Kim, S.H. Moon, Y.S. Cho, K.H. Lee, Targeted therapy of triple negative MDA-MB-468 breast cancer with curcumin delivered by epidermal growth factor-conjugated phospholipid nanoparticles, *Oncol. Lett.* 15 (2018) 9093–9100. <https://doi.org/10.3892/ol.2018.8471>.
- [110] N. Shekar, P. Mallya, D. V. Gowda, V. Jain, Triple-negative breast cancer: Challenges and treatment options, *Int. J. Res. Pharm. Sci.* 11 (2020) 1977–1986. <https://doi.org/10.26452/ijrps.v11i2.2127>.
- [111] C. Anders, L.A. Carey, Understanding and treating triple-negative breast cancer, *Oncology.* 22 (2008) 1233–1239.
- [112] L.A. Newman, Disparities in breast cancer and African ancestry: A global perspective, *Breast J.* 21 (2015) 133–139. <https://doi.org/10.1111/tbj.12369>.
- [113] E.C. Dietze, N. Carolina, N. Carolina, V.L. Seewaldt, Triple-negative breast cancer in African-American women: disparities versus biology, *Nat Rev Cancer.* 15 (2017) 248–254. <https://doi.org/10.1038/nrc3896>. Triple-negative.
- [114] O. Engebraaten, H.K.M. Vollan, A.L. Børresen-Dale, Triple-negative breast cancer and the need for new therapeutic targets, *Am. J. Pathol.* 183 (2013) 1064–1074. <https://doi.org/10.1016/J.AJPATH.2013.05.033>.
- [115] F.C. Geyer, F. Pareja, B. Weigelt, E. Rakha, I.O. Ellis, S.J. Schnitt, J.S. Reis-Filho, The

- Spectrum of Triple-Negative Breast Disease: High- and Low-Grade Lesions, *Am. J. Pathol.* 187 (2017) 2139–2151. <https://doi.org/10.1016/j.ajpath.2017.03.016>.
- [116] E. Lee, R. McKean-Cowdin, H. Ma, D. V. Spicer, D. Van Den Berg, L. Bernstein, G. Ursin, Characteristics of triple-negative breast cancer in patients with a BRCA1 mutation: Results from a population-based study of young women, *J. Clin. Oncol.* 29 (2011) 4373–4380. <https://doi.org/10.1200/JCO.2010.33.6446>.
- [117] F. Borri, A. Granaglia, Pathology of triple negative breast cancer, *Semin. Cancer Biol.* 72 (2021) 136–145. <https://doi.org/10.1016/j.semcancer.2020.06.005>.
- [118] P. Zagami, L.A. Carey, Triple negative breast cancer: Pitfalls and progress, *Npj Breast Cancer.* 8 (2022). <https://doi.org/10.1038/s41523-022-00468-0>.
- [119] L. Sweatt, S.K. Gower, B.A. Chieh, A.Y. Liu, Y. Li, 乳鼠心肌提取 HHS Public Access, *Physiol. Behav.* 176 (2016) 139–148. <https://doi.org/10.1158/1078-0432.CCR-14-0432.Comprehensive>.
- [120] T.F.S. Mendes, L.D. Kluskens, L.R. Rodrigues, Triple Negative Breast Cancer: Nanosolutions for a Big Challenge, *Adv. Sci.* 2 (2015) 1–14. <https://doi.org/10.1002/advs.201500053>.
- [121] F. Borri, A. Granaglia, Pathology of triple negative breast cancer, *Semin. Cancer Biol.* 72 (2021) 136–145. <https://doi.org/10.1016/j.semcancer.2020.06.005>.
- [122] R. Scully, J. Chen, A. Plug, Y. Xiao, D. Weaver, J. Feunteun, T. Ashley, D.M. Livingston, Association of BRCA1 with Rad51 in mitotic and meiotic cells, *Cell.* 88 (1997) 265–275. [https://doi.org/10.1016/S0092-8674\(00\)81847-4](https://doi.org/10.1016/S0092-8674(00)81847-4).
- [123] W. Zhao, J.B. Steinfeld, F. Liang, X. Chen, G. David, C.J. Ma, Y. Kwon, T. Rao, W. Wang, S. Chen, X. Song, Y. Deng, J. Jimenez-sainz, L. Lu, R.B. Jensen, G.M. Kupfer, C. Wiese, E.C. Greene, P. Sung, HHS Public Access, 550 (2018) 360–365. <https://doi.org/10.1038/nature24060.Promotion>.
- [124] R. Prakash, Y. Zhang, W. Feng, M. Jasin, Homologous recombination and human health: the roles of BRCA1, BRCA2, and associated proteins., *Cold Spring Harb. Perspect. Biol.* 7 (2015) a016600. <https://doi.org/10.1101/cshperspect.a016600>.
- [125] W.K. Holloman, Unraveling the mechanism of BRCA2 in homologous recombination., *Nat. Struct. Mol. Biol.* 18 (2011) 748–754. <https://doi.org/10.1038/nsmb.2096>.
- [126] S. Mylavarapu, A. Das, M. Roy, Role of BRCA mutations in the modulation of response to platinum therapy, *Front. Oncol.* 8 (2018) 1–11. <https://doi.org/10.3389/fonc.2018.00016>.

- [127] E. Choi, G. im Mun, J. Lee, H. Lee, J. Cho, Y.S. Lee, BRCA1 deficiency in triple-negative breast cancer: Protein stability as a basis for therapy, *Biomed. Pharmacother.* 158 (2023) 114090. <https://doi.org/10.1016/j.biopha.2022.114090>.
- [128] J. Zámorszky, B. Szikriszt, J.Z. Gervai, O. Pipek, Á. Póti, M. Krzystanek, D. Ribli, J.M. Szalai-Gindl, I. Csabai, Z. Szallasi, C. Swanton, A.L. Richardson, D. Szüts, Loss of BRCA1 or BRCA2 markedly increases the rate of base substitution mutagenesis and has distinct effects on genomic deletions, *Oncogene.* 36 (2017) 746–755. <https://doi.org/10.1038/onc.2016.243>.
- [129] A.J. Fulcher, D.M. Roth, S. Fatima, G. Alvisi, D.A. Jans, The BRCA-1 binding protein BRAP2 is a novel, negative regulator of nuclear import of viral proteins, dependent on phosphorylation flanking the nuclear localization signal, *FASEB J.* 24 (2010) 1454–1466. <https://doi.org/10.1096/fj.09-136564>.
- [130] 2012 Morris et al., 2012 et al., 基因的改变NIH Public Access, *Gerontology.* 61 (2015) 515–525. <https://doi.org/10.1038/nrm2831.BRCA1>.
- [131] M.Y.T. Keung, Y. Wu, J. V. Vadgama, PARP inhibitors as a therapeutic agent for homologous recombination deficiency in breast cancers, *J. Clin. Med.* 8 (2019). <https://doi.org/10.3390/jcm8040435>.
- [132] C. Valenza, B. Taurelli Salimbeni, C. Santoro, D. Trapani, G. Antonarelli, G. Curigliano, Tumor Infiltrating Lymphocytes across Breast Cancer Subtypes: Current Issues for Biomarker Assessment., *Cancers (Basel).* 15 (2023). <https://doi.org/10.3390/cancers15030767>.
- [133] B. Chaudhary, E. Elkord, Regulatory T Cells in the Tumor Microenvironment and Cancer Progression: Role and Therapeutic Targeting., *Vaccines.* 4 (2016). <https://doi.org/10.3390/vaccines4030028>.
- [134] J.-H. Kim, B.S. Kim, S.-K. Lee, Regulatory T Cells in Tumor Microenvironment and Approach for Anticancer Immunotherapy., *Immune Netw.* 20 (2020) e4. <https://doi.org/10.4110/in.2020.20.e4>.
- [135] R.R. Malla, P. Vasudevaraju, R.K. Vempati, M. Rakshmitha, N. Merchant, G.P. Nagaraju, Regulatory T cells: Their role in triple-negative breast cancer progression and metastasis, *Cancer.* 128 (2022) 1171–1183. <https://doi.org/10.1002/cncr.34084>.
- [136] M. Santoni, E. Romagnoli, T. Saladino, L. Foghini, S. Guarino, M. Capponi, M. Giannini, P.D. Cognigni, G. Ferrara, N. Battelli, Triple negative breast cancer: Key role of Tumor-Associated Macrophages in regulating the activity of anti-PD-1/PD-L1

- agents., *Biochim. Biophys. Acta. Rev. Cancer.* 1869 (2018) 78–84. <https://doi.org/10.1016/j.bbcan.2017.10.007>.
- [137] J. Lee, Current Treatment Landscape for Early Triple-Negative Breast Cancer (TNBC)., *J. Clin. Med.* 12 (2023). <https://doi.org/10.3390/jcm12041524>.
- [138] J. Cao, D. Huang, N.A. Peppas, Advanced engineered nanoparticulate platforms to address key biological barriers for delivering chemotherapeutic agents to target sites., *Adv. Drug Deliv. Rev.* 167 (2020) 170–188. <https://doi.org/10.1016/J.ADDR.2020.06.030>.
- [139] S.K. Sriraman, B. Aryasomayajula, V.P. Torchilin, Barriers to drug delivery in solid tumors., *Tissue Barriers.* 2 (2014) e29528. <https://doi.org/10.4161/tisb.29528>.
- [140] S. Barua, S. Mitragotri, Challenges associated with Penetration of Nanoparticles across Cell and Tissue Barriers: A Review of Current Status and Future Prospects., *Nano Today.* 9 (2014) 223–243. <https://doi.org/10.1016/j.nantod.2014.04.008>.
- [141] D. Rosenblum, N. Joshi, W. Tao, J.M. Karp, D. Peer, Progress and challenges towards targeted delivery of cancer therapeutics, *Nat. Commun.* 9 (2018). <https://doi.org/10.1038/s41467-018-03705-y>.
- [142] E. Blanco, H. Shen, M. Ferrari, Principles of nanoparticle design for overcoming biological barriers to drug delivery, *Nat. Biotechnol.* 33 (2015) 941–951. <https://doi.org/10.1038/nbt.3330>.
- [143] H. Matsumoto, A.A. Thike, H. Li, J. Yeong, S.-L. Koo, R.A. Dent, P.H. Tan, J. Iqbal, Increased CD4 and CD8-positive T cell infiltrate signifies good prognosis in a subset of triple-negative breast cancer., *Breast Cancer Res. Treat.* 156 (2016) 237–247. <https://doi.org/10.1007/s10549-016-3743-x>.
- [144] M. Niu, S. Valdes, Y.W. Naguib, S.D. Hursting, Z. Cui, Tumor-Associated Macrophage-Mediated Targeted Therapy of Triple-Negative Breast Cancer, *Mol. Pharm.* 13 (2016) 1833. <https://doi.org/10.1021/ACS.MOLPHARMACEUT.5B00987>.
- [145] F. Sobande, L. Dušek, A. Matějková, T. Rozkoš, J. Laco, A. Ryška, EGFR in triple negative breast carcinoma: significance of protein expression and high gene copy number., *Cesk. Patol.* 51 (2015) 80–86.
- [146] J. Anampa, D. Makower, J.A. Sparano, Progress in adjuvant chemotherapy for breast cancer: An overview, *BMC Med.* 13 (2015) 1–13. <https://doi.org/10.1186/s12916-015-0439-8>.
- [147] M. Burotto, J. Wilkerson, W.D. Stein, S.E. Bates, T. Fojo, Adjuvant and neoadjuvant

- cancer therapies: A historical review and a rational approach to understand outcomes, *Semin. Oncol.* 46 (2019) 83–99. <https://doi.org/10.1053/J.SEMINONCOL.2019.01.002>.
- [148] K. Kim, H.J. Park, K.H. Shin, J.H. Kim, D.H. Choi, W. Park, S. Do Ahn, S.S. Kim, D.Y. Kim, T.H. Kim, J.H. Kim, J. Kim, Breast Conservation Therapy Versus Mastectomy in Patients with T1-2N1 Triple-Negative Breast Cancer: Pooled Analysis of KROG 14-18 and 14-23., *Cancer Res. Treat.* 50 (2018) 1316–1323. <https://doi.org/10.4143/crt.2017.575>.
- [149] L. Guo, G. Xie, R. Wang, L. Yang, L. Sun, M. Xu, W. Yang, M.C. Chung, Local treatment for triple-negative breast cancer patients undergoing chemotherapy: breast-conserving surgery or total mastectomy?, *BMC Cancer.* 21 (2021) 717. <https://doi.org/10.1186/s12885-021-08429-9>.
- [150] M.Y. He, C. Rancoule, A. Rehailia-Blanchard, S. Espenel, J.C. Trone, E. Bernichon, E. Guillaume, A. Vallard, N. Magné, Radiotherapy in triple-negative breast cancer: Current situation and upcoming strategies, *Crit. Rev. Oncol. Hematol.* 131 (2018) 96–101. <https://doi.org/10.1016/J.CRITREVONC.2018.09.004>.
- [151] R. Baskar, K.A. Lee, R. Yeo, K.W. Yeoh, Cancer and radiation therapy: current advances and future directions, *Int. J. Med. Sci.* 9 (2012) 193–199. <https://doi.org/10.7150/IJMS.3635>.
- [152] C. Kan, J. Zhang, BRCA1 Mutation: A Predictive Marker for Radiation Therapy?, *Int. J. Radiat. Oncol. Biol. Phys.* 93 (2015) 281. <https://doi.org/10.1016/J.IJROBP.2015.05.037>.
- [153] B.S. Abdulkarim, J. Cuartero, J. Hanson, J. Deschênes, D. Lesniak, S. Sabri, Increased risk of locoregional recurrence for women with T1-2N0 triple-negative breast cancer treated with modified radical mastectomy without adjuvant radiation therapy compared with breast-conserving therapy, *J. Clin. Oncol.* 29 (2011) 2852–2858. <https://doi.org/10.1200/JCO.2010.33.4714>.
- [154] A.K. Mehta, E.M. Cheney, C.A. Hartl, C. Pantelidou, M. Oliwa, J.A. Castrillon, J.-R. Lin, K.E. Hurst, M. de Oliveira Taveira, N.T. Johnson, W.M. Oldham, M. Kalocsay, M.J. Berberich, S.A. Boswell, A. Kothari, S. Johnson, D.A. Dillon, M. Lipschitz, S. Rodig, S. Santagata, J.E. Garber, N. Tung, J. Yélamos, J.E. Thaxton, E.A. Mittendorf, P.K. Sorger, G.I. Shapiro, J.L. Guerriero, Targeting immunosuppressive macrophages overcomes PARP inhibitor resistance in BRCA1-associated triple-negative breast

- cancer., *Nat. Cancer.* 2 (2021) 66–82. <https://doi.org/10.1038/s43018-020-00148-7>.
- [155] D. Massihnia, A. Galvano, D. Fanale, A. Perez, M. Castiglia, L. Incorvaia, A. Listi, S. Rizzo, G. Cicero, V. Bazan, S. Castorina, A. Russo, Triple negative breast cancer: Shedding light onto the role of pi3k/akt/mTOR pathway, *Oncotarget.* 7 (2016) 60712–60722. <https://doi.org/10.18632/oncotarget.10858>.
- [156] W. Alshaer, H. Hillaireau, J. Vergnaud, S. Mura, C. Deloménie, F. Sauvage, S. Ismail, E. Fattal, Aptamer-guided siRNA-loaded nanomedicines for systemic gene silencing in CD-44 expressing murine triple-negative breast cancer model, *J. Control. Release.* 271 (2018) 98–106. <https://doi.org/10.1016/j.jconrel.2017.12.022>.
- [157] D. Cretella, A. Ravelli, C. Fumarola, S. La Monica, G. Digiacomo, A. Cavazzoni, R. Alfieri, A. Biondi, D. Generali, M. Bonelli, P.G. Petronini, The anti-tumor efficacy of CDK4/6 inhibition is enhanced by the combination with PI3K/AKT/mTOR inhibitors through impairment of glucose metabolism in TNBC cells, *J. Exp. Clin. Cancer Res.* 37 (2018) 1–12. <https://doi.org/10.1186/s13046-018-0741-3>.
- [158] A. Marra, G. Viale, G. Curigliano, Recent advances in triple negative breast cancer : the immunotherapy era, (2019) 1–9.
- [159] E.S. Stovgaard, D. Nielsen, E. Hogdall, E. Balslev, Triple negative breast cancer - prognostic role of immune-related factors: a systematic review., *Acta Oncol.* 57 (2018) 74–82. <https://doi.org/10.1080/0284186X.2017.1400180>.
- [160] X. Zhu, W. Zhou, The emerging regulation of VEGFR-2 in triple-negative breast cancer, *Front. Endocrinol. (Lausanne).* 6 (2015) 1–7. <https://doi.org/10.3389/fendo.2015.00159>.
- [161] J. Sukumar, K. Gast, D. Quiroga, M. Lustberg, N. Williams, Triple-negative breast cancer: promising prognostic biomarkers currently in development, *Expert Rev. Anticancer Ther.* 21 (2021) 135–148. <https://doi.org/10.1080/14737140.2021.1840984>.
- [162] S. Ghosh, A. Javia, S. Shetty, D. Bardoliwala, K. Maiti, S. Banerjee, A. Khopade, A. Misra, K. Sawant, S. Bhowmick, Triple negative breast cancer and non-small cell lung cancer: Clinical challenges and nano-formulation approaches, *J. Control. Release.* 337 (2021) 27–58. <https://doi.org/10.1016/j.jconrel.2021.07.014>.
- [163] K. Nakai, M.C. Hung, H. Yamaguchi, A perspective on anti-EGFR therapies targeting triple-negative breast cancer, *Am. J. Cancer Res.* 6 (2016) 1609–1623.
- [164] Y. Wang, T. Zhang, N. Kwiatkowski, B.J. Abraham, T.I. Lee, S. Xie, H. Yuzugullu, T. Von, H. Li, Z. Lin, D.G. Stover, E. Lim, Z.C. Wang, J.D. Iglehart, R.A. Young, N.S. Gray, J.J. Zhao, CDK7-Dependent Transcriptional Addiction in Triple-Negative Breast

- Cancer, *Cell*. 163 (2015) 174–186. <https://doi.org/10.1016/j.cell.2015.08.063>.
- [165] Y. Si, Y. Xu, J.S. Guan, K. Chen, S. Kim, E.S. Yang, L. Zhou, X.M. Liu, Anti-EGFR antibody-drug conjugate for triple-negative breast cancer therapy, *Eng. Life Sci.* 21 (2021) 37–44. <https://doi.org/10.1002/elsc.202000027>.
- [166] Y.-C. Su, P.-A. Burnouf, K.-H. Chuang, B.-M. Chen, T.-L. Cheng, S.R. Roffler, Conditional internalization of PEGylated nanomedicines by PEG engagers for triple negative breast cancer therapy., *Nat. Commun.* 8 (2017) 15507. <https://doi.org/10.1038/ncomms15507>.
- [167] J.J.J. Geenen, S.C. Linn, J.H. Beijnen, J.H.M. Schellens, PARP Inhibitors in the Treatment of Triple-Negative Breast Cancer, *Clin. Pharmacokinet.* 57 (2018) 427–437. <https://doi.org/10.1007/s40262-017-0587-4>.
- [168] T.G. Lyons, Targeted Therapies for Triple-Negative Breast Cancer, *Curr. Treat. Options Oncol.* 20 (2019). <https://doi.org/10.1007/s11864-019-0682-x>.
- [169] J.C. Amé, C. Spenlehauer, G. De Murcia, The PARP superfamily, *BioEssays*. 26 (2004) 882–893. <https://doi.org/10.1002/bies.20085>.
- [170] J.C. Amé, V. Rolli, V. Schreiber, C. Niedergang, F. Apiou, P. Decker, S. Muller, T. Höger, J. Ménissier-de Murcia, G. De Murcia, PARP-2, a novel mammalian DNA damage-dependent poly(ADP-ribose) polymerase, *J. Biol. Chem.* 274 (1999) 17860–17868. <https://doi.org/10.1074/jbc.274.25.17860>.
- [171] J.C. Morales, L. Li, F.J. Fattah, Y. Dong, E.A. Bey, M. Patel, J. Gao, D.A. Boothman, Review of poly (ADP-ribose) polymerase (PARP) mechanisms of action and rationale for targeting in cancer and other diseases, *Crit. Rev. Eukaryot. Gene Expr.* 24 (2014) 15–28. <https://doi.org/10.1615/CritRevEukaryotGeneExpr.2013006875>.
- [172] T. Lindahl, M.S. Satoh, G.G. Poirier, A. Klungland, Post-translational modification of poly(ADP-ribose) polymerase induced by DNA strand breaks, *Trends Biochem. Sci.* 20 (1995) 405–411. [https://doi.org/10.1016/S0968-0004\(00\)89089-1](https://doi.org/10.1016/S0968-0004(00)89089-1).
- [173] S. Godar, T.A. Ince, G.W. Bell, D. Feldser, J.L. Donaher, J. Bergh, A. Liu, K. Miu, R.S. Watnick, F. Reinhardt, S.S. McAllister, T. Jacks, R.A. Weinberg, Growth-Inhibitory and Tumor- Suppressive Functions of p53 Depend on Its Repression of CD44 Expression, *Cell*. 134 (2008) 62–73. <https://doi.org/10.1016/j.cell.2008.06.006>.
- [174] N.C. Synnott, A. Murray, P.M. McGowan, M. Kiely, P.A. Kiely, N. O'Donovan, D.P. O'Connor, W.M. Gallagher, J. Crown, M.J. Duffy, Mutant p53: a novel target for the treatment of patients with triple-negative breast cancer?, *Int. J. Cancer.* 140 (2017) 234–

246. <https://doi.org/10.1002/ijc.30425>.
- [175] S.P. Shah, A. Roth, R. Goya, A. Oloumi, G. Ha, Y. Zhao, G. Turashvili, J. Ding, K. Tse, G. Haffari, A. Bashashati, L.M. Prentice, J. Khattra, A. Burleigh, D. Yap, V. Bernard, A. McPherson, K. Shumansky, A. Crisan, R. Giuliany, A. Heravi-Moussavi, J. Rosner, D. Lai, I. Birol, R. Varhol, A. Tam, N. Dhalla, T. Zeng, K. Ma, S.K. Chan, M. Griffith, A. Moradian, S.-W.G. Cheng, G.B. Morin, P. Watson, K. Gelmon, S. Chia, S.-F. Chin, C. Curtis, O.M. Rueda, P.D. Pharoah, S. Damaraju, J. Mackey, K. Hoon, T. Harkins, V. Tadigotla, M. Sigaroudinia, P. Gascard, T. Tlsty, J.F. Costello, I.M. Meyer, C.J. Eaves, W.W. Wasserman, S. Jones, D. Huntsman, M. Hirst, C. Caldas, M.A. Marra, S. Aparicio, The clonal and mutational evolution spectrum of primary triple-negative breast cancers., *Nature*. 486 (2012) 395–399. <https://doi.org/10.1038/nature10933>.
- [176] Z. Lu, G. Jiang, P. Blume-Jensen, T. Hunter, Epidermal growth factor-induced tumor cell invasion and metastasis initiated by dephosphorylation and downregulation of focal adhesion kinase., *Mol. Cell. Biol.* 21 (2001) 4016–4031. <https://doi.org/10.1128/MCB.21.12.4016-4031.2001>.
- [177] S.A. Eccles, The epidermal growth factor receptor/Erb-B/HER family in normal and malignant breast biology., *Int. J. Dev. Biol.* 55 (2011) 685–696. <https://doi.org/10.1387/ijdb.113396se>.
- [178] F. Podo, L.M.C. Buydens, H. Degani, R. Hilhorst, E. Klipp, I.S. Gribbestad, S. Van Huffel, H. W.M. van Laarhoven, J. Luts, D. Monleon, G.J. Postma, N. Schneiderhan-Marra, F. Santoro, H. Wouters, H.G. Russnes, T. Sørli, E. Tagliabue, A.L. Børresen-Dale, Triple-negative breast cancer: present challenges and new perspectives, *Mol. Oncol.* 4 (2010) 209–229. <https://doi.org/10.1016/J.MOLONC.2010.04.006>.
- [179] C. Neophytou, P. Boutsikos, P. Papageorgis, Molecular Mechanisms and Emerging Therapeutic Targets of Triple-Negative Breast Cancer Metastasis, *Front. Oncol.* 8 (2018). <https://doi.org/10.3389/FONC.2018.00031>.
- [180] R. Dent, M. Trudeau, K.I. Pritchard, W.M. Hanna, H.K. Kahn, C.A. Sawka, L.A. Lickley, E. Rawlinson, P. Sun, S.A. Narod, Triple-negative breast cancer: clinical features and patterns of recurrence, *Clin. Cancer Res.* 13 (2007) 4429–4434. <https://doi.org/10.1158/1078-0432.CCR-06-3045>.
- [181] B. Arneth, Tumor Microenvironment, *Medicina (Kaunas)*. 56 (2019). <https://doi.org/10.3390/MEDICINA56010015>.
- [182] T.L. Whiteside, The tumor microenvironment and its role in promoting tumor growth,

- Oncogene. 27 (2008) 5904–5912. <https://doi.org/10.1038/ONC.2008.271>.
- [183] T. Yu, G. Di, Role of tumor microenvironment in triple-negative breast cancer and its prognostic significance., *Chin. J. Cancer Res.* 29 (2017) 237–252. <https://doi.org/10.21147/j.issn.1000-9604.2017.03.10>.
- [184] S.K. Deshmukh, S.K. Srivastava, N. Tyagi, A. Ahmad, A.P. Singh, A.A.L. Ghadhban, D.L. Dyess, J.E. Carter, K. Dugger, S. Singh, Emerging evidence for the role of differential tumor microenvironment in breast cancer racial disparity: a closer look at the surroundings., *Carcinogenesis.* 38 (2017) 757–765. <https://doi.org/10.1093/carcin/bgx037>.
- [185] D.F. Quail, J.A. Joyce, Microenvironmental regulation of tumor progression and metastasis, *Nat. Med.* 19 (2013) 1423–1437. <https://doi.org/10.1038/NM.3394>.
- [186] F. Xing, J. Saidou, K. Watabe, Cancer associated fibroblasts (CAFs) in tumor microenvironment, *Front. Biosci. (Landmark Ed.)* 15 (2010) 166–179. <https://doi.org/10.2741/3613>.
- [187] J. Zhou, X.-H. Wang, Y.-X. Zhao, C. Chen, X.-Y. Xu, Q. Sun, H.-Y. Wu, M. Chen, J.-F. Sang, L. Su, X.-Q. Tang, X.-B. Shi, Y. Zhang, Q. Yu, Y.-Z. Yao, W.-J. Zhang, Cancer-Associated Fibroblasts Correlate with Tumor-Associated Macrophages Infiltration and Lymphatic Metastasis in Triple Negative Breast Cancer Patients., *J. Cancer.* 9 (2018) 4635–4641. <https://doi.org/10.7150/jca.28583>.
- [188] Z. Zhao, A. Ukidve, V. Krishnan, S. Mitragotri, Effect of physicochemical and surface properties on in vivo fate of drug nanocarriers, *Adv. Drug Deliv. Rev.* 143 (2019) 3–21. <https://doi.org/https://doi.org/10.1016/j.addr.2019.01.002>.
- [189] S. Hejmady, R. Pradhan, A. Alexander, M. Agrawal, G. Singhvi, B. Gorain, S. Tiwari, P. Kesharwani, S.K. Dubey, Recent advances in targeted nanomedicine as promising antitumor therapeutics, *Drug Discov. Today.* 25 (2020) 2227–2244. <https://doi.org/10.1016/j.drudis.2020.09.031>.
- [190] R. Pradhan, S.K. Dubey, A. Puri, R. Taliyan, Development and validation of a stability-indicating reversed-phase-high-performance liquid chromatography method for quantification of 2-[1-hexyloxyethyl]-2-devinyl pyropheophorbide-a from lipid-polymeric hybrid nanoparticles, *Sep. Sci. Plus.* 6 (2023) 1–13. <https://doi.org/10.1002/sscp.202200061>.
- [191] R. Jain, R. Pradhan, S. Hejmady, G. Singhvi, S.K. Dubey, Fluorescence-based method for sensitive and rapid estimation of chlorin e6 in stealth liposomes for photodynamic

- therapy against cancer, *Spectrochim. Acta - Part A Mol. Biomol. Spectrosc.* 244 (2021) 118823. <https://doi.org/10.1016/j.saa.2020.118823>.
- [192] R. Pradhan, K. V. Krishna, G. Wadhwa, R. Taliyan, R. Khadgawat, G. Kachhawa, G. Singhvi, S.K. Dubey, QbD-driven development and validation of HPLC method for determination of Bisphenol A and Bis-sulphone in environmental samples, *Int. J. Environ. Anal. Chem.* 100 (2020) 42–54. <https://doi.org/10.1080/03067319.2019.1629585>.
- [193] R. Jain, R. Pradhan, S. Hejmady, G. Singhvi, S.K. Dubey, Fluorescence-based method for sensitive and rapid estimation of chlorin e6 in stealth liposomes for photodynamic therapy against cancer, *Spectrochim. Acta - Part A Mol. Biomol. Spectrosc.* 244 (2021) 118823. <https://doi.org/10.1016/j.saa.2020.118823>.
- [194] S.K. Puttrevu, T.S. Laxman, A.K. Tripathi, A.K. Yadav, S.K. Verma, A. Mishra, R. Pradhan, N.K. Verma, J.K. Ghosh, R.S. Bhatta, Liquid chromatography–tandem mass spectrometry based method development and validation of S016-1271 (LR8P), a novel cationic antimicrobial peptide for its application to pharmacokinetic studies, *J. Pharm. Biomed. Anal.* 169 (2019) 116–126. <https://doi.org/10.1016/j.jpba.2019.01.046>.
- [195] R. Pradhan, S. Hejmady, R. Taliyan, R. Khadgawat, T. Gupta, G. Kachhawa, R. Kumar, G. Singhvi, S. Kumar Dubey, Simultaneous estimation of parabens and bisphenol a in ready-to-eat foodstuffs by using QbD-driven high-pressure liquid chromatography method, *Int. J. Environ. Anal. Chem.* 00 (2020) 1–16. <https://doi.org/10.1080/03067319.2020.1756272>.
- [196] V.K. Rapalli, V. Kaul, S. Gorantla, T. Waghule, S.K. Dubey, M.M. Pandey, G. Singhvi, UV Spectrophotometric method for characterization of curcumin loaded nanostructured lipid nanocarriers in simulated conditions: Method development, in-vitro and ex-vivo applications in topical delivery, *Spectrochim. Acta - Part A Mol. Biomol. Spectrosc.* 224 (2020) 117392. <https://doi.org/10.1016/j.saa.2019.117392>.
- [197] V.K. Rapalli, G. Singhvi, S. Gorantla, T. Waghule, S.K. Dubey, R.N. Saha, M.S. Hasnain, A.K. Nayak, Stability indicating liquid chromatographic method for simultaneous quantification of betamethasone valerate and tazarotene in in vitro and ex vivo studies of complex nanoformulation, *J. Sep. Sci.* 42 (2019) 3413–3420. <https://doi.org/10.1002/jssc.201900538>.
- [198] V.K. Venishetty, N. Parikh, R. Sistla, F.J. Ahmed, P.V. Diwan, Application of validated RP-HPLC method for simultaneous determination of docetaxel and ketoconazole in

- solid lipid nanoparticles, *J. Chromatogr. Sci.* 49 (2011) 136–141. <https://doi.org/10.1093/chrsi/49.2.136>.
- [199] S.S. Mannemala, J.S.K. Nagarajan, Development and validation of a generic liquid chromatographic method for the simultaneous determination of five commonly used antimalarial drugs: Application to pharmaceutical formulations and human plasma, *J. Sep. Sci.* 38 (2015) 1521–1528. <https://doi.org/10.1002/jssc.201401465>.
- [200] N. Patani, M. Patel, R. Patel, Development and validation of HPLC methodology for quantitative estimation of Efinaconazole in topical pharmaceutical formulation prepared in-house for the treatment of onychomycosis, *Sep. Sci. Plus.* 3 (2020) 375–383. <https://doi.org/10.1002/sscp.202000019>.
- [201] A. Mahmoudi, M.S. Boukhechem, Simplified HPLC method for simultaneous determination of erythromycin and tretinoin in topical gel form, *Sep. Sci. Plus.* 3 (2020) 86–93. <https://doi.org/10.1002/sscp.201900093>.
- [202] P.J. Parmar, V.B. Patel, D.A. Shah, Stability indicating LC method for estimation of Valbenazine and its degradation kinetic study, *Sep. Sci. Plus.* 3 (2020) 94–101. <https://doi.org/10.1002/sscp.202000003>.
- [203] O. Esim, M. Gumustas, C. Hascicek, S.A. Ozkan, A novel stability-indicating analytical method development for simultaneous determination of carboplatin and decitabine from nanoparticles, *J. Sep. Sci.* 43 (2020) 3491–3498. <https://doi.org/10.1002/jssc.202000320>.
- [204] B. Mangla, K.S. Patel, P. Kumar, K. Kohli, Validation of forced degradation and stability indicating studies of Tamoxifen in nanoformulation using spectroscopic technique, *Mater. Today Proc.* 26 (2019) 3265–3270. <https://doi.org/10.1016/j.matpr.2020.02.910>.
- [205] N.S. Abdelwahab, M.M. Abdelrahman, Stability indicating RP-HPLC method for the determination of flubendazole in pharmaceutical dosage forms, *RSC Adv.* 5 (2015) 10927–10935. <https://doi.org/10.1039/c4ra11758a>.
- [206] H. Services, Analytical Procedures and Methods Validation for Drugs and Biologics Guidance for Industry Analytical Procedures and Methods Validation for Drugs and Biologics Guidance for Industry, (2015).
- [207] G. Mustafa, A. Ahuja, S. Baboota, J. Ali, Box-Behnken supported validation of stability-indicating high performance thin-layer chromatography (HPTLC) method: An application in degradation kinetic profiling of ropinirole, *Saudi Pharm. J.* 21 (2013) 93–

102. <https://doi.org/10.1016/j.jsps.2011.11.006>.
- [208] R. Pradhan, Development and validation of a stability-indicating reversed-phase – high-performance liquid chromatography method for quantification of 2- [1-hexyloxyethyl] -2-devinyl pyropheophorbide-a from lipid-polymeric hybrid nanoparticles, (2023) 1–13. <https://doi.org/10.1002/sscp.202200061>.
- [209] P. Daumar, R. Dufour, C. Dubois, F. Penault-Llorca, M. Bamdad, E. Mounetou, Development and validation of a high-performance liquid chromatography method for the quantitation of intracellular PARP inhibitor Olaparib in cancer cells, *J. Pharm. Biomed. Anal.* 152 (2018) 74–80. <https://doi.org/10.1016/j.jpba.2018.01.036>.
- [210] K.M. Patel, B.N. Suhagia, I. Singhvi, Analytical Method Development and Validation for Enrofloxacin in Bulk and Formulation by RP-HPLC Method, 8 (2018).
- [211] N. Caballero-Casero, L. Lunar, S. Rubio, Analytical methods for the determination of mixtures of bisphenols and derivatives in human and environmental exposure sources and biological fluids. A review, *Anal. Chim. Acta.* 908 (2016) 22–53. <https://doi.org/10.1016/j.aca.2015.12.034>.
- [212] R. Peraman, K. Bhadraya, Yp. reddy, Cs. reddy, T. Lokesh, Analytical quality by design approach in RP-HPLC method development for the assay of etofenamate in dosage forms, *Indian J. Pharm. Sci.* 77 (2016) 751. <https://doi.org/10.4103/0250-474x.174971>.
- [213] R.P.A.-R.P.A.-S.H.A.-R.T.A.-R.K.A.-T.G.A.-G.K.A.-R.K.A.-G.S.A.-S.K. Dubey, Simultaneous estimation of parabens and bisphenol a in ready-to-eat foodstuffs by using QbD-driven high-pressure liquid chromatography method, *Int. J. Environ. Anal. Chem.* v. 102 (2022) 2363-2378–2022 v.102 no.10. <https://doi.org/10.1080/03067319.2020.1756272>.
- [214] I.R. Kothari, K.S. Italiya, S. Sharma, A. Mittal, D. Chitkara, A rapid and precise liquid chromatographic method for simultaneous determination of alpha lipoic acid and docetaxel in lipid-based nanoformulations, *J. Chromatogr. Sci.* 56 (2018) 888–894. <https://doi.org/10.1093/chromsci/bmy064>.
- [215] I.P. Mabbu, G. Sumathi, N. Devanna, A novel LC-MS method development and validation for the determination of phenyl vinyl sulfone in eletriptan hydrobromide, *Futur. J. Pharm. Sci.* 7 (2021). <https://doi.org/10.1186/s43094-020-00175-2>.
- [216] D. Kavitaapu, A. Maruthapillai, S. Devikala, J.A. Selvi, M. Tamilselvi, S. Mahapatra, G.P. Kumar, P.K. Tyagi, New Rapid Stability indicating RP-UPLC Method for the Determination of Olaparib, its Related Substances and Degradation Products in Bulk

- drug and Dosage Form, *Mater. Today Proc.* 14 (2019) 492–503. <https://doi.org/https://doi.org/10.1016/j.matpr.2019.04.172>.
- [217] S.K. Puttrevu, T.S. Laxman, A.K. Tripathi, A.K. Yadav, S.K. Verma, A. Mishra, R. Pradhan, N.K. Verma, J.K. Ghosh, R.S. Bhatta, Liquid chromatography–tandem mass spectrometry based method development and validation of S016-1271 (LR8P), a novel cationic antimicrobial peptide for its application to pharmacokinetic studies, *J. Pharm. Biomed. Anal.* 169 (2019) 116–126. <https://doi.org/10.1016/j.jpba.2019.01.046>.
- [218] T.S. Laxman, S.K. Puttrevu, R. Pradhan, A. Mishra, S. Verma, Y.S. Chhonker, S. Srivastava, S.P. Singh, K. V. Sashidhara, R.S. Bhatta, Pharmacokinetics, metabolism, bioavailability, tissue distribution and excretion studies of 16 α -hydroxycyclohexa-3, 13(14) Z -dien-15, 16-olide—a novel HMG-CoA reductase inhibitor, *Naunyn-Schmiedeberg's Arch. Pharmacol.* 391 (2018) 965–973. <https://doi.org/10.1007/s00210-018-1518-0>.
- [219] S. Mohamed, R. Riva, M. Contin, Novel UHPLC-MS/MS method for the determination of rotigotine in the plasma of patients with Parkinson's disease, *Biomed. Chromatogr.* 31 (2017) 1–6. <https://doi.org/10.1002/bmc.3944>.
- [220] P. Sengupta, B. Chatterjee, U.K. Mandal, B. Gorain, T.K. Pal, Development and validation of a high throughput LC–MS/MS method for simultaneous quantitation of pioglitazone and telmisartan in rat plasma and its application to a pharmacokinetic study, *J. Pharm. Anal.* 7 (2017) 381–387. <https://doi.org/10.1016/j.jpha.2017.05.004>.
- [221] R. Ramakrishna, S. kumar Puttrevu, M. Bhateria, V. Bala, V.L. Sharma, R.S. Bhatta, Simultaneous determination of azilsartan and chlorthalidone in rat and human plasma by liquid chromatography-electrospray tandem mass spectrometry, *J. Chromatogr. B Anal. Technol. Biomed. Life Sci.* 990 (2015) 185–197. <https://doi.org/10.1016/j.jchromb.2015.03.018>.
- [222] M. Bhateria, R. Ramakrishna, S.K. Puttrevu, S. Yerrabelli, A.K. Saxena, R.S. Bhatta, Pre-clinical investigation of plasma pharmacokinetics and biodistribution of a novel antithrombotic agent S002-333 in mice using LC–MS/MS, *J. Chromatogr. B Anal. Technol. Biomed. Life Sci.* 1031 (2016) 154–162. <https://doi.org/10.1016/j.jchromb.2016.07.030>.
- [223] L. Hou, J. Yao, J. Zhou, Simultaneous LC-MS analysis of paclitaxel and retinoic acid in plasma and tissues from tumor-bearing mice, *Chromatographia.* 73 (2011) 471–480. <https://doi.org/10.1007/s10337-010-1903-4>.

- [224] B. Ni, S. Cao, L. Feng, X. Yin, W. Wang, X. Zhang, J. Ni, Simultaneous Analysis of Quercetin and Naringenin in Rat Plasma by Liquid Chromatography-Tandem Mass Spectrometry: Application to a Pharmacokinetic Study after Oral Administration, *J. Chromatogr. Sci.* 54 (2016) 1359–1364. <https://doi.org/10.1093/chromsci/bmw079>.
- [225] T. Margaryan, M. Elliott, N. Sanai, A. Tovmasyan, Simultaneous determination of LY3214996, abemaciclib, and M2 and M20 metabolites in human plasma, cerebrospinal fluid, and brain tumor by LC-MS/MS, *J. Pharm. Anal.* 12 (2022) 601–609. <https://doi.org/10.1016/j.jpha.2022.05.003>.
- [226] M. Al-Shehri, M. Hefnawy, H. Abuelizz, A. Alzamil, M. Mohammed, N. Alsaif, A. Almehezia, H. Alkahtani, M. Abounassif, Development and validation of an UHPLC-MS/MS method for simultaneous determination of palbociclib, letrozole and its metabolite carbinol in rat plasma and pharmacokinetic study application, *Arab. J. Chem.* 13 (2020) 4024–4034. <https://doi.org/10.1016/j.arabjc.2019.05.005>.
- [227] D. Li, G. Zhao, W. Ai, G. Li, L. Si, J. Huang, Y. Chen, S. Wu, Simultaneous LC-MS/MS bioanalysis of etoposide and paclitaxel in mouse tissues and plasma after oral administration of self-microemulsifying drug-delivery systems, *Biomed. Chromatogr.* 32 (2018) 1–9. <https://doi.org/10.1002/bmc.4192>.
- [228] X. Jin, F. Zhou, Y. Liu, C. Cheng, L. Yao, Y. Jia, G. Wang, J. Zhang, Simultaneous determination of parecoxib and its main metabolites valdecoxib and hydroxylated valdecoxib in mouse plasma with a sensitive LC-MS/MS method to elucidate the decreased drug metabolism of tumor bearing mice, *J. Pharm. Biomed. Anal.* 158 (2018) 1–7. <https://doi.org/10.1016/j.jpba.2018.05.034>.
- [229] M. Mehdizadeh, H. Rouhani, N. Sepehri, R. Varshochian, M.H. Ghahremani, M. Amini, M. Gharghabi, S.N. Ostad, F. Atyabi, A. Baharian, R. Dinarvand, Biotin decorated PLGA nanoparticles containing SN-38 designed for cancer therapy, *Artif. Cells, Nanomedicine, Biotechnol.* 45 (2017) 495–504. <https://doi.org/10.1080/21691401.2016.1178130>.
- [230] S. Mazumdar, K.S. Italiya, S. Sharma, D. Chitkara, A. Mittal, Effective cellular internalization, cell cycle arrest and improved pharmacokinetics of Tamoxifen by cholesterol based lipopolymeric nanoparticles, *Int. J. Pharm.* 543 (2018) 96–106. <https://doi.org/10.1016/j.ijpharm.2018.03.022>.
- [231] M.L. Chen, C.J. Lai, Y.N. Lin, C.M. Huang, Y.H. Lin, Multifunctional nanoparticles for targeting the tumor microenvironment to improve synergistic drug combinations and

- cancer treatment effects, *J. Mater. Chem. B.* 8 (2020) 10416–10427. <https://doi.org/10.1039/d0tb01733g>.
- [232] S. Sharma, S. Mazumdar, K.S. Italiya, R.I. Mahato, A. Mittal, D. Chitkara, Cholesterol and Morpholine Grafted Cationic Amphiphilic Copolymers for miRNA-34a Delivery Cholesterol and Morpholine Grafted Cationic Amphiphilic Copolymers for miRNA- Department of Pharmaceutical Sciences , University of Nebraska Medical Center, (2018). <https://doi.org/10.1021/acs.molpharmaceut.8b00228>.
- [233] P. Zhao, G. Xia, S. Dong, Z.-X. Jiang, M. Chen, An iTEP-salinomycin nanoparticle that specifically and effectively inhibits metastases of 4T1 orthotopic breast tumors, *Biomaterials.* 93 (2016) 1–9. <https://doi.org/https://doi.org/10.1016/j.biomaterials.2016.03.032>.
- [234] S. Agrawal, M. Dwivedi, H. Ahmad, S.B. Chadchan, A. Arya, R. Sikandar, S. Kaushik, K. Mitra, R.K. Jha, A.K. Dwivedi, CD44 targeting hyaluronic acid coated lapatinib nanocrystals foster the efficacy against triple-negative breast cancer, *Nanomedicine Nanotechnology, Biol. Med.* 14 (2018) 327–337. <https://doi.org/10.1016/j.nano.2017.10.010>.
- [235] S.S. Pukale, S. Sharma, M. Dalela, A. kumar Singh, S. Mohanty, A. Mittal, D. Chitkara, Multi-component clobetasol-loaded monolithic lipid-polymer hybrid nanoparticles ameliorate imiquimod-induced psoriasis-like skin inflammation in Swiss albino mice, *Acta Biomater.* 115 (2020) 393–409. <https://doi.org/10.1016/j.actbio.2020.08.020>.
- [236] D.H. Surve, A.B. Jindal, Development and validation of reverse-phase high-performance liquid chromatographic (RP-HPLC) method for quantification of Efavirenz in Efavirenz-Enfuvirtide co-loaded polymer-lipid hybrid nanoparticles, *J. Pharm. Biomed. Anal.* 175 (2019) 112765. <https://doi.org/10.1016/j.jpba.2019.07.013>.
- [237] S. Handali, E. Moghimipour, M. Rezaei, Z. Ramezani, M. Kouchak, M. Amini, K.A. Angali, S. Saremy, F.A. Dorkoosh, A novel 5-Fluorouracil targeted delivery to colon cancer using folic acid conjugated liposomes, *Biomed. Pharmacother.* 108 (2018) 1259–1273. <https://doi.org/10.1016/j.biopha.2018.09.128>.
- [238] Y.F. Zhang, Y.F. Wu, T.J. Lan, Y. Chen, S.H. Su, Codelivery of Anticancer Drug and Photosensitizer by PEGylated Graphene Oxide and Cell Penetrating Peptide Enhanced Tumor-Suppressing Effect on Osteosarcoma, *Front. Mol. Biosci.* 7 (2021) 1–9. <https://doi.org/10.3389/fmolb.2020.618896>.
- [239] M. Mehdizadeh, H. Rouhani, N. Sepehri, R. Varshochian, M.H. Ghahremani, M. Amini,

- M. Gharghabi, S.N. Ostad, F. Atyabi, A. Baharian, R. Dinarvand, Biotin decorated PLGA nanoparticles containing SN-38 designed for cancer therapy, *Artif. Cells, Nanomedicine Biotechnol.* 45 (2017) 495–504. <https://doi.org/10.1080/21691401.2016.1178130>.
- [240] N. Sharma, P. Madan, S. Lin, Effect of process and formulation variables on the preparation of parenteral paclitaxel-loaded biodegradable polymeric nanoparticles: A co-surfactant study, *Asian J. Pharm. Sci.* 11 (2016) 404–416. <https://doi.org/https://doi.org/10.1016/j.ajps.2015.09.004>.
- [241] S. Raman, A.A. Khan, S. Mahmood, Nose to brain delivery of selegiline loaded PLGA/lipid nanoparticles: Synthesis, characterisation and brain pharmacokinetics evaluation, *J. Drug Deliv. Sci. Technol.* 77 (2022) 103923. <https://doi.org/https://doi.org/10.1016/j.jddst.2022.103923>.
- [242] K.V. Krishna, G. Wadhwa, A. Alexander, N. Kanojia, R.N. Saha, R. Kukreti, G. Singhvi, S.K. Dubey, Design and Biological Evaluation of Lipoprotein-Based Donepezil Nanocarrier for Enhanced Brain Uptake through Oral Delivery, *ACS Chem. Neurosci.* 10 (2019) 4124–4135. <https://doi.org/10.1021/acscchemneuro.9b00343>.
- [243] M.R. Donthi, R.N. Saha, G. Singhvi, S.K. Dubey, Dasatinib-Loaded Topical Nano-Emulgel for Rheumatoid Arthritis: Formulation Design and Optimization by QbD, In Vitro, Ex Vivo, and In Vivo Evaluation, *Pharmaceutics.* 15 (2023) 736. <https://doi.org/10.3390/pharmaceutics15030736>.
- [244] J.R. Rodriguez Amado, A.L. Prada, J.L. Duarte, H. Keita, H.R. da Silva, A.M. Ferreira, E.H. Sosa, J.C.T. Carvalho, Development, stability and in vitro delivery profile of new loratadine-loaded nanoparticles, *Saudi Pharm. J.* 25 (2017) 1158–1168. <https://doi.org/10.1016/j.jsps.2017.07.008>.
- [245] K.S. Prayag, A.T. Paul, S.K. Ghorui, A.B. Jindal, Preclinical evaluation of quinapyramine sulphate-loaded lipidic nanocarriers for trypanocidal effect against *Trypanosoma evansi*, *J. Drug Deliv. Sci. Technol.* 81 (2023) 104215. <https://doi.org/10.1016/j.jddst.2023.104215>.
- [246] B. Sun, R. Chang, S. Cao, C. Yuan, L. Zhao, H. Yang, J. Li, X. Yan, J.C.M. van Hest, Acid-Activatable Transmorphic Peptide-Based Nanomaterials for Photodynamic Therapy, *Angew. Chemie.* 132 (2020) 20763–20769. <https://doi.org/10.1002/ange.202008708>.
- [247] S. Derman, Caffeic Acid Phenethyl Ester Loaded PLGA Nanoparticles: Effect of

- Various Process Parameters on Reaction Yield, Encapsulation Efficiency, and Particle Size, *J. Nanomater.* 2015 (2015). <https://doi.org/10.1155/2015/341848>.
- [248] J.H. Park, J. Ahn, S. Kim, How shall we treat early triple-negative breast cancer (TNBC): from the current standard to upcoming immuno- molecular strategies, (2018) 1–16. <https://doi.org/10.1136/esmooopen-2018-000357>.
- [249] Y. Xie, Q. Gou, Q. Wang, X. Zhong, H. Zheng, The role of BRCA status on prognosis in patients with triplenegative breast cancer, *Oncotarget.* 8 (2017) 87151–87162. <https://doi.org/10.18632/oncotarget.19895>.
- [250] J. Maksimenko, A. Irmejs, M. Nakazawa-Miklasevica, I. Melbarde-Gorkusa, G. Trofimovics, J. Gardovskis, E. Miklasevics, Prognostic role of BRCA1 mutation in patients with triple-negative breast cancer, *Oncol. Lett.* 7 (2014) 278–284. <https://doi.org/10.3892/ol.2013.1684>.
- [251] V. Ossovskaya, I.C. Koo, E.P. Kaldjian, C. Alvares, B.M. Sherman, Upregulation of poly (ADP-Ribose) polymerase-1 (PARP1) in triple-negative breast cancer and other primary human tumor types, *Genes and Cancer.* 1 (2010) 812–821. <https://doi.org/10.1177/1947601910383418>.
- [252] M. Rose, J.T. Burgess, K. O’Byrne, D.J. Richard, E. Bolderson, PARP Inhibitors: Clinical Relevance, Mechanisms of Action and Tumor Resistance, *Front. Cell Dev. Biol.* 8 (2020) 1–22. <https://doi.org/10.3389/fcell.2020.564601>.
- [253] R.J. Kong, X.Y. Li, J.Q. Huang, X. Zhou, F.A. Deng, Y.M. Li, L.S. Liu, S.Y. Li, H. Cheng, A self-delivery photodynamic sensitizer for enhanced DNA damage by PARP inhibition, *Biomater. Sci.* 11 (2022) 162–169. <https://doi.org/10.1039/d2bm01320g>.
- [254] P. Kaur, G.M. Nagaraja, H. Zheng, D. Gizachew, M. Galukande, S. Krishnan, A. Asea, A mouse model for triple-negative breast cancer tumor-initiating cells (TNBC-TICs) exhibits similar aggressive phenotype to the human disease, *BMC Cancer.* 12 (2012) 120. <https://doi.org/10.1186/1471-2407-12-120>.
- [255] H. Wu, X. Du, J. Xu, X. Kong, Y. Li, D. Liu, X. Yang, L. Ye, J. Ji, Y. Xi, G. Zhai, Multifunctional biomimetic nanoplatfrom based on photodynamic therapy and DNA repair intervention for the synergistic treatment of breast cancer, *Acta Biomater.* 157 (2023) 551–565. <https://doi.org/10.1016/j.actbio.2022.12.010>.
- [256] L. Yang, Y. Zhang, Y. Zhang, Y. Xu, Y. Li, Z. Xie, H. Wang, Y. Lin, Q. Lin, T. Gong, X. Sun, Z. Zhang, L. Zhang, Live Macrophage-Delivered Doxorubicin-Loaded Liposomes Effectively Treat Triple-Negative Breast Cancer, *ACS Nano.* 16 (2022)

- 9799–9809. <https://doi.org/10.1021/acsnano.2c03573>.
- [257] S. Taymouri, M. Alem, J. Varshosaz, M. Rostami, V. Akbari, L. Firoozpour, Biotin decorated sunitinib loaded nanostructured lipid carriers for tumor targeted chemotherapy of lung cancer, *J. Drug Deliv. Sci. Technol.* 50 (2019) 237–247. <https://doi.org/10.1016/j.jddst.2019.01.024>.
- [258] J. Wu, The Enhanced Permeability and Retention (EPR) Effect: The Significance of the Concept and Methods to Enhance Its Application., *J. Pers. Med.* 11 (2021). <https://doi.org/10.3390/jpm11080771>.
- [259] E.Y. Hanurry, T.W. Mekonnen, A.T. Andrgie, H.F. Darge, Y.S. Birhan, W.-H. Hsu, H.-Y. Chou, C.-C. Cheng, J.-Y. Lai, H.-C. Tsai, Biotin-Decorated PAMAM G4.5 Dendrimer Nanoparticles to Enhance the Delivery, Anti-Proliferative, and Apoptotic Effects of Chemotherapeutic Drug in Cancer Cells., *Pharmaceutics*. 12 (2020). <https://doi.org/10.3390/pharmaceutics12050443>.
- [260] S. Salatin, J. Barar, M. Barzegar-Jalali, K. Adibkia, F. Kiafar, M. Jelvehgari, Development of a nanoprecipitation method for the entrapment of a very water soluble drug into Eudragit RL nanoparticles., *Res. Pharm. Sci.* 12 (2017) 1–14. <https://doi.org/10.4103/1735-5362.199041>.
- [261] B.S. Zolnik, D.J. Burgess, Effect of acidic pH on PLGA microsphere degradation and release, *J. Control. Release.* 122 (2007) 338–344. <https://doi.org/10.1016/j.jconrel.2007.05.034>.
- [262] P. Rong, K. Yang, A. Srivastan, D.O. Kiesewetter, X. Yue, F. Wang, L. Nie, A. Bhirde, Z. Wang, Z. Liu, G. Niu, W. Wang, X. Chen, Photosensitizer loaded nano-graphene for multimodality imaging guided tumor photodynamic therapy, *Theranostics*. 4 (2014) 229–239. <https://doi.org/10.7150/thno.8070>.
- [263] L. Séguy, A.C. Groo, D. Goux, D. Hennequin, A. Malzert-Fréon, Design of non-haemolytic nanoemulsions for intravenous administration of hydrophobic APIs, *Pharmaceutics*. 12 (2020) 1–20. <https://doi.org/10.3390/pharmaceutics12121141>.
- [264] S. Sadat Abolmaali, S. Zarenejad, Y. Mohebi, H. Najafi, S. Javanmardi, M. Abedi, A. Mohammad Tamaddon, Biotin receptor-targeting nanogels loaded with methotrexate for enhanced antitumor efficacy in triple-negative breast cancer in vitro and in vivo models, *Int. J. Pharm.* 624 (2022) 122049. <https://doi.org/10.1016/j.ijpharm.2022.122049>.
- [265] E. Hatanaka, A. Dermargos, A.E. Hirata, M.A.R. Vinolo, A.R. Carpinelli, P. Newsholme, H.A. Armelin, R. Curi, Oleic, linoleic and linolenic acids increase ros

- production by fibroblasts via NADPH oxidase activation., *PLoS One*. 8 (2013) e58626. <https://doi.org/10.1371/journal.pone.0058626>.
- [266] X. Wang, J. Pan, H. Shi, N. Liang, S. Sun, Biotin-modified acid-sensitive micelles for enhancing antitumor effect of paclitaxel, *J. Drug Deliv. Sci. Technol.* 84 (2023) 104538. <https://doi.org/10.1016/j.jddst.2023.104538>.
- [267] Y. Li, Z. Zhan, X. Yin, S. Fu, X. Deng, Targeted Therapeutic Strategies for Triple-Negative Breast Cancer, *Front. Oncol.* 11 (2021) 1–14. <https://doi.org/10.3389/fonc.2021.731535>.
- [268] A.D. Pathade, N. Kommineni, U. Bulbake, M.M. Thummar, G. Samanthula, W. Khan, Preparation and Comparison of Oral Bioavailability for Different Nano-formulations of Olaparib, *AAPS PharmSciTech*. 20 (2019). <https://doi.org/10.1208/s12249-019-1468-y>.
- [269] K. Anwer, E.A. Ali, M. Iqbal, M.M. Ahmed, M.F. Aldawsari, A. Al Saqr, A. Alalaiwe, G.A. Soliman, Development of Chitosan-Coated PLGA-Based Nanoparticles and In Vivo Pharmacokinetic Studies, *Processes*. (2022).
- [270] R.J.C. Bose, R. Ravikumar, V. Karuppagounder, D. Bennet, S. Rangasamy, R.A. Thandavarayan, Lipid–polymer hybrid nanoparticle-mediated therapeutics delivery: advances and challenges, *Drug Discov. Today*. 22 (2017) 1258–1265. <https://doi.org/10.1016/j.drudis.2017.05.015>.
- [271] S.M. Talaat, Y.S.R. Elnaggar, M.A. Gowayed, S.O. El-Ganainy, M. Allam, O.Y. Abdallah, Novel PEGylated cholephyosomes for targeting fisetin to breast cancer: in vitro appraisal and in vivo antitumoral studies, *Drug Deliv. Transl. Res.* (2023). <https://doi.org/10.1007/s13346-023-01409-5>.
- [272] J. Dolai, K. Mandal, N.R. Jana, Nanoparticle Size Effects in Biomedical Applications, *ACS Appl. Nano Mater.* 4 (2021) 6471–6496. <https://doi.org/10.1021/acsanm.1c00987>.
- [273] N.D. Donahue, H. Acar, S. Wilhelm, Concepts of nanoparticle cellular uptake, intracellular trafficking, and kinetics in nanomedicine, *Adv. Drug Deliv. Rev.* 143 (2019) 68–96. <https://doi.org/10.1016/j.addr.2019.04.008>.
- [274] S. Jeon, J. Clavadetscher, D.K. Lee, S. V. Chankeshwara, M. Bradley, W.S. Cho, Surface charge-dependent cellular uptake of polystyrene nanoparticles, *Nanomaterials*. 8 (2018) 1–11. <https://doi.org/10.3390/NANO8121028>.
- [275] P. Foroozandeh, A.A. Aziz, Insight into Cellular Uptake and Intracellular Trafficking of Nanoparticles, *Nanoscale Res. Lett.* 13 (2018). <https://doi.org/10.1186/s11671-018-2728-6>.

- [276] Y. Gregoriou, G. Gregoriou, V. Yilmaz, K. Kapnisis, M. Prokopi, A. Anayiotos, K. Strati, N. Dietis, A.I. Constantinou, C. Andreou, Resveratrol loaded polymeric micelles for theranostic targeting of breast cancer cells, *Nanotheranostics*. 5 (2020) 113–124. <https://doi.org/10.7150/ntno.51955>.
- [277] Y. Herdiana, N. Wathoni, S. Shamsuddin, M. Muchtaridi, Drug release study of the chitosan-based nanoparticles, *Heliyon*. 8 (2022) e08674. <https://doi.org/10.1016/j.heliyon.2021.e08674>.
- [278] I. Amjadi, M. Rabiee, M.S. Hosseini, F. Sefidkon, M. Mozafari, Nanoencapsulation of *Hypericum perforatum* and doxorubicin anticancer agents in PLGA nanoparticles through double emulsion technique, *Micro Nano Lett.* 8 (2013) 243–247. <https://doi.org/10.1049/mnl.2012.0920>.
- [279] B. Mandal, N.K. Mittal, P. Balabathula, L.A. Thoma, G.C. Wood, Development and in vitro evaluation of core–shell type lipid–polymer hybrid nanoparticles for the delivery of erlotinib in non-small cell lung cancer, *Eur. J. Pharm. Sci.* 81 (2016) 162–171. <https://doi.org/https://doi.org/10.1016/j.ejps.2015.10.021>.
- [280] J. Vassoudevane, M. Mariebernard, V. Rajendran, Stearylamine Liposome as an Anti-Parasitic Agent, *Drugs Drug Candidates*. 2 (2023) 95–108. <https://doi.org/10.3390/ddc2010006>.
- [281] Z. He, K. Bao, J. Jian, Y. Zhao, Z. Jian, C. Hu, X. Gao, Biotin-Targeted Multifunctional Nanoparticles Encapsulating 10-Hydroxycamptothecin and Apoptin Plasmid for Synergistic Hepatocellular Carcinoma Treatment, *ACS Appl. Polym. Mater.* 4 (2022) 497–508. <https://doi.org/10.1021/acsapm.1c01393>.
- [282] D. Press, Effective use of nanocarriers as drug delivery systems for the treatment of selected tumors, (2017) 7291–7309.
- [283] S. Taymouri, M. Alem, J. Varshosaz, M. Rostami, V. Akbari, L. Firoozpour, Biotin decorated sunitinib loaded nanostructured lipid carriers for tumor targeted chemotherapy of lung cancer, *J. Drug Deliv. Sci. Technol.* 50 (2019) 237–247. <https://doi.org/10.1016/j.jddst.2019.01.024>.
- [284] X. Song, R. Wang, J. Gao, X. Han, J. Jin, C. Lv, F. Yu, Construction of a biotin-targeting drug delivery system and its near-infrared theranostic fluorescent probe for real-time image-guided therapy of lung cancer, *Chinese Chem. Lett.* 33 (2022) 1567–1571. <https://doi.org/10.1016/j.ccllet.2021.08.111>.
- [285] S. Lei, F. Ge, M. Lin, X. Wang, J. Shen, Y. Yang, J. Deng, Z. Wang, J. Wang, K. Li,

- PARP inhibitors diminish DNA damage repair for the enhancement of tumor photodynamic therapy, *Photodiagnosis Photodyn. Ther.* 40 (2022) 103058. <https://doi.org/10.1016/j.pdpdt.2022.103058>.
- [286] K. Sun, K. Mikule, Z. Wang, G. Poon, A. Vaidyanathan, G. Smith, Z.Y. Zhang, J. Hanke, S. Ramaswamy, J. Wang, A comparative pharmacokinetic study of PARP inhibitors demonstrates favorable properties for niraparib efficacy in preclinical tumor models, *Oncotarget.* 9 (2018) 37080–37096. <https://doi.org/10.18632/oncotarget.26354>.
- [287] V. Dave, K. Tak, A. Sohgaure, A. Gupta, V. Sadhu, K.R. Reddy, Lipid-polymer hybrid nanoparticles: Synthesis strategies and biomedical applications, *J. Microbiol. Methods.* 160 (2019) 130–142. <https://doi.org/10.1016/j.mimet.2019.03.017>.
- [288] S. Li, J. Zhao, Y. Guo, Y. Mei, B. Yuan, N. Gan, J. Zhang, J. Hu, H. Hou, Influence of the introduction of a triphenylphosphine group on the anticancer activity of a copper complex, *J. Inorg. Biochem.* 210 (2020) 111102. <https://doi.org/10.1016/j.jinorgbio.2020.111102>.
- [289] S.H. Nam, J. Park, H. Koo, Recent advances in selective and targeted drug/gene delivery systems using cell-penetrating peptides, *Arch. Pharm. Res.* 46 (2023) 18–34. <https://doi.org/10.1007/s12272-022-01425-y>.
- [290] L. Ye, Q. Yao, F. Xu, L. He, J. Ding, R. Xiao, L. Ding, B. Luo, Preparation and antitumor activity of triphenylphosphine-based mitochondrial targeting polylactic acid nanoparticles loaded with 7-hydroxyl coumarin, *J. Biomater. Appl.* 36 (2022) 1064–1075. <https://doi.org/10.1177/08853282211037030>.
- [291] G.W. BIRD, Blood compatibility tests., *J. Indian Med. Assoc.* 21 (1951) 67–68.
- [292] Jia Zhou , Wei-Yu Zhao , Xu Ma , Rui-Jun Ju , Xiu-Ying Li , Nan Li , Meng-Ge Sun , Ji-Feng Shi , Cheng-Xiang Zhang , Wan-Liang Lu , The anticancer efficacy of paclitaxel liposomes modified with mitochondrial targeting conjugate in resistant lung cancer, *Biomaterial*, Volume 34, Issue 14, May 2013, Pages 3626-3638
- [293] S. Parveen, P. Gupta, S. Kumar, M. Banerjee, Lipid polymer hybrid nanoparticles as potent vehicles for drug delivery in cancer therapeutics, *Med. Drug Discov.* 20 (2023) 100165. <https://doi.org/10.1016/j.medidd.2023.100165>.



APPENDIX-I



List of Publications, Patents and Book Chapters

Publications from Ph. D Thesis

1. **Pradhan Rajesh**, Shobha Kumari, Himaja Ambati, Tarun Kumar Patel, Balaram Ghosh, Anu Puri, Sunil Kumar Dubey, and Rajeev Taliyan.” Development of Biotin Decorated Olaparib Loaded Cationic Lipopolymeric Hybrid Nanoparticle and Evaluation of its Anticancer Effect and Pharmacokinetics for Triple Negative Breast Cancer”, Journal of Drug Delivery Science and Technology 94 (2024):105458.
2. **Pradhan Rajesh**, Sunil Kumar Dubey, Anu Puri, and Rajeev Taliyan.” Development and validation of a stability-indicating reversed-phase–high-performance liquid chromatography method for quantification of 2-[1-hexyloxyethyl]-2-devinyl pyropheophorbide-a from lipid-polymeric hybrid nanoparticles.” Separation Science Plus: 6, no. 1 (2023): 2200061.
3. **Pradhan, Rajesh**, Anuradha Dey, Rajeev Taliyan, Anu Puri, Sanskruti Kharavtekar, and Sunil Kumar Dubey.” Recent Advances in Targeted Nanocarriers for the Management of Triple Negative Breast Cancer.” Pharmaceutics 15, no. 1 (2023): 246.
4. Nitheesh, Yanamandala*, **Rajesh Pradhan***, Siddhant Hejmady, Rajeev Taliyan, Gautam Singhvi, Amit Alexander, Prashant Kesharwani, and Sunil Kumar Dubey.” Surface engineered nanocarriers for the management of breast cancer.” Materials Science and Engineering: C 130 (2021): 112441.
5. Hejmady, Siddhanth*, **Rajesh Pradhan***, Amit Alexander, Mukta Agrawal, Gautam Singhvi, Bapi Gorain, Sanjay Tiwari, Prashant Kesharwani, and Sunil Kumar Dubey.” Recent advances in targeted nanomedicine as promising antitumor therapeutics.” Drug discovery today 25, no. 12 (2020): 2227-2244.

Patent

1. **Pradhan Rajesh**, Rajeev Taliyan, Sunil Kumar Dubey, Balram Ghosh and. Shobha Kumari, “A drug delivery system for photodynamic therapy and method of preparing the same” (Indian Patent, filed on 19 Oct 2023; Application no. 202311071310)

Other Publications

1. **Pradhan Rajesh**, Diksha Mishra, Sunil Kumar Dubey, Rajesh Khadgawat, Garima Kachhawa, Tarang Gupta, and Rajeev Taliyan.” Simultaneous estimation of methyl paraben, propyl paraben, and Bisphenol A in the plasma of Indian pregnant women using liquid chromatography–tandem mass spectrometry.” *Separation Science Plus*: 2200163.
2. **Pradhan Rajesh**, Gautam Singhvi, Sunil Kumar Dubey, Gaurav Gupta, and Kamal Dua.” MAPK pathway: a potential target for the treatment of non-small-cell lung carcinoma.” *Future medicinal chemistry* 11, no. 08 (2019): 793-795.
3. **Pradhan Rajesh***, Siddhanth Hejmady*, Rajeev Taliyan, Gautam Singhvi, Rajesh Khadgawat, Garima Kachhawa, and Sunil Kumar Dubey.” Bioanalytical methodologies for clinical investigation of endocrine-disrupting chemicals: a comprehensive update.” *Bioanalysis* 13, no. 1 (2021): 29- 44.
4. **Pradhan Rajesh**, K. V. Krishna, Geetika Wadhwa, Rajeev Taliyan, Rajesh Khadgawat, Garima Kachhawa, Gautam Singhvi, and Sunil Kumar Dubey. ” QbD-driven development and validation of HPLC method for determination of Bisphenol A and Bis-sulphone in environmental samples.” *International Journal of Environmental Analytical Chemistry* 100, no. 1 (2020): 42-54.
5. **Pradhan Rajesh**, Siddhanth Hejmady, Rajeev Taliyan, Rajesh Khadgawat, Tarang Gupta, Garima Kachhawa, Rajesh Kumar, Gautam Singhvi, and Sunil Kumar Dubey.” Simultaneous estimation of parabens and bisphenol a in ready-to-eat foodstuffs by using QbD-driven high-pressure liquid chromatography method.” *International Journal of Environmental Analytical Chemistry* 102, no. 10 (2022): 2363-2378
6. Dubey, Sunil Kumar*, **Rajesh Pradhan***, Siddhanth Hejmady, Gautam Singhvi, Hira Choudhury, Bapi Gorain, and Prashant Kesharwani.” Emerging innovations in nano-enabled therapy against age-related macular degeneration: A paradigm shift.” *International Journal of Pharmaceutics* 600 (2021): 120499.
7. Siddhanth Hejmady*, **Pradhan Rajesh***, Shobha Kumari, Meghna Pandey, Sunil Kumar Dubey, and Rajeev Taliyan.” Pharmacokinetics and toxicity considerations for antibody-drug conjugates: an overview
8. Jain, Rupesh, **Rajesh Pradhan**, Siddhanth Hejmady, Gautam Singhvi, and Sunil Kumar Dubey.” Fluorescence-based method for sensitive and rapid estimation of chlorin e6 in stealth liposomes for photodynamic therapy against cancer.”

Spectrochimica Acta Part A: Molecular and Biomolecular Spectroscopy 244 (2021): 118823.

Book Chapters

1. **Pradhan Rajesh**, Siddhanth Hejmady, Amit Alexander, Gautam Singhvi, and Sunil Kumar Dubey.” Analytical quality by design for gas chromatographic method development.” In Handbook of Analytical Quality by Design, pp. 45-70. Academic Press, 2021.
2. Hejmady, Siddhanth, Dinesh Choudhury, **Rajesh Pradhan**, Gautam Singhvi, and Sunil Kumar Dubey.” Analytical quality by design for high-performance thin-layer chromatography method development.” In Handbook of Analytical Quality by Design, pp. 99-113. Academic Press, 2021.
3. **Pradhan Rajesh**, Meghna Pandey, Siddhanth Hejmady, Rajeev Taliyan, Gautam Singhvi, Sunil K. Dubey, and Sachin Dubey.” Antibody–Drug Conjugates: Development and Applications.” Targeted Drug Delivery (2022): 127-154.

Certificates/Poster presentations

1. Poster presented on pre-clinical pharmacokinetics of MEM-ALA conjugates in rat using UPLC-MS/MS at ISSX-2019, Bengaluru
2. Certificate course in “Improving the quality and outcome of experimental research” with hands-on training on cellular imaging and confocal technique, live cell imaging & in-vivo technique, conducted by NIPER-R, Lucknow
3. Certificate course in “Drug metabolism and pharmacokinetics” conducted by ISSX, India



APPENDIX-II





Biography of Dr. Rajeev Taliyan

Dr. Rajeev Taliyan is currently working as a Professor in the Department of Pharmacy, Birla Institute of Technology and Science, Pilani, Pilani-campus, Rajasthan. He has earned his PhD (Pharmacology) under the supervision of Prof. P.L Sharma (Emeritus, Prof. PGIMER) and Late Prof. Manjeet Singh (Ex Head, Dean, Punjabi University) from ISF college of Pharmacy, Punjab Technical University, Punjab. He has been involved in teaching and research for past two decade. He has vast experience in the field of Neuropharmacology, Cancer, Cardiovascular pharmacology and Drug toxicity. He has been awarded with various research projects from DST, UGC, ICMR and BITS-Pilani. He has also several research collaborations and projects with Pharmaceutical Industry such as Etica Clin Pharm Pvt Ltd, Emami Ltd. and Zeon life sciences Ltd. He has guided 7 PhD scholar and more than 25 students for their postgraduation dissertation. He has been awarded with many prestigious awards at international and national level including, Prof. Manjeet Singh Gold medal award at IPSCON-2015; PP Surya Kumari Gold Medal Award at IPSCON-2014. He has been invited by several Research and Academic institutes for delivering guest lectures including GLA University, Mathura, Rayat Bahra, Ram-Eesh University, Shoolini University. He was also a visiting Assistant Research Professor in the Department of Pharmacy at the University in Taipei, Taiwan. He has published several papers in peer reviewed international and national journals and in conferences of international and national repute. He is life member of Indian Pharmacological Society and British Pharmacological Society, UK.



Biography of Sunil Kumar Dubey

Dr. Sunil Kumar Dubey is presently working as the General Manager, Medical Research, R&D Healthcare Division at Emami Ltd, Kolkata. He is involved in planning and ensuring the timely execution of several preclinical and clinical studies. His expertise involves in validating the effectiveness of a vast range of healthcare products and providing business development-related insights. He is responsible for developing product concept notes, technical notes, monographs, and dossiers. His team is also involved in supporting medico-marketing, product licensing activities, and training personnel from marketing and sales teams. Collectively, his efforts are towards bridging the gap between the industry, consumers, and the scientific community.

Overall, he has more than 16 years of industrial, teaching, research, and administrative experience. Prior to this, he was Assistant Professor in the Department of Pharmacy, Birla Institute of Technology and Science (BITS), Pilani, India. He was also a visiting Assistant Research Professor in the Department of Chemical and Biomolecular Engineering at the University of Maryland, USA. Currently, he also serves as a guest faculty at various leading institutes including NIPER Guwahati, NIPER Raebareli, Jamia Hamdard, etc.

He has an extensive research experience in the area of pharmacokinetic pharmacodynamic modelling and simulations, development of phytopharmaceuticals and numerous nano-technology-based platforms. He has supervised Ph.D., postgraduate and undergraduate students. He has published more than 150 articles and book chapters in renowned high-impact journals and presented papers at conferences in India and abroad. He is included in the list of 'World's Top 2% Most-Cited Scientists' as per the Elsevier-Stanford University report.

He has successfully completed various government and industry funded projects related to new product development, pharmacokinetic and pharmacodynamic investigations. All these concerted efforts have led to the grant of patents to his name as well.



Biography of Rajesh Pradhan

Currently, **Mr. Rajesh Pradhan** is pursuing PhD degree from Department of Pharmacy, BITS-Pilani, Pilani campus, Rajasthan. He has obtained MS (Pharm.) Pharmaceutics from NIPER-Raebareli, India. He has qualified national level entrance exams including GPAT and NIPER-JEE. He is having more than 5 years of research experience in the field of Advance Drug Delivery, Pharmacokinetics and Cancer therapeutics and 2 years of expertise in Pharmacology for the treatment of Breast Cancer. He has also gained industrial experience of 1.8 years in the field of BA/BE and DMPK particularly in Bioanalysis, In-vitro pharmacokinetics and In-vivo pharmacokinetics. He has published several articles in peer reviewed journals and filed a patent at national and international level.

